The Geochemical Modelling of Emergent Life from Submarine Hydrothermal Environments

A thesis submitted for the award of PhD

March 2002

by Laiq Rahman

Division of Earth Sciences

University of Glasgow

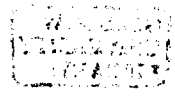

Acknowledgements

Thanks to Prof. Michael J. Russell and Dr. Allan J. Hall, without whom this thesis could not have been. Equally, my gratitude extends to all in the Division of Earth Sciences who provided advice, encouragement, and technical support. Thanks also to the Natural Environment Research Council (UK) for providing the necessary funding. Last but not least, this thesis is dedicated to my parents, Jamil and Asifa.

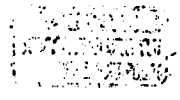

Declaration of Originality

This thesis is my original work and has not been presented for a degree in any other University

"Why am I doing this? Only the tiny sea of my cells replies, reminding me that I am the sea and the sea is in me."

Jacques-Yves Cousteau

Abstract

As knowledge improves in the study of early atmospheric, oceanic, and crustal composition, and in planetary science in general, it rejects previous origin of Life models such as that of Haldane (1929), Oparin (1938); Urey (1952), Miller (1953), and perhaps more recently, Wächtershäuser, (1988a). Consequently, the idea that submarine hydrothermal systems could have produced and harboured the necessary prebiotic reactants for Life has become increasingly popular among many scientists since their discovery in 1977 (Corliss *et al.*, 1979). This idea, in particular the origin of Life model proposed by Russell and Hall (1997), was the primary focus for this study.

Since it is difficult to simulate hydrothermal conditions in laboratory experiments, equilibrium thermodynamic models provide an alternative approach and are the main concern of this thesis. These help to investigate the availability, redox behaviour, and fate of chemical species around hydrothermal systems (in particular, hydrogen, iron, sulfur, carbon dioxide and amino acids), and the physicochemical properties of hydrothermal systems (temperature and pH). A secondary aim was to evaluate the advantages and shortcomings of this approach. Most models used in this study were created using the Geochemist's Workbench (GWB) speciation/solubility code (Bethke, 1998), in tandem with thermodynamic data for minerals, aqueous species and gases, available from the Lawrence Livermore National Laboratory (LLNL) facility, USA (Delaney and Lundeen, 1990). Where thermodynamic data were not available for a particular component, the LLNL database was updated using data from alternative published sources. Results obtained by others using the SUPCRT92 code (Johnson *et al.*, 1992), and a comparison of GWB and EQ3NR/EQ6 (Wolery, 1992; Wolery and Daveler, 1992), were used to demonstrate the consistency of results between geochemical codes.

This study began with an attempt to understand and convey the significant advances in knowledge that have been made in the 20th century, in pursuit of the solution to the origin of Life, and of early conditions to provide the necessary experimental controls for the investigation. Early oceanic crust models were based on the oldest rocks found today (Archaean greenstones, ophiolites and dunites). These mafic (Mg-Fe rich) and ultramafic rocks usually contain olivines and are often serpentinised. Seawater models were based on a mainly carbonic acid Hadean Ocean. The production of hydrogen (a key metabolite for chemolithoautotrophy) from olivine-seawater interaction was investigated, as well as the controls on pH in the reaction settings. Hydrogen was produced in sufficient quantities (≤40

mmoles) for chemolithoautotrophic metabolism, and pH was controlled by temperature and the presence of magnesium and calcium. Sulfur availability (~10 mmoles) in hydrothermal fluids, critical to the Russell and Hall (1997) hypothesis for the formation of a primitive membrane in hydrothermal fluids was confirmed and concluded to be controlled by mineral assemblages buffering the hydrothermal fluid.

The Theory of Surface Metabolism by Wächtershäuser (1988a) implies that high-temperature hydrothermal environments enhance iron sulfide's ability to catalyse organic synthesis by a surface-promoted reaction (Wächtershäuser, 1988b; Wächtershäuser, 1990; Huber and Wächtershäuser, 1997). This so-called 'pyrite-pulled' mechanism was rejected in a detailed thermodynamic study by Schoonen *et al.* (1999). To emphasise their point, their complex SUPCRT92 model was simplified and recast using GWB, which confirmed the SUPCRT92 result and Schoonen *et al.*'s (1999) statement.

Hydrothermal systems may have been more widespread in the Hadean due to a greater heat flux. To investigate this possibility, and unravel the mechanism(*s*) by which the pH of high-temperature vent fluids become acidic and what produces their distinctive black colour, reactions between model seawater and mafic/ultramafic rock were conducted. Results indicated that ancient, medium to high temperature (150-300°C), alkaline hydrothermal fluids would have precipitated carbonates, brucite, and calcite upon re-mixing with cold, slightly alkaline seawater and may have predominated in the Hadean. Acid pH was effected by the loss of magnesium from seawater and calcium loss from mafic rock. Black-smokers were unlikley in the Hadean as the ocean was probably acidic due to high levels of CO_2.

If the early crust contained vestigial native iron and nickel (Ballhaus, 1995; Righter and Drake, 1997), its overall oxidation state would have been more reducing than today (Kasting and Brown, 1998). Oxidation states of mineral assemblages (pyrite-pyrrhotite-magnetite, PPM; fayalite-magnetite-quartz, FMQ; nickel/nickel-oxide, Ni/NiO) with respect to the C-O-H system were evaluated at various temperatures and compared with the relatively reduced iron-wüstite assemblage. However, the availability of thermodynamic data for investigating novel, reduced mineral assemblages was limited, and unexpected results indicated the need to reassess the approach used.

Water-rock reaction models were constructed to test the possibility that simple amino acids could have been generated in early hydrothermal fluids, and to see how pH and redox conditions affect their distribution (*cf.* Amend and Shock, 1998). Though concentrations of

amino acids produced were negligible, amino acids were stable in low-temperature, alkaline, and reduced hydrothermal fluids and may have concentrated in the colloidal sieve comprising a hydrothermal mound. An extension of the experiment to determine if glycine could be condensed to higher carbon number amino acids (alanine, valine, leucine) under hydrothermal conditions, indicated that condensation may be 'pulled' by a decrease in H_2O activity of the fluid.

In conclusion, this study improved on previous environmental and reactant constraints by simulating the generation of *inorganic* prebiotic reactants from the local geochemical hydrothermal environment. Consequently, the quantity of chemical species such as hydrogen and sulfide available for organic synthesis were limited by the local geochemical settings in the model, whereas others have, often admittedly, used reactants in higher concentrations than were probably available when Life emerged.

This thesis is a thermodynamic feasibility study which supports the notion that in the Hadean, key prebiotic reactants such as hydrogen, iron-sulfides, and amino acids could have been available and conditions were thermodynamically favourable to establish primitive membranes and chemolithoautotrophic metabolism. In addition, the ability to model organic compounds in an inorganic geochemical system demonstrate the applicability of the modelling codes to a variety of geochemical and biochemical situations. Thus, they are particularly suitable for investigating a geochemical origin of Life.

Preface

The thesis presented here is the result of three years work carried out at the Division of Earth Sciences at Glasgow University and funded by a Natural Environment Research Council (UK) studentship.

The primary aim of this research was to investigate the role of minerals, fluids, gases, temperature and pH in the emergence and early evolution of life at or near submarine alkaline hydrothermal seepages, approximately 4.2 billion years ago. The work investigates the proposed hydrothermal fluid-rock reactions among minerals, aqueous and gaseous species featuring in the reaction pathways leading towards the first cell, as described in Russell and Hall (1997). The latest developments in their hypothesis can be examined online at http://www.gla.ac.uk/projects/originoflife (Russell *et al.*, WWW, 2001).

In general, the question to be answered in this study was: Assuming that heavy meteoritic impacts (Melosh, 1989) on the early Earth provided a significantly different (higher energy, more reduced), mineralogy to that of today (Turcotte, 1980; Ballhaus, 1995; Righter *et al.*, 1997; Francis *et al.*, 1999), how then did this affect the chemistry of the early atmosphere and oceans (Kasting and Brown, 1998) and the availability of prebiotic reactants in early hydrothermal systems?

The origin of Life is of interest to people from many disciplines. Therefore, it seems appropriate to mention some key Earth Science textbooks and papers for an introduction to some of the principles behind the subject of geology and aqueous geochemistry (Brown *et al.*, 1992; Krauskopf, 1967; Appelo and Postma, 1993). An understanding of models of the evolution of the early atmosphere, ocean and crust (Lafon and MacKenzie, 1974; Holland, 1984, Kasting and Brown, 1998) and geophysiology, the coupling of Life and the planet (Lovelock, 1989), will undoubtedly prove invaluable to visualise geochemical conditions and cycles on the early Earth. In 1991, the Scientific Committee on Oceanic Research (SCOR) created a working group of scientists from various disciplines who set out the terms of reference for the study of submarine hydrothermal systems as a plausible environment for the origin of Life. As a result of this collaboration, a set of papers were published (Holm (ed.), 1992) summarising the state of knowledge by 1992, six years before the commencement of this study. The discussions presented in these papers may convert even some of the most sceptical into accepting that extreme conditions in hydrothermal systems *are* plausible environments for life. The discussions range from the availability and fate of chemical species around hydrothermal systems, to the physical and chemical properties of

the hydrothermal systems themselves. This collection of published works is ideal as a primer to understanding the scientific reasoning behind the chemistry to be investigated, and the unusual conditions that prevail in hydrothermal systems, and it provides a very useful starting point for this research.

The sheer complexity of the geochemical and physical processes leading up to the emergence of life makes it impossible to include a thorough investigation of all the stages of the proposed prebiotic evolutionary process. As mentioned above the thesis focused on hydrothermal fluid-rock and hydrothermal fluid-seawater reactions (MacLeod *et al.*, 1994; Hochella Jr. and White, (eds.), 1990) to investigate what role the geochemistry of minerals, fluids, gases, temperature and pH played in what are considered to be the important chemical reactions, as well as the reaction pathways, leading towards the formation of the first cells (Russell and Hall, 1997). Elements and compounds that are studied in this work include hydrogen, carbon oxides, nitrogen, iron, sulfur and amino acids. The results help in the investigation of proposed key reactions, concentrations, and stability of chemical species in a prebiotic hydrothermal environment in the Russell-Hall theory (1997).

Similar research, modelling the potential of hydrothermal or broadly analogous environments to produce and harbour the chemical species and energy necessary for the emergence of life is currently being investigated or reviewed by others (Shock, 1990, 1992a, 1992b, 1995; Shock and Schulte, 1998; Schulte and Shock, 1995; Amend and Shock, 1998; Schoonen *et al.*, 1999; Wächtershäuser, 1988b), including individuals in our own research group (Russell *et al.*, 1998). Their expertise in thermodynamic modelling is undeniable and unparalleled in this field, possibly due to working with some of the pioneers of the early thermodynamic modelling codes such as Hal Helgeson, author of the Helgeson-Kirkham-Flowers (Helgeson *et al.*, 1981) equations of state for modelling minerals, aqueous species and gases; Tom Wolery, author of the EQ3NR/EQ6 modelling code; and Craig Bethke, author of the Geochemist's Workbench), and to their rigorous definitions of the thermodynamic parameters used in their work. Therefore, their work is of essential reading for a thermodynamic study such as this.

The investigators listed examine the ability of hydrothermal systems to sustain (in sufficient concentrations) the organic reactants for the initiation of the first biochemical cycle, (perhaps the pentose phosphate cycle or the reverse tricarboxylic acid (TCA) cycle). They also suggest how the same environment may have later supported or encouraged the formation of the first amino acids and proteins.

In particular, this work investigates the thermodynamics of reactions under significantly more reducing conditions than those tested by others on the basis that the early crust had a significantly higher native iron and nickel content than today. Other significant differences between this work and the work of these authors are listed below.

(i) The majority of conclusions by these authors were arrived at using the SUPCRT codes whereas this work utilised the Geochemist's Workbench (GWB) codes and includes a comparison of results obtained from GWB and EQ3NR/6 computer codes. High pressures (500-5000 bars) are regularly used in the calculations by these authors. In this thesis it is assumed that pressure has little influence in low temperature reactions. The main advantages of GWB over SUPCRT and EQ3NR/EQ6 are graphic output, ease of use and rapidity, it is also biochemically friendly in that organic species can be modelled.

(ii) This research utilises improved environmental and reactant constraints whereas others have, often admittedly, used reactants in higher concentrations than were probably available on the early Earth and not considered their genesis or even the initial conditions. One of the ways it does this is by placing an upper limit to the availability of the *inorganic* prebiotic reactants by utilising only the reactants available from the local environment or reaction settings.

(iii) It could be argued that Shock, Seyfried, Schoonen, and their co-workers have already undertaken thermodynamic studies on the subject of organic synthesis, or stability and concentration of chemical species under hydrothermal conditions, but their experiments are limited in their applicability to the origin of Life. Most of their work focuses on the key steps between the inorganic and organic, and in the subsequent stability of the organic molecules once formed. Many of their experiments are performed with experiments buffered to modern oxidation states of the Earth. Although they have tackled the more difficult problem of organic synthesis, in this study the mechanisms by which the prebiotic 'ingredients' are produced, their available concentrations, the influence of pH on their availability, are thought to be just as important. These important issues have generally not been addressed by many authors who just focus on organic synthesis.

(iv) Russell and Hall have formulated their pre-life reactions within the context of the Hadean environment. They address why life began, and envisage a chemolithoautotrophic rather than an autotrophic origin. They also emphasise the important contribution of pH to the driving force for Life (Russell and Hall, 1997). Their hypothesis depends very much on the availability of key reactants in sufficient concentrations, and pH is also important in

determining the availability of a particular chemical species. For example, H_2S is predominantly stable in acidic conditions, whereas HS^- is stable in alkaline conditions. This approach has the support of biochemists who understand reactions in terms of *Eh*-pH diagrams, since *Eh* and pH conditions influence many biochemical reactions. In addition, their post emergence of life predictions are supported by feasible mechanisms for information transfer and replication and estimates of timescales for key evolutionary processes.

To summarise, a brief description of each chapter follows.

Chapter 1 introduces the historical aspects and recent advances of the subject to be tackled in the thesis, as well as the specific aims and objectives of this research. The reader is introduced to the basic inner workings of the thermodynamic databases and geochemical packages used. For readers unfamiliar with the typical output of geochemical packages, some special assistance is given to help in the interpretation of results in this study.

The thesis pays particular attention to the role of hydrogen as a prebiotic reactant. Hydrogen has recently been shown to provide a source of energy for reactions involved in cell metabolism for many chemolithoautotrophic organisms (Wood, 1991; Stevens and McKinley, 1995; Vargas *et al.*, 1998; Martin and Müller, 1998; Kral *et al*, 1998). It is suggested that hydrogen detected near serpentinised rock/basalts is abiogenic in origin (Neal and Stanger, 1983; Coveney *et al.*, 1987; Stevens and McKinley, 1995). Hydrogen production could be commonplace in many other subsurface environments where serpentinisation is taking place (Neal and Stanger, 1983; Berndt *et al.*, 1996). If the same is true of the early Earth, then early organisms could have survived on the energy available from hydrogen produced from such water-rock reactions.

Chapter 2 investigates the production of hydrogen from reactions between the Hadean seawater and minerals assumed to be present beneath the vents and seepages of early hydrothermal systems. In cases such as this, where the field evidence is not conclusive, computer-simulated water-rock experiments can help to show whether such hypotheses are thermodynamically feasible in a particular geochemical environment. Thus, it includes a description of what the Hadean environment may have been like for the purpose of defining the initial environmental constraints for creating models. The crust today is composed of layers of basalt, gabbro and peridotites, but the models in this work focus on the oldest rocks found today such as Archaean greenstones, ophiolites and dunites. These ultramafic and mafic rocks usually contain serpentinised olivines and serpentines (Neal and Stanger, 1983).

The result is a set of computer-generated diagrams helpful in visualising the geochemical processes that may have led to the production and stability of hydrogen.

In Chapter 3 attempts were made to determine whether there would have been sufficient quantities of iron-sulfide available to form membranous structures to assimilate organic reactants, as suggested by Russell and Hall (1997). Thus, models were created to examine what controls the stability and availability of sulfur in a hydrothermal fluid. Sulfur and sulfur compounds (particularly iron sulfides and H_2S) found in and around hydrothermal vents are of particular interest for several reasons (Russell *et al*, 1997; Clark *et al*, 1998). Iron(nickel)-sulfide containing proteins are at the root of metabolic processes in all life (Silver (ed.), 1993) and are likely to have been present in the earliest life-form (Eck and Dayhoff, 1966). Iron sulfides may also help overcome thermodynamic barriers with their ability to catalyse important biological reactions in surface-promoted reactions (Wächtershäuser, 1988b; Wächtershäuser, 1990; Huber and Wächtershäuser, 1997). In addition experiments by Heinen and Lauwers (1996, 1997) hinted that the route to organic synthesis may be more easily facilitated by the formation of organic thiols (R-SH) as intermediates. This idea was confirmed theoretically in a thermodynamic study by Schoonen *et al.* (1999). Naturally, iron and sulfur are two components that feature prominently in this thesis. Wächtershäuser's (1988a) Theory of Surface Metabolism is also questioned. His proposed "pyrite-pulled mechanism" to reduce CO_2 and produce activated acetic acid has been shown to have inherent flaws (de Duve and Miller, 1991; McDowall *pers. comm.*, 1997; Schoonen *et al.*, 1999), though later he did have success with CO and iron-nickel sulfide as a catalyst. However, the reaction in the latter experiment was not coupled to the generation of pyrite as initially proposed, and is the subject of much discussion elsewhere in the scientific community. The discussion serves to provide the basis for subsequent experiments in the chapter.

Chapter 4 has a dual purpose. The first is to question whether hydrothermal systems could have been present in the Hadean and to attempt to unravel the mechanism by which modern or ancient vent fluids become acidic or alkaline and what makes vent-plumes black. This is achieved by experimenting with mixing a model seawater with mafic and ultramafic rock at various temperatures, Recent investigations indicate that perhaps they were abundant in the early oceanic crust (de Wit *et al.*, 1982; de Ronde *et al.*, 1994; Appel *et al.*, 2001). In addition to these questions, this chapter also incorporates the testing of the integrity of the geochemical modelling software by evaluating two different modelling codes (Geochemist's Workbench and EQ3/6) with the same data. The experiment also uses the modelling codes

to attempt to generate a fluid (from water-rock reactions) that resembles those sampled at hydrothermal vents. The author is not aware of previous work that has attempted to do this.

Many researchers have based their research under conditions resembling the oxidation state imposed by mineral assemblages of the early crust, pyrrhotite/pyrite-magnetite (PPM) for example (Frost, 1985; Shock and Schulte, 1998; Hennet *et al.*, 1992). However, if native iron and nickel were present in the early crust (Ballhaus, 1995; Righter and Drake, 1997), it is possible that the overall oxidation state of the early crust could have been much more reduced (Kasting and Brown, 1998). In Chapter 5, in anticipation of calculations now and in future work to be performed using these lower oxidation states, various mineral assemblages are tested and their oxidation state evaluated at different temperatures. For example, mineral buffers that are relatively more reduced than those tested by these authors are also investigated, such as iron-wüstite as Fe-FeO.

Chapter 6 extended on work done by others (Amend and Shock 1998; Shock and Schulte, 1998; Schoonen *et al.*, 1999; Hennet *et al.*, 1992). Specifically, models of early hydrothermal systems were created to test the possibility that simple amino acids can exist in a hydrothermal fluid and to see how pH and redox conditions affect their distribution (*cf.* Amend and Shock, 1998). Although amino acid formation and stability in hydrothermal systems have been investigated by Shock and his co-workers, this thesis experiments further by attempting to model the actual condensation reactions of glycine to higher carbon number amino acids such as alanine, valine and leucine under hydrothermal conditions as shown experimentally by Ferris *et al.* (1996), and Imai *et al.* (1999).

All experimental work in this thesis was performed using thermodynamic data available from the Lawrence Livermore National Laboratory, LLNL (Delaney and Lundeen, 1990). This database (*thermo.com.v8.r6.full*) is one of the most reliable with respect to its internal consistency of methods and thermodynamic variables used to obtain the data. Occasionally a smaller subset of the data is used with the GWB modelling software and will be referred to as *thermo.dat*.

Contents

Chapter 1. Introduction

1.1 Introduction

Oparin (1938) may be credited for providing the foundations for modern research pertaining to the phenomenon of Life. He proposed that Life resulted from a series of probable steps of increasing complexity, inevitably leading to the living state. His "materialistic" view was different. It was opposed to the "mechanistic" chance combination of the elements, or reductionism, which was popular during the earlier part of the 20th century, and instead incorporated the application of natural laws of physics and chemistry.

Oparin described three stages for the evolutionary process:

1. The development of a primary reducing atmosphere that promoted the formation of organic molecules. This stage was later endorsed by Bernal (1949, 1951) and Urey's (1952) discussion of available free energies and reducing atmospheres on the Early Earth, and seemingly substantiated by Miller's (1953) success in producing amino acids in a reducing atmosphere.

2. The autotrophic formation of progressively complex organic substances as a result of condensation, polymerisation, and redox reactions assisted by the warm waters of the early oceans. Echoes of this idea may be seen in Pringle, (1953), Oberholzer *et al.* (1995), Russell and Hall, (1997), Schwartzman *et al.* (1994), Russell, Daia and Hall, (1998).

3. The third stage, which could not be explained by the natural laws of physics and chemistry, required new laws – referring to the laws of biological factors such as Darwin's (1859) theory of natural selection, where "new systems of co-ordination of chemical processes appeared" and "which hitherto were entirely unthinkable" (Farley, 1977).

To escape from the vague notions of spontaneous generation formulated in the 19th century, Oparin presented this hypothetical sequence of key stages leading to the emergence of life for the purpose of providing a framework for future investigations. This ideology led to Miller's synthesis of amino acids in electric discharge experiments (1953) which was hailed as a major breakthrough. He had created simple organic molecules by simulating lightning in an atmosphere modelled on Urey's reduced atmospheric gases: hydrogen, methane, ammonia; and then water as his 'ocean' in which to collect the amino acids.

However, new findings began to contradict Urey's reducing atmosphere. Evidence from the presence of sulfates in 3.5 billion year old rocks from Western Pilbara, Australia (Schopf, 1983; Walter, 1983; Rasmussen, 2000) show that these sulfates could not have formed without some oxygen-containing compound (such as sulfur dioxide and carbon dioxide) in the atmosphere. Volcanic outgassing during the early stages of the Earth's formation would have contributed large amounts of the carbon oxides, CO and/or CO_2, to the atmosphere (Kasting, 1993). Together, they predominated over methane. Any methane or ammonia present in the early atmosphere would have been dissociated by strong UV radiation (Kasting and Brown, 1998). Thus, it became generally accepted that the early atmosphere, although anoxic (lacking in oxygen), could not have been reducing but was probably mildly oxidised, consisting mainly of a mixture of carbon oxides and nitrogen rather than methane and ammonia. In addition, Miller's experiments with reduced atmospheric gases, with the ocean being the recipient of amino-acids, hinted that life initially thrived near the surface of the early earth. Such ideas were classed as organic 'soup' or 'broth' theories and were typical in that they did not explain how possible prebiotic molecules such as ammonia, and life itself would have been protected against strong UV radiation or several global catastrophic events such as heavy bombardment from meteorites and the consequent vaporisation of the oceans.

Thus, the basic framework for future investigations had to be adjusted to consider the possibility of mildly oxidised conditions and environments that offered protection from impacts and solar radiation. A major advance in planetary science was made when in the 1950s, sonar maps of the Atlantic seafloor showed the presence of an abyssal mid-ocean ridge (Heezen, Tharp and Ewing, 1959). Studies in magnetometry which led to the discovery of magnetic anomalies in rocks (Raff and Mason, 1961) and later, the symmetry of these anomalies on either side of the ocean-ridge systems (Vine and Matthews, 1963) contributed to advance the theory of plate tectonics (Morgan, 1968; Le Pichon, 1968). This important theory along with new advances in deep-sea submersible technology, led to the discovery of ocean-floor magmatic hydrothermal systems by oceanographer Jack Corliss and geochemist John Edmond. In 1977, during an expedition of the East Pacific Rise in the deep-sea submersible Alvin, their team came across fauna living independently of photosynthesis on the ocean floor, around the vents of hydrothermal systems. These vents were spewing out magmatically super-heated, acidic 'black' fluids up to temperatures of 400°C, black because they were rich in iron sulfides. What was particularly surprising was that life was thriving in and around such extreme conditions. This led to Corliss's suggestion that the ocean floor was a potential site for the origin of life and with the absence of any link to photosynthesis here, he suggested that this ecosystem was somehow dependent on the

sulfides and a local energy source. Though not widely accepted at the time, his hypothesis was later strengthened by the discovery of fossilised hydrothermal systems. Fossilised flora and fauna similar to those surrounding present hydrothermal systems were discovered in the Carboniferous (360 ma) seafloor deposit at Silvermines by Larter *et al.* (1981), Boyce *et al.* (1983), and also at Tynagh (Banks, 1985), both in Ireland. Fossilised tubeworms and giant clams of Silurian (430 ma) age, similar to those found around present day hydrothermal systems, were found in the Yaman Kasy volcanogenic massive sulfide (VMS) deposit in the Urals of Russia (Little, C. and Herrington, R., WWW, 1995). Add to this the evidence of a of 3.75 billion year old fossilised ocean floor spreading ridge-system discovered in Isua Greenland (Moorbath *et al.*, 1973; Appel *et al.*, 2001), and in the Barberton district (3.3 - 3.5 Ga) in South Africa (de Wit *et al.*, 1982) and the Corliss theory looked the more attractive. It is further supported by the fact that these hydrothermal systems were predominant on the young Earth. The basaltic pillow lavas found in Isua and Barberton provide indisputable evidence of an ocean floor spreading ridge system from the Archaean and the increased likelihood of early hydrothermal systems. Additionally, amongst these rocks in the Barberton district, there are what appear to be the fossilised remains of Archaean black smokers (de Wit *et al.*, 1982).

Discoveries of bacteria and photosynthetic plant material, preserved or thriving in what were previously considered to be inhospitable conditions for life, have now become commonplace. Bacteria thrive at 113°C in hot sulfur springs in Yellowstone park (Stahl *et al.*, 1985; Stetter *et al.*, 1987) and in volcanic mudpools (Daniel, 1992). At other extreme conditions, bacteria and algae survive in sub-zero temperatures in the permafrost at the polar ice caps, Alaska, and in the Siberian Tundra, or in acidic or alkaline lakes or under lethal doses of ionizing radiation (*Deinococcus radiodurans*, Battista, *et al.*, 1999). They can also survive at great depths (Stevens and McKinley, 1995) and without the presence of UV light or oxygen. It is commonly known now that some anaerobic bacteria may rely on metabolic cycles incorporating iron and sulfur as electron donors/transporters or an energy source such as hydrogen, rather than organic carbon and photolytic energy, to synthesise key metabolites (Stevens and McKinley, 1995; Adams, 1992; Stetter *et al.*, 1987). In many species, their 16s RNA assigns them to the lower branches of the 'evolutionary tree of life', (Woese *et al.*, 1990). Thus, their close relatives are considered to be archaebacteria, mainly hyperthermophilic, or at least thermophilic organisms. New discoveries such as the methanogenic archaebacteria living at submarine hydrothermal sites at 100°C discovered by Huber *et al.* (1989), or the 3.5 Ga fossilised mud pools (a nutrient-rich haven for primitive bacteria?) found in the Barberton district, serve to further substantiate the claims for a hot

origin of life. The fact that life can persevere and be preserved under such depths and extreme conditions makes it conceivable that, once life was established, many global catastrophes in the early history of the Earth might not have 'sterilised' the planet. There have been claims that bacteria and algae have been reanimated from the meltwater of deep permafrost drill core samples, thought to date back to tens of thousands if not millions of years!

After they found the submarine seeps at the Galapogos rift, Corliss and Edmond, his co-diver, calculated the fluids to have been 350°C on their trace element content. He and his co-workers published a hypothesis (Corliss *et al.*, 1979), in which they suggest just how life may have originated in such a hostile environment. They indicated possible reaction zones for synthesis of organic molecules and their subsequent concentration within the black-smoker hydrothermal systems. However, it was argued (Miller and Bada, 1988) that since temperatures of black-smoker systems often approached 400°C, these high temperatures would destroy any complex organic compounds that might form in such an environment (an argument convincingly rejected in a thermodynamic study performed by Shock, 1990). Further investigations revealed that black-smokers represented just one type of submarine hydrothermal system. Away from the spreading mid-ocean ridges there were many smaller-scale vents and seepage sites. These were emanating fluids with a myriad of chemistries, but predominantly alkaline and somewhat cooler (4-150°C) than the 400°C black-smoker fluids. Russell *et al.* (1998) suggested that these lower-temperature seepage sites, which existed under more moderate conditions, might have been more favourable for life's beginnings as a reposte to the criticisms of Miller and Bada (1988). It was the discovery by Russell and his research students of what seemed like miniature pyrite vent chimney's in Ireland (Larter *et al.*, 1981; Boyce *et al.* 1983), which led to the Russell-Hall hypothesis. Russell and Hall had made many other observations in the field, Russell as a mine geologist, and Hall, as an expert in mineralogy. They began to notice, as did many other geologists at that time, that the gap between life and its dependency on the mineralogical environment was ever decreasing. This naturally led them to believe that not only can geological studies provide insights into Earth's history, but perhaps to Life's history as well. Inspired by Corliss and his co-workers hypothesis, Russell and Hall began to evaluate possible geological mechanisms and reaction pathways for overcoming many of the hurdles that life would have had to face in establishing a foothold on Earth (Russell and Hall, 1997).

A key feature of the Russell-Hall hypothesis is the spontaneous generation of an iron-sulfide film that may have had basic membranous properties (Chapter 3). Membranes offer

protection from the environment, such as the extreme dilution of newly formed organic molecules in the ocean. Closer examination of samples of modern-day hydrothermal vents (Baross and Hoffman, 1985) and examination of iron-sulfide structures prepared in laboratory simulations (Russell and Hall, 1997) of hydrothermal fluid and seawater mixing, revealed a honeycomb of small iron-sulfide 'compartments' where fluids might be exchanged. Organic molecules trapped within these compartments could have avoided dilution by the ocean and attain concentrations for biosynthesis of an organic membrane. The redox and catalytic properties of iron and sulfur are known to play a crucial role in biological reactions, for example in ferredoxins. Ferredoxins are a group of iron-sulfur enzymes present in lower animal forms, green plants and bacteria. They are proteins containing iron and sulfur, and function as electron carriers during photosynthesis, nitrogen fixation, or other oxidation-reduction reactions in biochemical processes (Russell *et al.*, 1989). Unlike the protein (heme) units involved in the transport of oxygen for anoxic life-forms, they have ligands in which the binding sites are sulfur atoms. With iron and sulfur having such a central metabolic role between energy and life in all life-forms, Russell and Hall (1997) suggested that these iron-sulfide 'compartments' might have been analogous to the first cell membranes. They may have formed the basis for the first metabolising cell, since all other requirements for life were, theoretically speaking, available locally. Using a combination of thermodynamic calculations and laboratory experiments, Russell and Hall set out to analyse the possible distribution of minerals, species, gases, and energy that might have been available from the early Earth's hydrothermal systems which in turn would promote the formation of such iron-sulfide membranes. Russell and Hall demonstrated in laboratory experiments that a pH gradient could be maintained between a hydrothermal fluid and seawater by a semi-permeable iron-sulfide barrier, while still allowing selective exchange of ions and molecules. They suggest that essential organic ingredients could have been similarly concentrated in hydrothermal iron-sulfide bubbles on the ocean floor of the early Earth, if interactions with the hydrosphere and atmosphere provided favourable conditions for the formation of organic molecules. Many scientists have stressed the importance of a cellular membrane structure prior to the establishment of a primitive metabolic cycle.

Other materials and environments for the production of early membranes have also been proposed, for example, membranes composed of amphipathic lipids (Deamer, 1986), in which the R groups are fatty acids ($CH_3(CH_2)_nCOOH$) bonded to glycerol ($C_3H_8(OH)_3$ by ester (R-COO-R) linkages (Brock *et al.*, 1997). Presently, gene studies of early organisms have uncovered no evidence of lipid membranes in the early stages of life on Earth

(Wächtershäuser, 1998). However, the lipids in Archea consist of *isoprene* R groups ($CH_2C(CH_3)CHCH_2$) bonded to glycerol by *ether* (R-O-R) linkages, possibly for increased protection from harsh environments. Thus, the detection of isoprene in microfossils in Archean rocks may function as an important biomarker (Michaelis and Albrecht, 1979; Hahn and Haug, 1986). Further support for lipids come from work by Allamandola *et al.* (1997), who suggest an extraterrestrial source of organic molecules and membranes. They have made cellular membranes by simulating UV irradiation on interstellar ice, containing complex organic molecules typically found in space.

The iron-sulfide membrane hypothesis is an idea that suggests that life originated from a water-rock reaction, which some at first may have found difficult to accept. Since Oparin's vision in the 1930s, the interdependence between Life and Earth processes is practically undisputed, and the Russell and Hall hypothesis has its roots in these processes. Russell and Hall's encouraging results in the iron-sulfide membrane experiments and the synthesis of simple organic molecules using iron-sulfide as a catalyst by others (Heinen and Lauwers, 1996, 1997; Huber and Wächtershäuser, 1997) lends some weight to their hypothesis. Heinen and Lauwers (1997) generated hydrogen ($\geq$50 °C) and 50 nanomoles of organic sulfur compounds ($\geq$75 °C) such as thiols, of which 2.3% included dimethyldisulfide and CS_2 from CO_2 (0.26 bar), H_2S (1-10 ml) or HCl (1 ml), and in the presence of iron-sulfide (0.57 mmol) subjected to a range of temperatures under anoxic conditions and normal pressures. Huber and Wächtershäuser (1997) reported the generation of biologically important organic molecules, such as acetate ($CH3COO^-$) and thioester ($CH_3CO(SCH_3)$) at 100°C from basic raw materials (1 mmol of Ni-Fe sulfides, 1 bar of CO and 100 μmol methyl thiol (CH_3SH) at a yield of up to 40%. However, more repeatable evidence is still required. Whether the concentrations of CO used in Huber and Wächtershäuser's experiments reflected the actual concentrations found in and around submarine hydrothermal systems is an issue that is still being debated (Schoonen *et al.*, 1999; de Duve and Miller, 1991). Even if Wächtershäuser's results are applicable, the synthesis of pyruvate in significant quantities ($CH_3(CO)_2OH$) rather than activated acetic acid would have been the ultimate prize. With pyruvate, the energy requirements for initiating a primitive, autocatalytic metabolic cycle, akin to the reverse citric acid cycle, are subsequently lower. This objective was achieved recently by Cody *et al.* (2001) who reported small quantities of pyruvate as a by-product during experiments investigating the formation of decanoic acid ($CH_3(CH_2)_8COOH$). They used nonyl thiol ($CH_3(CH_2)_8SH$) and powdered iron-sulfide as a catalyst. Formic acid (HCOOH) was used as a source of CO and water for the pyruvate to

form (and is more likely to have been present in higher concentrations at hydrothermal vents than CO (Pinto, 1980)). Specifically, Cody *et al.* (2001) have shown that, when iron sulfide is subjected to high (250°C) temperatures such as those found at deep-sea hydrothermal vents, it will react with certain organic molecules to form mixed iron-sulfur-carbon (organometallic) compounds. These compounds were formed when mixtures of organic compounds and iron sulfide were subjected to temperatures of 250°C and pressures of 50, 100, and 200 MPa to simulate hydrothermal conditions. These CO-bearing phases could have led to the formation of the metabolic enzymes known to contain active iron-sulfur centres. However, these results have just recently been released (Cody *et al.*, 2001) and must be accepted with the usual caution. The formation of pyruvate could have been a by-product of the complex chemical derivitation techniques, or of contamination during the various stages involved, for example by the use of ethanol to wash the iron sulfide.

1.2 Aims and objectives

The geochemical history of the early earth has long been of great interest, but our knowledge of this previously elusive domain has been rapidly evolving with new advances in technology and discoveries in the physical and astronomical sciences, and this thesis attempts to help continue this trend. The feasibility of the hypothetical steps of early evolution (Russell and Hall, 1997) is tested using the geochemical modelling software packages Geochemist's Workbench (GWB; Bethke, 1988) and EQ3NR/EQ6 (Wolery, 1992). The software utilises the LLNL thermodynamic database (Delaney and Lundeen, 1990), *thermo.com.v8.r6.full*, maintained and made freely available by the courtesy of Jim Johnson (Johnson *et al.*, 1992, and see §1.4) at the Lawrence Livermore National Laboratory (LLNL), and the GWB database *thermo.dat* (Bethke, 1998).

Since submarine hydrothermal systems have become priority sites for investigation in future missions to other planetary bodies in the search for signs of Life (Holm, 1992), it is hoped that this work will further contribute to the understanding of the development, evolution and sustenance of the Earth's biosphere. This will provide us *a priori* with ideas of what geochemical processes may have occurred or are still occurring on other planets. In particular this research has the objectives to:

(i) refine, develop and extend existing computational techniques to demonstrate convincingly, a continuity in the chemical processes between submarine oceanic hydrothermal systems on the early Earth and the life-sustaining metabolism of the most primitive prokaryotes (such as the

hyperthermophilic methanogens, and the iron and sulfate-reducing organisms).

(ii) investigate the impact of early aqueous geochemistry on early evolution with respect to 'chemolithoautotrophic' (§2.1) metabolism. For example, by the nature and composition of the early crust, hydrothermal fluids, ocean, and atmosphere.

(iii) help understand life's processes through the generation of explanatory diagrams.

(iv) use the software packages GWB and EQ3NR/EQ6 to model, understand, explain, and demonstrate relevant geochemical processes related to energy transfer and dissipation on the early abiogenic Earth. In particular the software will be used to:

a) model possible geochemical processes

b) provide geochemical diagrams

c) compare the results from the thermodynamic databases with the calculated and experimental results obtained by other researchers.

(v) update and extend the thermodynamic databases to include other minerals, gases, and perhaps biochemical molecules in addition to simple inorganic and organic complexes.

(vi) since the basic elemental requirements for life are known to involve carbon, hydrogen, oxygen, iron, nickel, sulfur, nitrogen, and phosphorous, we use this chemical system C-H-O-Fe-Ni-S-N-P as the basis of the computational geochemistry. These elements play crucial roles in the formation of prebiotic compounds and in some biological reactions. Examples of the roles of these compounds are as follows:

hydrogen - for energy, and underpinning electrons in redox reactions
sulfur - for FeS in ferredoxins, amino acids, Co-enzyme A
iron - for FeS in ferredoxins, valence change for electron transfer, catalytic surface
carbon - CO/CO_2, and for versatile C-C bonding for organic molecules
HCN/NH_3 - for amino and nucleic acids
phosphorus - for phosphates

nickel - for catalytic properties

Phosphorus in the form of pyrophosphate, is more important in the latter stages of chemical evolution in phosphorylation, the ATP/ADP reaction, and the formation of nucleic acids. It is not included in the chemistry or calculations examined here, (though see Russell and Hall (1997) for more on the role of pyrophosphate in their hypothesis). Phosphates were probably widespread on the early earth, as indicated from their ubiquitous presence in early rocks, and are found in gases sampled from present-day volcanic regions (Yamagata *et al.*, 1991). Phosphate availability is not considered as a major problem in geochemical studies

It can be gathered from this discussion that one of the major aims of this research is to model, test, and provide theoretical evidence for the hypothesis by Russell and Hall (1997). In particular, evidence is required that after the interaction between seawater and crust, the resultant hydrothermal fluid, should approach equilibrium with its surrounding environment, be alkaline, rich in sulfur, and carry traces of organic molecules. During the course of this research, some of the questions listed below, though not tackled individually, are addressed or incorporated into the final thesis.

(i) How did the chemistry of Hadean ocean water assist the onset of life on the early Earth?

(ii) What were the range of chemistries of seafloor springs and what was their potential role in the origin of life?

(iii) What inorganic processes were adopted as biochemical processes?

(iv) How did pH and redox energy potentials in the ambient environment lead to intermediaries in energy transfer processes?

(v) Can progression from inorganic geochemistry through organic geochemistry to simple organic biochemistry be incorporated usefully into computer packages for geochemistry?

1.3 Variables and terms used in geochemical modelling

The fundamentals underlying some of the variables and terms used for measurements in this thesis are provided (Polya, D. *pers. comm.*; Moore, WWW, 2001; Wolery, 1992; Bethke, 1996).

1.3.1 Activity

The *activity* (a) represents the chemical activity of an aqueous species. Activities are often used instead of concentrations in geochemistry because standard Gibbs free energies of ions measured or extrapolated to infinite dilutions may be substantially different from Gibb's free energies for the same ions in ionic solutions due to the strong influence of electrostatic shielding. This shielding effect is important in influencing the ion's ability to dissolve or be precipitated out of water as a mineral. The symbol for activity is a, and for concentration is M (moles per litre of water) but square brackets, for example $[Fe^{2+}]$, which conventionally denote concentration, or curly brackets $\{Fe^{2+}\}$, are commonly used to represent the activity of an ion in water. In addition, *activity coefficients* (γ) are a mathematical correction that can be used to convert concentration to activity or vice versa. Values of this coefficient range from 0 to 1, and its relationship with molality (m, moles per kilogram of water) is such that as $m \rightarrow 0, \gamma \rightarrow 1$. In other words, as the concentration of an ion in solution decreases, the value of the activity coefficient tends towards one. Since the majority of the modelling in this thesis will be based on dilute solutions, molarities can be used (where 1kg of water is assumed to be equivalent to 1 L of solution) without introducing significant error. Activity is assumed to be numerically equal to fugacity except that activity is dimensionless whereas f has units of pressure, for example, bars or atmospheres (Greenwood, 1977).

1.3.2 Fugacity

Similar in purpose to activity, fugacity (f) functions as an effective substitute for pressure, to allow a real gas system to be considered by the same equations that apply to an ideal gas (Fletcher, 1993; p131). The fugacity is related to the change in chemical potential (μ) of species i from its standard state (μ^0), so that for any gas or gas mixture:

$$\mu_i - \mu_i^0 = RT \ln\left(\frac{f_i}{f_i^0}\right)$$

where R is the gas constant and T is the temperature (Greenwood, 1997).

1.3.3 pH

pH (Sörenson, 1909) is a measure of H_3O^+ activity (H_3O^+ is the hydrated proton). However, H_3O^+ is commonly written as H^+ since it is generally understood that H^+ is hydrated, just as all other dissolved ions are hydrated.

$H(H_2O)^+_n$, n is large

The pH is defined as the negative base ten logarithm of the hydrogen ion activity expressed as moles per litre.

$$pH \equiv -\log_{10}\{H^+\} \qquad (1.1)$$

The pH is especially important to the mobility of metals, and many biochemical reactions. It is not a simple solubility effect in most cases. Adsorption-desorption equilibria are also important.

1.3.4 *Eh*, E^0, p*e*, ΔG, K_{eq}, and Q

The *Eh* is a measure of the activity of electrons in redox reactions. This free energy (in kJ/mol) can be converted to an electrical potential, E^0 (V), by the equation

$$\Delta G^0 = -nFE^0 \qquad (1.2)$$

where ΔG^0 is the molar free energy of the reaction under standard temperature and pressure (STP, standard conditions imply 1 M concentrations of all reactants at one atmosphere pressure and at 25°C). E^0 is referred to as the standard electromotive force or standard potential of the reaction and is measured in volts (V). If a reaction proceeds forward spontaneously, ΔG is negative (the system gives up energy or does work), and E is positive. F is the Faraday constant, 96.42 kJ/V gram equivalent (or 96487 coulombs/equivalent), and n is the number of equivalents (mols of electrons) involved in a reaction.

$$pe \equiv -\log_{10}\{e^-\} \qquad (1.3)$$

The p*e* value is analogous to pH. The quantity $\{e^-\}$ is the electron activity. p*e* and *Eh* are easily convertible parameters that describe the redox state of a reaction. Many reaction equilibria can be described in terms of the sum of pH and pe.

ΔG is the free energy under non-standard conditions, and E (or *Eh*) the electromotive force of the reaction, and

$$\Delta G = -nFE \qquad (1.4)$$

For a chemical reaction that can be written as:

$$aA + bB \rightleftharpoons cC + dD \qquad (1.5)$$

$$K_{eq} = \frac{\{C\}^c\{D\}^d}{\{A\}^a\{B\}^b} \quad \text{or} \quad K_{eq} = \frac{[C]^c[D]^d}{[A]^a[B]^b} \tag{1.6}$$

where a, b, c, and d represent the number of moles of reactants and products, and A, B, C, and D represent the reactants and products, the equilibrium constant K_{eq} for that reaction may

$$Q = \frac{\{C\}\{D\}}{\{A\}\{B\}} \tag{1.7}$$

be derived either by the activity or concentration, as shown in Equation *1.6*: where { } is the activity or [] the concentration of a chemical species. Under non-equilibrium conditions, the equilibrium constant expression is defined as Q: The value of ΔG under non-standard conditions (different concentrations, different temperatures) can be calculated by the expression

$$\Delta G = \Delta G^0 + RT \ln Q \tag{1.8}$$

where R is the gas constant (8.3143 J Kelvin^{-1} mol^{-1}) and T is the absolute temperature (in Kelvin). At equilibrium, $\Delta G = 0$ and $Q = K$, so the expression reduces to

$$\Delta G = - RT \ln K \tag{1.9}$$

This means that the equilibrium constant can be calculated from the free energy of the reaction, or vice versa (Equation *1.10*). Since the redox potential of the reaction can be calculated from the free energy, this means that it is possible to calculate Eh if E^0 is known:

$$Eh = E^0 - \frac{RT}{nF} \ln Q \tag{1.10}$$

Many redox potentials are calculated using half reactions, for example,

$$Fe^{2+} \rightarrow Fe^{3+} + e^- \qquad E^0 = -0.771 \text{ V} \tag{1.11}$$

and,

$$2\,H_2O_{(l)} \rightarrow O_2 + 4\,H^+ + 4\,e^- \qquad E^0 = -1.229 \text{ V} \tag{1.12}$$

The rules for manipulating these equations are fairly simple: if an equation is written backwards, the sign of the potential changes. If the entire equation is multiplied by a constant (for example, if everything is doubled), the potential is unchanged. This is because the units are volts - joules per coulomb - so doubling the coulombs does not change the volts.

In other words, the voltage for a one atom reaction, or a many atom reaction, is the same. Thus the E^0 for a half-reaction is independent of concentration. The half-reactions above can be combined to get the reaction potential for the oxidation of Fe^{2+} to Fe^{3+} by oxygen in acid solution. First, the equation for the iron half-reaction is doubled:

$$2Fe^{2+} \rightarrow 2Fe^{3+} + 2e^- \qquad E^0 = -0.771\ V \qquad (1.13)$$

Then oxygen half-reaction equation is reversed and halved:

$$\tfrac{1}{2}O_2 + 2H^+ + 2e^- \rightarrow H_2O \qquad E^0 = +1.229\ V \qquad (1.14)$$

Combining the two gives,

$$2Fe^{2+} + \tfrac{1}{2}O_2 + 2H^+ \rightarrow 2Fe^{3+} + H_2O \qquad E^0 = +0.458\ V \qquad (1.15)$$

Note that this relationship is valid at 1 atmosphere oxygen pressure and at pH 0 (1 M acid). Half-reaction redox potentials are listed in tables in various chemistry handbooks. There is another application for the half-reaction. If a half-reaction is considered as a complete reaction, with the electron as a solute, it can be worked out what (fictitious) electron activity corresponds to a given *Eh*. Considering the iron half-reaction again, and writing it as an oxidation:

$$Fe^{2+} \rightarrow Fe^{3+} + e^- \qquad E^0 = -0.771\ V \qquad (1.16)$$

Assuming that Fe^{2+} and Fe^{3+} are at unit concentrations and that the electron activity is sufficient to keep the system at equilibrium (so $E^0 = 0$ when $pe = pe^0$). Then

$$Eh = 0 - \frac{RT}{nF} \ln\left[\frac{\{Fe^{3+}\}\{e^-\}}{\{Fe^{2+}\}}\right] \qquad (1.17)$$

Converting to base 10 logarithms,

$$Eh = 0 - \frac{2.303RT}{nF} \log_{10}\left[\frac{\{Fe^{3+}\}\{e^-\}}{\{Fe^{2+}\}}\right] \qquad (1.18)$$

As an example, if T = 10 °C (= 283 K) then,

$$Eh = -0.05615 \log_{10} \{e^-\} = 0.05615\ pe \qquad (1.19)$$

if Eh is expressed in volts (note that the Fe^{2+} and Fe^{3+} activities cancel out), or

$$pe = 17.81\ Eh \qquad (1.20)$$

at 10 °C. More generally,

$$pe = (5040.1/T)\ Eh \qquad (1.21)$$

Eh is customarily measured using a platinum electrode. It only measures voltages that are generated by chemical species that react readily on the platinum surface. Eh refers to a specific reaction. When referring to "system Eh" it is assumed that all potential reactions are at equilibrium. Except in a few simple systems at low pH, this is generally not true. Thus, "system Eh" is term that should be used carefully (Moore, WWW, 2001; Wolery, 1992, p26; Bethke, 1996, p100).

1.4 Introduction to geochemical modelling

Though based on a technique that has been established for nearly a century, geochemical modelling has its opponents as well as its adherents. It is understandable that some scientists working laboriously to make direct measurements of chemical and physical phenomena in their laboratories find it difficult to see their hard earned data used not merely to interpolate but also in extrapolations far from the data points. Indeed, this author would probably have had leanings towards the latter critical group had he not been intrigued by this theoretical method of research. How was it possible, given the current technology, that a computer program could be used to model chemical and physical processes as complex as those that led to life? Surely even the latest number-crunching installation by IBM at the world's largest supercomputing facility, currently at the Lawrence Livermore National Laboratory (LLNL) in the USA, could not answer such a question? Recollections of a similar scenario in Douglas Adams (1979) science fiction comedy novel 'The Hitchhikers Guide to the Galaxy' could not help but spring to mind. Here, a supercomputer posed with such a question produces a unexpected and meaningless result after several centuries of calculations, hinting that the original query was too general and perhaps should have been more specific. However in reality, the approach could be much more simple. Geochemical modelling codes utilise many standard techniques already used in chemical laboratories when experimental data is unavailable or direct measurements are impossible. In these

laboratories, techniques such as thermodynamic equilibrium calculations, extrapolation, approximation, and simplification, are used with care and serve as supplementary tools for the investigator. This is also how the codes must also be utilised, since they offer similar tools to the geochemist. The diagrams produced by such programs are useful in that they provide a quick overview of the relative stability of species, minerals or gases present in an unfamiliar system (in this case, environments on the early Earth, but equally applicable to other planets). In contrast to the comic novel mentioned above, a difficult task such as to explain the origins of Life, is broken down into many smaller problems - ones that *can* be tackled within one lifetime!

The high pressures, relatively high temperatures and slow reaction-rates of geological processes have always inhibited or limited direct observations in the field and also in simulations in laboratory experiments. For the geochemist, a method is required to simulate aqueous processes in the crust and mantle, and equilibrium thermodynamic theory is possibly the only available recourse. However, this method often involved the computation of a large number of iterations of thermodynamic chemical equations to find the equilibrium state of a geochemical system. Therefore, it was deemed impractical to apply the theory to chemical processes in complex aqueous solutions such as those found in nature. Reductions in computation time became possible thanks to advances in semiconductor technology. Since the 1960s, the efforts of several scientists (Garrels and Mackenzie, 1967; Helgeson, 1968; Helgeson *et al.*, 1969; and Wolery, 1979) have paved the way for thermodynamic equlilibrium theory to be applied to geochemical systems. Their expertise in equilibrium thermodynamics, coupled with the new digital technology, produced software that was particularly useful in allowing investigations into complex aqueous solutions. Thermodynamic calculations that were previously too large to calculate manually could now be performed on a computer in a few minutes or days rather than months and years. Today, there are several software applications for modelling reactions between minerals and molecular species in aqueous solutions. The ease with which the user can create the necessary models is also an important factor in their widespread use today in many industries and in agencies that have an interest in the environment.

In general, geochemical modelling codes are based on the laws of equilibrium and thermodynamics, so their individuality and suitability for a particular task is often dependent on the thermodynamic data, and the equations that can be used for the calculations. Some thermodynamic databases are available freely (Delaney and Lundeen, 1990). Certain databases are suitable for dilute, low-temperature aqueous geochemical modelling, while

some others are better suited for modelling concentrated brine solutions. The quality of the results obtained using a particular database are determined by the consistency of the data entered into the database, with respect to the equations used to calculate data, thermodynamic laws, units, definitions, standard states, fundamental constants and experimental measurements (Fletcher, 1993). However, the quality of the results obtained from a particular modelling package are also determined by the choice and efficiency of the mathematical methods, equations and of algorithms that are used in the program code.

The thermodynamic databases consist of values for the chemical and physical properties of minerals, elements, aqueous species, and gases, over various temperatures and pressures. Examples of the type of data and its input format in the LLNL database are presented below. Which of these chemical or physical components and their corresponding values are selected for manipulation by the program depends on the chemical system or process to be modelled and is of course determined by the user. An input file for the modelling program is created, which contains (constrains) the initial concentrations or pressures of the key phases in the system to be evaluated. The input file also specifies any reactants that are to be added or any other changes that are to be made to the original system over the course of the reaction. The file may also specify numerous other options. For example, whether the system to be modelled is an open or closed thermodynamic system, or a variable such as pH is to be held constant during the reaction

Excerpts from the LLNL database are given below, in the 'header' block (Figure 1.1), note the pressures that are used at each temperature. These values for pressure correspond to the boiling curve of water at each temperature (0.010°C to 300°C, see Figure C, Appendix 1A). However, intermediate values of temperatures, pressures, coefficients and equilibrium constants can be interpolated from the existing data by the modelling program. Next, the activity coefficients for each temperature are listed for three variations of the Debye-Hückel equation (Helgeson and Kirkham, 1974b; Wolery, 1992, p38; Bethke, 1996, p108). Note that lines marked with an asterisk in the database below signify a comment or other information for the user. This information may be a heading, comment, or a reference to the source of the data or the values of thermodynamic variables used to calculate equilibrium constants or other data. The information contained within these lines is not used nor required for the program to run.

There are currently 81 elements listed in the 'elements' block (Fig 1.2), and it is possible to add more using the format below. The modelling program will use these values for mass balance calculations for the geochemical system under investigation.

The next block of data is the set of species called the basis species, that is, the minimum set of species required to build the progressively more complex chemical molecules. This block (Figure 1.3), must contain the minimal data required for each species. Note the reference sources of the data (e.g. `92joh/oel`) and the values for key thermodynamic variables such as the standard free energy of formation, ΔG^o_f (`delG0f`). For an explanation of the fundamental variables mentioned below, such as *Eh*, pe, and pH, see §1.3.

Next, in the 'redox couples' block (Figure 1.4), species are included that may have a redox relation with a basis species. In the example below HS^- would normally be coupled with $SO4^{2-}$ from the 'basis species' block. Similarly, acetic acid is coupled with $HCO3^-$. Sometimes it is necessary to model environments where there is no redox interaction between common redox couples, and both the GWB and EQ3NR/EQ6 programs can simulate this by allowing the coupling to be disabled.

Header

```
dataset of thermodynamic data for gwb programs
dataset format: oct94
activity model: debye-huckel
*  THERMODYNAMIC DATABASE: thermo.com.V8.R6.full
*  generated by GEMBOCHS.V2-Jewel.src.R6 03-dec-1996 16:55:04
*  Output package:  gwb
*  Data set:        com


* temperatures
0.0100   25.0000   60.0000  100.0000
150.0000  200.0000  250.0000  300.0000
* pressures
1.0132    1.0132    1.0132    1.0132
4.7572   15.5365   39.7365   85.8378
* debye huckel a (adh)
0.4939    0.5114    0.5465    0.5995
0.6855    0.7994    0.9593    1.2180
* debye huckel b (bdh)
0.3253    0.3288    0.3346    0.3421
0.3525    0.3639    0.3766    0.3925
* bdot
0.0374    0.0410    0.0440    0.0460
0.0470    0.0470    0.0340    0.0000
```

Figure 1.1. Excerpt from the *'thermo.com.V8.R6.full'* thermodynamic database maintained by the Lawrence Livermore National Laboratory (LLNL) showing the 'Header' block.

```
                              Elements
Oxygen              (O )          mole wt.=   15.9994
Silver              (Ag)          mole wt.=  107.8682
Aluminum            (Al)          mole wt.=   26.9815
```

Figure 1.2. Excerpt from the *'thermo.com.V8.R6.full'* thermodynamic database maintained by the Lawrence Livermore National Laboratory (LLNL) showing the 'Elements' block.

The 'aqueous species' block (Figure 1.5), contains thermodynamic data for organic and inorganic aqueous species and also for potentially useful prebiotic reactants such as amino acids such as glycine or isoleucine (Figure 1.5). The next two blocks of data, 'minerals' (Figure 1.6) and 'gases' (Figure 1.7), similarly contain the appropriate data. The last block (Figure 1.8.), lists the references for various sources of the thermodynamic data. At the top of each reference is the corresponding code that is referenced throughout the database.

```
                              Basis species
Fe++
     1.0000 Fe charge=  2.0      ion size=  6.0 A      mole wt.=
55.8470 g
     1 elements in species
*    gflag = 1 [reported delG0f used]
*    extrapolation algorithm: supcrt92 [92joh/oel]
*    reference-state data source = 88sho/hel
*         delG0f =    -21.870 kcal/mol
*         delH0f =    -22.050 kcal/mol
*         S0PrTr =    -25.300 cal/(mol*K)

MoO4--
     charge= -2.0      ion size=  4.5 A      mole wt.=  159.9376 g
     2 elements in species
      1.0000 Mo             4.0000 O
*    gflag = 1 [reported delG0f used]
*    extrapolation algorithm: supcrt92 [92joh/oel]
*    reference-state data source = 88sho/hel
*         delG0f =   -199.900 kcal/mol
*         delH0f =   -238.500 kcal/mol
*         S0PrTr =      6.500 cal/(mol*K)
```

Figure 1.3. Excerpt from the *'thermo.com.V8.R6.full'* thermodynamic database maintained by the Lawrence Livermore National Laboratory (LLNL) showing the 'Basis Species' block.

Redox couples

```
HS-
     charge= -1.0       ion size=  3.5 A       mole wt.=    33.0739 g
     3 species in reaction
 -2.0000 O2(aq)        1.0000 H+          1.0000 SO4--
       152.0993   138.3169   122.1371   107.0295
        91.7855    79.4025    69.0257    60.0062
*    gflag = 1 [reported delG0f used]
*    extrapolation algorithm: supcrt92 [92joh/oel]
*    reference-state data source = 88sho/hel
*         delG0f =       2.860 kcal/mol
*         delH0f =      -3.850 kcal/mol
*         S0PrTr =      16.300 cal/(mol*K)
```

Figure 1.4. Excerpt from the *'thermo.com.V8.R6.full'* thermodynamic database maintained by the Lawrence Livermore National Laboratory (LLNL) showing the 'Redox Couples' block.

Aqueous Species

```
Glycine(aq)
         4.1510     3.7266     2.9573     2.0325
         0.9029    -0.1736    -1.1974    -2.1632
*    gflag = 1 [reported delG0f used]
*    extrapolation algorithm: supcrt92 [92joh/oel]
*    reference-state data source = 95sho/kor
*         delG0f =    -156.477 kcal/mol
*         delH0f =    -221.770 kcal/mol
*         S0PrTr =      63.000 cal/(mol*K)

Isoleucine(aq)
*    formula= C6H13NO2
     charge=  0.0       ion size=  3.0 A       mole wt.=  131.1748 g
     4 species in reaction
 -3.0000 O2(aq)              -2.0000 NH3(aq)              2.0000 H2O
  3.0000 Glycine(aq)
       237.4093   217.0619   193.1630   170.8251
       148.2796   130.0056   114.8020   101.8250
*    gflag = 1 [reported delG0f used]
*    extrapolation algorithm: supcrt92 [92joh/oel]
*    reference-state data source = 90sho/hel
*         delG0f =     -82.200 kcal/mol
```

Figure 1.5. Excerpt from the *'thermo.com.V8.R6.full'* thermodynamic database maintained by the Lawrence Livermore National Laboratory (LLNL) showing the 'Aqueous Species' block.

Minerals

```
Magnetite                              type=oxide
     formula= Fe3O4
     mole vol.=   44.524 cc       mole wt.=  231.5386 g
     4 species in reaction
 -8.0000 H+                  1.0000 Fe++                  2.0000 Fe+++
  4.0000 H2O
        13.8989   10.4724    6.4420    2.6912
        -1.1245   -4.3319   -7.2074   -9.9523
*    gflag = 1 [reported delG0f used]
*    extrapolation algorithm: supcrt92 [92joh/oel]
*    reference-state data source = 78hel/del
*         delG0f =   -242.574 kcal/mol
*         delH0f =   -267.250 kcal/mol
*         S0PrTr =     34.830 cal/(mol*K)
```

Figure 1.6. Excerpt from the *'thermo.com.V8.R6.full'* thermodynamic database maintained by the Lawrence Livermore National Laboratory (LLNL) showing the 'Minerals' block.

Gases

```
H2(g)
     mole wt.=    2.0159 g
     2 species in reaction
 -0.5000 O2(aq)              1.0000 H2O
        47.4693   43.0016   37.8323   33.0786
        28.3653   24.6162   21.5521   18.9808
*    gflag = 1 [reported delG0f used]
*    extrapolation algorithm: supcrt92 [92joh/oel]
*    reference-state data source = 82wag/eva
*         delG0f =      0.000 kcal/mol
*         delH0f =      0.000 kcal/mol
*         S0PrTr =     31.234 cal/(mol*K)
```

Figure 1.7. Excerpt from the *'thermo.com.V8.R6.full'* thermodynamic database maintained by the Lawrence Livermore National Laboratory (LLNL) showing the 'Gases' block.

References

```
92joh/oel
Johnson, J.W., Oelkers, E.H., and Helgeson, H.C., 1992, SUPCRT92: A
software package for calculating the standard molal thermodynamic
properties of minerals, gases, aqueous species, and reactions from 1
to 5000 bar and 0 to 1000degC:  Computers Geosci., 18, 899-947.
```

Figure 1.8. Excerpt from the *'thermo.com.V8.R6.full'* thermodynamic database maintained by the Lawrence Livermore National Laboratory (LLNL) showing the 'References' block.

However, the GWB program has the advantage in that it is significantly easier to use and produces graphical output in the form of plots and, if required, textual output in the form of tables. The EQ3NR/EQ6 program requires more skill and patience, and displays the

results as text only. Both of these modelling programs are largely based on original work of Helgeson (mentioned above) and use many of the same thermodynamic calculations. The following description is a very simplistic and general explanation of the key steps and the chemical and mathematical equations used by the programs in determining the equilibrium state of a geochemical system. For a comprehensive analysis of the theoretical concepts behind the programs, refer to Wolery (1992), Wolery and Daveler, (1992) and Bethke (1996). It should be noted here that the user should understand the theoretical concepts involved in the running of the program but need only provide sensible input constraints for the calculations to proceed to completion. After reading the input file, the program identifies balanced chemical equations for each independent reaction that takes place in the system being modelled. Accordingly, the program ensures that the law of the conservation of matter is adhered to, by incorporating a facility for mass balance calculations in the code. The law of neutrality of electrolytic solutions is also maintained, by balancing the charges of all the aqueous species involved in the model. Adjusted concentrations, activity coefficients and associated equilibrium constants of all species and reactions present in the geochemical system are also determined. Depending on the nature of the solution to be modelled, the computed activity coefficients are incorporated into various forms of the Debye-Hückel equation (Helgeson and Kirkham, 1974a, 1974b) for dilute aqueous solutions or the Pitzer equation for highly concentrated brine solutions. The thermodynamic data can then be used to evaluate the saturation indices (*SI*) of various minerals to predict precipitation of the minerals out of aqueous solutions (Wolery, 1992; Bethke, 1996).

$$SI = \log Q/K \qquad (1.22)$$

Here, Q is the activity product of the aqueous species in the reaction and K the equilibrium constant the reaction at a certain temperature. Thermodynamic affinities (A), the measure of the driving force of each reaction (A), are also evaluated , where R is the gas constant and T the absolute temperature.

$$A = -2.303\, RT \log Q/K \qquad (1.23)$$

In reactions that involve a redox aspect, *Eh*, *pe*, oxygen activity, and redox affinity (*Ah*) are also computed (Wolery, 1992, p31). The fugacities of any gaseous phases with respect to the initial equilibrium state of the fluid are also calculated.

So far, the preceding steps serve only to determine the primary equations (or more commonly known as the governing equations) required to solve the initial equilibrium state

of an aqueous solution. Some of the unknowns in the governing equations however exhibit exponential properties and therefore simple linear algebra will not suffice to provide a solution. An appropriate method is required to solve them, and by far the best way to approach a solution is to use a well-known iterative numerical method known as the Newton-Raphson approximation equation (Wolery, 1992, p171; Bethke, 1996, p61). However, this technique requires that the unknowns be initially calculated to within an order of magnitude to the mathematical solution. Therefore, prior to running the main calculation a method known as Newton's method (or pre-Newton-Raphson optimisation) is employed to satisfy this requirement. Any discrepancies that arise as a result of the calculations are corrected at the end of each iteration of the optimisation procedure. Such discrepancies may be in the value of the activity coefficients of aqueous species or of the charge balance of the aqueous solution or in the mass of minerals. Once the Newton-Raphson calculation converges to a solution, the bulk composition of the system can be calculated according to the mass balance equations for the reactions involved in the model. Finally, any minerals that become undersaturated during the iterative process can be identified by a negative *SI* in the program output A negative value for the *SI* indicates that the mineral was consumed during the reaction. Undersatured minerals are removed from the system one at a time. On each removal, the iterative process is restarted with the next most appropriate aqueous species, this secondary species (which must be present in a sufficient concentration to allow the iteration process to continue) is swapped into the calculation. When there are no undersaturated minerals left, the most supersaturated minerals are added back into the calculation and the iteration is restarted. When there is no undersaturated or supersaturated mineral remaining, the final equilibrium state in terms of the minerals, aqueous species and gases remaining in the system is solved.

1.5 The Geochemist's Workbench and the EQ3NR/EQ6 modelling software

In this study, it is predominantly the Geochemist's workbench (GWB) program that is used to create environmental models. In Chapter 4 however, the EQ3NR/EQ6 code is used for comparison of results with GWB. Results are regularly compared to those obtained by others using the SUPCRT92 code (Johnson *et al.*, 1992).

Within the GWB package there are several subprograms (ACT2, REACT, TACT, RXN, GTPLOT). The ACT2 subprogram is used to generate activity-activity (Figure 1.11) or activity-fugacity diagrams, which show the distribution of components in a simulated environmental system with respect to their activities or fugacities. In the default settings of

the GWB programs, the oxidation state is calculated by the amount of dissolved oxygen $O_{2(aq)}$ in the fluid. Likewise, the pH is a variable dependent on the amount of H^+ ions present in the fluid, and to satisfy the law of charge balance in electrolytic solutions, the program corrects any imbalance with Cl^- ions.

These variables are set by default but the user can alter these settings. For example, to display the various oxidation states of iron in terms of the redox potential (*Eh*), the user can add a trace of iron to water and then substitute the activity of dissolved oxygen, $O_{2(aq)}$, with the activity of electrons e^- (Figure 1.9, line 2). In nature, and accordingly in the ACT2 program, there are other ways that the overall oxidation state of a geochemical system can be influenced. For example, we could use the activity of a redox pair such as HS^- and SO_4^{2-}. However, in an anoxic environmental model it is more appropriate to use H_2 fugacity as a redox variable to measure relative oxidation state than it is to use *Eh* or $O_{2(aq)}$,. Examples and the logic of using this approach can be found in Eckstrand (1975), Shock (1992a), and Schoonen *et al.* (1999).

Another subprogram within GWB, REACT, is used for reaction modelling. REACT calculates the initial and final equilibrium states of a geochemical system and helps to determine the route taken (reaction path) between the two (Figure 1.12). Reaction paths can reflect various changes to the system; the addition or the removal of components, temperature gradients, or fugacity gradients. The program's facility to combine reaction path diagrams with activity-activity or activity-fugacity diagrams allows the user to evaluate the distribution of components within a geochemical system that results from each change to the system. This composite diagram (Figure 1.18) also gives a view of the system from which we can follow the change to the redox properties of the simulated environment. The results are determined by the nature and value of the environmental constraints set by the user for a proposed model (Figure 1.9), and by the laws of equilibrium thermodynamics.

For the majority of the research, the LLNL database *thermo.com.V8.R6.full* is used, and occasionally for convenience, a smaller version *thermo.dat.* As stated above, the GWB subprograms use the databases to populate and maintain a set of aqueous chemical species. These are listed at the beginning of the database file and GWB uses these 'basis' species to write chemical reactions when modelling a geochemical system. This set of species can be altered by the user to reflect the chemical environment to be simulated in a model by substituting other aqueous species, minerals, or gases for entries in the original set (Figure 1.9, line 2). Note that in all the GWB programs, unless otherwise specified by the user, the

temperature by default is 25 °C and the mass of water is 1kg. The program script below (Fig 1.9) demonstrates an example of an input file for the GWB ACT2 program.

ACT2 input script for Figure 1.11

```
1. data = thermo.dat
2. swap e- for O2(aq)
3. diagram Fe++ on Eh vs pH
4. log activity main = -6
5. log activity SiO2(aq) = -6
6. x-axis from 0 to 14 increment 1
7. y-axis from -1 to 1.5 increment .25
8. suppress  FeO(c)
```

Figure 1.9. Example GWB input file for the program ACT2 (Bethke, 1998) which generates activity-activity diagrams (see Figure 1.11).

Line 1 determines the thermodynamic database to be used.

Line 2 specifies that oxidation state is to be represented by the concentration of electrons in the system in volts, better known as the *Eh*.

Line 3 instructs the program to plot the distribution of Fe^{2+} species on an *Eh*-pH (Pourbaix, 1949) diagram (Krauskopf, 1967).

Line 4 sets the total activity of Fe^{2+} at 10^{-6}. This low value is used because the thermodynamic dataset (thermo.com.v8.r6.full) is valid for dilute aqueous solutions only.

Line 5 sets the total activity of $SiO_{2(aq)}$ at 10^{-6}. This value also complies with the requirement for low concentrations.

Lines 6 and 7 constrain the ranges of pH and *Eh* respectively to be shown on the plot. Note that the ACT2 diagram produced from this code will incorporate a wide range of pH (0-14) and oxidation states (-1 to 1.5 volts) for theoretical waters (environments).

Line 8 shows how it is possible to easily suppress species that are known not to form under certain conditions, in this case $FeO_{(c)}$.

Although similar to the ACT2 script, the REACT script (Figure 1.10) demonstrates how it is possible to easily constrain the oxygen availability to resemble an anoxic environment (line 3). Charge balancing the aqueous solution with H^+ (line 6) will help to demonstrate the sensitivity of the system to pH. Finally, line 7 specifies the type of change that is to be imposed on the geochemical system, in this case the addition of 1 millimole of fayalite.

REACT input script for Figures 1.12 to1.17

```
1. data = thermo.com.v8.r6.full
2. swap O2(g) for O2(aq)
3. fugacity O2(g) = 1e-40
4. total mmol Fe++ = 1e-6
5. total mmol SiO2(aq) = 1e-6
6. balance on H+
7. react 1 mmol of Fayalite
8. suppress  FeO(c)
```

Figure 1.10. Example GWB input file for the program REACT (Bethke, 1998).

REACT (Bethke, 1998), allows modelling of the path taken by a reaction (reaction-path, see Figure 1.12). Reaction-paths reflect various changes to the system; the addition or the removal of components, temperature gradients, or fugacity gradients.

1.6 Interpretation of modelling results

Environmental systems are governed by many redox reactions that are rarely at equilibrium, but the results presented from Pourbaix (1949) diagrams (*Eh*-pH) are equilibrated values. This means that important components that exist in an intermediate state (*out-of-equilibrium* or *metastable*) in an environmental system may not be represented in the results and may be missed altogether. A good example is nitrogen, which can exist in various thermodynamically stable forms such as nitrogen N_2, ammonia NH_3, ammonium NH_4^+, and nitrate NO_3^-. It is well known that natural waters and soils contain organisms that produce the metastable species nitrite, NO_2^-. However, in a Pourbaix diagram representing the stable phases of nitrogen, nitrite would not have a stability field.

In contemplating whether the resulting plot can represent natural processes, it is realised that any environmental factors not considered will influence the validity of the diagram to a greater or lesser extent. With the major components and environmental factors identified and included in the script, the plot should suggest the forms of iron that might be found in different redox environments in nature. However, from field experience and with background knowledge and reasoning, we can also argue that certain products would not be formed as predicted by the results (such as $FeO_{(c)}$ above), especially in cases where the model is oversimplified for the purposes of clarity and discussion.

Additionally we know the lower and upper limits of pH commonly found in nature are around 3 and 10 respectively and the lower and upper limits of redox potentials in natural environments are around 0 volts and 1.2 volts respectively. It is worthwhile to note at this point that this range in redox potential is closely related to the lower and upper limits of the

dissociation of water. Therefore, we have to be sceptical about whether complexes that plot outside these natural boundaries would be found in nature. It is recommended that the reader be familiar with the use of *Eh*-pH (Pourbaix) diagrams by referring to an appropriate text such as Krauskopf (1967).

Some electron transfer reactions can be very slow and reaction kinetics (reaction rates) must be considered before arriving at any conclusions. Questions arise when geochemical modelling is used to make quantitative statements, since these kinetic barriers must first be overcome. For example in Chapter 2, where the amount of hydrogen released from the reaction between olivine and water is examined, the quantitative statements obtained from the environmental model are not based on theoretical equilibrium values alone. The results are corroborated with the relevant literature (Berndt *et al.*, 1996; Neal and Stanger, 1983; Coveney *et al.*, 1987; Stevens and McKinley, 1995) and serve to establish that a model substantiates field evidence or laboratory results. This allows the model to be used for further development with a certain degree of confidence. The difficulty (and occasionally the danger) of simulating environmental processes and measuring the products in the laboratory is also a valid reason for the theoretical approach. It *is* possible to incorporate kinetic constraints into a geochemical model, but suitable reaction rate data required for this purpose are not readily available. This is not as much of a limitation as it may initially seem. It is often the mechanism or direction of reactions, the relative stability of components, or the distribution of components in a system and not solely the rate at which a reaction proceeds that can be of interest. For example, in Chapter 2 where the influence of pH on the olivine-water reaction and the potential production of hydrogen were assessed, it is revealed from the environmental model that the interaction between forsterite and water does not involve a redox aspect whereas the reaction between fayalite and water does. Such information regarding the sensitivity or behaviour of a geochemical system to a particular change can be of immense value to environmental studies. The advantages of Pourbaix diagrams are that they offer a quick overview of an unfamiliar system and possible stable phases can be identified at a glance, the influence of pH on redox reactions can be viewed in complicated systems. The disadvantages of such diagrams are that they display only equilibrated systems, whereas natural systems may play host to many redox processes that never reach equilibrium and remain in a metastable state. In addition, intermediate (metastable) phases may be missed and more detailed calculations are often needed to confirm critical aspects.

1.7 Initial computations

The initial computations involved simulating and testing the water-rock reactions proposed in the hydrothermal origin of life hypothesis (Russell and Hall, 1997). The approach was to create and test a simple system and, if successful, to increase the complexity in stages, in order to build a relatively more complex model.

The simulations were performed using GWB and carried out in a controlled manner analogous to a controlled laboratory experiment (by testing reactions over a range of environmental conditions). Examples of the GWB plots are presented below. All plots describe the system at STP (25°C/1 atmosphere).

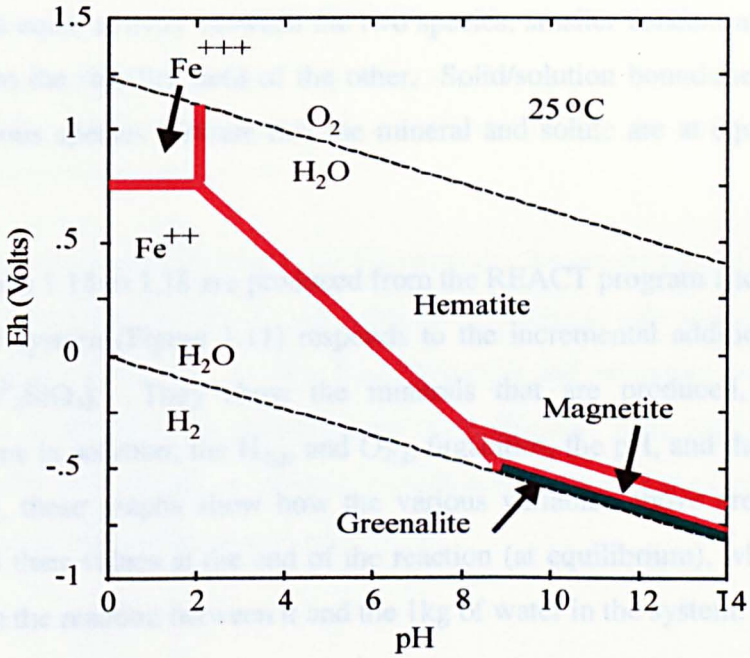

Figure 1.11. Stable minerals and aqueous species in the Fe-SiO_2-H_2O system at STP. Activity Fe^{++} = 10^{-6}, activity $SiO_{2(aq)}$ =10^{-6}. $FeO_{(c)}$ precipitation suppressed.

Figure 1.11, produced from ACT2 represents the stability of iron species and minerals in terms of the activity of electrons (*Eh*) and the activity of H^+ (pH) in a geochemical system containing trace amounts of Fe^{2+} and $SiO_{2(aq)}$. Note that the horizontal line between Fe^{2+} and Fe^{3+} indicates that the transition from Fe^{2+} to Fe^{3+} is strictly *Eh* controlled at low pH. Yet with increasing pH, the line between Fe^{2+} and hematite ($Fe^{3+}{}_2O_3$) is sloping because Fe^{3+} becomes increasingly insoluble relative to Fe^{2+} in alkaline conditions. Conversely, a vertical line between two species or minerals would indicate that a transition was strictly pH-controlled. The plot also indicates that at this temperature and pressure, magnetite and greenalite are stable in extremely reducing conditions in neutral to alkaline conditions. The dashed lines designate the water stability limits. Outside these boundaries,

hydrogen and oxygen exist as gases. In natural environments, water cannot exist outside these *Eh*-pH conditions. In natural environments, there are usually no oxidants or reductants that are strong enough to drive the reactions below (Equations *1.24* and *1.25*) to the right otherwise H_2 and O_2 gas would be produced from water.

$$H_2O \rightleftharpoons 2e^- + 2H^+ + \tfrac{1}{2}O_{2(g)} \qquad (1.24)$$

$$H^+ + e^- \rightleftharpoons \tfrac{1}{2}H_2 \qquad (1.25)$$

The boundaries between two dissolved species (solute/solute) in the diagrams represent the activity ratio between those species in a given solution. Although the boundary represents an equal activity between the two species, smaller concentrations of each species are present in the stability field of the other. Solid/solution boundaries between a mineral and an aqueous species indicate that the mineral and solute are at equilibrium for a given activity.

Figures 1.12 to 1.18 are produced from the REACT program and show how the same geochemical system (Figure 1.11) responds to the incremental addition of 1 millimole of fayalite ($Fe^{II}_2SiO_4$). They show the minerals that are produced, the Fe^{2+} and Fe^{3+} concentrations in solution, the $H_{2(g)}$ and $O_{2(g)}$ fugacities, the pH, and the redox potential. In other words, these graphs show how the various variables above are affected during the reaction and their values at the end of the reaction (at equilibrium), when all the fayalite is consumed in the reaction between it and the 1kg of water in the system.

$$6\,Fe_2SiO_4\,(\text{fayalite}) + 7\,H_2O \rightarrow Fe_3O_4\,(\text{magnetite}) + 3\,[Fe_3Si_2O_5(OH)_4]\,(\text{greenalite}) + H_{2(g)} \qquad (1.26)$$

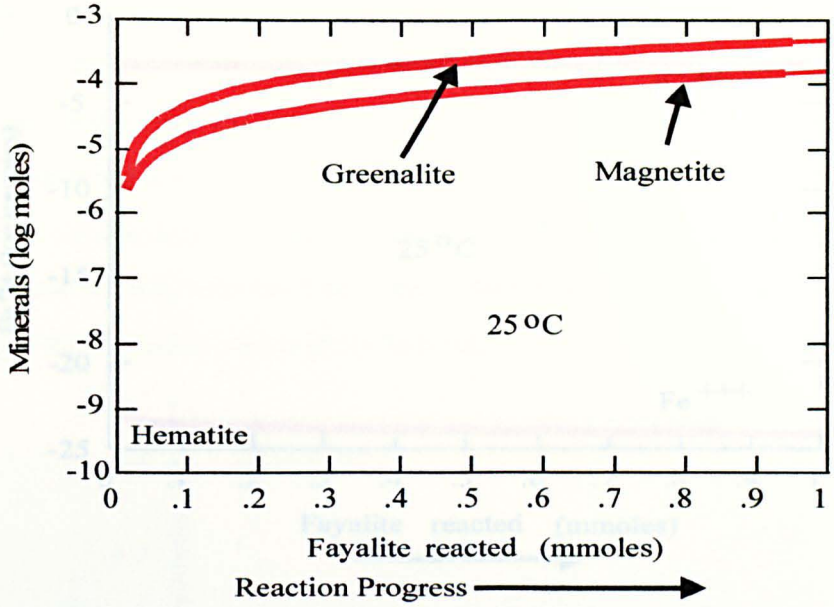

Figure 1.12. Mineral stabilities of the Fe-SiO_2-H_2O system at STP, as a function of the amount of fayalite (Fe_2SiO_4) reacted. Fugacity $O_{2(g)} = 1e^{-40}$, total $[Fe^{++}] = 10^{-6}$ mmol, total $[SiO_2]_{(aq)} = 10^{-6}$ mmol $FeO_{(c)}$ precipitation suppressed.

The reaction path (Figure 1.12) demonstrates the production of greenalite ($Fe^{II}{}_3Si_2O_5$) and magnetite ($Fe_2{}^{III}Fe^{II}O_4$) as water reacts progressively with fayalite in the absence of oxygen ($\log f\ O_{2(g)} = -40$). Both greenalite and magnetite are stable at the end of the reaction when the system comes to equilibrium. Note that hematite ($Fe^{III}{}_2O_3$) is initially precipitated, but then is immediately consumed back into the reaction. $FeO_{(c)}$ precipitation suppressed.

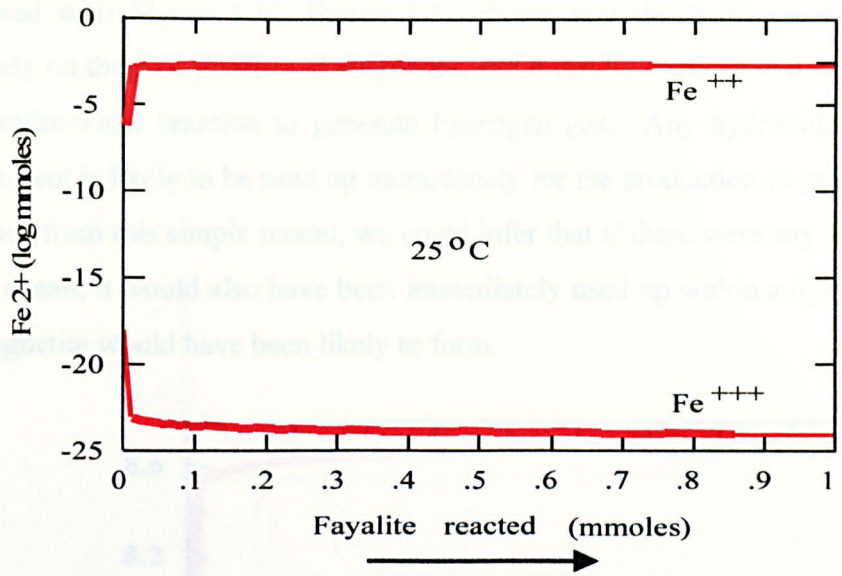

Figure 1.13. Fe^{++} activity in the Fe-SiO_2-H_2O system at STP, as a function of the amount of fayalite (Fe_2SiO_4) reacted. Fugacity $O_{2(g)} = 1e^{-40}$, total $[Fe^{++}] = 10^{-6}$, total $[SiO_2]_{(aq)} = 10^{-6}$. $FeO_{(c)}$ precipitation suppressed.

If compared alongside Figure 1.12, it can be deduced (Figure 1.13) that on precipitation of magnetite, a conjugated Fe^{2+}/Fe^{3+} mineral, there is a corresponding decrease in Fe^{3+} in the aqueous solution. However, the production of greenalite (a Fe^{2+} mineral) does not show a corresponding decrease in Fe^{2+}, but an increase in Fe^{2+}. This is due to the addition of fayalite itself (also a Fe^{2+} mineral).

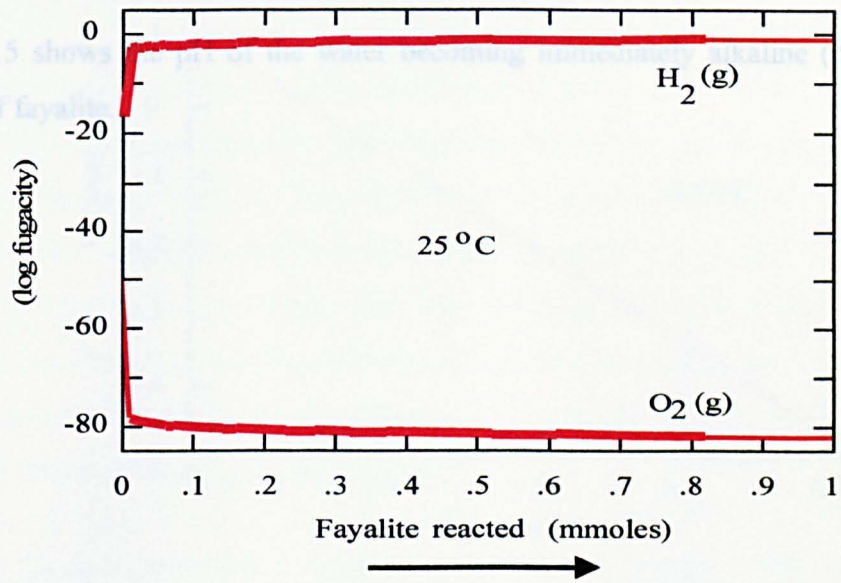

Figure 1.14. Fugacity of O_2 and H_2 in the Fe-SiO_2-H_2O system at STP, as a function of the amount of fayalite (Fe_2SiO_4) reacted. Fugacity $O_{2(g)} = 1e^{-40}$, $[Fe^{++}] = 10^{-6}$, $[SiO_2]_{(aq)} = 10^{-6}$. $FeO_{(c)}$ precipitation suppressed.

If compared with Figure 1.12, Figure 1.13 shows that the hydrogen fugacity increases immediately on the precipitation of magnetite, and it can be deduced that water is dissociated in the fayalite-water reaction to generate hydrogen gas. Any hydroxide released or free oxygen present is likely to be used up immediately for the production of greenalite (Equation 1.26). Thus from this simple model, we could infer that if there were any free oxygen in the primitive ocean, it would also have been immediately used up within a hydrothermal system where magnetite would have been likely to form.

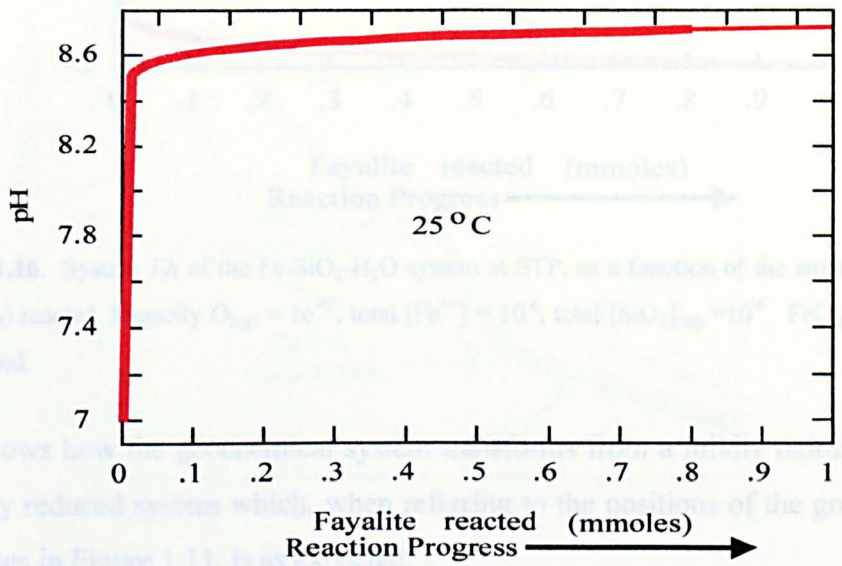

Figure 1.15. System pH of the Fe-SiO_2-H_2O system at STP, as a function of the amount of fayalite (Fe_2SiO_4) reacted. Fugacity $O_{2(g)} = 1e^{-40}$, $[Fe^{++}] = 10^{-6}$, $[SiO_2]_{(aq)} = 10^{-6}$. $FeO_{(c)}$ precipitation suppressed.

Figure 1.15 shows the pH of the water becoming immediately alkaline (pH ~8.6) on the addition of fayalite.

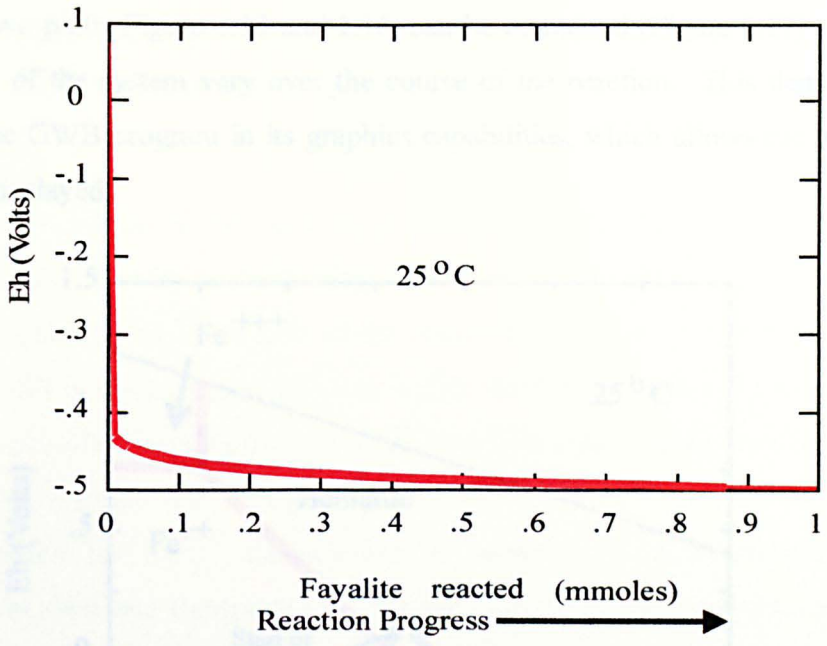

Figure 1.16. System *Eh* of the Fe-SiO_2-H_2O system at STP, as a function of the amount of fayalite (Fe_2SiO_4) reacted. Fugacity $O_{2(g)} = 1e^{-40}$, total $[Fe^{++}] = 10^{-6}$, total $[SiO_2]_{(aq)} = 10^{-6}$. $FeO_{(c)}$ precipitation suppressed.

Figure 1.16 shows how the geochemical system transforms from a mildly oxidising system to an extremely reduced system which, when referring to the positions of the greenalite and magnetite phases in Figure 1.11, is as expected.

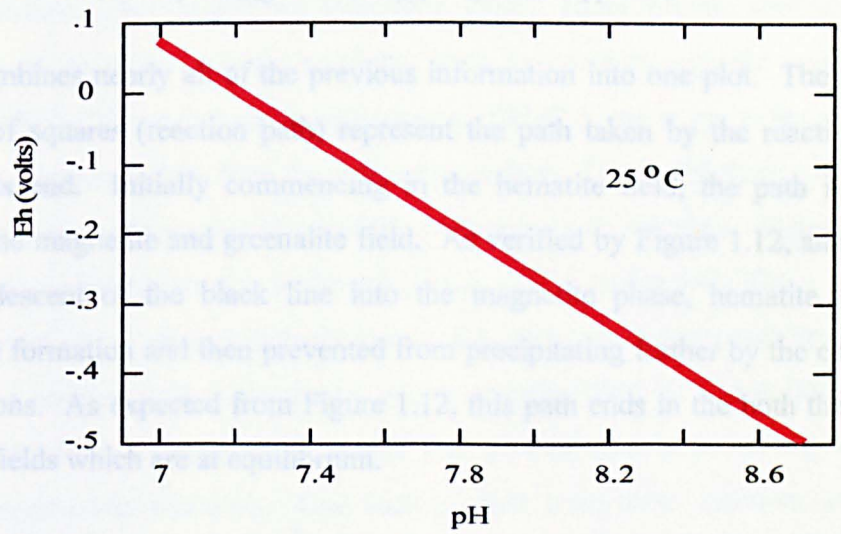

Figure 1.17. Redox state of the Fe-SiO_2-H_2O system at STP, as a function of pH as 1 mmole of fayalite (Fe_2SiO_4) is reacted. Fugacity $O_{2(g)} = 1e^{-40}$, total $[Fe^{++}] = 10^{-6}$, total $[SiO_2]_{(aq)} = 10^{-6}$. $FeO_{(c)}$ precipitation suppressed.

The previous two plots, Figure 1.15 and 1.16, can be combined (Figure 1.17) to show how the *Eh* and pH of the system vary over the course of the reaction. This demonstrates the flexibility of the GWB program in its graphics capabilities, which allows the user to select the data to be displayed.

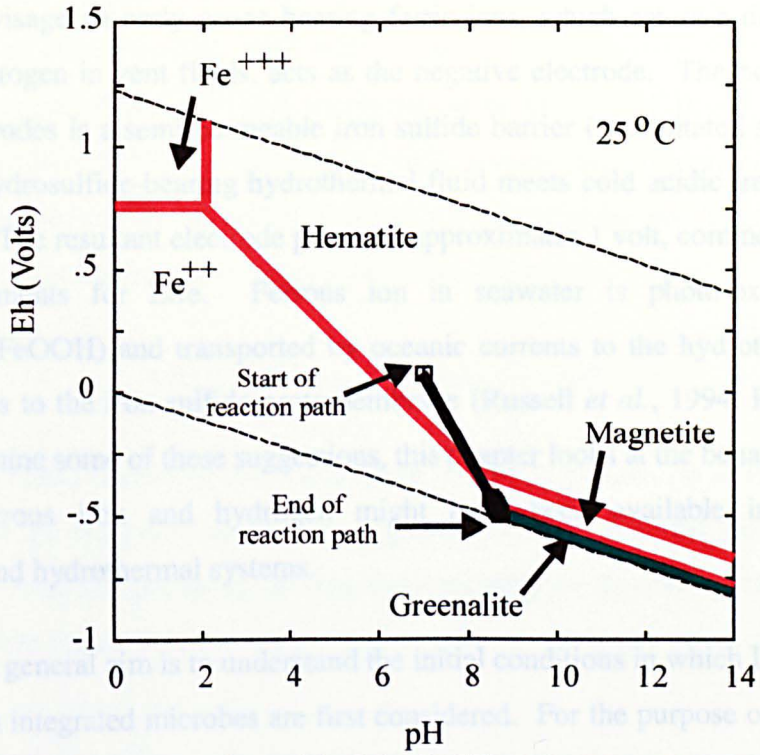

Figure 1.18. Thermodynamic model of the Fe-SiO_2-H_2O system at STP. The thick black line represents *Eh* and pH as a function of fayalite (Fe_2SiO_4) added to the system. Fugacity $O_{2(g)} = 1e^{-40}$, activity $Fe^{++} = 10^{-6}$, activity $SiO_{2(aq)} = 10^{-6}$. $FeO_{(c)}$ precipitation suppressed.

Figure 1.18 combines nearly all of the previous information into one plot. The thick black line made up of squares (reaction path) represent the path taken by the reaction from its beginning to its end. Initially commencing in the hematite field, the path immediately descends into the magnetite and greenalite field. As verified by Figure 1.12, and suggested by the steep descent of the black line into the magnetite phase, hematite is used up immediately on formation and then prevented from precipitating further by the changing pH and *Eh* conditions. As expected from Figure 1.12, this path ends in the both the magnetite and greenalite fields which are at equilibrium.

This is but the first impression to be perceived from the output, a simple evaluation at this stage. To be sure of its success as a realistic or appropriate model and use it for further work, it is necessary to refer to field evidence and to the available literature to assess its suitability for the purpose which it is intended.

Chapter 2. Iron and olivine: The water-rock reaction and the generation of H_2 and control of pH

2.1 Introduction

In their description of the Earth as a giant photoelectrochemical cell, Russell and Hall (1997) envisage an early ocean bearing ferric ions, which act as a dispersed positive electrode. Hydrogen in vent fluids, acts as the negative electrode. The boundary between these two electrodes is a semi-permeable iron sulfide barrier (precipitated spontaneously as hot, alkaline, hydrosulfide-bearing hydrothermal fluid meets cold acidic iron-bearing ocean water, §3.1.1). The resultant electrode potential approximates 1 volt, commensurate with the energy requirements for Life. Ferrous ion in seawater is photo-oxidised to ferric oxyhydroxide (FeOOH) and transported by oceanic currents to the hydrothermal seepages where it adheres to the iron-sulfide protomembrane (Russell *et al.*, 1994; Russell and Hall, 1997). To examine some of these suggestions, this chapter looks at the behaviour of iron and how much ferrous iron and hydrogen might have been available in early oceanic environments and hydrothermal systems.

As the general aim is to understand the initial conditions in which Life emerged, the simplest known integrated microbes are first considered. For the purpose of this discussion, bacteria can be classed into one of two broad categories, heterotrophic or autotrophic. Heterotrophic organisms are thought to predominate over the autotrophic in subsurface sediments and surface soils (Stevens and McKinley, 1988). Heterotrophic organisms require chemical energy from biotic organic nutrients, such as complex organic compounds of nitrogen (urea $(NH_2)_2CO$) or carbon (carbohydrates, $(CH_20)_n$), made by bacteria and plants fixing inorganic nitrogen or CO_2 from the soil or atmosphere. The metabolism of autotrophic organisms is however, independent of other life with respect to nutrition. Instead, they use simple inorganic compounds such as hydrogen ($H_{2(g)}$), nitrate, sulfur and $CO_{2(g)}$. Autotrophs must use photosynthesis or chemosynthesis as a source of energy to form carbohydrates from simple inorganic sources. The autotrophs which are classified as chemolithoautotrophs obtain their energy from chemosynthesis rather than photosynthesis, for example, from the products of mineral-water reactions. One such product from these reactions is hydrogen (Brock *et al.*, 1997; Martin and Müller, 1998; Wood, 1991). The oxidation of hydrogen to water yields enough energy to allow the synthesis of carbohydrate for cell material (Equation *2.1*).

$$2H_{2(g)} + CO_{2(g)} \rightarrow (CH_2O) + H_2O \qquad (2.1)$$

Stevens and McKinley (1995) reported the existence of hydrogen-dependent chemolithoautotrophic bacteria living on geochemically produced hydrogen, deep in the rock aquifers of the Columbia River Basalt Group (CRB), the groundwater there being typically alkaline (pH 8-10.6). They concluded that the only local source of hydrogen was from the interaction between the groundwater and the basalt (most probably serpentinisation reactions in which reduced iron minerals react with water). Their water-rock experiments using crushed rock samples from the CRB produced up to 60 μM of dissolved H_2 at 22°C. Additionally, enriched ^{13}C levels from their stable carbon isotope studies indicate that the depletion of dissolved inorganic carbon (*DIC*) in the groundwater was coupled to bacterially mediated methane production as in the reaction below (Equation 2.2).

$$4\,H_{2(g)} + CO_{2(aq)} \rightarrow CH_{4(g)} + 2\,H_2O \qquad (2.2)$$

Since many bacterially-mediated redox equilibria involve hydrogen (as in Equation 2.2), it is possible to relate the $H_{2(g)}$ concentration of a given environment to the dominant bacterially mediated redox reaction occurring in that environment, as demonstrated by Lovely and Goodwin (1998) in Figure 2.1.

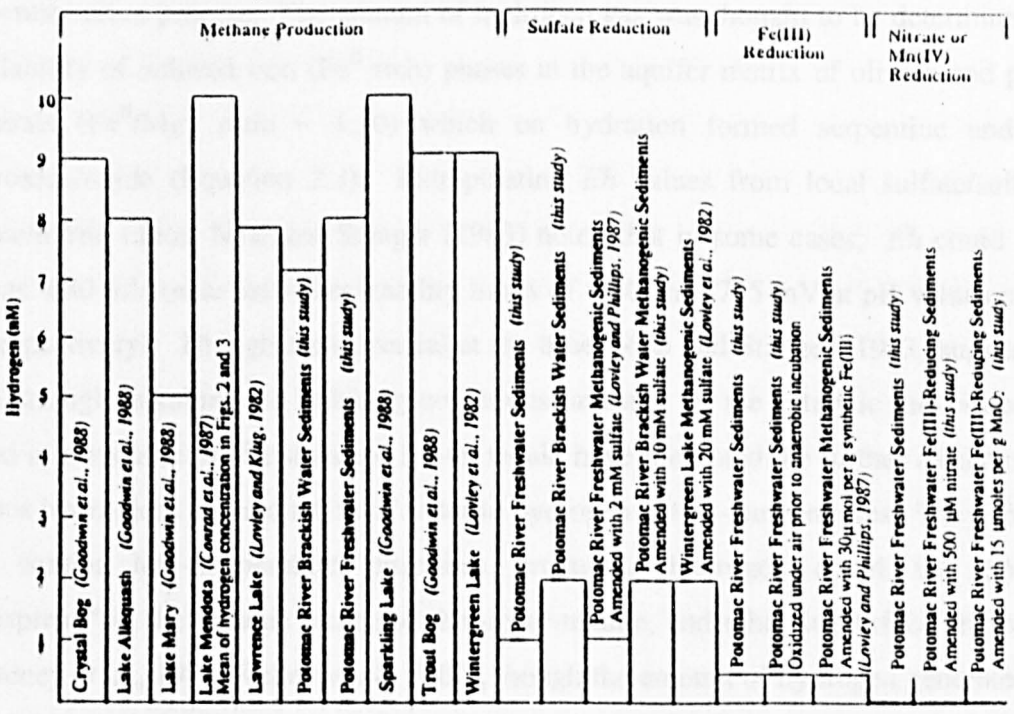

Figure 7.11. H_2 concentrations in sediments with different predominant electron accepting processes (reproduced with permission, Lovley and Goodwin, 1988).

Figure 2.1. H_2 concentrations in sediments with different predominant electron accepting processes. From Lovely and Goodwin (1988).

Figure 2.1 shows that bacterial processes producing methane are coupled with significantly higher levels of H_2 (≤10nM) in these sediments. Environments that contain Fe(III) reducing bacteria, have a much lower H_2 content, approximately 0.5 nM H_2. Nitrate and $Mn^{(IV)}$ reducing bacteria produce even lower levels of H_2 (≤0.1 nM). In comparison, Stevens and McKinley reported ~10nM H_2 in the groundwater samples from the CRB. However, this study is concerned with finding evidence for the presence of H_2 in early hydrothermal fluids. Evans *et al.* (1988) sampled vent fluids from the southern Juan de Fuca ridge at 2300m depth, at 285°C, and recorded 148-313 μm H_2, but estimated there to be 270-527 μm H_2 by considering the relative contributions of the fluids and seawater to each sample, and assuming all of the magnesium in the sample originated from the seawater (see Chapter 4). If even a fraction of the concentrations of hydrogen described by Evans *et al.*, (1988) could have been produced from the Hadean lithosphere, then it is possible that there was enough hydrogen to support chemolithoautotrophic metabolism even allowing for escape of H_2 to the atmosphere given that there was also a direct or indirect source of carbon dioxide (or monoxide). Neal and Stanger (1983) reported the generation of up to 97% by volume of inorganically produced H_2 gas as a result of low temperature, alkaline (pH 10-12) water-rock reactions, in an anoxic, closed groundwater environment in the Oman Ophiolite. They suggested that the generation of hydrogen and the anoxic conditions were coupled to the serpentinisation process. The amount of hydrogen gas was thought to be determined by the availability of reduced iron (Fe^{II}-rich) phases in the aquifer matrix of olivine and pyroxene minerals (Fe^{II}/Mg^{II} ratio ~ 1:10) which on hydration formed serpentine and ferrous hydroxide/oxide (Equation *2.3*). Extrapolating *Eh* values from local sulfate/sulfide and nitrate/nitrite ratios, Neal and Stanger (1983) noted that in some cases, *Eh* could reach as low as -630 mV (near the water stability limits of -650 and -715 mV at pH values of 11 and 12 respectively). Though controversial at the time, Neal and Stanger (1983) suggested that such strongly alkaline and reducing conditions, assisted by the catalytic nickel-iron alloys found in serpentinites (Krishnarao, 1964), would have promoted the further oxidation of the ferrous hydroxides and reduction of water to hydrogen at low-temperatures. They concluded that similar low-temperature processes producing hydrogen could be "potentially widespread" in the oceanic crust and the upper-mantle, and other subsurface environments (Coveney *et al.*, 1987; Kelley *et al.*, 2001), though the amount of hydrogen generated would be limited by the availability of Fe^{II} hydroxide.

In this study, the objectives were to examine the olivine-water reaction, and decide whether hydrogen production was possible from such reactions in a Hadean crust. The controls on pH of early hydrothermal fluids is also discussed. To accomplish this task it is

necessary to ascertain the probable environmental conditions in the Hadean. These are difficult to constrain due to the absence of geological evidence from this era; thus there are a large number of uncertainties to consider. This is discussed in §2.2 below, where the environmental constraints to be used for this study are contemplated. The accepted early Earth conditions that were eventually used were those that have been proposed after much discussion in the scientific community. However, some of these proposals are regularly challenged.

2.2 Environmental conditions in the Hadean

It is assumed that the pH of the ocean water about 4.2 billion years ago (4.2 Ga) was imposed by the carbon oxides. The ratio between the monoxide and dioxide will depend on the overall oxidation state of the Hadean mantle (but the pH of seawater is unlikely to be affected by the monoxide). This is disputed. Canil (1997) argues for a mantle similar to today's (i.e., FMQ or Fayalite-Magnetite-Quartz) whereas Kasting and Brown (1998) argue for a mantle with an oxygen fugacity one to four units more reducing than FMQ (§5.5). Kasting's argument centres on the assumption that incoming asteroids consisting in part of nickel-iron as well as the carbonaceous chondrites, comprised a significant proportion of the Hadean crust. With such a low redox state, hydrogen would have gravitated rapidly to space and methane would have been photo-oxidised. Thus, the early Earth is left with an atmosphere that, while containing a similar nitrogen content to today, has an unknown pressure of the carbon oxides at an unknown ratio. Supposing that of all the carbon present on and in the Earth today, two per cent were available to the Hadean atmosphere, then the pressure would approximate to one bar (Walker, 1985). And clearly a ten bar atmosphere would be within the bounds of possibility. Considering that Venus has 90 bars of CO_2 today, this figure may even be conservative. Given the lack of certainty and the likely inhomogeneity of the Hadean crust, a CO/CO_2 ratio of 1:1 is arbitrarily chosen. However, Kasting and Brown (1998) consider the ratio could reach 9:1. Against this is the fact that CO is nearly insoluble in mafic magma, whereas CO_2 can achieve a 1% solubility and is readily degassed from volcanoes (Gerlach, 1989a; 1989b). The lack of free oxygen in the Hadean atmosphere is undisputed, therefore anoxic atmospheres are reflected in the models.

As for temperatures and pressures, they increase with depth in the crust where solids, fluids and gases may have supercritical properties or exhibit other unusual behaviour. Pressures in early hydrothermal systems may have been hydrostatic or lithostatic. If the fluids in the fractures were open to the interface between the ocean and it's crust then the pressure would be hydrostatic. If the fractures or pore spaces were sealed from the surface

by precipitated minerals then the density of the overlying rock would have to be considered (Shock, 1992a). Since this study deals with early hydrothermal systems discharging fluids into the early ocean, the pressures are assumed to be hydrostatic. At temperatures of 373.9°C, 220.5 bars, and 407°C, 298.5 bars, H_2O and seawater reach their supercritical points respectively. At these conditions the physical properties of H_2O such as molal volume (V°, $cm^3\ mol^{-1}$), dielectric constant, and properties related to density such as isobaric expansivity, α ($K^{-1}.10^2$), isothermal compressibility β ($bar^{-1}.10^2$), and the standard molal isobaric heat capacity $C°_p$ ($cal\ mol^{-1}K^{-1}$), control the upper limits of the temperatures of venting fluids to around 350-400°C. At lower temperatures, particularly <200°C, pressures ranging from 1-5 Kbars have relatively little effect on certain properties of H_2O such as the density of the fluid, compared with temperature changes. Similarly, the dielectric constant of H_2O is also barely affected by similar pressures (see Shock, 1992a; Bischoff and Rosenbauer, 1984). However, the ionisation constant ($K_w = [H^+][OH^-]$), and thus the pH, of water *is* influenced by temperature and pressure (see Shock, 1992a; and Figure B in Appendix 1A). Although temperature has a more noticeable effect on pH, an increase in pressure of 2 kilobars can decrease neutral pH (~7.5 at 0°C) by about 0.4 units. However, a similar increase in pressure at 350°C will decrease neutral pH (~5.9 at 350°C) by about 0.8 units (see *Figure 15*, Shock, 1992a). In addition, at temperatures above 200°C, the pH of many submarine hydrothermal vent fluids is controlled by the hydrolysis of Ca-plagioclase to epidote ($Ca_2FeAl_2Si_3O_{12}OH$). This is a reaction whose equilibrium constant is highly sensitive to pressure, especially at temperatures and pressures near the critical point of water (Seyfried *et al.*, 1991; Polya, D., *pers. comm.*).

2.3 The fayalite and water reaction

To theoretically determine how much hydrogen could have been generated from water-rock reactions it is necessary to create a model to reflect the early seawater as it permeates, percolates and flows through the early oceanic crust. The most likely composition of the Hadean crust and seawater is still debatable. Komatiites are thought to have made up the bulk of the oceanic crust during the Archaean (Nisbet, 1987), and may be used in a proposed model of the Hadean (*cf.* Macleod *et al.*, 1994). However, in this investigation the focus is on certain key minerals in the komatiitic crust, such as the olivine end-members forsterite and fayalite. Therefore, it is not necessary to model a complex rock such as komatiite, but instead create a model rock of olivine - the dominant mineralogical constituent of the ocean crust. Olivines are a group of silicate minerals that have the general formula $(Mg, Fe >> Mn >> Ca)_2SiO_4$ and generally exist in some combination of these

metallic elements. They are widespread in basalt, peridotite, and other igneous rocks. Knowing that oxidation of iron produces hydrogen, our interest lies in olivine that contains the iron-rich silicate, fayalite (Fe_2SiO_4). Fayalite is present in olivine with forsterite (Mg_2SiO_4), usually in a 1:9 ratio in mafic/ultramafic igneous rocks. Many ultramafic bodies show evidence of two distinct reactions, talc-carbonate alteration and serpentinisation (Eckstrand, 1975). The reaction between olivine and water during serpentinisation (Equation *2.3*) is of particular interest in this chapter. The reactions are widely documented (Moody, 1976, Neal and Stanger, 1983, and references therein; Coveney *et al.*, 1987) and show that the fayalite end-member of olivine reacts with water to produce magnetite (Fe_3O_4); an iron-rich serpentinite-type mineral (for example, greenalite, $3[Fe_3Si_2O_5(OH)_4]$); and hydrogen (Equation *2.3*, Figure 2.2). Similarly, the reaction between the forsterite end-member of olivine and water produces a magnesian-rich serpentine (typically lizardite, $Mg_6[Si_4O_{10}](OH)_8$ ± brucite ($Mg(OH)_2$) ± talc ($Mg_3Si_4O_{10}(OH)_2$ (Janecky and Seyfried, 1986).

$$\text{(fayalite) } 6Fe_2SiO_4 + 7H_2O \rightarrow \text{(magnetite) } Fe_3O_4 + \text{(greenalite) } 3[Fe_3Si_2O_5(OH)_4] + H_{2(g)} \qquad (2.3)$$

$$\text{(forsterite) } 4Mg_2SiO_4 + 6H_2O \rightarrow \text{(lizardite) } Mg_6[Si_4O_{10}](OH)_8 + \text{(brucite) } 2Mg(OH)_2 \qquad (2.4)$$

One of the aims in this chapter is to determine whether the early environmental conditions proposed for the Russell and Hall model (1997) will allow reaction *2.3* to proceed and if so, how much hydrogen could be produced from it. However, the stability of iron with respect to redox conditions is discussed prior to modelling the olivine-water reaction.

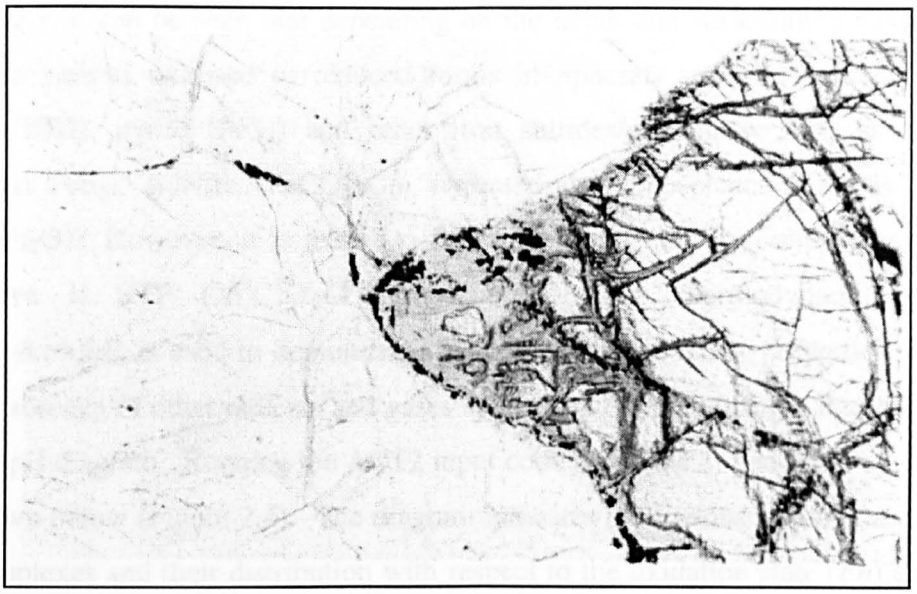

Figure 2.2. Photomicrograph (transmitted light, plane-polarised-light) showing altered olivine in thin section. The olivine (crystal on right) is altering to serpentine (in fractures) and magnetite (black). Photograph courtesy of A. J. Hall

2.4 The stability of iron and its compounds in redox environments

2.4.1 The Fe system

In sedimentary environments redox conditions may be *oxic* ($O_{2(aq)}$ > ~1 μM), or *anoxic* ($O_{2(aq)}$ < ~1 μM), sulfidic or postoxic/methanic. For an anoxic environment, if sulfide (C_{H2S}) species are >1 μM, it is *sulfidic*. If sulfide species are <1 μM, it is *postoxic* or *methanic*. The system of the classification of redox environments suggested by Berner (1981), though mainly of relevance to sediments and soils, is a useful guide and is tabulated below (Table 2.1).

Table 2.1

Environment	*Characteristic Phases*
I. Oxic ($C_{O2} \geqq 10^{-6}$)	hematite, goethite, MnO_2-type minerals; no organic matter
II. Anoxic ($C_{O2} < 10^{-6}$)	
A. Sulfidic ($C_{H2S} \geqq 10^{-6}$)	pyrite, marcasite, rhodochrosite, alabandite; organic matter
B. Nonsulfidic ($C_{H2S} < 10^{-6}$)	
1. Postoxic	glauconite and other Fe^{2+}, Fe^{3+} silicates (also siderite, vivianite, rhodochrosite); no sulfide minerals; minor organic matter
2. Methanic	siderite, vivianite, rhodochrosite: earlier formed sulfide minerals: organic matter

Table 2.1. Berner's (1981) classification of redox environments together with solids which are expected to form in each environment. The environments from top to bottom also correspond to increasing depth. (C = molar concentration)

From Table 2.1, it can be seen that depending on the depth and surrounding environment, iron exists in various oxidised or reduced forms in minerals such as hematite (Fe_2O_3), goethite (FeOOH), pyrite (FeS_2) and other iron sulfides/carbonates such as marcasite (orthorhombic FeS_2), siderite ($FeCO_3$), or hydrated iron phosphates such as vivianite ($Fe_3(PO_4)_2.8H_2O$). However, it is useful to first understand how iron and its compounds might behave at STP (25°C / 1 atmosphere). The thermodynamic database, *thermo.com.v8.r6.full*, is used to demonstrate the behaviour and redox properties of iron in water in the absence of other radicals and gases apart from oxygen, using a Pourbaix (1949, 1963) or *Eh*-pH diagram. Running the ACT2 input code (Figure 2.3) generates the Pourbaix diagram shown below (Figure 2.4). The diagram indicates the various stable phases of iron and iron complexes and their distribution with respect to the oxidation state (*Eh*) and pH at STP (25°C / 1 atmosphere) in 1kg water according to the thermodynamic data in the database. Of course, the phases of iron that are stable in natural environments are determined by very different chemical and physical conditions, and kinetic barriers. Bacterial activity may also influence the distribution of minerals, species and gases. Additionally, in out-of-equilibrium conditions, metastable entities may well precipitate first (see §5.1).

ACT2 input script for Figure 2.4

```
1.    data = thermo.com.v8.r6.full
2.    swap e- for O2(aq)
3.    diagram Fe++ on Eh vs pH
4.    log activity main = -6
5.    x-axis from 0 to 14
6.    y-axis from -1 to 1.5
7.    suppress FeO(c)
```

Figure 2.3. Input code used to generate the Pourbaix diagram for iron in 1kg water at 1.013 bar and 25°C, as shown in Figure 2.4.

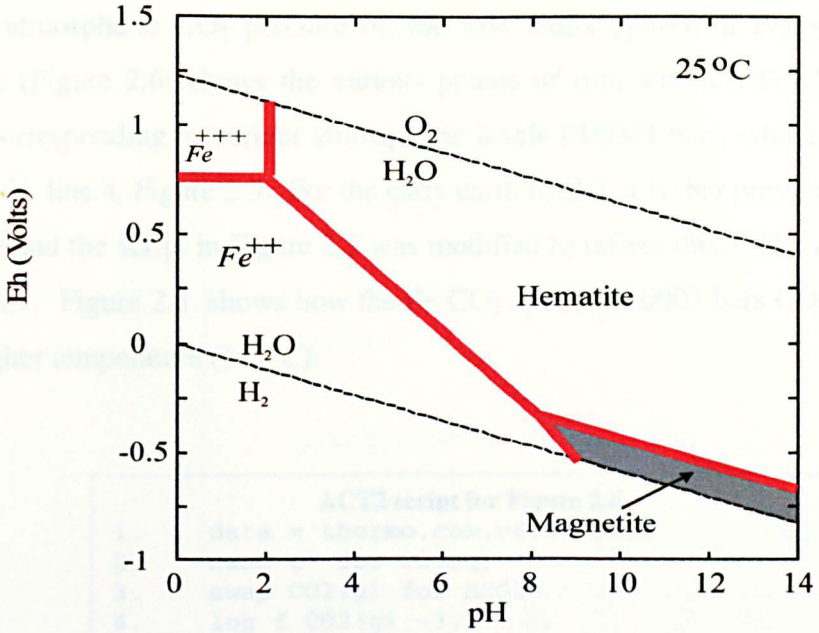

Figure 2.4. Mineral phases and aqueous species of the Fe-H_2O system, showing the stability of iron minerals and iron compounds in water at STP (25°C / 1 atmosphere) with respect to *Eh* and pH conditions. Activity $Fe^{++} = 10^{-6}$. $FeO_{(c)}$ suppressed

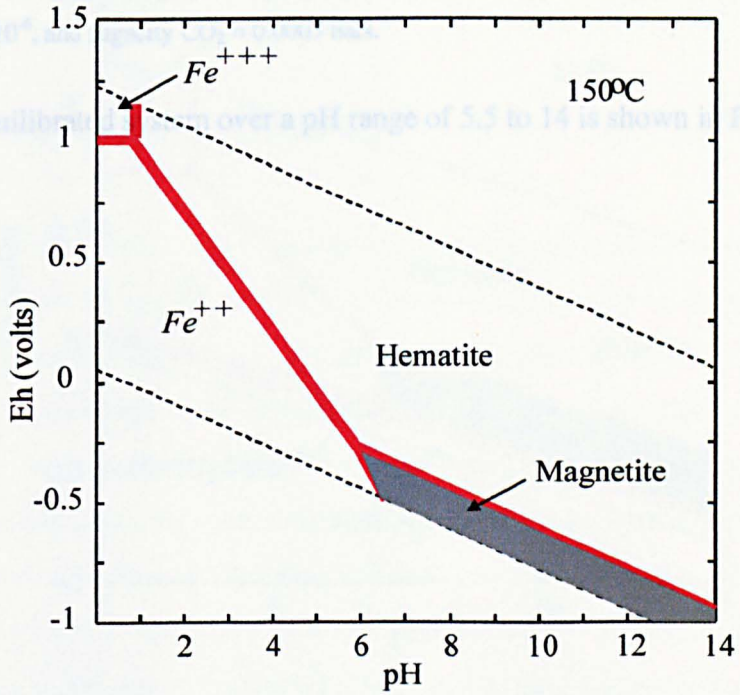

Figure 2.5. Mineral phases and aqueous species of the Fe-H_2O system with respect to *Eh* and pH conditions at 150°C and 4.757 bar in 1kg H_2O. actibity $Fe^{++} = 10^{-6}$. The pressure corresponds to the boiling curve of H_2O (Appendix 1A, Figure B).

2.4.2 The Fe-CO_2 System

The CO_2 concentration expected in the Hadean atmosphere is expected to be much higher than today therefore it is useful to examine what influence the high pressures of CO_2 in the atmosphere may have had on the stable phases of iron. To consider the influence of

current atmospheric CO_2 pressure on the iron redox system in Figure 2.4, the Pourbaix diagram (Figure 2.6) shows the various phases of iron within a Fe-CO_2 redox system at 25°C, corresponding to current atmospheric levels (0.0003 bars, which is equivalent to log f_{CO2} $10^{-3.5}$, line 4, Figure 2.5. For the early earth model, a 10 bar pressure of CO_2 fugacity is possible and the script in Figure 2.5 was modified to reflect this. The result is presented in Figure 2.7. Figure 2.8 shows how the Fe-CO_2 system (0.0003 bars CO_2) would be affected by a higher temperature (150°C).

ACT2 script for Figure 2.6

```
1.    data = thermo.com.v8.r6.full
2.    swap e- for O2(aq)
3.    swap CO2(g) for HCO3-
4.    log f CO2(g) -3.5
5.    diagram Fe++ on Eh vs pH
6.    log activity main = -6
7.    x-axis from 5.5 to 14
8.    y-axis from -.85 to 1.15
```

Figure 2.5. ACT2 script showing input parameters for system at 25°C containing 1kg H_2O, activity Fe++ = 10^{-6}, and fugacity CO_2 = 0.0003 bars.

The equilibrated system over a pH range of 5.5 to 14 is shown in Figure 2.6.

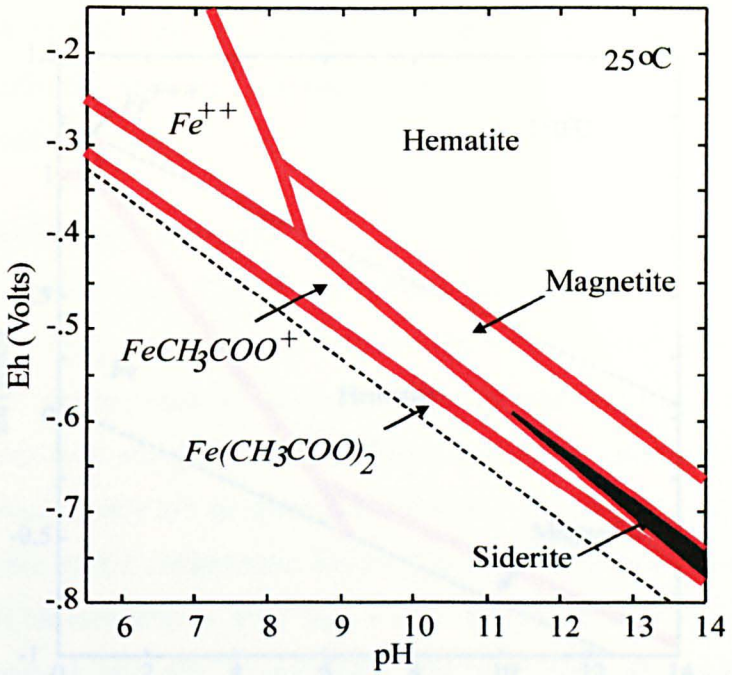

Figure 2.6. Mineral phases and aqueous species of the Fe-H_2O-CO_2 system with respect to *Eh* and pH conditions at STP. Total $CO_{2(g)}$ = 0.0003 bars, activity $Fe^{++} = 10^{-6}$.

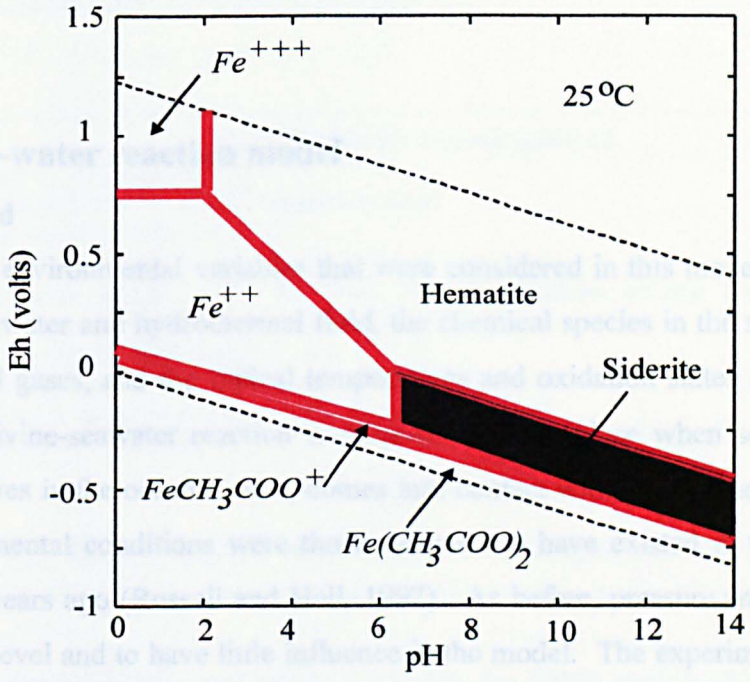

Figure 2.7. Mineral phases and aqueous species of the Fe-H_2O-CO_2 system with respect to *Eh* and pH conditions at STP. Total $CO_{2(g)}$ = 10 bars, activity $Fe^{++} = 10^{-6}$.

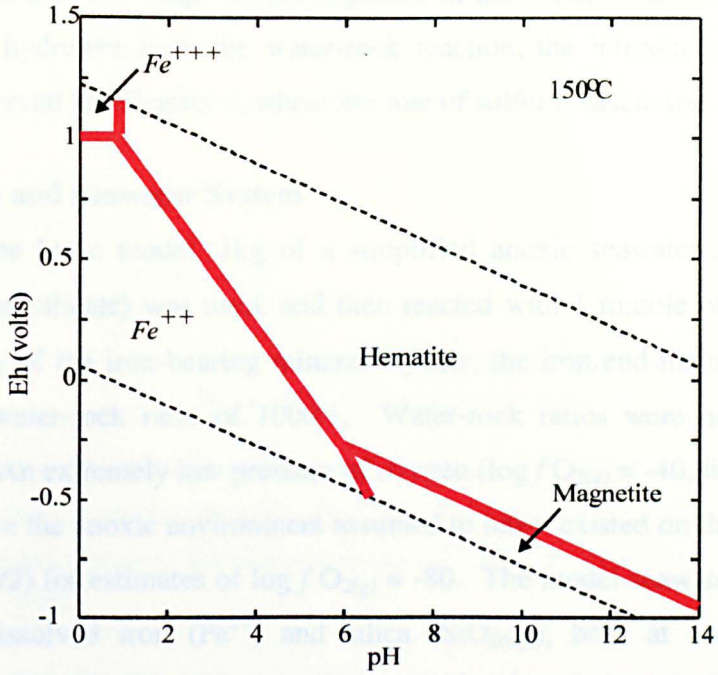

Figure 2.8. Mineral phases and aqueous species of the Fe-H_2O-CO_2 system with respect to *Eh* and pH conditions at 150°C. Total $CO_{2(g)}$ = 0.0003 bars, activity Fe^{++} = 10^{-6}.

2.5 Olivine-water reaction model

2.5.1 Method

The environmental variables that were considered in this model were temperature, pH of the seawater and hydrothermal fluid, the chemical species in the system, atmospheric and dissolved gases, and the typical temperatures and oxidation states in the oceanic crust where the olivine-seawater reaction is proposed to take place when seawater, gravitating through fissures in the oceanic crust, comes into contact with the olivine at a depth of 5km. The environmental conditions were those assumed to have existed in the Hadean ~4.2 to ~4.4 billion years ago (Russell and Hall, 1997). As before, pressure was assumed to be at atmospheric level and to have little influence in the model. The experimental approach was to create a basic model, test it for stability, then to gradually add more complexity. Once the robustness of the basic model was confirmed, other components and constraints were introduced into the model with subsequent testing. Using the GWB reaction modelling program REACT, a geochemical model was constructed of the water-rock (seawater-fayalite) interaction. The Russell and Hall (1997) hypothesis stipulates that after the interaction between the seawater and olivine, the resultant fluid should be in equilibrium with its surrounding environment, alkaline, and contain sulfur as hydrosulfide (HS^-) but have vanishingly small concentrations of iron (MacLeod *et al.*, 1994). However, since the

primary objective at this stage of development in the model was the investigation of the production of hydrogen from the water-rock reaction, the introduction of sulfur into the model was reserved for Chapter 3, where the role of sulfur is discussed.

2.5.2 Fayalite and Seawater System

For the basic model, 1kg of a simplified anoxic seawater analogue (containing ferrous iron and silicate) was used, and then reacted with 1 mmole of a 'simplified' rock, composed only of the iron-bearing mineral fayalite, the iron end-member of olivine. This constitutes a water-rock ratio of 1000:1. Water-rock ratios were not varied during the experiments. An extremely low pressure of oxygen ($\log f O_{2(g)} = -40$, line 5, Figure 2.9) was used to simulate the anoxic environment assumed to have existed on the early earth, though see Shock (1992) for estimates of $\log f O_{2(g)} = -80$. The model seawater contained nominal amounts of dissolved iron (Fe^{2+}) and silica ($SiO_{2(aq)}$), both at concentrations of 10^{-6} millimoles, allowing the REACT program to consider them in its calculations (lines 6 and 7, Figure 2.9). These low concentrations were used because the thermodynamic data in the database are accurate only for dilute solutions.

REACT script for Figures 2.10-2.12

```
1.    data = thermo.dat
2.    temperature = (Set temperature)
3.    swap O2(g) for O2(aq)
4.    1 kg free H2O
5.    fugacity O2(g) = 1e-40 (Set PPM oxidation state for s/water)
6.    total mmol Fe++ = 1e-6
7.    total mmol SiO2(aq) = 1e-6
8.    balance on H+
9.    react 1 mmol of Fayalite
10    suppress  FeO(c)
```

Figure 2.9. REACT script for water-rock reaction involving fayalite and H_2O at STP, see Figures 2.10-2.12. Thermodynamic data obtained from GWB database, *thermo.dat* (Bethke, 1998)

Using the REACT script in Figure 2.9 with the GWB code enabled the production of a variety of diagrams describing changes to the system as the reaction progressed (Figures 2.10-2.12). Balancing the electrolytic charge of the ionic solution with hydrogen ions allowed calculation of the pH (line 8, Figure 2.9) of the fluid at each stage of the reaction. Three types of diagram were selected to portray events during the reaction (minerals produced or consumed, Figure 2.10; fugacities of gases as they are produced or consumed, Figure 2.11; and changes in oxidation state and pH, Figure 2.12).

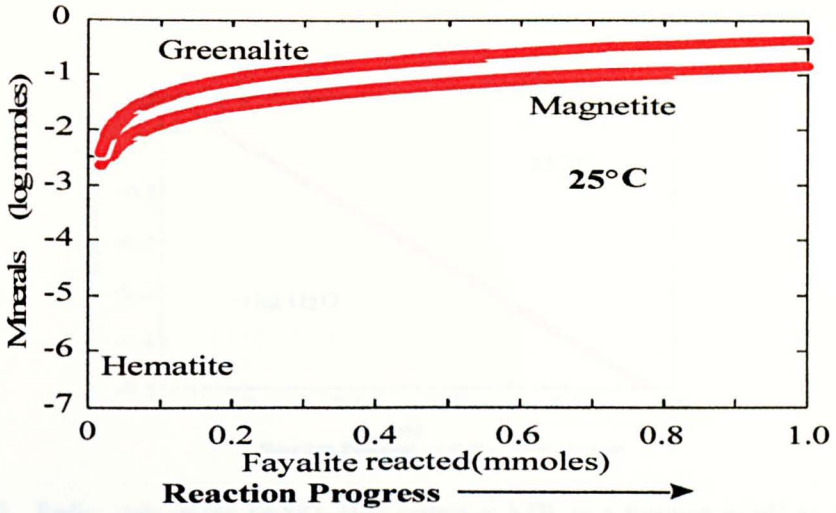

Figure 2.10. Mineral stabilities of the Fe-SiO_2-H_2O system at STP, as a function of the amount of fayalite (Fe_2SiO_4) reacted. Initial fugacity $O_{2(g)} = 1e^{-40}$, total $[Fe^{++}] = 10^{-6}$, total $[SiO_2]_{(aq)} = 10^{-6}$. $FeO_{(c)}$ precipitation suppressed. Graph produced using GWB REACT code and GWB database *thermo.dat* (Bethke, 1998).

Figure 2.10 shows minerals produced or consumed as 1 mmol of fayalite is titrated into 1kg of water at STP. A small amount of hematite is precipitated, but it is used up as soon as it is formed. Graph produced using GWB REACT code and GWB database *thermo.dat* (Bethke, 1998).

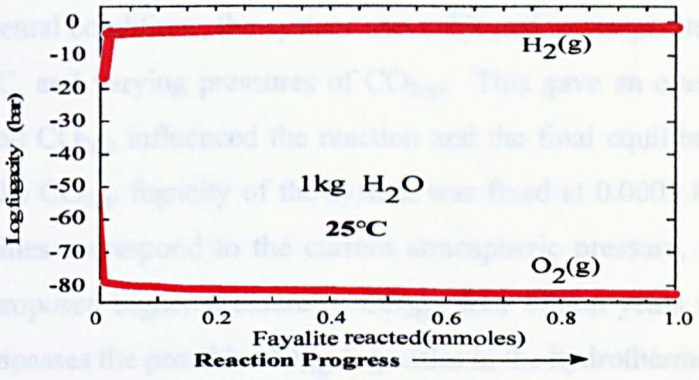

Figure 2.11. Fugacity of O_2 and H_2 in the Fe-SiO_2-H_2O system at STP, as a function of the amount of fayalite (Fe_2SiO_4) reacted. Initial fugacity $O_{2(g)} = 1e^{-40}$, total $[Fe^{++}] = 10^{-6}$, total $[SiO_2]_{(aq)} = 10^{-6}$. $FeO_{(c)}$ precipitation suppressed. Graph produced using GWB REACT code and GWB database *thermo.dat* (Bethke, 1998).

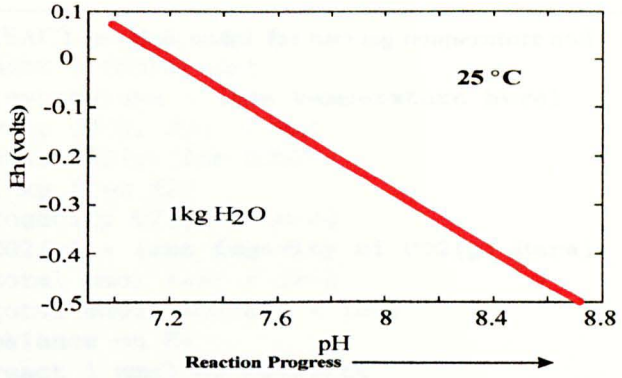

Figure 2.12. Redox state of the Fe-SiO_2-H_2O system at STP, as a function of pH as 1 mmole of fayalite (Fe_2SiO_4) is reacted into 1 kg of water at STP. Initial fugacity $O_{2(g)} = 1e^{-40}$, total $[Fe^{++}] = 10^{-6}$, total $[SiO_2]_{(aq)} = 10^{-6}$. $FeO_{(c)}$ precipitation suppressed. Graph produced using GWB REACT code and GWB database *thermo.dat* (Bethke, 1998).

The fayalite and simple seawater system was subjected to a series of tests to determine how it may respond to fluctuations of temperature and $CO_{2(g)}$ pressure.

2.5.3 Temperature, CO_2 pressure, and the fayalite, forsterite and seawater system

Having shown that the modelling software produced the expected results, in that the seawater and fayalite reaction does indeed produce hydrogen (Figure 2.11) under the proposed environmental conditions, the system was subjected to temperatures of 10, 50, 90, 150, 200 and 250°C, and varying pressures of $CO_{2(g)}$. This gave an overall impression of how temperature and $CO_{2(g)}$ influenced the reaction and the final equilibrated system. For each temperature, the $CO_{2(g)}$ fugacity of the system was fixed at 0.0003 bars, 1 bar and 10 bars. These fugacities correspond to the current atmospheric pressure, the standard state pressure, and the proposed higher pressure of $CO_{2(g)}$, four billion years ago (4 Ga). This range at least encompasses the possible $CO_{2(g)}$ fugacities in the hydrothermal environment.

The REACT script in Figure 2.9 was updated as necessary to reflect each temperature and CO_2 pressure of interest (lines 2 and 7, Figure 2.13). In addition, the experiments were repeated with the mineral forsterite, the magnesian end-member of olivine, substituted for fayalite. Finally, the experimental system was updated to reflect a more realistic olivine by using both fayalite and forsterite in a ratio of 1:9 (Neal and Stanger, 1986). A large number of graphs can be generated using this approach, and the data extracted

REACT template script for varying temperature and $CO_{2(g)}$

```
1.   data = thermo.dat
2.   temperature = (set temperature here)
3.   swap O2(g) for O2(aq)
4.   swap CO2(g) for HCO3-
5.   1 kg free H2O
6.   fugacity O2(g) = 1e-40
7.   CO2(g) = (set fugacity of CO2(g) here)
8.   total mmol Fe++ = 1e-6
9.   total mmol SiO2(aq) = 1e-6
10.  balance on H+
11.  react 1 mmol of Fayalite
```

Figure 2.13. REACT template script for varying temperature and $CO_{2(g)}$ in fayalite and seawater system.

from them even larger. Thus, the values of key variables (temperature, dominant mineral concentrations, fugacities of $H_{2(g)}$ and $O_{2(g)}$, and *Eh* and pH) were recorded and tabulated from each mineral, fugacity and *Eh*-pH diagram, as each reaction reached equilibrium. The results can be viewed in Appendix 1B (Tables A1 - A12). The products for each system tested were plotted (Figures A1-A78, Appendix 2) to provide, at a glance, how the entire system varied with temperature and $CO_{2(g)}$ fugacity. The results are summarised in §2.6 below.

2.6 Discussion

2.6.1 Fe-H_2O system

Figure 2.4. demonstrates that at 25°C and in very acidic environments (pH < 2), regardless of the oxidation state, iron tends to remain in solution as Fe^{2+} or Fe^{3+} ions. Iron solubility can be seen to depend very much on the pH of the system. As the pH of the environment rises above approximately 8.7, iron becomes insoluble (<1 ppm approximately) regardless of the redox potential of the system, and precipitates out of the solution mainly as hematite. Magnetite is stable in moderate to extreme redox conditions. Further analysis of Figure 2.4 reveals what is fairly well known about iron:

(i) iron oxides, in this case magnetite (Fe_3O_4, a conjugated Fe^{2+}/Fe^{3+} mineral), and hematite (Fe_2O_3, an Fe^{3+} mineral), are the possible stable minerals controlling iron solubility.

(ii) in anoxic environments (*less O_2, more reducing, hence lower Eh*) and in non-oxidising acids, Fe^{2+} is the dominant oxidation state of dissolved iron. However, in oxic environments (*more O_2, more oxidising, higher Eh*) or in oxidising acids, some

of the iron would be present as Fe^{3+}, but this can only occur at extremely acidic/oxidising conditions.

Oxidation of iron from Fe(II) to Fe(III) produces more acid in many moderate to extreme environments such as in the precipitation of iron hydroxides, $Fe(OH)_3$, since Fe^{3+} removes hydroxide ions from water and releases hydronium ions from water as shown in Equation *2.5*.

$$2\,Fe^{2+} + \tfrac{1}{2}\,O_2 + 5\,H_2O \rightarrow 2\,Fe(OH)_3 + 4\,H^+ \qquad (2.5)$$

The magnetite phase is shown to be dominant only in extremely reducing (low *Eh*) and alkaline (high pH) environments (Figure 2.4). If we suggest that the surface redox environments were moderate and anoxic in the Hadean, Figure 2.4 predicts that magnetite rather than hematite deposits would be more likely to be formed in sediments and within the crust. The simple iron system calculated at 25°C (Figure 2.4) was also tested to reflect possible higher temperatures (150°C) in the model (Figure 2.5). This had had no obvious effect on the overall distribution of the iron species in the system, except that the magnetite field extended to slightly acidic conditions (pH ~6.2).

The iron stability diagrams in Figures 2.4 and 2.5 are simple models describing the behaviour of iron and it's complexes in water alone. A more realistic model for the emergence of life would have to incorporate sulfur and carbon, and thus other minerals could form preferentially. The thermodynamic calculations that produce Figure 2.4 and 2.5 would have also shown that iron oxide ($FeO_{(c)}$) could be precipitated. However, $FeO_{(c)}$ does not constitute a stable phase at these temperatures. $FeO_{(c)}$ would instead be incorporated into silicates, oxyhydroxides and carbonates. For this reason, the production of $FeO_{(c)}$ was suppressed in the calculations by issuing the appropriate instructions to the program in the ACT2 code (line 7, Figure 2.3).

2.6.2 Fe-H_2O-CO_2 system

With carbon dioxide in the Fe-H_2O-CO_2 system (Figure 2.6), hematite still occupies much of the computed redox and pH space. At low temperatures (25°C), high pH (>11) and reducing conditions (*Eh* < -600mV), magnetite production becomes less likely, and siderite ($FeCO_3$), iron in its carbonate form, is progressively favoured. When the system was subjected to a higher pressure of CO_2 (10 bars), it showed that under alkaline and reducing conditions, the siderite stability field occupies a much larger Eh-pH space (Figure 2.7). An important point can be drawn from Figures 2.6 and 2.7. One of the requirements of the

origin of life model is to convert CO_2 to acetate (CH_3COO). In these figures, $CO_{2(g)}$ is shown to be reduced to acetate, and that the acetate is thermodynamically stable. This does not happen readily in an abiotic environment. Although the conversion of $CO_{2(g)}$ to acetate is shown to be thermodynamically feasible in the calculations, it is the overcoming of the kinetic barrier which poses the difficulty in natural abiotic systems. How then is it possible for these organic compounds to be synthesised? This problem provides the foundation for much of the work in Chapter 5, where the role of mineral buffers in organic synthesis is discussed.

In Figures 2.6 and 2.7, it can be seen then that the presence of even very small amounts of CO_2 (0.0003 bars) in the system may allow the precipitation of some siderite, under appropriate pH and redox conditions. Many Archaean iron formations contain some siderite layers (Dymick and Klein, 1988) as do the Maar Lakes in the Cameroon such as Lake Nyos and Monoun (Sigurdsson, 1987; Kling *et al.*, 1989). Thus given higher CO_2 partial pressure, the dominant chemical sediment in the Hadean is likely to have been siderite. This could be significant in terms of the synthesis of organic molecules. After all, French (1971) generated organic acids, alcohols, ketones, and hydrocarbons during the synthesis of siderite from ferrous oxalate, though the production of organic molecules was not the main focus of the investigation, and as such, not taken further. Thus it is possible to imagine that if such sediments were to be covered by komatiitic flows they could be subsequently thermally metamorphosed by later magmatic intrusions in the presence of magmatic or hydrothermal hydrogen and similar organic molecules generated. If CO_2 was present in early seawater, then it would be consumed as the seawater-rock reaction progresses and siderite precipitates. Eventually, magnetite would be the dominant precipitate from a seawater with low concentrations of CO_2 at depth in a hydrothermal system. Interlaminations of these two minerals may be expected from cycles of saturation-supersaturation-nucleation-settling cycles.

In Figure 2.8 (produced from the script in Figure 2.5 and modified for 150°C), it can be seen that higher temperatures favour the production of hematite and magnetite at current CO_2 levels over a similar *Eh*-pH space, and no siderite or acetates are stable at this temperature. In additional tests with 10 bars CO_2, the results were similar to Figure 2.8 in that magnetite was predominantly stable at alkaline and reducing conditions.

2.6.3 Simple Fayalite and seawater system

Several observations were made. In the minerals diagram (Figure 2.10), the introduction of fayalite into the system was perceived as the moment when seawater comes

into contact with olivine, causing minerals such as hematite ($Fe_2^{III}O_3$), magnetite ($Fe^{II}Fe_2^{III}O_4$) and greenalite ($Fe^{II}_3Si_2O_5(OH)_4$) to immediately precipitate from the seawater. The initial redox conditions allowed a small amount of hematite to precipitate, but it was used up as soon as it was formed (Figure 2.10). This could be explained by the rapid assimilation of oxygen (Figure 2.11), quickly making the system strongly reducing and consequently, making hematite unstable again. As indicated by the levelling of the curves and the presence of both minerals at the end of the reaction (Figure 2.10), the fluid was in equilibrium with greenalite, the dominant mineral, and some magnetite. The model confirmed that as seawater reacts with olivine (in particular, the mineral fayalite, the iron end-member of olivine) hydrogen gas is produced (Figure 2.11). The results were as expected (see Equation *2.3*, and the iron-silicate stability diagram in Figure 1.11, §1.7). The hydrogen content in the system increased from $\sim\log f\,H_{2(g)} = 10^{-15}$ to $\sim\log f\,H_{2(g)}\ 10^{-3}$ at the end of the reaction. Oxygen levels depleted rapidly from $\log f\,O_{2(g)} = 10^{-40}$ to $\log f\,O_{2(g)} = 10^{-90}$ which agree with Shock (1992) results.

Consulting the *Eh*-pH values of the reaction path (Figure 2.12), the pH is initially neutral (pH 7), and the redox environment moderate. In the *Eh*-pH diagram (Figure 2.12), the pH of the seawater was calculated by REACT to be initially neutral at pH 7, and finally alkaline at pH 8.7 after its contact with the rock. The initial and final oxidation state of the system was transformed from a slightly oxidising 0.1 V to a strongly reducing –0.5 V. The equation for the fayalite reaction (Equation *2.3*) may provide an explanation for the higher pH as follows. Fayalite reacts with water to produce magnetite, greenalite and hydrogen. Greenalite is a form of serpentine and consists of silica ($2SiO_2$), iron oxide (FeO), and iron hydroxide ($2Fe(OH)_2$). Serpentine is a secondary mineral formed from minerals such as olivine, and often occurs in igneous rocks, but mainly in serpentinites which have formed by the hydration of olivine-bearing rocks (Garcia *et al.*, 1995). The reaction is thought to proceed as $FeO_{(silicate)}$ reacts with water to form iron hydroxides (Equation *2.6*).

$$FeO_{(silicate)} + H_2O \rightarrow Fe(OH)_2 \qquad (2.6)$$

Some of the iron hydroxide produced is dissociated into its component parts to the ferrous ion, Fe^{++}, and the hydroxyl ion, OH^-, thereby increasing the pH (Equation *2.7*).

$$Fe(OH)_2 \rightarrow Fe^{2+} + 2OH^- \qquad (2.7)$$

The liberation of hydrogen gas by water dissociation (Equation *2.3*) may also increase the presence of the hydroxyl ion OH^-, and may have sufficiently increased the alkalinity of the

solution to allow magnetite and greenalite to form. The reaction proceeds in this direction until all the fayalite has been reacted. Therefore, assuming that the reaction goes to completion, the results show that in a reduced, alkaline fluid, and reaction between seawater and olivine, in a water-rock ratio of 1000:1, greenalite and magnetite are the products that are favoured. The maximum concentrations that can be achieved are approximately log $10^{-0.3}$ mmoles (~0.5 mmoles) greenalite and log $10^{-0.8}$ mmoles (~0.17 mmoles) magnetite. Thus, greenalite is the dominant phase and its concentration exceeds that of magnetite by a ratio of ~3:1.

2.6.4 Olivine (fayalite, forsterite) - seawater system

All plots in Appendix 2 (except the 'minerals' diagrams) show reaction products and system variables at initial (seawater) and final (fluid) values. In all of the systems tested the result was influenced by the initial conditions, hence the initial oxygen fugacity, set at log f $O_{2(g)}$ = -40, was the same at all temperatures and the system was in effect less oxic at higher temperatures (Appendix 2, Figures A3, A8, A13, A18, A25, A32, A39, A46, A53, A60, A67 and A74). Thus, the plots in Appendix 2 show that many of the lines merge at high temperature, concluding that the redox change from seawater to fluid was less with increasing initial temperature. It is presumed that fewer mmoles of H_2 are generated at high temperatures to attain equilibrium conditions (and thus there is less dissociation of H_2O). The forsterite and seawater reactions did not show any redox aspect as evidenced by the overlap of the seawater and fluid lines in the hydrogen and oxygen fugacity plots for forsterite and seawater, and thus no change in oxygen or hydrogen fugacity was produced from them. This was to be expected (Equation *2.4*) as it is the fayalite reaction (Equation *2.3*) that involves the dissociation of water and the production of hydrogen. The increase that is evidenced in the forsterite plots for hydrogen fugacity is merely the numeric value of H_2 fugacity changing with temperature and corresponding to the initial O_2 value (log f $O_{2(g)}$ = -40). In the E*h* plots, initial seawater E*h* also reflects the initial fugacity of O_2 in seawater which is fixed at each temperature. Thus, log f $O_{2(g)}$ = -40 gives a lower E*h* at high temperature. However, the redox aspect of the reaction is of more interest at lower temperatures where there is a greater redox contrast between the initial seawater and the final fluid.

Influence of temperature on fayalite and seawater system

(Table A1, Appendix 1B; Figures A1-A5, Appendix 2).

From Table A1 and Figures A1-A5, at temperatures below 150°C, greenalite or a similar serpentine-type mineral is expected to be the dominant mineral and stable with magnetite (Figure A1). At temperatures of between 150°C and 250°C, magnetite is the stable mineral, with concentrations of greenalite dropping to zero. Hydrogen production can be seen to be indifferent to temperature variations, though it may not reach the 1 bar level as indicated in Figure A2. Shock calculated H_2 fugacities ranging from 0.01 bars to 0.17 bars at 285°C from H_2 activities of samples of hydrothermal fluid, and 0.19 bars H_2 at oxidation states fixed by PPM assemblage values (Chapter 5). Figure A3 indicates that although the system remains anoxic (approximately log $f\ O_{2(g)}$ -85 to -40) over the temperature range tested (0-250°C), $O_{2(g)}$ levels seem to vary with temperature, though on inspection of the forsterite system (Figure A8) it could be argued that it is the fayalite reaction that is responsible for the change and not the temperature..

The values calculated for the oxidation state of the hydrothermal fluid (Figure A3) correspond to the $O_{2(g)}$ fugacities calculated for the PPM assemblage over the same temperature range (Figure 5.1, Chapter 5) indicating that the fluid is buffered at PPM $O_{2(g)}$ fugacities over this temperature range. If temperature alone influenced the $O_{2(g)}$ levels in the system then the curves would be superimposed, but it can be seen that the hydrothermal fluid is depleted of oxygen more so than in the seawater indicating the reductive power of Fe^{II}. Figure A4 indicates from the oxidation states of the seawater and fluid, that the hydrothermal fluid assumed to be produced at the end of the reaction is considerably reduced (-0.5V at 50 C) relative to the original seawater (~ 0.1V at 50°C) used in the model. Ignoring pH contrasts, this is the redox contrast necessary for life as suggested by Russell and Hall (1997). The voltage that could be generated by this contrast is indicated to be from ΔEh ~0.6 volts at 50°C to ΔEh ~ 0.18 volts at 200°C.

The pH of the original seawater varies from slightly alkaline to slightly acidic, but the hydrothermal fluid is initially strongly alkaline at lower temperatures (~ 0-50°C). Taking into consideration that neutral pH varies with temperature, it may be as low as 5.5 (Amend and Shock, 2001), both seawater and fluid are around neutral pH at higher temperatures. The pH contrast (ΔpH) between the seawater and fluid indicated from the graph is about one unit (i.e. ~60 millivolts). The voltage produced from ΔpH contrast and ΔEh contrast are interdependent but are approximately cumulative.

Influence of temperature on forsterite and seawater system

(Table A2, Appendix 1B; Figures A6-A10, Appendix 2)

Under the same conditions, 1 mmol of forsterite, the dominant end-member mineral of olivine, is reacted. The minerals stable here are predominantly brucite ($Mg(OH)_2$) with small amounts of antigorite ($Mg_6[Si_4O_{10}](OH)_8$. Brucite is known to occur in low-temperature hydrothermal veins, and antigorite is another form of serpentine. Although the hydrogen fugacity is shown to increase with temperature, its concentration in the seawater and fluid are the same, indicating that as expected, forsterite does not promote the production of hydrogen: it is the fayalite component which does this. The oxygen fugacity remains constant throughout the temperature range tested (Fig A8). This confirms that the fayalite reaction must be responsible for the change in $O_{2(g)}$ fugacities in Figure A3. Though the oxidation state is indicated to be relatively reduced as in the fayalite model, there is no redox aspect to the calculation and is simply a numerical value generated. The pH of the hydrothermal fluid is initially slightly more alkaline than in the fayalite reaction, but as in the fayalite reaction it drops to about neutral at higher temperatures.

Influence of temperature on fayalite, forsterite and seawater system

(Table A3, Appendix 1B; Figures A11-A15, Appendix 2)

Forsterite and fayalite are introduced into the system in a ratio of 9:1 respectively, resembling the typical composition of olivine. Brucite, magnetite and antigorite are the main mineral products, with brucite the dominant phase. Hydrogen production is favoured at lower temperatures. The influence of the fayalite component can be seen by the variations in $O_{2(g)}$ fugacity. The contrast in oxidation state between the fluid and seawater is ~ 0.1V higher than the fayalite reaction alone (at lower temperatures). The pH of the fluid is initially alkaline but drops to around neutral at higher temperatures (*cf.* Figure 2.20).

Influence of temperature on fayalite, and seawater system, with 0.0003 bars CO_2

(Table A4, Appendix 1B; Figures A16-A22, Appendix 2)

The influence of temperature and current atmospheric $CO_{2(g)}$ levels (0.0003 bars) on the fayalite reaction is tested. In addition, the fugacities of $CH_{4(g)}$ and $CO_{2(g)}$ are compared. Unlike the systems tested in Table A1 and Table A2, the seawater will be slightly acidic due to the exchange of $CO_{2(g)}$ from the atmosphere to the seawater. Figure A22 indicates that this is so with seawater remaining buffered at pH ~5.5 over the temperature range tested. Greenalite and magnetite production is influenced little by the low levels of carbon dioxide present. Hydrogen fugacities in the fluid are unaffected by temperature or low levels of $CO_{2(g)}$. At lower temperatures, where the system is reducing, $CO_{2(g)}$ concentrations in the

fluid are low (as expected, since $CO_{2(g)}$ is the more oxidised phase of the CH_4/CO_2 redox couple), while the $CH_{4(g)}$ concentrations in the fluid are correspondingly high. This relationship between CH_4/CO_2 is reversed for seawater, which is relatively oxidised compared to the hydrothermal fluid. The redox contrast seen in Figure A21 is ~ 0.05V greater at 50°C (ΔEh ~ 0.65V) with the presence of $CO_{2(g)}$

Influence of temperature on fayalite, and seawater system, with 1 bar CO_2

(Table A5, Appendix 1B; Figures A23-A29, Appendix 2)

With increased concentrations of $CO_{2(g)}$ in the model, siderite is stable with quartz between ~50°C to ~100°C, and at lower temperatures between (~0°C-50°C). Magnetite is the only stable phase at temperatures above 150°C. Hydrogen production however is hindered by the presence of higher $CO_{2(g)}$ levels, presumably because CO_2 removes Fe^{2+} from the system. The system remains anoxic, and the CH_4/CO_2 relationship is similar to that under 0.0003 bars of $CO_{2(g)}$.

Influence of temperature on fayalite, and seawater system, with 10 bars CO_2

(Table A6)

(Table A6, Appendix 1B; Figures A30-A36, Appendix 2)

At lower temperatures (<150°C) quartz and siderite are precipitated, magnetite and then graphite at higher temperatures (>150°C). Hydrogen production is not completely impaired, but it can be seen that the system is saturated with CO_2, and CO_2 is only reduced at temperatures above 200°C

Influence of temperature on forsterite, CO_2 and seawater system, with 0.0003 bars CO_2

(Table A7, Appendix 1B; Figures A37-A43, Appendix 2)

Minerals precipitated are mainly brucite and small amounts of antigorite. No hydrogen since no fayalite is present in model. System becomes increasingly reducing as reaction progresses, thus methane levels rise. pH ranges from approximately 6-8 at 150°C, but is much more alkaline at lower temperatures.

Influence of temperature on forsterite, CO_2 and seawater system, with 1 bar CO_2

(Table A8, Appendix 1B; Figures A44-A50, Appendix 2)

Quartz may be stable at lower temperatures (0-100°C), though at higher temperatures it is predominantly magnesite with lesser amounts of antigorite that are stable. No hydrogen production is evident. The system becomes increasingly reducing as the reaction progresses, as do concentrations of methane. However, there is a decrease of CO_2 halfway through the reaction at a temperature of ~150°C possibly due to the production of magnesite. pH is low due to high levels of CO_2.

Influence of temperature on forsterite, CO_2 and seawater system, with 10 bars CO_2

(Table A9, Appendix 1B; Figures A51-A57, Appendix 2)

Siderite is the dominant mineral that is stable at moderate temperatures, though at 250°C only graphite is stable, with minor magnetite. No hydrogen, since no fayalite. As expected, there is a substantial decrease in CO_2 as siderite precipitates. This does not cause a corresponding increase in pH. pH contrast remains at about 1.4 units throughout reaction. Fluid pH ranges from acidic (3.8) at low temperature, to slightly acidic (5.5) at 300°C (see Figure B, Appendix 1A)

Influence of temperature on fayalite, forsterite, CO_2 and seawater system, with 0.0003 bars CO_2

(Table A10, Appendix 1B; Figures A58-A64, Appendix 2)

Mainly brucite, and minor magnetite and antigorite, Hydrogen production evident at low to moderate temperatures. pH ranges from highly alkaline to moderately alkaline.

Influence of temperature on fayalite, forsterite, CO_2 and seawater system, with 1 bar CO_2

(Table A11, Appendix 1B; Figures A65-A71, Appendix 2)

At low to moderate temperatures, quartz is stable. However, at higher temperatures and more CO_2 magnesite is stable with minor talc, magnetite and antigorite. Hydrogen production is evident as before though its generation is not as rapid as in the previous system. Methane is also produced. pH change is moderate and the fluid remains acidic.

Influence of temperature on fayalite, forsterite, CO_2 and seawater system, with 10 bars CO_2

(Table A12, Appendix 1B; Figures A72-A78, Appendix 2)

Predominantly graphite at higher temperature (250°C), some hydrogen produced at low to moderate temperatures. System is reduced relative to initial conditions, pH in the acidic domain.

2.7 Conclusions

This work on iron geochemistry and the olivine-water reaction shows that the reaction products ascertained by thermodynamic calculations confirm that hydrogen is produced when slightly acidic seawater reacts with olivine-bearing oceanic rock. The model confirms that hydrogen production is coupled to the fayalite-water reaction. The basic model indicates that under extremely reducing conditions fayalite can be altered to an iron-rich serpentine (greenalite), and an iron oxide (magnetite).

Overall the results indicated that low-temperature (<150°C) alteration of olivine rock produces serpentine, brucite, quartz, antigorite, and siderite give greater redox and pH contrasts. However, higher temperatures and pressures of CO_2 increase CH_4 production due to the lower oxidation state, and smaller redox and pH contrasts, as well as increased precipitation of carbonates (e.g. siderite, magnesite) and graphite, and lesser magnetite and antigorite

Up to 1 bar $H_2(g)$ is possible (or ~40 mmoles) and at low temperatures when seawater reacts with olivine quantities. The hydrogen production does not seem to be influenced by temperature (except perhaps kinetically). Berndt *et al.* (1996) reported 11.5 mmoles after 48 hours at higher temperatures and pressures (300°C and 500 bar). The results also indicate significant E*h* (0.85 volts) and pH (4.5 units) contrasts at low temperatures, even when CO_2 is introduced into the experiments, though with higher concentrations of CO_2 and temperature the redox contrast is reduced and the pH of the fluid passes from neutral to acidic (Table 1B, Appendix 1A). This suggests that significant energy potential would be available for emergent Life in the Hadean. Increased iron availability would have positive impact on the amount of hydrogen produced. However, increased CO_2 levels would use up any available iron and favour the precipitation of siderite instead unless pH of the ocean remains low.

Though the systems were varied over a range of temperatures and CO_2 pressures, hydrogen was produced in significant quantities in most of the tests. Thus its occurrence at hydrothermal seepages on the early Earth was very likely if the crust contained significant fayalite. In general, the results agree with the findings of Neal and Stanger (1983). Coupled with pH reaching as high as 9.5 at low temperatures, additional support for the presence of low-temperature, methane and hydrogen-rich, alkaline fluids generated from serpentinisation reactions at off-axis ultramafic vent systems as witnessed by Kelley *et al.* (2001) and suggested by MacLeod *et al*, 1994; see Chapter 4). Since the results are in excellent agreement with observed behaviour in natural systems, it is concluded that the model is a successful one and can be extended further if required.

To understand more about the controls on pH, it would have been desirable to look at temperatures above ~300°C, as $HCl^0_{(aq)}$ and some OH^-- bearing aqueous complexes are more stable above this temperature and would impact on pH (Seyfried *et al.*, 1991). However, the thermodynamic data was only valid for up to 300°C and this study is concerned with low- to moderate-temperature hydrothermal systems.

Chapter 3 - Sulfur and Sulfides and the generation of H_2 and HS^-

3.1 Introduction

"...the cradle of Life reeked of hydrogen sulfide...", de Duve (1995)

And so do the laboratories of research groups investigating the origin of Life (much to the discomfort of their colleagues). Sulfur, though toxic in some forms and nasally unpleasant, is present in living systems today as a minor constituent of fats, body fluids, and skeletal minerals. As the comment above by Christian de Duve (1995) indicates, the role of iron and sulfur in living systems may be traced back to the very beginnings of Life. Sulfur complexed with iron is thought to have been absolutely central to the emergence of Life (Russell & Hall, 1997). Perhaps this is because iron and sulfur are unusual elements in that they can form a variety of complex structures due to the wide range of valence states and variable co-ordination ligands available to them. In support of this notion is the fact that iron- and sulfur-reducing bacteria were probably the first organisms that were able to thrive in a hot, anoxic and sulfur-rich environment, such as that of the Hadean Earth, as they do today in hot sulfur springs in the Yellowstone calderas and deep-sea hydrothermal vents. Furthermore, hyperthermophilic Fe(III) reducers were probably among the earliest organisms as indicated in the phylogenetic tree of life (Stetter, 1996; Liu *et al.* 1997; Vargas *et al.* 1998). Important electron-transport reactions in cell metabolism are performed by biological catalysts (ferredoxins) which have an iron-sulfur centre. Iron and sulfur enzymes are present in prokaryotic membranes today and may also have been constituents of early cell membranes. In addition, iron, nickel or other transition-metal sulfides may have played a part in the reductive formation of organic molecules from CO_2, such as activated acetate or pyruvate, that could have initiated a primitive metabolic cycle.

Another useful form of sulfur, in the form of hydrosulfide, is present in thioesters (CH_3COSCH_3). The role of thioesters (or thiol esters) in early metabolism was emphasised by de Duve (1991). Nature currently makes prominent use of thioesters to provide organic resonance structures that are energetically favourable in helping to build longer or cyclic carbon compounds, especially the thioester, acetylcoenzyme A ($CoA\text{-}SCO\text{-}CH_3$). This behaviour can be attributed to the relative lack of stability of their resonance structures compared with ordinary esters, making the carbonyl group in the thioester resonance structure more susceptible to nucleophilic attack. In addition, the carbon-sulfur bond of a thioester is weaker than an ordinary ester. This makes the S-R functional group in a thioester a better leaving group than the O-R group in an ordinary ester. For this reason, thioesters make effective acylating agents. Resonance contributions from resonance structures of

thioesters can also make their α-hydrogens more acidic, thus making thioesters effective alkylating agents (Solomons, 1980). The formation of activated organic compounds such as esters, thioesters and acetates by carbon oxide reduction, in the presence of iron-sulfide, would be able to initiate a primitive autocatalytic metabolic cycle on the early Earth, which would resemble the reversed citric acid cycle (Wächtershäuser, 1988a; Morowitz *et al.*, 2000; Russell and Hall, 1997; Buchanan and Arnon, 1990). A further role for iron and sulfur has been discussed in an analogy of the Earth as a giant photo-electrochemical cell (Russell and Hall, 1997) which proposes that iron sulfide precipitates behave as an electrolyte at submarine hydrothermal seepage mounds.

From the many biological roles of iron and sulfur, such as those cited above, it seems reasonable to conclude that iron and sulfur have many roles to play in metabolism. Thus, the primary focus of this chapter is to determine thermodynamically the availability of the key iron or sulfur compounds, and the energy available from them for the synthesis of organic molecules which can be utilised in a primitive metabolic cycle.

3.1.1 Iron sulfur/hydroxide membranes

One of the major challenges of origin of Life theories is the abiotic synthesis of organic molecules. Friedrich Wöhler (1828) is credited as the first to synthesise organic molecules from inorganic chemicals by heating ammonium cyanate, NH_4CNO, made from inorganic salts, and obtaining urea H_2NCONH_2. Since then, major advances have included the synthesis of amino acids (Miller, 1953), organic sulfur compounds such as methane thiol, CH_3SH, (Heinen and Lauwers, 1996), activated thioesters and acetate (Huber and Wächtershäuser, 1997), and more recently pyruvate CH_3COCOO^-, (Cody *et al.*, 2000, 2001), all via simple inorganic molecules that may have been available on the early Earth. The next hurdle which remains to be overcome is to formulate a hypothesis that explains rigorously how newly formed organic molecules accumulated in significant concentrations on the prebiotic Earth. In addition, for newly formed organic molecules to have any chance of polymerisation and stability, the hypothesis would have to include some method of preventing dispersion and hydrolysis. The solution to these two problems may lie with iron-sulfide/hydroxide compounds.

Russell and Hall (1997) developed a theoretical mechanism that explains how these problems were overcome. They envisage the spontaneous precipitation of ferrous-nickel monosulfide (FeNiS)/ferric oxyhydroxide (FeOOH) bubbles around hydrothermal seepages as hot (≤150°C), alkaline, reduced hydrothermal fluids encounter the cold, mildly oxidised, acidic Hadean Ocean. Minerals likely to be present in such environments include

mackinawite ($Fe_{1+x}S$), greigite (Fe_3S_4), violarite ($FeNi_2S_4$), mixed valence iron-magnesium hydroxides, the double-layered hydroxide greenrust ~$[(Fe^{II},Mg)_2Fe^{III}(OH)_6]Cl$, and siderite, $FeCO_3$ (Russell *et al.*, 1994, 1998, ; Russell and Hall, 2001; *cf.* Huber and Wächtershäuser, 1997; Arrhenius, 1986; Eschenmoser, 1994; Kassim *et al.*, 1982) and may have been primitive metabolic catalysts. Such minerals may have assisted in the development of complex organic molecules, cell formation, and subsequent cell reproduction (Russell and Hall, 1997). Russell and Hall (1997) describe how a ferric/ferrous mineral such as greigite, as $[2(FeS_2)\ (Fe_4^{2.5+}S_4)]$ would, with the help of thiols sequestered from the hydrothermal fluid (Heinen and Lauwers, 1996, 1997), resemble the structure of ferredoxins, which also have variable valence Fe^{2+}/Fe^{3+} cations and a Fe_4S_4 centre ligated to various organic molecules (*cf.* Bonomi *et al.*, 1985). Russell and Hall's ideas are reinforced by the fact that a spectrum of iron-sulfur minerals of increasing oxidation state can be found in aqueous systems: as amorphous iron(II) monosulfide (FeS_{am}), mackinawite (tetragonal FeS), pyrrhotite ($Fe_{(1-x)}S$), greigite (Fe_3S_4), and the stable pyrite FeS_2 (Krupp, 1994; Rickard *et al.*, 2001). Ferredoxins have also been suggested to be the first biological catalysts (Eck and Dayhoff, 1966; Hall *et al.*, 1971; Daniel and Danson, 1995). Daniel and Danson (1995) argue that primitive ('proto-') ferredoxins probably had a more reduced iron-sulfur cubane centre ($[Fe_4S_4]^{2+/+}$) than modern ferredoxins and would be able to catalyse redox reactions at low redox potentials. Further evidence is in the formation of iron-sulfide bubbles at hydrothermal seepages, as revealed in the pyritic boytroids found on a fossilised hydrothermal seepage mound at Tynagh, Ireland (Banks, 1985). Such iron-sulfide boytroidal bubbles would be inflated with medium temperature hydrothermal fluid containing dissolved abiotic organic molecules such as formaldehyde (HCOH) and acetates (RCOOH) (Shock, 1992a; 1996). Other molecules in the fluid would also include hydroxide (OH^-), hydrosulfide (HS^-), thiols (RSH), hydrogen and ammonia. Catalytic transition-metal ions of cobalt and nickel, ultimately derived from 400°C springs at oceanic spreading centres, were also available in the somewhat acidic seawater. The iron-monosulfide bubbles could potentially have performed the most basic bio-cellular functions. For example, they could have helped protect and concentrate organic molecules, and acted as primitive prebiotic semi-permeable cell membranes allowing selective ion-exchange and energy exchange for simple metabolism. In addition, the membrane surface may have helped stereospecific orientation of organic ligands for oligomerisation. Furthermore, the membranous structure would assist the transport of protons and electrons through the membrane, and thus provide the physical setting for a chemiosmotic source of energy whereby 'protons' could be translocated from the acidic ocean to the alkaline interiors as discussed in the following paragraph.

A necessary function of any prebiotic cell would be to maintain the disequilibrium (or in other words, a potential difference) that is required for Life, by the maintenance of an ion gradient (concentration ratio) between two fluids. For example, a concentration ratio (between monovalent ions) of just 10 would generate a membrane potential of 60mV at 27°C (Wrigglesworth, 1997). In living systems, a mechanism is required for transporting ions across a membrane. Redox reactions coupled to the ion transport process provide one such mechanism. Since the ions which are involved in these reactions are often protons, the membrane potential that is generated is known as the proton-motive force (pmf). As pH is a measure of proton concentration, a pH difference (ΔpH) between two fluids is a concentration ratio of protons which can generate a membrane potential. The ΔpH between the hydrothermal fluid (pH ~9) and seawater (pH ~4.5) provides approximately ~240 mV to contribute to the energy for Life in the Russell-Hall model (one pH unit = ~60mV, Garrels and Christ (1965)). pH experiments with model fluids have demonstrated the precipitation of an iron-sulfide (FeS) barrier and the enforced separation of fluids by such a barrier (Russell *et al.*, WWW, 2001, Figures 9e, 14). The recorded voltages were similar to the pmf measured between fluids in living systems. Additionally the experiments demonstrated that this pmf can be maintained from a few hours to several days. Redox potentials (ΔEh) would have resulted from the redox contrast between the mildly-oxidised ocean and highly-reduced hydrothermal fluid (ΔEh results from the redox contrast between the oxidised Fe^{3+} produced by the photolytic oxidation of Fe^{2+} in the ocean and the reduced hydrothermal hydrogen from the olivine-water reaction described in Chapter 2 (redox couple Fe^{2+}/Fe^{III} vs. H_2/H^+). The redox potential ranges from ~300 mV to ~700 mV across the precipitated membrane and contributes to the overall disequilibrium (for example, the iron(II)monosulfide and greigite couple, FeS/Fe_3S_4, ΔEh = approx. -0.5 V, at pH 7 and 120°C, Russell *et al.*, 1998). The cumulative potentials generated would be more than sufficient to drive cellular metabolism (de Duve, 1991). The reader is referred to Russell *et al.* (1994, 1998) for a more detailed description of the chemistry taking place within or on the surface of the membranes. In these papers, the catalytic activity of membrane constituents (for example, transition metal ions, Fe>>Ni>Co, in mineral structures such as mackinawite), and the mechanisms by which CO or CO_2 may be reduced to organic compounds are discussed in the context of the Russell and Hall hypothesis.

Rickard (1995) has established that although iron(II)monosulfides are initially precipitated as cubic FeS in low temperature aqueous conditions, they rapidly crystallise to form mackinawite (Rickard, 1995). Mackinawite can then be subsequently oxidised to greigite, or further oxidised to pyrite. The catalytic potential of hydrothermal fluid

constituents (such as aldehydic carbonyl groups) determine the oxidation state achieved, and the amount of greigite or pyrite precipitated (Rickard *et al.*, 2001). Aldehyde adsorption prevents H_2S oxidation to pyrite because it is the iron and not the sulfur that is oxidised, thus producing greigite. In the absence of aldehyde, pyrite is generated, as sulfur but not the iron, is oxidised. Thus, bonding of the aldehyde ligands to the inner membrane surface may have protected the membrane from being oxidised to pyrite. Concentrated thus it may have polymerised and assisted in the eventual organic take-over of the membrane.

3.1.2 Ferric hydroxides/oxyhydroxides

At low temperatures and near-neutral pH, ferric iron's solubility is minimal (Figure 2.4, §2.4.1). Oxidation by photolysis would result in the kinetically favoured formation of amorphous ferric oxyhydroxides (for example, ferrihydrite, $Fe(OH)_3$). One such ferric oxyhydroxide, greenrust (Equation *3.1*), can comprise a "precipitate-membrane" at high pH (Turner, D. *pers. comm.*, 1999). In laboratory simulations of the mixing of early hydrothermal fluid using Na_2S and early seawater using $FeCl_2$ (Russell, Hall and Turner, 1989), the precipitate formed in the resultant alkaline fluid (pH>10) was analysed by X-ray diffraction (XRD). The peaks produced from the XRD analysis matched those of the iron oxyhydroxide mineral, greenrust, $Fe^{II}_2Fe^{III}(OH)_6Cl$ as well as of mackinawite. Later, it was demonstrated that greenrust can catalyse the formation of ribose-2,4-biphosphate from glycolaldehyde phosphate and glyceraldehyde-2-phosphate (Krishnamurthy *et al.*, 1999), synthesised from formaldehyde. In addition, iron oxyhydroxides have been shown to adhere to extracellular polymers of cells of organisms that live off energy from the oxidation of ferrous iron in low oxygen environments in the Earth's crust (Barker *et al.*, WWW, 2001).

The stability of greenrust with respect to redox conditions is examined to provide further insights into its behaviour. There are several descriptions of greenrust in the literature. Some contain the carbonate group ($Fe_6(OH)_{12}CO_3$) rather than the oxyhydroxyl group (-OOH), one likely formula considering the carbonic nature of the early ocean. The general formula of the double layer hydroxide minerals is given in Equation *3.1*,

$$\left[M^{2+}_{3-x}M^{3+}_{x}(OH)_6\right]\left\{\frac{x}{n}A^{n-}.mH_2O\right\} \qquad (3.1)$$

where m~ 4, square brackets denote the main hydroxide layer, and curly brackets denote the hydrate interlayer of mono and divalent anions (A^- bicarbonate, A^{2-} carbonate). However, the thermodynamic data for the oxyhydroxide greenrust that is to be expected to form in strongly reducing conditions were not available. Instead, the data for the carbonate greenrust

(already present in the database, Figure 3.1) were modified to reflect the oxyhydroxide greenrust (Figure 3.2). The molecular weight for the oxyhydroxide (573.1842g, Figure 3.2) and the molar volume (158.58cc, Figure 3.2) was calculated. Since the carbonate (Figure 3.1) was not required to form the oxyhydroxide, it was removed from the calculations (Figure 3.2). Two options were available to estimate the equilibrium constant for greenrust. The first would be to calculate the constants for each species in the reaction and then summing them to give an overall constant for greenrust, but theoretical constants have to be supported by experimentally obtained values. Alternatively, the equilibrium constant (as well as Fe^{++} availability) could be varied and the effect on greenrust production in the chosen system can be observed. The second option was chosen since the true value of the equilibrium constant for greenrust is uncertain. The value of the equilbrium constant for the oxyhydroxide was set to that of the carbonate for a temperature of 25°C, thus all experiments were limited to this temperature constraint. The new oxyhydroxide was renamed to *rustgreen* to differentiate it from the carbonate greenrust in the database (Figure 3.2) and entered into the *thermo.com.v8.r6.full* database. The calculations can now include *rustgreen.* The script for the iron stability diagram (§2.4.1, Figure 2.3) was rerun to read the updated database. On completion, the calculations showed that under alkaline and reducing conditions, magnetite precipitation is possible but perhaps with some $Fe(OH)_3^-$. Assuming that $Fe(OH)_3^-$ would be unlikely to form, it was excluded from the calculations and the script was rerun. The results showed that with an equilibrium constant (log K) equal to 42.535, STP, *rustgreen* is likely to be precipitated under certain *Eh*-pH conditions (Figure 3.4) given that $Fe(OH)^{3-}$ production is hindered in some way. In further experiments, an increase in the value of log K resulted in a decrease of the *rustgreen* stability field. A decrease in log K resulted in an increase in the stability of *rustgreen.* A log K of 47.54 resulted in no *rustgreen* at all. An increase in Fe^{++} activity resulted in an increase in the *rustgreen* field, whereas a decrease in Fe^{++} activity resulted in a decrease in the *rustgreen* field.

```
Greenrust                          type=carbonate
formula= Fe6(OH)12CO3
mole vol.=  158.8 cc          mole wt.=  599.1788 g
5 species in reaction
4.000 Fe++                  -13.000 H+            12.000 H2O
1.000 HCO3-                   2.000 Fe+++
500.0000   42.535   500.0000   500.0000
500.0000  500.0000  500.0000   500.0000
```

Figure 3.1. Entry for the carbonate greenrust in the database *thermo.com.v8.r6.full.*

```
Rustgreen                                type=hydroxide
     formula= Fe6(OH)14
     mole vol.=  158.58 cc                mole wt.=  573.1842 g
     4 species in reaction
4.000 Fe++                    -14.000 H+                    14.000
H2O
2.000 Fe+++
          500.0000   42.535   500.0000   500.0000
          500.0000  500.0000  500.0000   500.0000
```

Figure 3.2. New entry for the oxyhydroxide greenrust, renamed to rustgreen to prevent conflict in the modified database, *thermo.com.v8.r6.full.*

ACT2 script for Figure 3.4

```
1.    data = rustgreen.thermo.com.v8.r6.full
2.    swap e- for O2(aq)
3.    diagram Fe++ on Eh vs pH
4.    log activity main = -6
5.    x-axis from 0 to 14
6.    y-axis from -1 to 1.5
7.    suppress Fe(OH)3-
```

Figure 3.3. Input code for the ACT2 program, modified from Figure 2.3 by substituting the *rustgreen.thermo.com.v8.r6.full* database.

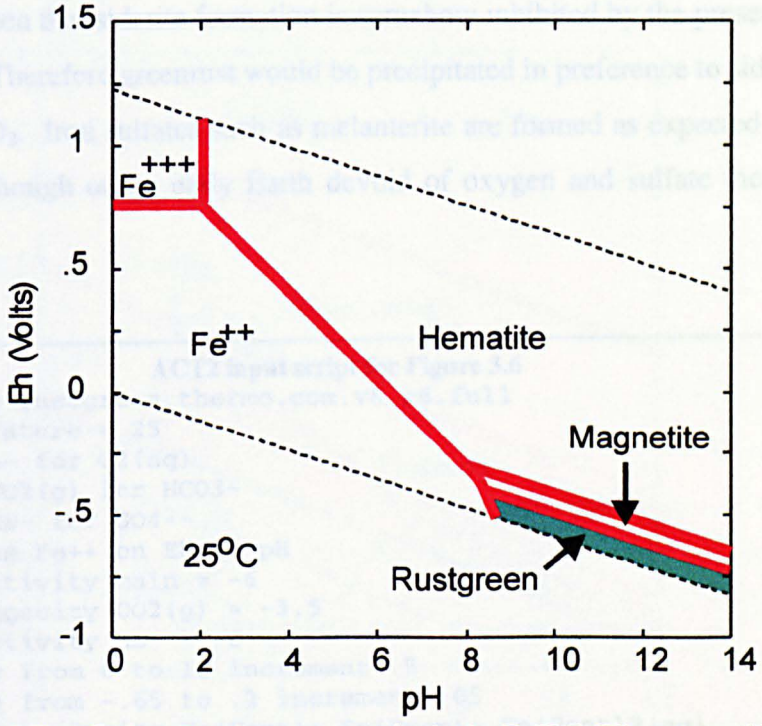

Figure 3.4. Stability of minerals and aqueous species in the Fe-H_2O-CO_2 system with respect to *Eh* and pH at STP. Total activity $Fe^{++} = 10^{-6}$, total activity $SiO_{2(aq)} = 10^{-6}$. $Fe(OH)^{3-}$ formation suppressed.

Since the database now includes thermodynamic data for the oxyhydroxide greenrust, Figure 3.4 suggests that the oxyhydroxide greenrust (*rustgreen*) may perhaps be thermodynamically stable at low temperatures (25°C) in alkaline and reduced conditions, but

note that magnetite too could be precipitated under a very narrow set of *Eh*-*p*H conditions (the magnetite field in Figure 3.4 has been slightly enlarged for clarity). However, the calculations have thus far not considered the early atmosphere, and the sulfide that would be present in hydrothermal fluids. The presence of low to high pressures of CO_2 and small amounts of sulfide are considered in the Fe-CO_2-S system in the next section.

3.1.3 The Fe-CO_2-S system

Figure 3.6 and 3.7 display the Fe-CO_2-S system. The system is identical to the Fe-CO_2 system in Figure 2.6 (§2.4.2) except that in Figure 3.6, trace amounts of sulfide are added (activity $HS^- = 10^{-6}$), and later in Figure 3.7, sulfide concentration is increased by one order of magnitude (activity $HS^- = 10^{-5}$). Pyrite, along with some complex organic iron compounds would not be expected to form in reduced conditions, and are therefore excluded from this calculation (Figure 3.5). The graph in Figure 3.6 displays possible effects of trace amounts of HS^- in a system containing iron, carbon dioxide and water. The system is at low temperature (25°C) and at low concentrations of CO_2 (0.0003 bars). It can be seen that in alkaline conditions, troilite (or more likely, pyrrhotite), or perhaps other FeS minerals such as greigite or mackinawite (Rickard, 1995) may be precipitated along a possible reaction path and it can be seen that siderite formation is somehow inhibited by the presence of small amounts of sulfur. Therefore greenrust would be precipitated in preference to siderite at such low pressures of CO_2. Iron sulfates such as melanterite are formed as expected in the more oxidising regions, though on an early Earth devoid of oxygen and sulfate their formation would be unlikely.

ACT2 input script for Figure 3.6

```
data = rustgreen.thermo.com.v8.r6.full
temperature = 25
swap e- for O2(aq)
swap CO2(g) for HCO3-
swap HS- for SO4--
diagram Fe++ on Eh vs pH
log activity main = -6
log fugacity CO2(g) = -3.5
log activity HS- = -6
x-axis from 6 to 12 increment .5
y-axis from -.65 to .2 increment .05
suppress  Pyrite Fe(Pent)+ Fe(Prop)+ Fe(Pent)2(aq)
suppress  Fe(But)+ Fe(But)2(aq) Fe(Prop)2(aq)
```

Figure 3.5. ACT2 input script for Figure 3.6 modifying the Fe-CO_2 system in §2.4.2 by including a trace amount of sulfide, (total activity $HS^- = 10^{-6}$). Note that pyrite is suppressed as well as some complex organics.

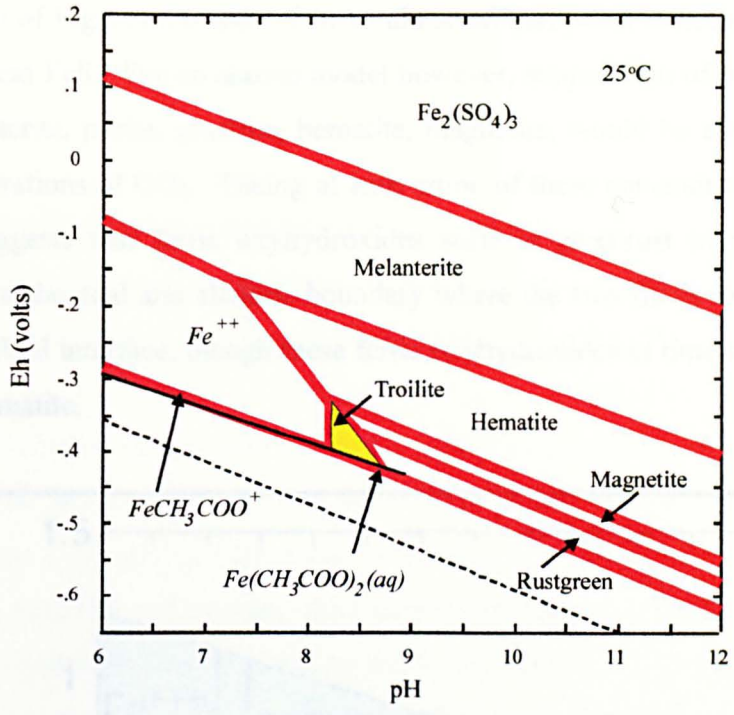

Figure 3.6. Stability of minerals and aqueous species in the Fe-H_2O-CO_2-S system with respect to *Eh* and pH at STP. Total $CO_{2(g)}$ = 0.0003 bars, total activity $Fe^{++} = 10^{-6}$, total activity $HS^- = 10^{-6}$. Pyrite and some complex iron organic molecules suppressed (see Figure 3.5). Melanterite is a hydrated iron sulfate, ($FeSO_4.7H_2O$)

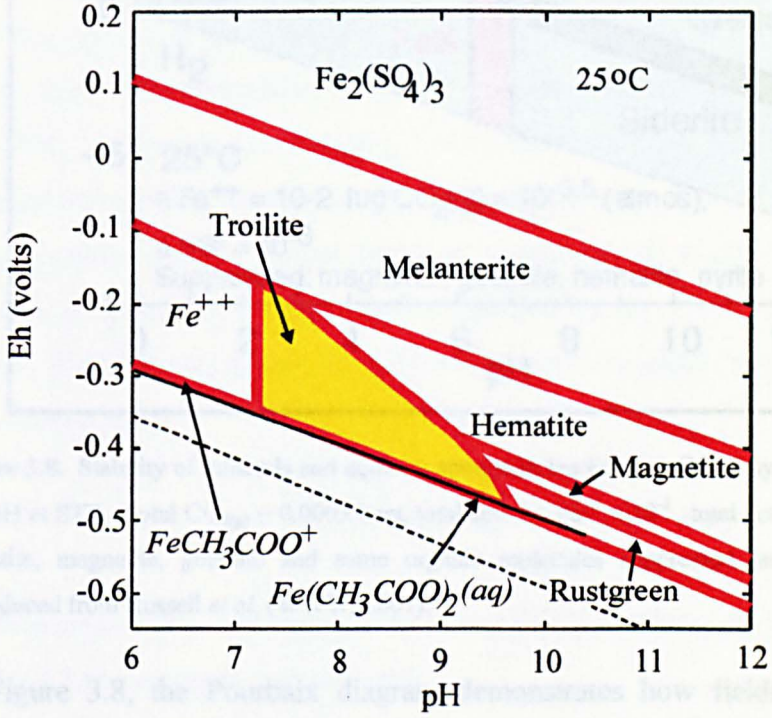

Figure 3.7. Stability of minerals and aqueous species in the Fe-H_2O-CO_2-S system with respect to *Eh* and pH at STP. Total $CO_{2(g)}$ = 0.0003 bars, total activity $Fe^{++} = 10^{-6}$, total activity $HS^- = 10^{-5}$. Pyrite and some organic molecules suppressed (see Figure 3.5).

The activities of sulfide used in Figure 3.6 and 3.7 were 10^{-6} and 10^{-5} respectively. On comparison of Figures 3.6 and 3.7, it would seem that lower concentrations of available sulfide mean less FeS. For an anoxic model however, suppression of oxidised components such as melanterite, pyrite, goethite, hematite, magnetite, would be appropriate as well as higher concentrations of CO_2. Taking at least some of these constraints into consideration, Figure 3.8 suggests that ferric oxyhydroxides such as greenrust may coexist with iron monosulfides at the acid and alkaline boundary where the two fluids meet at the seawater-hydrothermal fluid interface, though these ferric oxyhydroxides in time would convert to the more stable hematite.

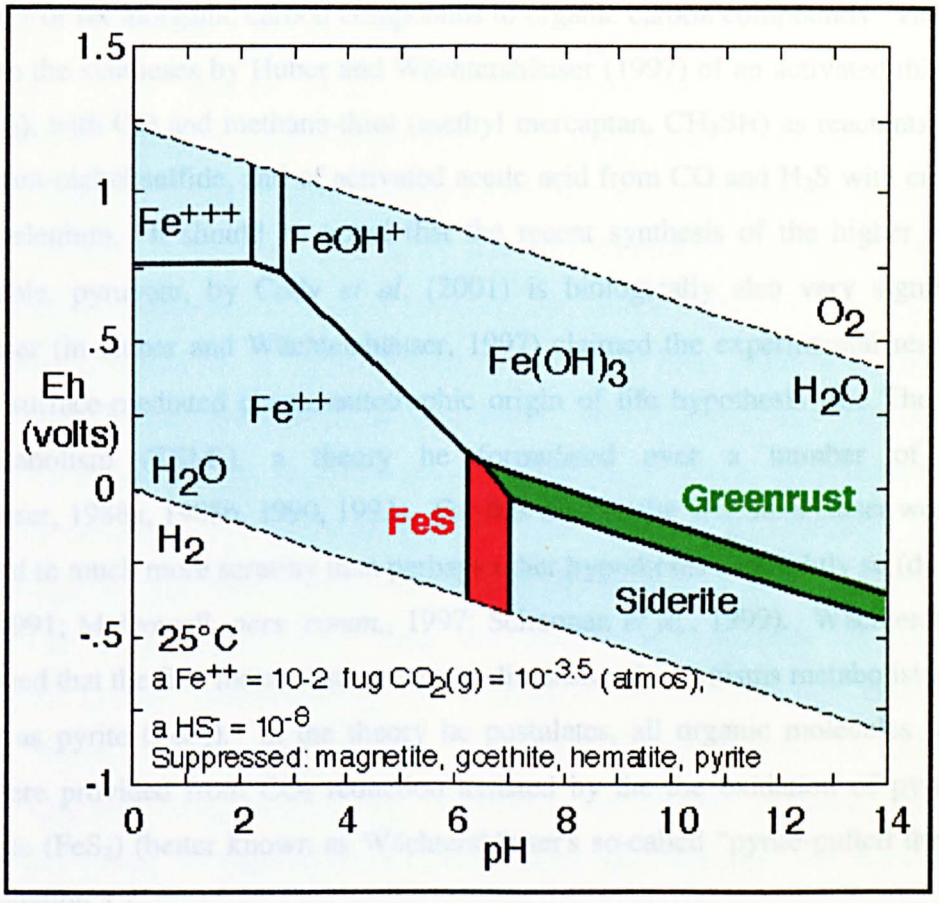

Figure 3.8. Stability of minerals and aqueous species in the Fe-H_2O-CO_2-S system with respect to *Eh* and pH at STP. Total $CO_{2(g)}$ = 0.0003 bars, total activity $Fe^{++} = 10^{-2}$, total activity $HS^- = 10^{-8}$. Pyrite, hematite, magnetite, goethite and some organic molecules suppressed (see Figure 3.5). Figure reproduced from Russell *et al.* (WWW, 2001).

In Figure 3.8, the Pourbaix diagram demonstrates how fields of greenrust and mackinawite (FeS) are likely to be met as alkaline fluids interface with the acidulous ocean. Using Geochemist's Workbench (Bethke 1998), a maximum concentration of HS^- of ~10 millimoles was calculated. Hematite is suppressed to show $(FeOH)_3$, which is taken to control Fe-solubility in near surface environments. Fields of

magnetite, Fe_3O_4 and siderite, $FeCO_3$ are shown. Pyrite, (FeS_2) is thermodynamically stable but 'FeS' phases are favoured kinetically (Rickard, 1995) therefore it is suppressed.

3.1.4 Carbon fixation experiments involving transition-metal sulfides

In many origin of life hypotheses and experiments (Wächtershäuser, 1988a, 1998b; Hennet *et al.*, 1992; Russell and Hall, 1997; Russell *et al.*, 1998; Huber & Wächtershäuser, 1997; Heinen & Lauwers, 1996, 1997; Schoonen *et al.*, 1999; Cody *et al.*, 2000, 2001) transition metal-sulfides such as iron and nickel-sulfides are used to promote catalysis in the effort to reduce or fix inorganic carbon compounds to organic carbon compounds. The most impressive are the syntheses by Huber and Wächtershäuser (1997) of an activated thioester, (CH_3COSCH_3), with CO and methane-thiol (methyl mercaptan, CH_3SH) as reactants in the presence of iron-nickel sulfide, and of activated acetic acid from CO and H_2S with catalytic amounts of selenium. It should be noted that the recent synthesis of the higher energy though unstable, pyruvate, by Cody *et al.* (2001) is biologically also very significant. Wächtershäuser (in Huber and Wächtershäuser, 1997) claimed the experimental results as proof of his surface-mediated chemo-autotrophic origin of life hypothesis (the Theory of Surface Metabolism (TSM)), a theory he formulated over a number of years (Wächtershäuser, 1988a, 1988b, 1990, 1992). For this reason, the Wächtershäuser work has been subjected to much more scrutiny than perhaps other hypotheses and rightly so (de Duve and Miller, 1991; McDowall, *pers. comm.*, 1997; Schoonen *et al.*, 1999). Wächtershäuser (1988b) claimed that the first metabolists were two-dimensional organisms metabolising on a surface such as pyrite (FeS_2). In the theory he postulates, all organic molecules for the metabolist were provided from CO_2 reduction assisted by the the oxidation of pyrrhotite (FeS) to pyrite (FeS_2) (better known as Wächtershäuser's so-called "pyrite-pulled theory"), notionally Equation *3.2*,

$$2FeS + 2H_2S + CO_2 \rightarrow 2FeS_2 + CH_2O + H_2O \qquad (3.2)$$

In fact, Wächtershäuser has only managed to reduce CO (Equation *3.3*), and not reduce CO_2 as in Equation *3.2* and no pyrite was reported.

$$CH_3SH + CO + H_2O \rightarrow CH_3COOH + H_2S \qquad (3.3)$$

Later, Wächtershäuser (1997) proposed that submarine hydrothermal environments or volcanic settings would be ideal environments for the reactions in his hypothesis to proceed.

The Theory of Surface Metabolism is novel, visionary, and a fruitful advance on organic 'broth' or 'soup' theories, but the 'proofs' offered by Wächtershäuser (2000) in support of the pyrite-pulled theory are not fully convincing. Furthermore, many of the remaining assertions in the Theory of Surface Metabolism have still to be demonstrated. The surface-catalysed reduction of CO_2 is purported to have been demonstrated in various experiments. However, in a paper by Schoonen *et al.* (1999), it is argued that the mechanics of the pyrite-pulled mechanism have never been adequately tested and that only two recent experiments have a bearing on the pyrite-pulled mechanism of CO_2 reduction, referring to the experiments published by Keefe *et al.* (1995) and Heinen and Lauwers, (1996, 1997). In any case, it is difficult to envisage a surface mechanism when the products in these experiments have been found in the reaction solution or 'broth', rather than on the pyrite surface (McDowall, WWW, 1998; as quoted *in* Russell *et al.*, 1998 website) the "broth" being a feature Wächtershäuser (1988a, 1988b) ardently rejects as a source of organic molecules in his Theory of Surface Metabolism. The theory was also claimed to be suspect from what was then understood about surface catalysts (de Duve and Miller, 1991), but others disagree pointing out that peculiarities in ligand sphere bonds might help promote a myriad of reactions on a pyrite surface (McDowall, WWW, 1998). Other concerns regarding the TSM are the lack of relevance of the experimental conditions in the Huber & Wächtershäuser (1997) study to submarine hydrothermal systems. In addition, Wächtershäuser (1988a), asserts that the pyrite-pulled mechanism was energetically favourable at room temperature, and more so at higher temperatures such as those in hydrothermal environments. Wächtershäuser's (1988) thermodynamic calculations to substantiate this claim were unconvincing, in part due to performing the free energy calculations at STP (25°C / 1 atmosphere) only, and using what is now believed to be suspect thermodynamic data (Schoonen *et al.*, 1999). In light of these discrepancies, the theoretical and experimental evidence that Wächtershäuser has cited in favour of his hypothesis seem unsatisfactory for some critical stages of the Theory of Surface Metabolism.

Perhaps Wächtershäuser's theory of carbon dioxide reduction by a surface mechanism has been most convincingly addressed in the thermodynamic evaluation by Schoonen *et al.* (1999). Schoonen *et al.* (1999) re-evaluate the thermodynamic feasibility of the pyrite-pulled reduction of CO_2, and attempt to provide an explanation for the results of Keefe *et al.* (1995) and Heinen and Lauwers (1996). Schoonen *et al.*'s (1999) pretext for the investigation stems from the inconsistencies in Wächtershäuser's theory that are outlined above. In the next section, Schoonen *et al.*'s (1999) methods are discussed and investigated.

3.2 The reducing potential of the pyrrhotite-H_2S/pyrite redox couple

3.2.1 Schoonen's critique of Wächtershäuser's pyrite-pulled hypothesis

The redox equilibria showing the oxidation of pyrrhotite to pyrite suggested by Wächtershäuser (1988a, 1988b) can be written as shown in Equation *3.4*:

$$FeS_{(pyrrhotite)} + H_2S_{(aq)} \rightleftharpoons FeS_{2(pyrite)} + H_{2(g)} \qquad (3.4)$$

Wächtershäuser (1998a, 1998b) asserts that the oxidation of FeS to FeS_2 in Equation *3.4* is the redox reaction that is coupled with, and provides the energy for, carbon fixation for formation of activated organic molecules that could be initiated into a primitive metabolic cycle. He suggests that reaction *3.4* is favourable at room temperature and would provide even more reducing energy at higher temperatures. In contrast, the reduction of CO_2 by the energy available from the pyrrhotite-H_2S/pyrite redox couple was demonstrated theoretically by Schoonen *et al.* (1999) to be difficult at high temperatures and at low activities of $H_2S_{(aq)}$, but much more facile at low temperatures coupled with high activities of $H_2S_{(aq)}$.

My objective was to simplify and recast the diagram presented in Schoonen *et al.* (Figure 3.15b, from Schoonen *et al.*, 1999), to review their result and conclusion, and to compare results of thermodynamic calculations generated by the SUPCRT92 code (Johnson *et al.*, 1992) used in their investigation, with the results obtained by the Geochemist's Workbench, GWB (Bethke, 1998).

3.2.2 Geochemist's Workbench Approach

Equation *3.4* can be rearranged to show how the reducing potential of the FeS-H_2S/FeS_2 redox couple can be described in terms of the $H_{2(g)}$ fugacity ($f H_2$) of the reaction (Equation *3.5*).

$$fH_2 = \frac{a_{pyrrhotite} \cdot a_{H_2S}}{a_{pyrite}} K \qquad (3.5)$$

To enable the measurement of the reduction potential of the FeS-H_2S/FeS_2 redox couple, the Geochemist's Workbench (GWB) subprogram 'ACT2' was used to generate fugacity-activity plots (Figures 3.10-3.14) to reflect Equation *3.5*. These plots show how both hydrogen gas (log $f H_{2(g)}$), and dissolved hydrogen sulfide (log $a H_2S_{(aq)}$) influence the distribution of iron and sulfur minerals in an aqueous system (1kg H_2O) with an activity of pyrite = 1 (since activity coefficients for uncharged species are close to unity activity), over a

temperature range of 50-250°C. By extrapolating a line from where the log activity of $H_2S_{(aq)}$ is equal to -3 (~0.001 millimoles, Figure 3.10), it is possible to infer directly from each plot the fugacity of $H_{2(g)}$ at the FeS/FeS_2 (pyrrhotite/pyrite) phase boundary where FeS/FeS_2 are at equilibrium (in other words, when reaction *3.4* has gone to completion at the specified temperature). Note that the log $f\,H_{2(g)}$ values in Figure 3.10 and 3.11 are outwith the stability field of water. However, this need not be of concern as $H_{2(g)}$ fugacity is only being used as a numeric value to measure the reduction potential; it is not implied that hydrogen gas will evolve in the amounts shown on the graphs .

ACT2 script for Figures 3.10 to 3.14

```
1. data = thermo.dat
2. temperature = 50, 100, 150, 200, 250C
3. swap Pyrite for Fe++
4. swap H2(g) for O2(aq)
5. swap H2S(aq) for SO4--
6. diagram Pyrite on H2(g) vs H2S(aq)
7. log activity main = 0
8. x-axis from -9 to 1 increment .5
9. y-axis from -15 to 2 increment 1
10.suppress  Troilite FeO(c)
```

Figure 3.9. ACT2 script for Geochemist's Workbench (Bethke, 1998), used to generate Figures 3.10 to 3.14. The model reflects the distribution of iron-sulfur minerals with respect to temperature changes (line 2). Troilite is suppressed to favour the stability of pyrrhotite in the plots. $FeO_{(c)}$ is suppressed to favour stability of magnetite.

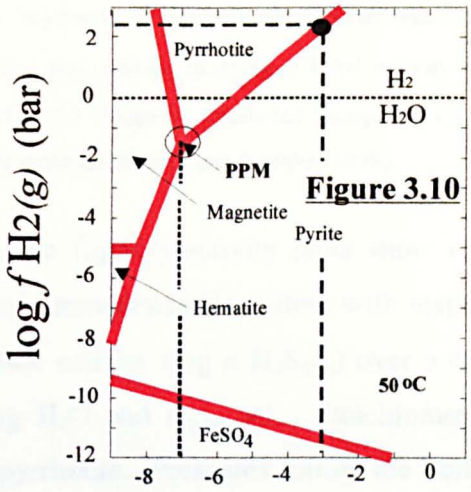

Figure 3.10

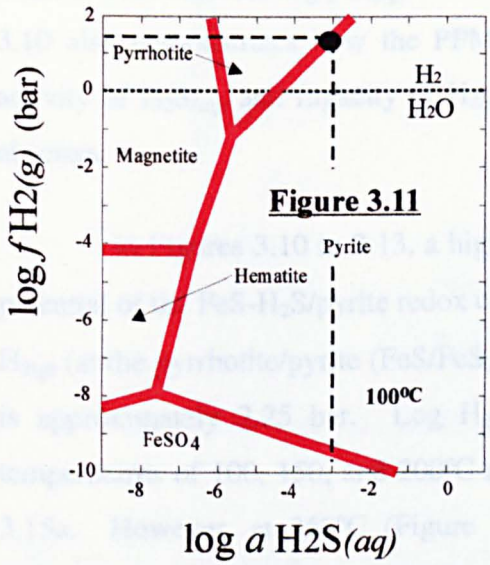

Figure 3.11

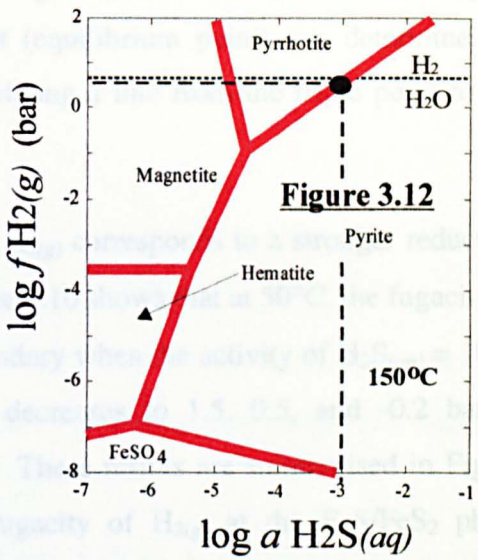

Figure 3.12

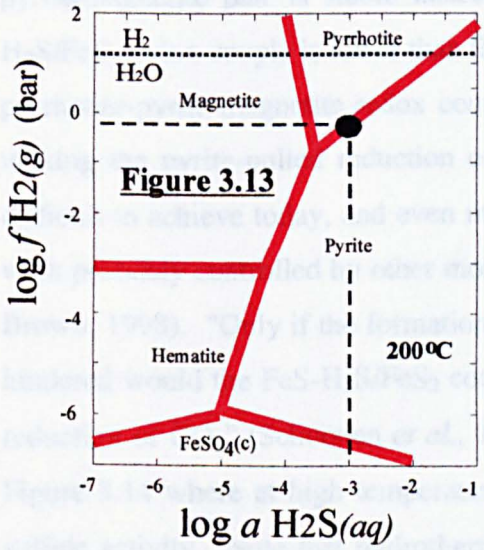

Figure 3.13

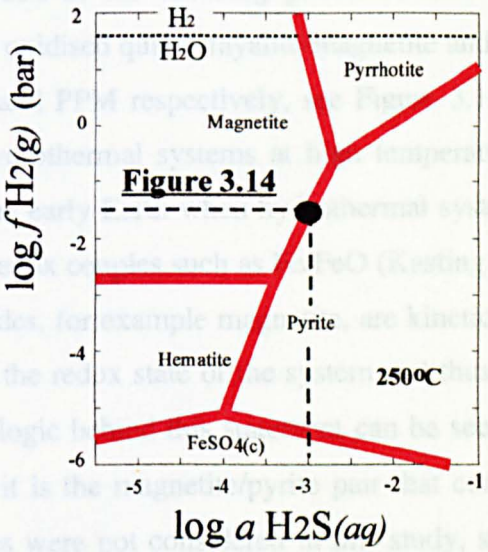

Figure 3.14

Figures 3.10 to 3.14. Stabilities of minerals and aqueous species in the Fe-H_2O-S system with respect to the fugacity of $H_{2(g)}$ and activity of $H_2S_{(aq)}$. Total activity of pyrite =1. Troilite and $FeO_{(c)}$ formation suppressed. All diagrams produced using the Geochemist's Workbench subprogram 'ACT2' and the GWB database *thermo.dat* (Bethke, 1998).

In Figures 3.10 to 3.13, the fugacity-activity plots show the stability of iron and sulfur minerals in an equilibrated thermodynamic system with respect to hydrogen fugacity ($\log f H_{2(aq)}$) and hydrogen sulfide activity ($\log a H_2S_{(aq)}$) over a temperature range of 50-250°C. Each model contains 1kg H_2O and a_{pyrite} =1. Stoichiometric FeS (troilite) formation is suppressed in favour of pyrrhotite. Pressures follow the boiling curve of water (Appendix 1A, Figure B). Dotted lines represent the water stability limits ($H_{2(g)}/H_2O_{(aq)}$ boundary). Dashed lines indicate $\log f H_{2(g)}$ at the point where $\log a H_2S = -3$ (0.001 mmoles). Figure 3.10 also demonstrates how the PPM triple point (equilibrium point) can determine the activity of $H_2S_{(aq)}$ and fugacity of $H_{2(g)}$ by extrapolating a line from the triple point to the abscissa.

In Figures 3.10 to 3.13, a higher value of $H_{2(g)}$ corresponds to a stronger reduction potential of the FeS-H_2S/pyrite redox couple. Figure 3.10 shows that at 50°C, the fugacity of $H_{2(g)}$ (at the pyrrhotite/pyrite (FeS/FeS_2) phase boundary when the activity of $H_2S_{(aq)} = 10^{-3}$), is approximately 2.25 bar. Log $H_{2(g)}$ fugacity decreases to 1.5, 0.5, and -0.2 bar at temperatures of 100, 150, and 200°C respectively. These results are summarised in Figure 3.15a. However, at 250°C (Figure 3.14), the fugacity of $H_{2(g)}$ at the FeS/FeS_2 phase boundary (when the activity of $H_2S_{(aq)} = 10^{-3}$) is not available since at this temperature, the pyrite/magnetite pair is stable instead. Above 250°C, the reducing power of the FeS-H_2S/FeS_2 redox couple is lower than the relatively oxidised quartz-fayalite-magnetite and the pyrrhotite-pyrite-magnetite redox couples (FMQ and PPM respectively, see Figure 3.15b), making the pyrite-pulled reduction of CO_2 in hydrothermal systems at high temperatures difficult to achieve today, and even more so on the early Earth when hydrothermal systems were probably controlled by other more reduced redox couples such as Fe/FeO (Kasting and Brown, 1998). "Only if the formation of iron-oxides, for example magnetite, are kinetically hindered would the FeS-H_2S/FeS_2 couple control the redox state of the system and thus the reduction of CO_2" (Schoonen *et al.*, 1999). The logic behind this statement can be seen in Figure 3.14 where at high temperatures (250°C) it is the magnetite/pyrite pair that control sulfide activity. Note that hydrothermal pressures were not considered in this study, since Schoonen *et al*, (1999) also demonstrate that the pressure dependence of reaction *3.4* is minimal compared to that of temperature (Table 3.1). Figure 3.10 also indicates that at 50°C the activity of $H_2S_{(aq)}$ at the PPM triple point (the point at which all three lines of pyrrhotite,

pyrite and magnetite meet) is $\sim 10^{-7.1}$. Using the PPM triple point, the activity of $H_2S_{(aq)}$ can be seen to increase as temperature increases from 100°C to 250°C, by approximately four orders of magnitude to $\sim 10^{-2.7}$.

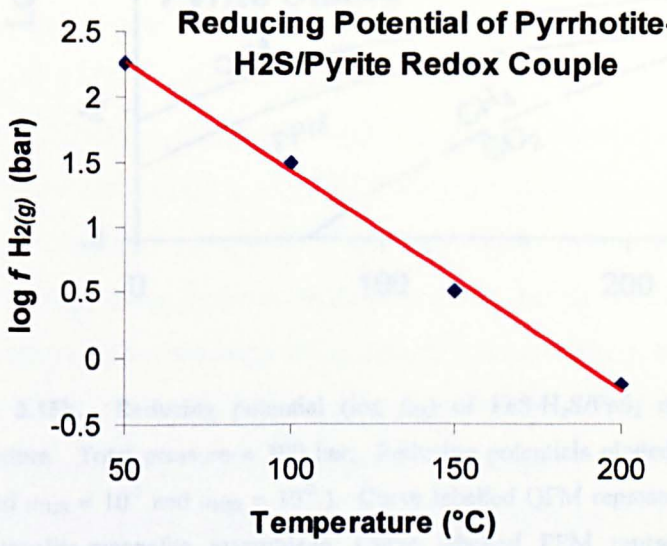

Figure 3.15a. Reducing potential (log f_{H2}) of the FeS-H_2S/FeS_2 redox couple as a function of temperature. Activity of $H_2S_{(aq)} = 10^{-3}$, total activity of pyrite = 1.

The results summarised (Figure 3.15a) from Figures 3.10 to 3.14, show that the pyrite-pyrrhotite-H_2S redox system is less exergonic (lower fugacity H_2) at higher temperatures.

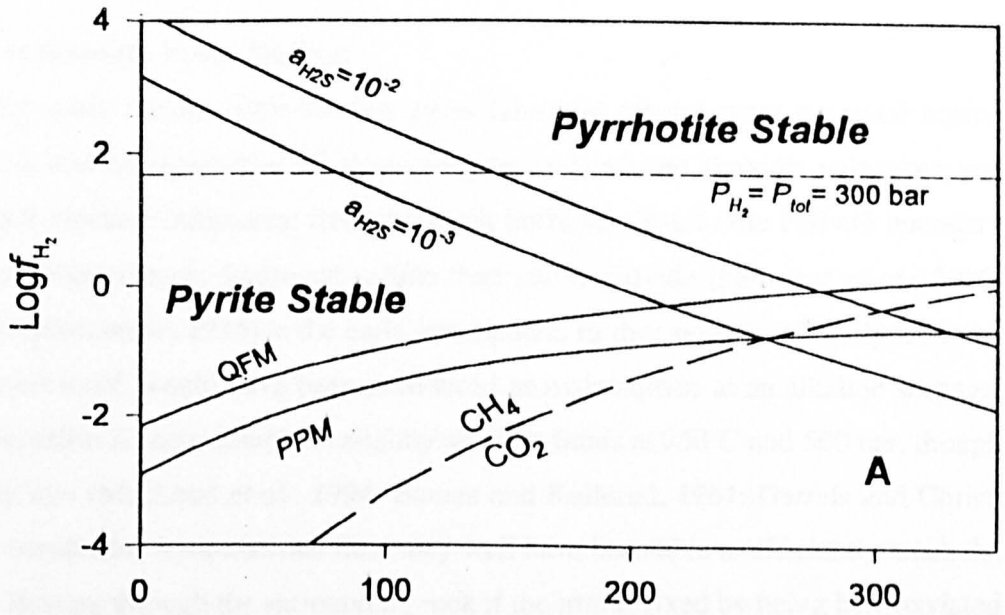

Figure 3.15b. Reducing potential (log f_{H2}) of FeS-H_2S/FeS_2 redox couple as a function of temperature. Total pressure = 300 bar. Reducing potentials plotted for 2 concentrations of $H_2S_{(aq)}$ (labelled $a_{H2S} = 10^{-3}$ and $a_{H2S} = 10^{-2}$). Curve labelled QFM represents the reducing potential of the quartz-fayalite-magnetite assemblage. Curve labelled PPM reprsents the reducing potential of pyrrhotite-pyrite-magnetite assemblage. Curve labelled CO_2-CH_4 indicates the fugacity of H_2 in equilibrium in solution with equal activities of dissolved CH_4 and CO_2. Figure reproduced from Schoonen *et al.* (1999), calculated using the SUPCRT92 modelling code (Johnson *et al.*, 1992).

Confident that Schoonen *et al.*'s results from the SUPCRT92 program can be replicated, and having verified the integrity of the results obtained by the GWB software, the question that remains to be answered in this chapter is: *how much sulfide can be provided by a hydrothermal fluid at around 150°C by the oxidation of pyrrhotite?* In the next section the availability of sulfur from hydrothermal systems in the Hadean is discussed.

3.3. Controls on Sulfur Availability

A possible difficulty for the Russell and Hall (1997) hypothesis is in producing the amount of reduced sulfur (in the form of the hydrosulfide, HS^-, that is stable in an alkaline hydrothermal fluid; see Krauskopf, 1967, p51) that would be available from hydrothermal systems in the Hadean to enable the formation of an iron-sulfide membrane. For an iron-monosulfide membrane to form at all, and depending on iron concentration, (MacLeod *et al.*, 1994), laboratory tests indicate that at least 250 millimoles of hydrosulfide would be required to form 'solid' membranous compartments. However, weak iron-sulfide membranes do

precipitate using ~10 millimoles of Na_2S as a model hydrothermal fluid, and $FeCl_2$ as a model seawater (Russell *et al.*, WWW, 2001, Figure 9d).

3.3.1 Sulfur availability in the Hadean

On the early Earth, sulfur-bearing gases (amongst others) were exsolved during depressurisation and crystallisation of rising magma and exhaled through volcanoes and fractures. Since volcanic outgassing from the Earth buffered close to the Fe/FeO boundary would have contributed more hydrogen sulfide than sulfur dioxide (Farquhar *et al.*, 2000; Walker and Brimblecombe, 1985) to the early atmosphere, further sulfur, ultimately from the rocks in the crust itself, would have been introduced as hydrosulfide at an alkaline seepage. This is because sulfur is more soluble in slightly alkaline fluids at 250°C and 500 bar, though it is limited by iron (MacLeod *et al.*, 1994; Barnes and Kullerud, 1961; Garrels and Christ, 1965, p222). An alkaline hydrothermal fluid may well have been able to efficiently leach the sulfide whilst flowing through the surrounding rock if the iron is fixed by being hydroxylated and/or carbonated. The production of hydrogen from serpentinisation reactions in the crust could have maintained the reducing conditions necessary for hydrosulfide to remain stable in sufficient concentrations and be transported to the hydrothermal fluid-seawater interface for iron-monosulfide membrane development. Sulfur may have even have outweighed iron in localities where volcanogenic sulfide emanated into the deep sea (Walker and Brimblecombe, 1985).

Dunitic rocks provide estimates for constraining the sulfur content of ultramafic rock compositions for modelling. Studies of nickeliferous mineral assemblages in weakly serpentinised ultramafic bodies (Eckstrand, 1975), which have been altered by CO_2 bearing fluids, show that mineral assemblages present as a result of hydrothermal alteration are controlled by Fe-related redox mechanisms. These assemblages are characterised by the presence of sulfide-rich minerals, for example, metal-sulfides such as millerite (NiS). However, studies of strongly serpentinised nickel deposits, reveal a much higher iron sulfide content, with minerals such as pyrrhotite (± pyrite), as well as pentlandite ($(Fe,Ni)_9S_8$) and occasionally heazlewoodite (Ni_3S_2) (Eckstrand, 1975; Krishnarao, 1964; Barnes and Hill, 2000) thus more sulfide may be available. Evidence is also present of the migration of sulfur from magmatic sulfide "blebs" within the serpentinised body (Eckstrand, 1975; de Vusse, 1983), possibly due to a f_{O2} gradient (Frost, 1985), and this may have led to finely dispersed sulfur particles within the rock. These "diffuse, sulfide-poor disseminations" (Barnes and Hill, 2000) can be within large extrusive bodies of olivine, for example, the Mt. Keith deposit in the Agnew-Wiluna Belt of Western Australia, and are a better source of sulfur

since they afford more surface area for reactions with hydrothermal fluids. Although these findings are helpful in providing constraints for rock models, the availability of sulfide still depends on its solubility in alkaline solution.

3.3.2 Method

An iron-sulfur stability diagram was created using the GWB (Bethke, 1998) program 'ACT2' to examine why sulfide availability may be limited (Figures 3.16). In addition, water-rock reactions were conducted between a simple Hadean seawater and ultramafic rock with troilite, under prebiotic (anoxic) conditions, and tested at various temperatures (50°C-300°C). The water-rock reaction in Figures 3.17a, 3.17b, and 3.17c involved a sulfide-poor ultramafic rock. However, the system described in Figure 3.17a was modified to resemble a sulfide-rich ultramafic rock by the addition of more troilite (Figure 3.18). The temperature in this system was varied from 50°C to 300°C to help understand how temperature may influence sulfur availability (Figure 3.18). In addition, hydrogen and sulfate were added to the script to allow the overall redox of the system to be manipulated. More hydrogen makes the system reducing, more sulfate makes the fluid acidic (these variables were used to see how they influenced the solubility of sulfide in the fluid). The thermodynamic models were created using the GWB program 'REACT' (Figures 3.19 to 3.23). Thus, the initial model reflects a simple, anoxic, sulfide-poor (Figure 3.17a, lines, 5 and 12 respectively) Hadean seawater containing ferrous and magnesium ions (both a_{Fe}^{2+} and $a_{Mg}^{2+} = 10^{-6}$, lines 6, 9, Figure 3.17a), flowing through rock representing the diffuse, sulfide-poor olivine body (9 mmoles forsterite, 1 mmole fayalite, and 0.5 mmoles of troilite). While the second model is similar, it uses a sulfide-rich rock (5 mmoles troilite) and the temperature is varied. Plots of mineral products, sulfide activity, and total sulfur were generated. The FeS analogue troilite (which has an Fe:S molar ratio of 1:1) was used for simplicity since natural pyrrhotite is slightly sulfur-rich.

3.3.3 Results

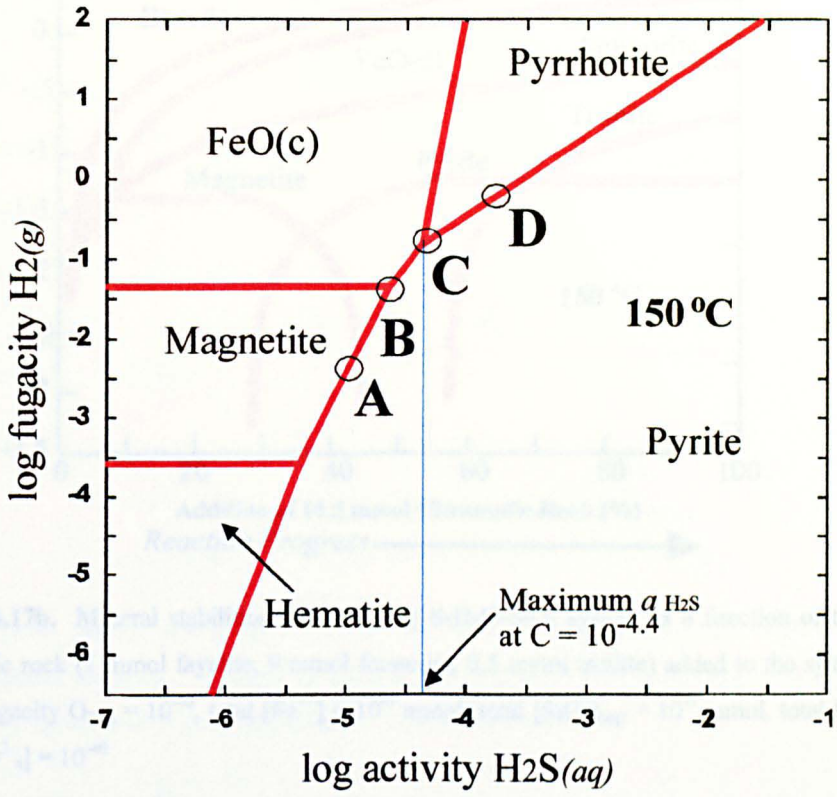

Figure 3.16. Stabilities of minerals and aqueous species in the Fe-H_2O-S system with respect to the fugacity of $H_{2(g)}$ and activity of $H_2S_{(aq)}$ at 150°C. Points A, B, C, and D represent different phase boundaries that control sulfur activity (log a $H_2S_{(aq)}$), A = pyrite-magnetite, B = pyrite-magnetite-FeO(c), C = pyrite-FeO(c)-pyrrhotite, D = pyrite-pyrrhotite. Produced by the Geochemist's Workbench (Bethke, 1998) program ACT2.

GWB REACT script for Figures 3.17b and 3.17c

```
1. data = thermo.dat
2. temperature = 150
3. swap O2(g) for O2(aq)
4. 1 kg free H2O
5. fugacity O2(g) = 1e-40
6. total mmol Fe++ = 1e-6
7. total mmol SiO2(aq) = 1e-6
8. balance on H+
9. total mmol Mg++ = 1e-6
10. total mmol SO4-- = 1e-40
11. react 1 mmol of Fayalite
12. react .5 mmol of Troilite
13. react 9 mmol of Forsterite
```

Figure 3.17a. Reaction constraints for the water-rock reaction between simple anoxic, sulfate-deficient Hadean seawater model and sulfide-deficient ultramafic rock containing forsterite, fayalite and some troilite.

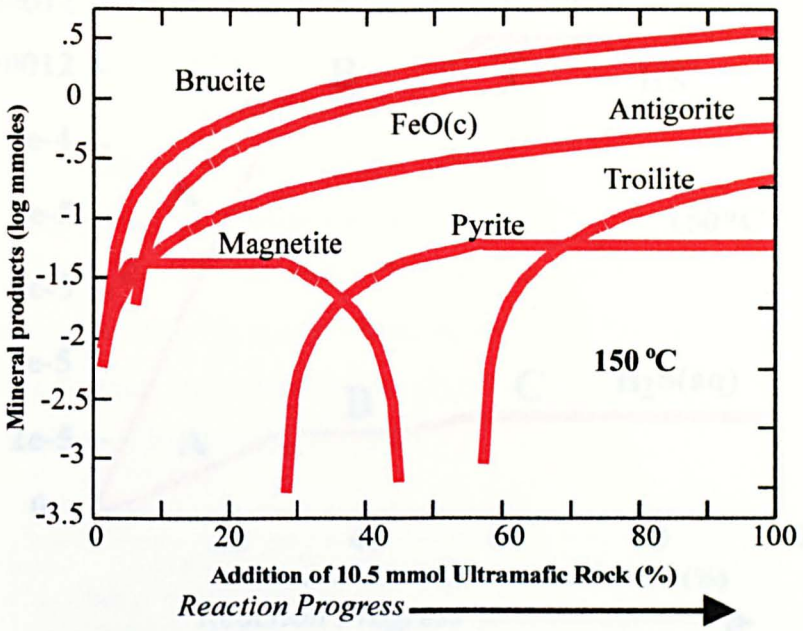

Figure 3.17b. Mineral stabilities in the Fe-Mg-S-H_2O-SiO_2 system as a function of the amount of ultramafic rock (1 mmol fayalite, 9 mmol forsterite, 0.5 mmol troilite) added to the system at 150°C. Initial fugacity $O_{2(g)} = 10^{-40}$, total $[Fe^{++}] = 10^{-6}$ mmol, total $[SiO_2]_{(aq)} = 10^{-6}$ mmol, total $[Mg^{++}] = 10^{-6}$, total $[SO^{2-}_4] = 10^{-40}$

In Figure 3.17b, the theoretical reaction products are produced at 150°C when 10.5 mmoles of simple ultramafic rock is added to 1kg of a simple Hadean model seawater. Brucite ($Mg(OH)_2$), FeO(c), antigorite ($Mg_{48}Si_{24}O_{85}(OH)_{62}$), troilite (FeS), and pyrite (FeS_2) are the final reaction products. System is relatively oxidised at 0% and relatively reduced at 100%.

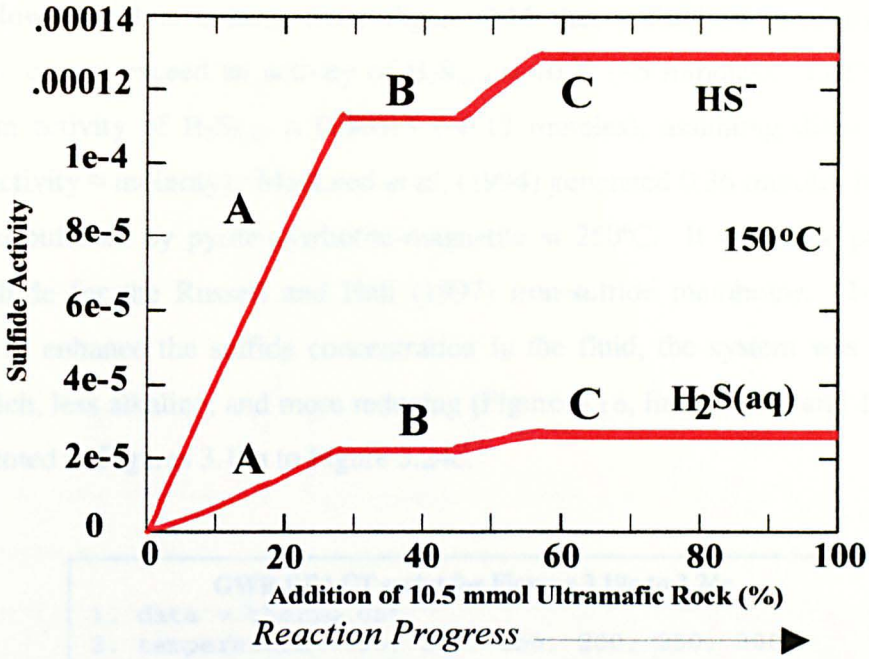

Figure 3.17c. Sulfide activity at 150°C as 10.5 mmoles of simple ultramafic rock is added to 1kg simple Hadean seawater. A, B, and C represent different phase boundaries that control sulfur activity. A, B and C correspond to the positions of A, B, and C in Figure 3.16.

In Figure 3.16, HS^- and $H_2S_{(aq)}$ are produced at stage A, but then buffered by pyrite-magnetite-$FeO_{(c)}$ at B. At C, HS^- and $H_2S_{(aq)}$ are buffered by pyrite-$FeO_{(c)}$-pyrrhotite. Figure 3.16 demonstrates that in the environment envisaged, sulfide activity (log *a* $H_2S_{(aq)}$) can be controlled by pyrite-magnetite (**A**), pyrite-magnetite-$FeO_{(c)}$ (**B**), pyrite-$FeO_{(c)}$-pyrrhotite (**C**), and pyrite-pyrrhotite (**D**). To increase sulfide availability conditions need to become increasingly reducing (higher fugacity of H_2). For example, at point **D**, sulfur is more soluble (higher H_2S activity). However, from Figure 3.17b, we can see that as the water-rock reaction proceeds, magnetite (Fe_3O_4) is initially stable. As more rock is added to the system, magnetite is transformed to FeO(c) and minor pyrite. At the point where the amount of rock reacted exceeds ~58 % of its total mass, further addition of the ultramafic rock does not produce more pyrite (Figure 3.17b), or increase the quantity of sulfide in the solution (Figure 3.17c) There is therefore a progression whereby the activity of $H_2S_{(aq)}$ increases, though it is buffered by magnetite-$FeO_{(c)}$-pyrite (points **B**, in Figures 3.16 and 3.17a), and then by $FeO_{(c)}$-pyrite-pyrrhotite at points **C** (Figures 3.16 and 3.17a). Note that pyrrhotite is present here in the form of the reactant troilite (it is analogous to pyrrhotite in Figure 3.16). The conditions at point **D** in Figure 3.16 are not achievable because of the stability of the $FeO_{(c)}$-pyrite-pyrrhotite (troilite) minerals after 58% of the reaction has proceeded (Figure 3,17b).

However, it is evident from Figure 3.16 that a fluid buffered by $FeO_{(c)}$-pyrite-pyrrhotite cannot exceed an activity of $H_2S_{(aq)} = 10^{-4.4}$ (~5 mmoles). In Figure 3.17c, the maximum activity of $H_2S_{(aq)}$ is 0.00013 (~0.13 mmoles), assuming dilute concentrations (where activity ≈ molarity). MacLeod *et al.* (1994) generated 0.36 mmoles $H_2S_{(aq)}$ (13 ppm) in a fluid buffered by pyrite-pyrrhotite-magnetite at 250°C. It would be preferable to get more sulfide for the Russell and Hall (1997) iron-sulfide membrane. To see if it was possible to enhance the sulfide concentration in the fluid, the system was modified to be sulfide-rich, less alkaline, and more reducing (Figure 3.18, lines 12, 14 and 16). The results are presented in Figures 3.19a to Figure 3.24c.

GWB REACT script for Figures 3.19a to 3.24c

```
1. data = thermo.dat
2. temperature = 50, 100, 150, 200, 250, 300
3. swap O2(g) for O2(aq)
4. 1 kg free H2O
5. fugacity O2(g) = 1e-40
6. total mmol Fe++ = 1e-6
7. total mmol SiO2(aq) = 1e-6
8. balance on H+
9. total mmol Mg++ = 1e-6
10. activity SO4-- = 1e-40
11. react 1 mmol of Fayalite
12. react 5 mmol of Troilite
13. react 9 mmol of Forsterite
14. react 20 mmol of SO4--
15. react 20 mmol of Mg++
16. react 50 mmol of H2(g)
```

Figure 3.18. Reaction constraints for the water-rock reaction between simple anoxic, sulfate-poor Hadean seawater and sulfide-rich ultramafic rock containing forsterite, fayalite and some troilite, under reducing and less alkaline conditions as indicated by the increased amount of sulfate and addition of hydrogen for the initial system (lines 14 and 16).

Figures 3.19a-Figure 3.21c show the reaction products produced when 15 mmoles of simple sulfide-rich ultramafic rock is added to 1 kg of simple Hadean seawater between temperatures of 50°C to 150°C. Brucite ($Mg(OH)_2$), pyrite (FeS_2), and antigorite ($Mg_{48}Si_{24}O_{85}(OH)_{62}$) are the final reaction products. The system is relatively oxidised at 0% and relatively reduced at 100%

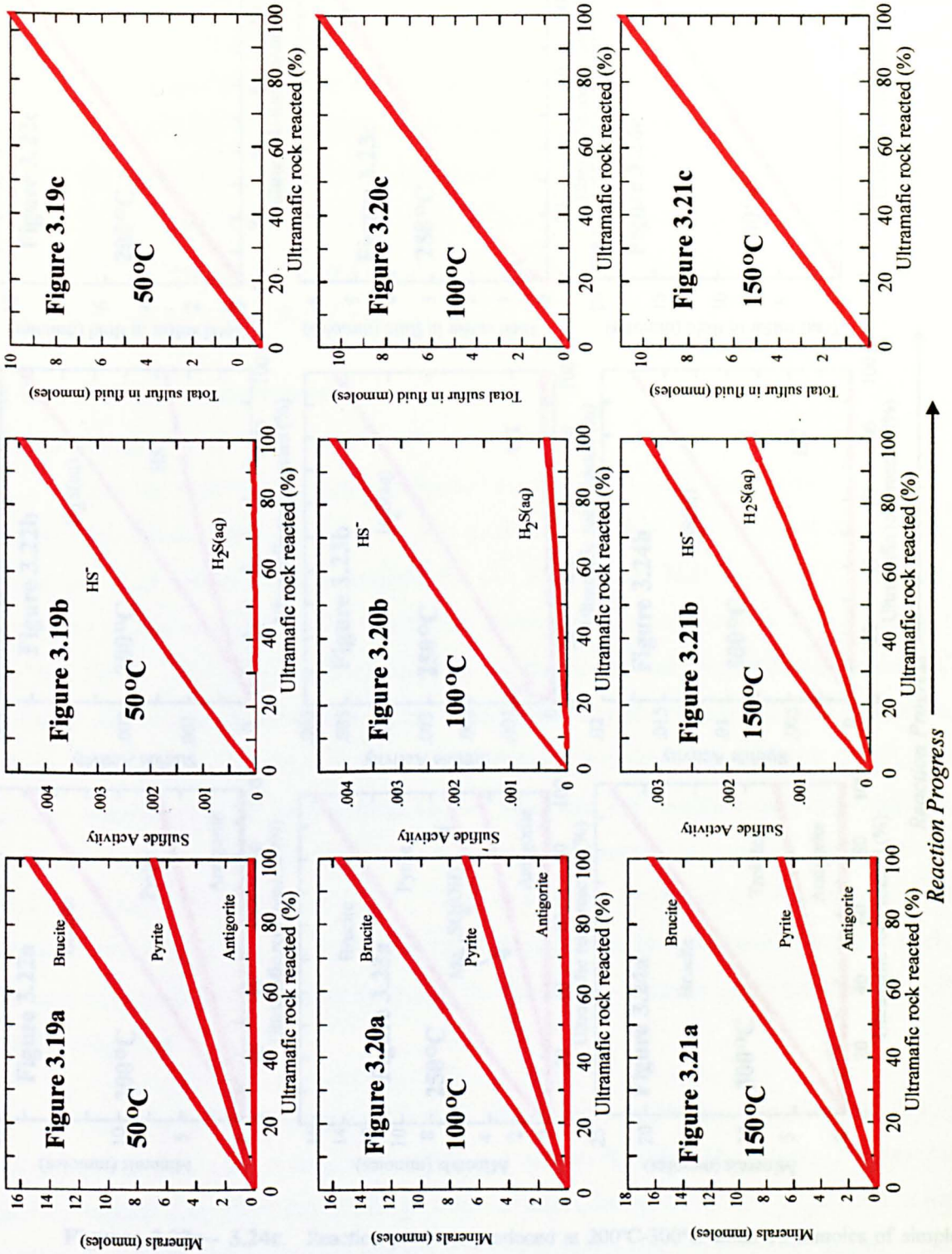

Figure 3.19a-Figure 3.21c. Mineral stabilities, sulfide activities, and total sulfur under reducing (50 mmol $H_{2(g)}$) and slightly alkaline conditions (20 mmol SO^{2-}_4 and Mg^{2+}), when ultramafic rock (1 mmol fayalite, 5 mmol troilite, 9 mmol forsterite) is titrated into the Fe-H_2O-SiO_2-Mg system. Initial fugacity $O_{2(g)} = 10^{-40}$, total mmol $Fe^{2+} = 10^{-6}$, total mmol $SiO_{2(aq)} = 10^{-6}$, total mmol $Mg^{2+} = 20$, activity $SO^{2-}_4 = 10^{-40}$, activity $Mg^{2+} = 10^{-6}$.

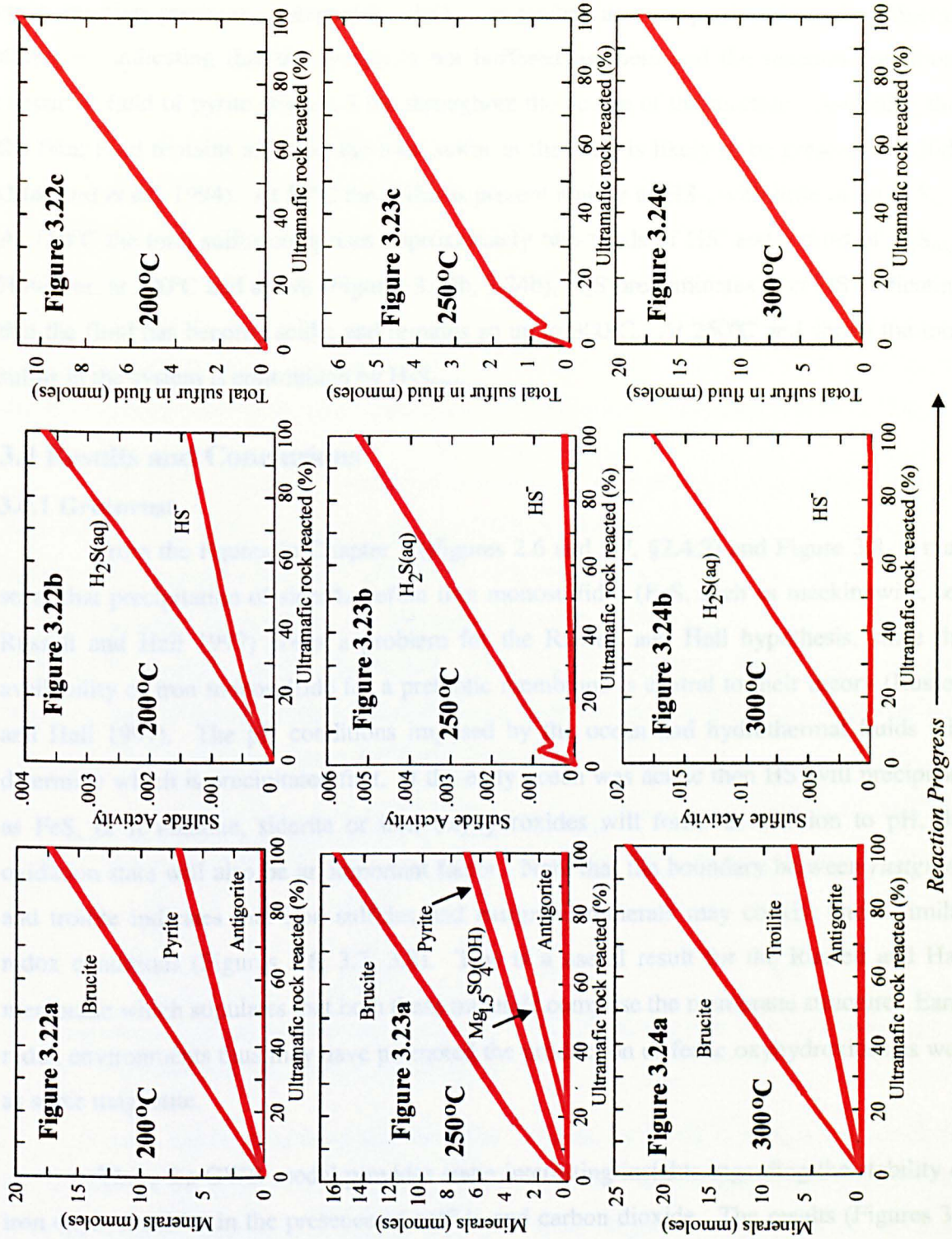

Figures 3.22a-- 3.24c. Reaction products produced at 200°C-300°C when 15 mmoles of simple sulfide-rich ultramafic rock is added to 1kg simple Hadean seawater. Brucite ($Mg(OH)_2$), pyrite (FeS_2), antigorite ($Mg_{48}Si_{24}O_{85}(OH)_{62}$), troilite (FeS), and pyrite (FeS_2) are the final reaction products. At 200C, $H_2S_{(aq)}$ is the predominant sulfide species. Note the precipitation of $Mg_{1.5}SO_4(OH)$ at 250°C. System is relatively oxidised at 0% and relatively reduced at 100%

The immediate conclusion from these graphs is that there is no buffering (i.e. the graphs do not level out as in Figure 3.17c). In addition, pyrite, brucite, and antigorite are the

main reaction products. Magnetite, $FeO_{(c)}$, or troilite are not produced in the minerals diagrams, indicating that the system is not buffered by them and the reaction conditions remain in field of pyrite (Figure 3.16) throughout the course of the reaction. Assuming that the final fluid remains alkaline, the total sulfur in the fluid is likely to be present as sulfide (Macleod *et al.*, 1994). At 50°C the sulfur is present mainly as HS-, with little or no $H_2S_{(aq)}$. At 150°C the total sulfur comprises approximately two-thirds of HS^- and a third of $H_2S_{(aq)}$. However, at 200°C and above (Figures 3.23b, 3.24b), H_2S predominates over HS^- indicating that the fluid has become acidic and remains so up to 300°C. At 250°C and above the total sulfur in the system is contributed by $H_2S_{(aq)}$.

3.4 Results and Conclusions

3.4.1 Greenrust

From the figures in Chapter 2 (Figures 2.6 and 2.7, §2.4.2) and Figure 3.8, it may seem that precipitation of siderite before iron monosulfides (FeS, such as mackinawite, see Russell and Hall 1997) poses a problem for the Russell and Hall hypothesis, since the availability of iron monosulfide for a prebiotic membrane is central to their theory (Russell and Hall 1997). The pH conditions imposed by the ocean and hydrothermal fluids will determine which is precipitated first. If the early ocean was acidic then HS^- will precipitate as FeS, or if alkaline, siderite or iron oxyhydroxides will form. In addition to pH, the oxidation state will also be an important factor. Note that the boundary between *rustgreen* and troilite indicates that iron sulfides and *rustgreen* minerals may coexist under similar redox conditions (Figures 3.6, 3.7, 3.8). This is a useful result for the Russell and Hall membrane which stipulates that both these minerals comprise the membrane structure. Early redox environments thus may have promoted the production of ferric oxyhydroxides as well as some magnetite.

Thus, the GWB model provides some interesting insights regarding the stability of iron oxyhydroxides in the presence of sulfide and carbon dioxide. The results (Figures 3.6 and 3.7) indicate that, given the estimated value of log K for *rustgreen* is ~42.54, and in the presence of sulfide, the hydroxide greenrust is stable under low-temperature, alkaline, and reducing conditions, perhaps with some magnetite or other iron oxide/hydroxide. On addition of small amounts of CO_2, iron-sulfides such as pyrrhotite (rather than troilite as shown), may form (Figures 3.6 and 3.7). Siderite formation is hindered, most likely by the presence of the sulfide. An increase in sulfide concentrations favours a corresponding increase in pyrrhotite formation (Figure 3.7). The strength of the model (and thus the conclusions above) are however very dependent on the estimated value of the equilbrium

constant. The formation of rustgreen was very sensitive to a change in the equilibrium constant of ±1, with a change of +5 resulting in no formation of rustgreen at all (Figure 3.4).

3.4.2 Schoonen versus Wächtershäuser

Using thermodynamic calculations, the reduction potential of the FeS-H_2S/FeS_2 redox couple for carbon fixation was demonstrated by Schoonen *et al.*(1999) to be less effective at higher temperatures but more facile at lower temperatures and higher activities of $H_2S_{(aq)}$. The results show that the pyrite-pyrrhotite-H_2S redox system is more exergonic (at equilibrium and at high fugacity H_2) at lower temperatures. This is confirmed by the decrease in $H_{2(g)}$ fugacity (or redox potential) with increasing temperature (Figure 3.15a).

The GWB model was considered to be a success for the following reasons. Though Schoonen *et al.*'s (1999) calculations are for 300 bars pressure, the GWB results calculated at much lower pressures agree with SUPCRT92 (*Figure 1* **B**, Schoonen *et al.*, 1999) that there is no significant influence to the hydrogen fugacity. The results between GWB and SUPCRT92 are very similar (Table 3.1). The SUPCRT92 results for hydrogen fugacity were obtained by extrapolating a line at the required temperature to the the point at which the activity of $H_2S = 10^{-3}$ (see Figure 3.15b and Table 3.1).

Table 3.1. Hydrogen fugacities at 50-200°C buffered by PPM

Temperature (°C)	GWB pressures (bar)	GWB results	SUPCRT92 results at 300 bar
50	1.103	2.25	2.3
100	1.103	1.5	1.5
150	4.7572	0.6	0.6
200	15.5365	-0.2	-0.2

Approximate hydrogen fugacities calculated by GWB and SUPCRT92 for the PPM buffer at $a_{H2S(aq)} = 10^{-3}$ (GWB pressures from Figure 3C, Appendix 1A)

Thus it can be concluded that the result obtained by GWB is in agreement with the result obtained using SUPCRT92 (Schoonen *et al.*, 1999). On comparison of Figure 3.15a with the stability diagram presented in Schoonen *et al.* (Figure 3.15b), it can be concluded that the GWB result is obviously less complex. It shows much more clearly that Wächtershäuser's (1988a) claim that CO_2 reduction with FeS-H_2S/FeS_2 would be energetically favoured at the higher temperatures typical of some hydrothermal systems to be erroneous.

The increasing influence of the hematite-magnetite buffer over PPM on $H_2S_{(aq)}$ stability at higher temperatures is acknowledged by Schoonen *et al.*, (1999). The GWB model demonstrates this influence whereas the Schoonen *et al.* SUPCRT92 model does not.

Furthermore, Schoonen *et al.*'s, calculation are for up to 350°C though PPM buffering is only evident at less than 250°C in the GWB model. Thus $H_2S_{(aq)}$ values could be erroneously extracted from the SUPCRT92 model if PPM buffering is assumed by the reader to continue to 350°C. In addition, the GWB model (Figures 3.10 to 3.14) shows how sulfide availability is affected by hydrogen fugacity and temperature. However, the SUPCRT92 model does have a greater bearing on the influence of PPM on organic synthesis by showing the CH_4/CO_2 phase boundary (Shock, 1992a; and see Chapter 5).

Wächtershäuser (1988b, 1990, 1992, and 1993) has frequently suggested that the reduction of CO_2 to form simple organic acids, for example formic acid (HCOOH), might be facilitated by reactions such as Equation *3.6* at 25°C in which CO_2 is the electron acceptor.

$$FeS_{(pyrrhotite)} + H_2S_{(aq)} + CO_{2(aq)} \rightleftharpoons FeS_{2(pyrite)} + HCOOH_{(aq)} \qquad (3.6)$$

Wächtershäuser's (1988) thermodynamic calculations resulted in a negative change in the Gibbs free energy. He used his results to suggest that such reactions (with an overall negative ΔG°_{r}) were thermodynamically favourable. However, experimental evidence has shown that the rate of reaction is such that no appreciable amount of organic molecules would form (*cf.* Keefe *et al.*, 1995). It is the activation energy that needs to be overcome to allow reaction *3.4* to proceed significantly. Schoonen *et al.* (1999) state that the high activation energy is due to the fact that "CO_2 reduction must involve an energetically unfavourable step in which electrons from the valence band of pyrrhotite are transferred into the Lowest Unoccupied Molecular Orbital (LUMO) of CO_2". In their study of the energetics of similar reactions proposed by Wächtershäuser (1992), Schoonen *et al.* (1999) evaluated all possible scenarios in which this step may have been facilitated, but concluded that CO_2 is not capable of accepting electrons to form formic acid. Huber and Wächtershäuser (1997) did however succeed in synthesising acetate by using CO. Schoonen *et al.* (1999) suggest that the CO reduction was made easier by the fact that "the energy position of the CO LUMO is ~ 3eV lower than that for CO_2". Wächtershäuser cited the findings of Merlivat *et al.* (1987) as evidence of CO being readily available in hydrothermal fluids today. However, Schoonen *et al.*, (1999) point out that Merlivat *et al.* (1987) had concluded in their investigation that the CO detected from hydrothermal fluids was a sampling artefact (as a result of the reaction between CO_2-rich fluids and the catalytic titanium containers used). Nevertheless, some reduction of CO_2 to CO is to be expected as volcanic exhalations migrate through lavas buffered at the iron/wüstite boundary (Righter and Drake, 1997). Schoonen *et al.* (1999) do offer an explanation as to why Keefe *et al.* (1995) and Heinen & Lauwers (1996) were able

to reduce CO_2 to form thiols via a possible CS_2 or COS pathway. The LUMO's of CS_2 and COS are much more accessible to the electrons in the valence band of pyrrhotite than the LUMO of CO_2.

Figure 3.15a in this study supports at least part of Schoonen *et al.*'s (1999) scepticism. However, assessments of Wächtershäuser's (1998b) idea regarding the temperature dependence of the favourability of the coupled reduction of $CO_{2(aq)}$ and oxidation of $FeS_{(po)}$ requires not only consideration of reaction *3.4*, but also of reaction *3.7*.

$$2CO_{2(aq)} + H_{2(aq)} \leftrightharpoons CH_3COOH_{(aq)} + 2H_2O_{(aq)} \qquad (3.7)$$

Wächtershäuser's (1988b) calculations address reaction *3.6* by calculating and summing the free energy of formation of reactions *3.4* and *3.7* at STP, thus they do not verify his suggestion that, at higher temperatures, reaction *3.6* is more favourable. In addition, the kinetics of the reaction are not discussed by Wächtershäuser (1998b), it is simply assumed that the overall negative free energy of reaction *3.6* will allow the reaction to proceed favourably and more so at higher temperatures. Schoonen *et al.* (1999, Figure 2) calculated the thermodynamics of reaction *3.6*, where the thermodynamics of $CO_{2(aq)}$ reduction to $CH_3COOH_{(aq)}$ are compared to the reducing power of the FeS-H_2S/FeS_2 redox couple. Again, their findings show an opposite trend in the reducing power required to reduce $CO_{2(aq)}$ to $CH_3COOH_{(aq)}$ and the reducing power of the FeS-H_2S/FeS_2 redox couple as temperatures increase.

It is concluded here that in light of the numerous discrepancies outlined above and elsewhere (de Duve and Miller, 1991; McDowall, 1998), the theoretical and experimental evidence that Wächtershäuser has cited in favour of his hypothesis seem unsatisfactory for some critical stages of the Theory of Surface Metabolism. Schoonen *et al.* have made a significant dent in the Theory of Surface Metabolism and as yet there is no published response by Wächtershäuser regarding these results. Schoonen *et al.*'s (1999) analysis is thorough and considers instances where Wächtershäuser's mechanisms might be feasible, so does not rule them out completely, but deems them to be very unlikely in hydrothermal conditions. Schoonen *et al.*'s investigation also highlights the need for thorough thermodynamic evaluations. Some of Wächtershäuser's (2000) experiments and statements, and some relevant studies by other researchers (Keefe *et al.*, 1995) proved difficult to test in the Schoonen *et al.* (1999) investigation, limited by the availability of thermodynamic and other data. Therefore some necessary assumptions had to be made in the Schoonen *et al.* study, making those arguments against Wächtershäuser slightly weaker. Further difficulties

were also encountered by Schoonen *et al.* (1999) as Wächtershäuser does not specify temperature or pH limits for many of the reactions proposed in the Theory of Surface Metabolism, making it difficult to verify his statements experimentally.

3.4.3 Controls on sulfur availability

Figures 3.10 to 3.14 also indicate that higher temperatures would make greater quantities of sulfide available, and higher $H_2S_{(aq)}$ activities provide a greater reducing potential for the reduction of CO_2. By starting at the triple point of PPM and extrapolating to the abscissa in each diagram, it can be seen that the activity of log a $H_2S_{(aq)}$ steadily increases with higher temperature. This is another useful result for the Russell and Hall (1997) model where the availability of sufficient sulfur for the iron-sulfide membrane is critical. More sulfide is 'advantageous' to the Russell and Hall (1997) membrane formation model in the need for a hydrosulfide-rich solution. Figures 3.10 to 3.14 indicate that the sulfur availability is likely to be controlled by PPM. However, sulfur availability can be increased if the environment becomes more reducing. The presence of $H_{2(g)}$ as a consequence of the serpentinisation of olivine from fluid-mixing with seawater could enhance the reducing potential of such environments.

However, Seyfried *et al.* (1991) note from their calculations $H_2S_{(aq)}$ decreases with increasing Cl. Hot spring fluids of *seawater salinity* are characterised by $H_2S_{(aq)}$ concentrations which range from ~7 to 9 mmolal (Seyfried *et al.*, 1991)

The total sulfur achieved in solution remains at about 11 mmolar between 25°C to 200°C (Figure 3.19c to 3.21c). However, at 250°C, the sulfur content is almost halved to approximately 6 mmolar (Figure 3.23c). Figure 3.23a indicates that this could be due to the precipitation of the mineral $Mg_{1.5}SO_4(OH)$. However, this is unlikely, as the sulfate stability field is not attainable in such reducing conditions. Then at 300°C (Figure 3.24c), the sulfur content increases to about 17.5 mmolar. Presumably, all the FeS (troilite) has dissolved as the results show that 5 mmolar troilite produce 11 mmolar sulfur. More sulfur could have come from the reduction of sulfate.

On comparison with laboratory experiments which were conducted by Turner, (*pers. comm.*), where it was determined that at least 25 mmolar sulfide would be needed to produce a sulfide membrane capable of maintaining a pH difference, this may seem short of the required concentrations, but field evidence indicates that more may be available, perhaps from degassing magma at depth. However, sulfur solubility can be increased if the environment can become more reducing. For example the presence of $H_{2(g)}$ as a

consequence of the serpentinisation of olivine (as demonstrated in Chapter 2) could enhance the reducing potential of such environments and increase the availability of hydrosulfide for membrane formation (Eckstrand, 1975; Frost, 1985).

Chapter 4 - Modern High Temperature Hydrothermal Systems

4.1 Introduction

Since the discovery of submarine hydrothermal systems and sulfide chimneys by the deep-sea submersible 'Alvin' in 1977 (Corliss *et al.*, 1979), it is understood that hydrothermal fluids form today when seawater reacts with mafic (Shanks, 1995), or ultramafic magmatic intrusions (Bischoff and Dickson, 1975; Seyfried and Dibble, 1979; Seyfried and Bischoff, 1981). The depth of knowledge of the geological settings, mechanics, mineralogy and chemistry of modern (Corliss *et al.*, 1979; Edmond *et al.*, 1979; Seyfried and Janecky, 1985; Von Damm, 1990; Seyfried *et al.*, 1991; Seyfried and Ding, 1992; Holm and Hennet, 1992; Krasnov *et al.*, 1995; Elderfield & Schultz, 1996; Butler *et al.*, 1998; Mottl *et al.*, 1998; Jupp and Schultz, 2000; Kelley *et al.*, 2001), and evidence from fossilised hydrothermal systems (Nehlig and Juteau, 1988; Alt *et al.*, 1986; Mottl, 1983), is improving steadily with improved detection methods and real-time studies *in situ*. Such information can be used in conjunction with theoretical models of Hadean seawater and oceanic crust to make better-informed inferences about the physicochemical properties of hydrothermal systems on the early Earth.

Although venting may occur in a range of tectonic settings along plate boundaries (Holm and Hennet, 1992; German *et al.*, 1995), high-temperature vents predominate near on-axis (mafic rock and rock-dominated) hydrothermal systems at fast-spreading ridges, where the heat and chemical flux is more focused than the diffuse-flow hydrothermal systems of off-axis (ultramafic rock and water-dominated) systems at slow-spreading ridges (Elderfield and Schultz, 1996). The metal-sulfide/oxide plumes emanating from the vents of high-temperature systems are typically black in colour and are termed as 'black-smokers'. The temperatures of modern hydrothermal fluids are known to vary from ~4°C to ~400°C, though black-smokers are always ≥350°C. In general, fluid temperatures may be high (≥250°C to ≤400°C), moderate (≥150°C to ≤250°C) or low (≥4°C to ≤150°C). The upper limit of temperature (§2.2) is controlled by how close the seawater can get to the magma (Figure 4.1, **B**), at pressures between 200 to 400 bars at several kilometres depth (Corliss, 1986, Von Damn, 1995). pH may range from ~3 to 9 and above (von Damm, 1985, Kelley *et al.*, 2001). However, the sampling and accurate determination of heat and chemical flux is still problematic (Elderfield and Schultz, 1996), and species concentrations determined from fluid samples have to be corrected by considering the relative contributions of the fluids and seawater to each sample. For example, many calculations assume all the magnesium in the fluid samples is due to the entrainment of ambient seawater (Von Damm, 1990). This can introduce errors if seawater-rock ratios are greater than 50, where magnesium is not

completely removed from the seawater as it reacts with oceanic rock (Seyfried and Bischoff, 1979).

Each expedition of new (Rona *et al.*, 1986; Murton *et al.*, 1994; Kelley *et al.*, 2001) or revisited (Baker, 1994; Edmond *et al.*, 1995) vent fields "expands the range of known compositional diversity" (Von Damm, 1990). For example, relatively little was known about off-axis vent systems at slow-spreading ridges, where seawater can circulate deeper and react with ultramafic peridotites, rather than the mafic basalts at the shallower depths of fast-spreading ridges. Neal and Stanger (1983, 1984) had predicted such systems from their studies of serpentinisation in the Oman Ophiolite, and though there was no firm indication of the nature of off-axis vent fluids, the geochemical model of MacLeod *et al.* (Figure 6, 1994) hinted at the presence of very alkaline fluids at low temperature (≤100°C) generated from seawater-rock reactions with ultramafic rocks. Since the commencement of this study, the discovery of the Lost City Field vent system, in the North Atlantic, 15 km off-axis of the slow-spreading Mid-Atlantic Ridge (Kelley *et al.*, 2001), provided a new insight into seafloor geochemistry where ultramafic-hosted vent systems form carbonate and magnesium hydroxide chimneys rather than the sulphide chimneys typical of vent systems at fast-spreading ridges, and the fluid properties (40-75°C and pH 9.0-9.8) are close to those described by MacLeod *et al.*'s (1994) predictions. Kelley *et al.*'s (2001) discovery supports the notion that on off-axis systems, the heat from serpentinisation reactions between seawater and ultramafic rock generate the relatively cool, alkaline, hydrogen-rich fluids and, 15 km away from the slow-spreading ridge, provide the more stable conditions necessary for organic compounds to concentrate (Russell and Hall, 1997).

If model modern high-temperature springs can be successfully modelled, then the possibility of using theoretical seawater and oceanic crust compositions in a similar model to establish the composition of Hadean high-temperature springs can then be considered. The remarkable agreement between anticipated fluid compositions from geochemical models (Mottl and Holland, 1978; MacLeod *et al.*, 1994) and sampled fluid compositions (Von Damm, 1985, Kelley *et al.*, 2001) provides confidence in this approach. The problem for modelling fluid compositions in relation to the origin of Life is that the dominant constituents of the oceanic crust and seawater in the Hadean are unknown. This makes it difficult to establish the nature and composition of the early hydrothermal systems and their fluids. Although high-temperature hydrothermal systems equivalent to modern 'black smokers" would have existed in the Hadean, they may have had a different chemistry and

chemical interaction with the Hadean ocean water, itself of a different chemistry. Thus, they may not have been characterised by 'black smoke' created by iron-sulfide precipitates

4.2 Modelling the formation and nature of vent fluids.

The objectives of this chapter were to construct geochemical models using Geochemist's Workbench (GWB) to show the formation and nature of modern high-temperature (≤300°C), and moderate-temperature (150°C, to compare with high-temperature) hydrothermal vent fluids (Figure 4.1) resulting from reactions between cold, oxidised, and slightly alkaline seawater with hot mafic and ultramafic rock, and to determine and demonstrate the possible mechanism(s) by which they attain their chemical properties. It would have been desirable to model modern high-temperature springs at up to 400°C to give more confidence in modelling early seafloor hydrothermal systems. However, the thermodynamic databases used for this study are only applicable for investigations up to 300°C. Water-rock ratios influence fluid composition and alteration products, thus the models were tested at water rock ratios of 10 and 100. Though it is known that 'black smoker' fluids are given their distinctive black colour due to the precipitation of metal-sulfides/oxides on mixing with seawater, this chapter also attempts to model the mechanism by which this occurs.

This exercise was undertaken to understand not only the factors that control the chemistry of the hydrothermal fluid, but to compare results generated from the Geochemist's Workbench (Bethke 1998) and EQ3NR/EQ6 (Wolery, 1992), and overall, to provide more confidence in modelling early high-temperature submarine hydrothermal systems. The success of the model will be determined by how close the fluid compositions and mineral products match field evidence and laboratory simulations of water-rock reactions (Mottl and Holland, 1978; Seyfried and Bischoff, 1979; Seyfried and Dibble, 1980; Seyfried and Bischoff, 1981; Mottl, 1984; Janecky and Seyfried, 1986; Seyfried *et al.*, 1991; Mottle and Wheat, 1994), and then the question of whether it is the concentration of magnesium that is present in seawater that ultimately determines the pH of the emergent hydrothermal fluid is discussed. In particular, whether acidity is due to the Mg^{2+} content of seawater in convective downdrafts producing $Mg(OH)_2$-bearing silicates on hydrothermal alteration of mafic rock and thereby releasing protons as in Equation *4.1* (Seyfried and Bischoff, 1981; Seyfried and Janecky, 1985; Seyfried *et al.*, 1991; Seyfried and Ding, 1992; Von Damm, 2000), or whether the acidity of hydrothermal fluids is primarily a response to the loss of magnesium from the fluid (Seyfried and Bischoff, 1979).

$$Mg^{2+} + 2\,H_2O \rightarrow Mg(OH)_{2\,(silicate)} + 2\,H^+ \qquad (4.1)$$

A complicating factor in modern day measurements, not considered here, is the contribution of sulfide oxidation to the generation of protons, as indicated by the production of sulfuric acid in Equation *4.2*.

$$2\,FeS_2 + 4\,H_2O + 7½\,O_2 \rightarrow 4\,H_2SO_4 + Fe_2O_3 \qquad (4.2)$$

4.3 The Geochemist's Workbench (GWB) Approach

4.3.1 Method

The GWB reaction-path modelling code REACT and the GWB database *thermo.dat* (Bethke, 1998) were used to produce simple models of the chemistry of the acidic and alkaline fluids emanating from on-axis and off-axis vent chimneys respectively, as shown in Figure 4.1.

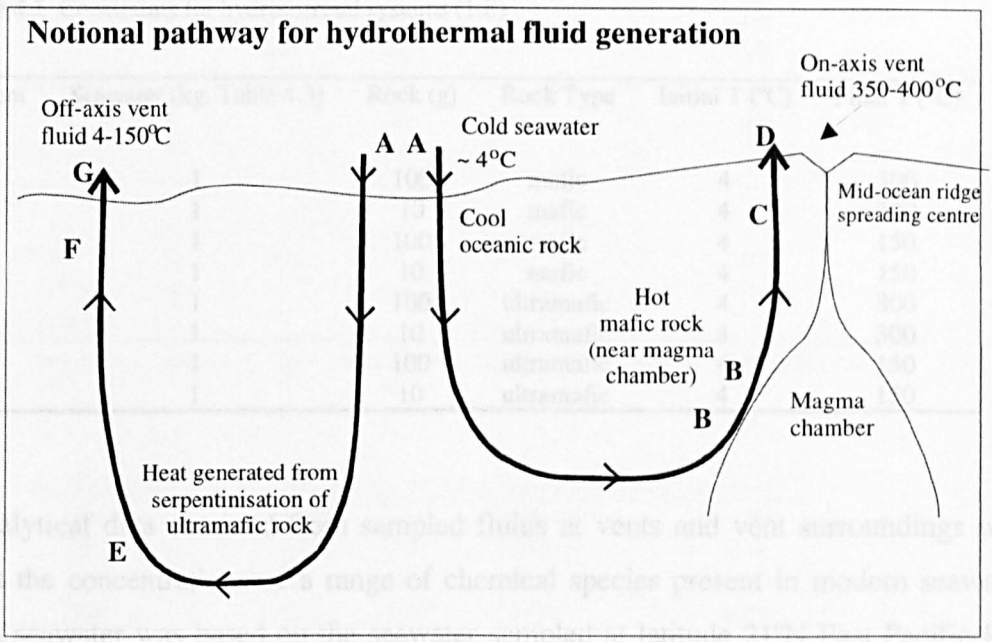

Figure 4.1. Diagram showing seawater flow and sequence of events **A-G** as seawater entering fissures in the oceanic crust metamorphoses into a hydrothermal fluid and, heated under pressure, exits near the spreading centre (**D**), or off-axis at **G**.

In Figure 4.1 at point **A**, cold, oxidised, and slightly alkaline seawater enters fissures in the oceanic crust. At **B**, seawater can be heated under pressure to temperatures of ≤400°C by magmatically-heated mafic rock, or to ~150°C assisted by serpentinisation of ultramafic rock at greater depth at off-axis vent systems (**E**). As the seawater is heated it rises back up through the crust. At **C**, the original seawater has been transformed into superheated, reduced, and acidic hydrothermal fluid, whereas at **F**, it is a relatively cool, reduced alkaline

fluid. At **D**, the hot, reduced, acidic hydrothermal fluid exits the on-axis vent and remixes with cold, oxidised, and slightly alkaline seawater, creating the 'black-smoker' vent plumes and entrained fresh precipitates. At **G**, the relatively cool alkaline fluids exit into seawater but with perhaps clear or 'white' coloured plumes.

Models representing the reactions occurring between seawater and rock at stages **B** and **E** in Figure 4.1 were created to produce the hydrothermal fluid at stage **C** and **F** respectively. To determine the influence of temperature on fluid composition and mineral alteration, experiments were conducted at 150°C and 300°C. Two seawater-rock ratios were tested (1kg seawater to 100g rock, and 1kg seawater to 10g rock) to represent a rock-dominated system and water-dominated system respectively. At water depths exceeding ~1 km, pressure has a negligible effect on pH compared with temperature (see §2.2, and Shock, 1992a; Schoonen *et al.*, 1999), thus pressure is not considered in the model. The constraints for each system modelled is summarised in Table 4.1

Table 4.1 Constraints for hydrothermal systems (1-8)

System	Seawater (kg, Table 4.3)	Rock (g)	Rock Type	Initial T (°C)	Final T (°C)
1	1	100	mafic	4	300
2	1	10	mafic	4	300
3	1	100	mafic	4	150
4	1	10	mafic	4	150
5	1	100	ultramafic	4	300
6	1	10	ultramafic	4	300
7	1	100	ultramafic	4	150
8	1	10	ultramafic	4	150

Analytical data obtained from sampled fluids at vents and vent surroundings were used to set the concentrations of a range of chemical species present in modern seawater. The model seawater was based on the seawater sampled at latitude 21°N East Pacific Rise spreading centre (von Damm *et al.*, 1985; Mottl and McConachy, 1990; Butterfield *et al.*, 1990; Drever, 1988; see Table 4.2), and is highly oxidised and moderately alkaline. The oxidation state of the seawater was constrained to be relatively oxidising by setting the activity of $O_{2(aq)}$ to 150 μmolal, though oxidation states vary between 30-200 μmolal (Table 4.2).

The model seawater in Table 4.3 was equilibrated at 4°C and then reacted with 100g of the mafic rock composition described in Table 4.4, while increasing the temperature from 4°C to 300°C over the course of the reaction. In addition, pH was set to an initial value (pH

= 7.7, Table 4.3) that would closely resemble the slightly alkaline nature of the seawater at the seafloor. It is helpful to set an approximate value for pH to reduce the number of mathematical operations that are required for the equilibrium values to be calculated. In addition, constraints which are too far from equilibrium will prevent the reaction from reaching equilibrium.

An assemblage of minerals (Tables 4.4 and 4.5) were used in appropriate quantities to represent the typical composition of mafic and ultramafic rock in the model (forsterite, Mg_2SiO_4; fayalite, Fe_2SiO_4; diopside, $CaMgSi_2O_6$; anorthite, $CaAl_2Si_2O_8$; albite, $NaAlSi_3O_8$; and troilite, FeS).

4.3.2 Reaction modelling constraints

Table 4.2 End-member Compositions of Seawater and Hydrothermal Fluids - East Pacific Rise near 21°N

mmolal	NGS field	OBS field	Seawater	µmolal	NGS field	OBS field	Seawater
Na+	510	432	464	Sr++	97	81	87
K+	25.8	23.2	9.78	Ba++	>15	>7	0.14
Mg++	~0	~0	52.7	Al+++	4	5.2	0.005
Ca++	20.8	15.6	10.25	Mn++	1002	960	0.0023
Cl-	579	489	541	Fe++	871	1664	0.0034
HCO3-	N/a	N/a	2.4	Cu+	<0.02	35	0.004
SO4--	~0	~0	29	Zn++	40	106	0.012
H2S	6.57	7.3	~0	O2	~0	~0	30-200
SiO2	19.5	17.6	0.178				
T(°C)	273	350	4	T(°C)	273	350	4
pH (25 °C)	3.8	3.4	7.8	pH (25 °C)	3.8	3.4	7.8
pH (273 °C)	4.5			pH (273 °C)	4.5		

Sources: Von Damm *et al.*, 1985; Mottle and McConaghy, 1990; Butterfield *et al.*, 1990; Drever, 1998

Table 4.3 - *GWB constraints used for 1kg modern seawater at 4°C

Species	mmolal	Species	µmolal
Cl^-	541	Ba^{++}	0.14
Na^+	464	Zn^{++}	0.012
Mg^{++}	52.7	Al^{+++}	0.005
SO_4^{--}	29	Cu^+	0.004
Ca^{++}	10.25	Fe^{++}	0.0034
K^+	9.78	Mn^{++}	0.0023
HCO_3^-	2.4	$O_{2(aq)}$	150
$SiO_{2(aq)}$	0.16		
Sr^{++}	0.087		
Initial pH	7.7		
Initial T (°C)	4		

*All values taken from Table 4.2

The water-rock reactions were repeated at 150°C, and again for the reaction between seawater and ultramafic rock at 300°C and 150°C (systems 5-8, Table 4.1). The ultramafic rock file is described in Table 4.5.

Table 4.4 - Rock composition representing mafic rock

	110g	11g
Forsterite (Mg_2SiO_4)	6.3	0.63
Fayalite (Fe_2SiO_4)	2.7	0.27
Diopside ($CaMgSi_2O_6$)	40	4
Anorthite ($CaAl_2Si_2O_8$)	30	3
Albite ($NaAlSi_3O_8$)	20	2
Troilite (FeS)	10	1

Table 4.5 - Rock composition representing ultramafic rock

	100g	10g
Forsterite (Mg_2SiO_4)	72	7.2
Fayalite (Fe_2SiO_4)	8	0.8
Diopside ($CaMgSi_2O_6$)	15	1.5
Anorthite ($CaAl_2Si_2O_8$)	3.6	0.36
Albite ($NaAlSi_3O_8$)	0.4	0.04
Troilite (FeS)	1	0.1

4.3.3 Results

Hydrothermal systems originating from seawater and mafic/ultramafic rock

Results for each temperature and type/amount of rock are presented as a series of plots. These show the concentration of dominant minerals, dominant magnesium and sulfur species, pH and oxidation state of the system as the reaction progresses towards equilibrium.

Although the main objective is to understand the pH of the fluids rather than the minerals precipitated, the minerals produced should resemble those observed in the field to assess the success of the model, and help to explain possible controls on pH. Thus plots of dominant mineral products described in Table 4.6 are also presented.

Table 4.6 - Minerals precipitated in systems 1-8

Mineral Name	Group	Formula
Albite	Feldspar	$NaAlSi_3O_8$
Amesite-14A	Silicate	$Mg_4Al_4Si_2O_{10}(OH)_8$
Anhydrite	Sulfate	$CaSO_4$
Antigorite	Serpentine	$Mg_{48}Si_{24}O_{85}(OH)_{62}$
Beidellite-Mg	Smectite	$Mg_{0.165}Al_{2.33}Si_{3.67}O_{10}(OH)_2$
Brucite	Hydroxide	$Mg(OH)_2$
Calcite	Carbonate	$CaCO_3$
Chalcopyrite	Sulfide	$CuFeS_2$
Clinochlore-14A	Chlorite	$Mg_5Al_2Si_3O_{10}(OH)_8$
Dolomite	Carbonate	$CaMg(CO_3)_2$
Epidote	Epidote	$Ca_2FeAl_2Si_3O_{12}OH$
Heulandite	Zeolite	$Ba_{0.065}Sr_{0.175}Ca_{0.585}K_{0.132}Na_{0.383}Al_{2.165}Si_{6.835}O_{18:6}$
Magnetite	Oxide	Fe_3O_4
Magnesite	Carbonate	$MgCO_3$
Maximum Microcline	Silicate	$KAlSi_3O_8$
Monticellite	Silicate	$CaMgSiO_4$
Muscovite	Mica	$KAl_3Si_3O_{10}(OH)_2$
Prehnite	Smectite	$Ca_2Al_2Si_3O_{10}(OH)_2$
Pyrite	Sulfide	FeS_2
Saponite-Ca	Smectite	$Ca_{0.165}Mg_3Al_{0.33}Si_{3.67}O_{10}(OH)_2$
Saponite-Na	Smectite	$Na_{0.33}Mg_3Al_{0.33}Si_{3.67}O_{10}(OH)_2$
Saponite-Mg	Smectite	$Mg_{3.165}Al_{0.33}Si_{3.67}O_{10}(OH)_2$
Sphalerite	Sulfide	ZnS
Tremolite	Amphibole	$Ca_2Mg_5Si_8O_{22}(OH)_2$
MHSH	sulfate	magnesium hydroxide sulfate hydrate

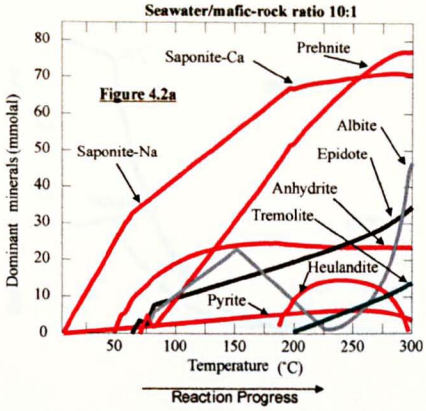
Seawater/mafic-rock ratio 10:1
Figure 4.2a
Saponite-Ca
Prehnite
Saponite-Na
Albite
Epidote
Anhydrite
Tremolite
Heulandite
Pyrite
Dominant minerals (mmolal)
Temperature (°C)
Reaction Progress

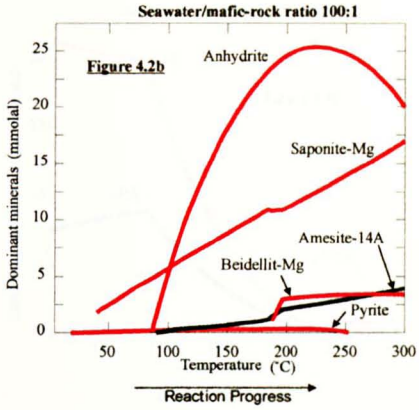
Seawater/mafic-rock ratio 100:1
Figure 4.2b
Anhydrite
Saponite-Mg
Amesite-14A
Beidellit-Mg
Pyrite
Dominant minerals (mmolal)
Temperature (°C)
Reaction Progress

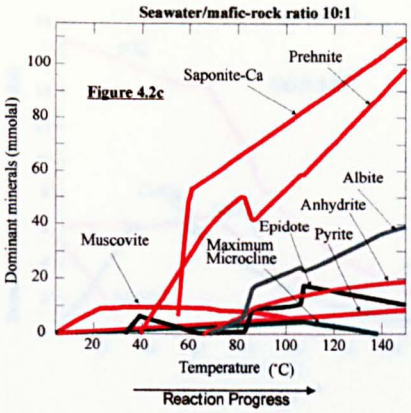
Seawater/mafic-rock ratio 10:1
Figure 4.2c
Prehnite
Saponite-Ca
Albite
Anhydrite
Epidote
Pyrite
Muscovite
Maximum Microcline
Dominant minerals (mmolal)
Temperature (°C)
Reaction Progress

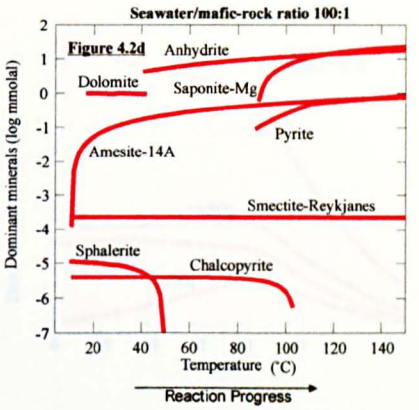
Seawater/mafic-rock ratio 100:1
Figure 4.2d
Anhydrite
Dolomite
Saponite-Mg
Pyrite
Amesite-14A
Smectite-Reykjanes
Sphalerite
Chalcopyrite
Dominant minerals (log mmolal)
Temperature (°C)
Reaction Progress

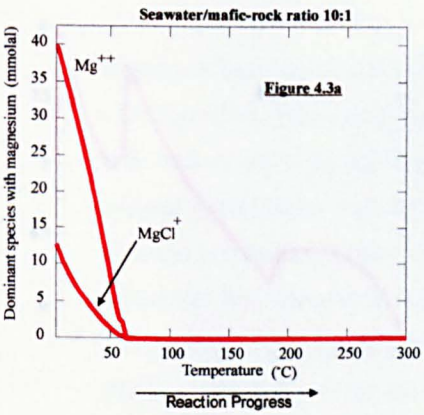
Seawater/mafic-rock ratio 10:1
Figure 4.3a
Mg++
MgCl+
Dominant species with magnesium (mmolal)
Temperature (°C)
Reaction Progress

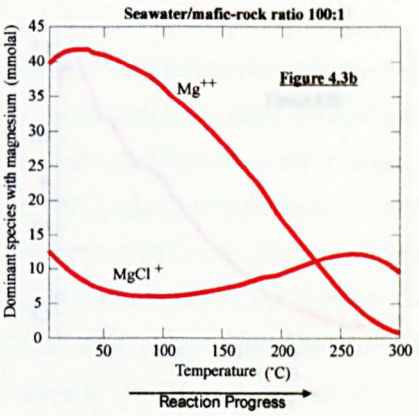
Seawater/mafic-rock ratio 100:1
Figure 4.3b
Mg++
MgCl+
Dominant species with magnesium (mmolal)
Temperature (°C)
Reaction Progress

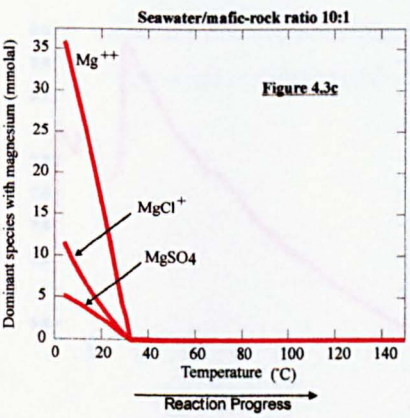
Seawater/mafic-rock ratio 10:1
Figure 4.3c
Mg++
MgCl+
MgSO4
Dominant species with magnesium (mmolal)
Temperature (°C)
Reaction Progress

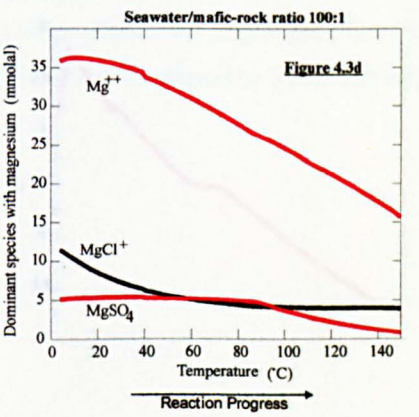
Seawater/mafic-rock ratio 100:1
Figure 4.3d
Mg++
MgCl+
MgSO4
Dominant species with magnesium (mmolal)
Temperature (°C)
Reaction Progress

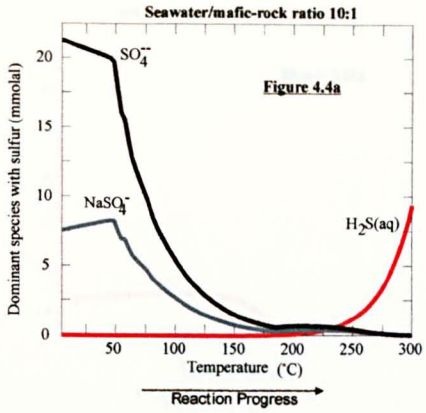
Seawater/mafic-rock ratio 10:1
Figure 4.4a
Dominant species with sulfur (mmolal)
SO_4^{--}
$NaSO_4^-$
$H_2S(aq)$
Temperature (°C)
Reaction Progress

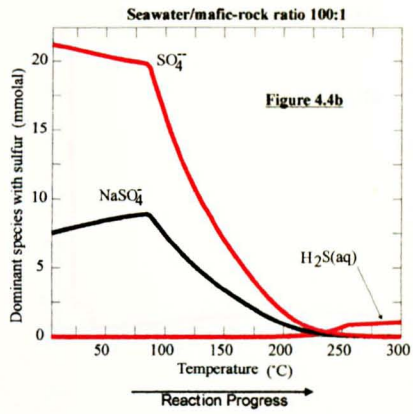
Seawater/mafic-rock ratio 100:1
Figure 4.4b
Dominant species with sulfur (mmolal)
SO_4^{--}
$NaSO_4^-$
$H_2S(aq)$
Temperature (°C)
Reaction Progress

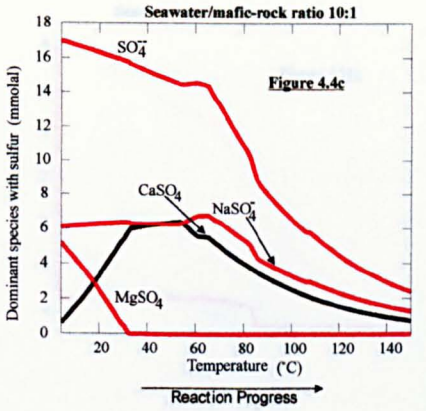
Seawater/mafic-rock ratio 10:1
Figure 4.4c
Dominant species with sulfur (mmolal)
SO_4^{--}
$CaSO_4$
$NaSO_4^-$
$MgSO_4$
Temperature (°C)
Reaction Progress

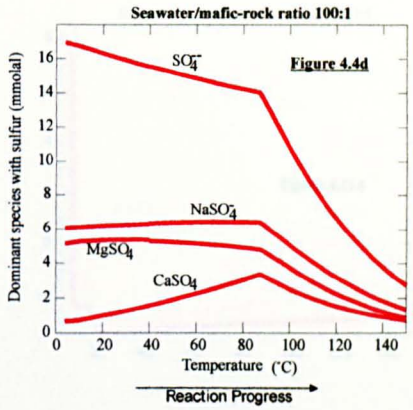
Seawater/mafic-rock ratio 100:1
Figure 4.4d
Dominant species with sulfur (mmolal)
SO_4^{--}
$NaSO_4^-$
$MgSO_4$
$CaSO_4$
Temperature (°C)
Reaction Progress

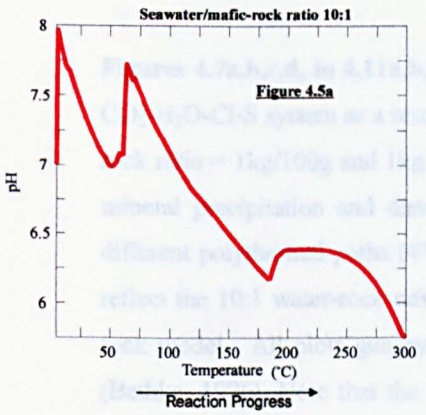
Seawater/mafic-rock ratio 10:1
Figure 4.5a
pH
Temperature (°C)
Reaction Progress

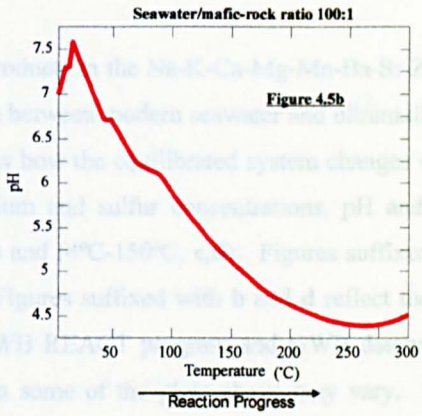
Seawater/mafic-rock ratio 100:1
Figure 4.5b
pH
Temperature (°C)
Reaction Progress

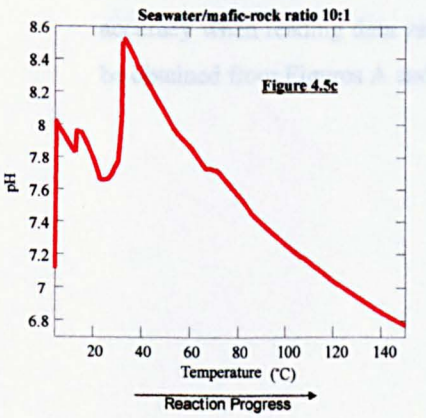
Seawater/mafic-rock ratio 10:1
Figure 4.5c
pH
Temperature (°C)
Reaction Progress

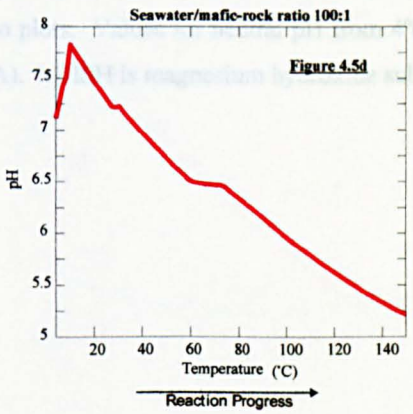
Seawater/mafic-rock ratio 100:1
Figure 4.5d
pH
Temperature (°C)
Reaction Progress

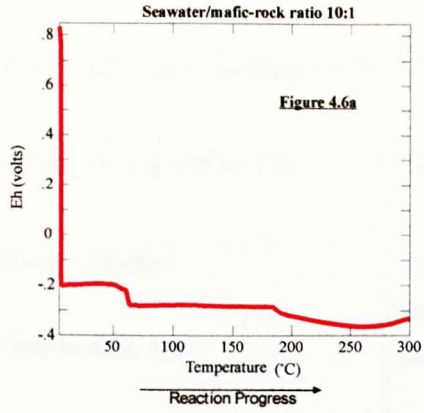

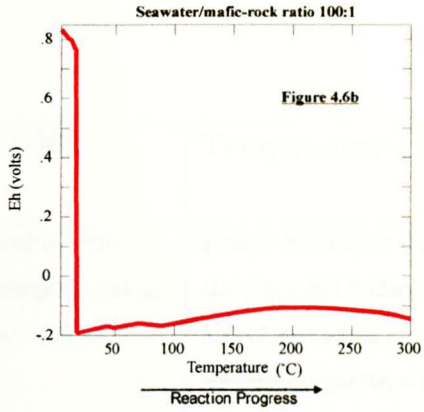

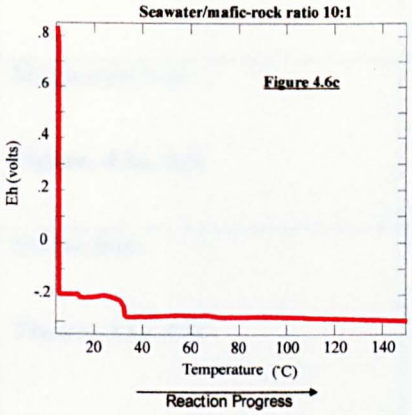

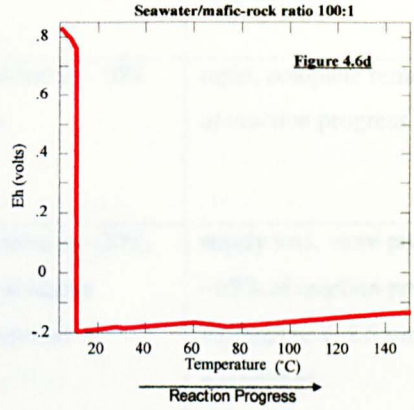

Figures 4.2a -4.6d. Reaction products in the Na-K-Ca-Mg-Mn-Ba-Sr-Zn-Fe-Al-SiO_2-CO_2-H_2O-Cl-S system as a result of the reaction between modern seawater and mafic rock (water-rock ratio = 1kg/100g and 1kg/10g). Plots show how the equilibrated system changes with respect to mineral precipitation and dissolution, magnesium and sulfur concentrations, pH and Eh over two different polythermal paths (4°C to 300°C, Figures **a** and **b**) and (4°C-150°C, Figures **c** and **d**). Figures **a** and **c** reflect the 10:1 water-rock ratio model, while Figures **b** and **d** reflect the 100:1 water-rock model. All plots generated using the GWB REACT program and GWB database *thermo.dat* (Bethke, 1998). Note that the ordinate scale on some of the plots above may vary. Logarithmic plots have been used in some cases to improve presentation and scale is adjusted to maximise accuracy when reading data values directly from plots. Values for neutral pH from 4°C to 300°C can be obtained from the graph in Figures A and B (Appendix 1A)

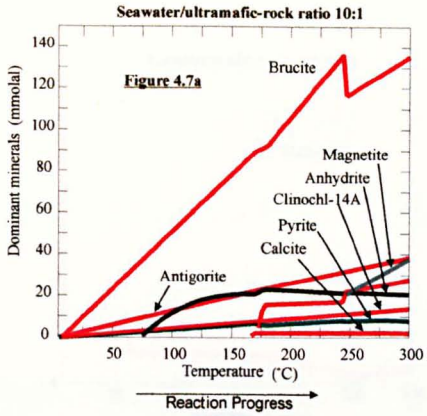
Seawater/ultramafic-rock ratio 10:1
Figure 4.7a
Brucite
Magnetite
Anhydrite
Clinochl-14A
Pyrite
Calcite
Antigorite
Dominant minerals (mmolal)
Temperature (°C)
Reaction Progress

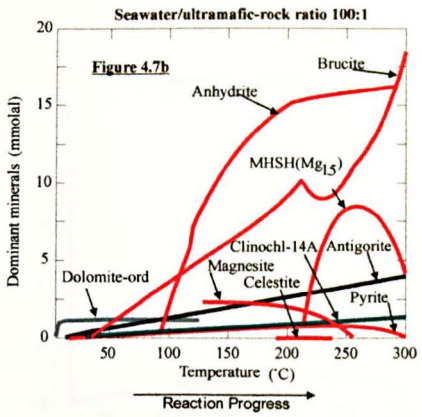
Seawater/ultramafic-rock ratio 100:1
Figure 4.7b
Brucite
Anhydrite
MHSH(Mg15)
Clinochl-14A
Antigorite
Magnesite
Celestite
Pyrite
Dolomite-ord
Dominant minerals (mmolal)
Temperature (°C)
Reaction Progress

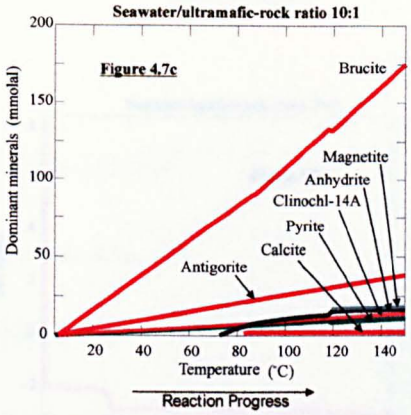
Seawater/ultramafic-rock ratio 10:1
Figure 4.7c
Brucite
Magnetite
Anhydrite
Clinochl-14A
Pyrite
Calcite
Antigorite
Dominant minerals (mmolal)
Temperature (°C)
Reaction Progress

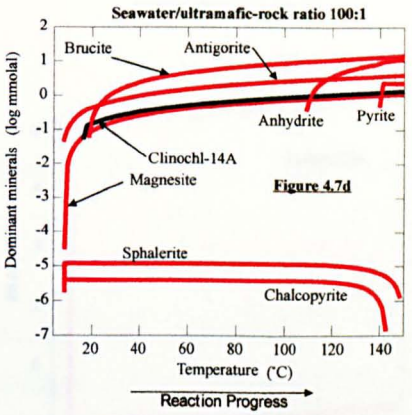
Seawater/ultramafic-rock ratio 100:1
Brucite
Antigorite
Anhydrite
Pyrite
Clinochl-14A
Magnesite
Figure 4.7d
Sphalerite
Chalcopyrite
Dominant minerals (log mmolal)
Temperature (°C)
Reaction Progress

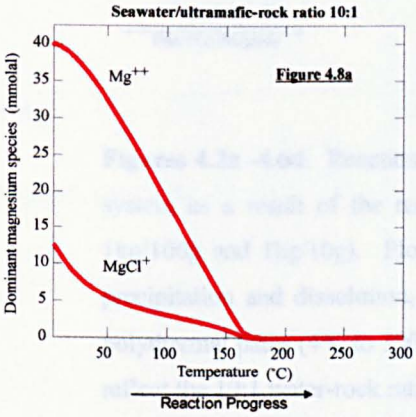
Seawater/ultramafic-rock ratio 10:1
Figure 4.8a
Mg++
MgCl+
Dominant magnesium species (mmolal)
Temperature (°C)
Reaction Progress

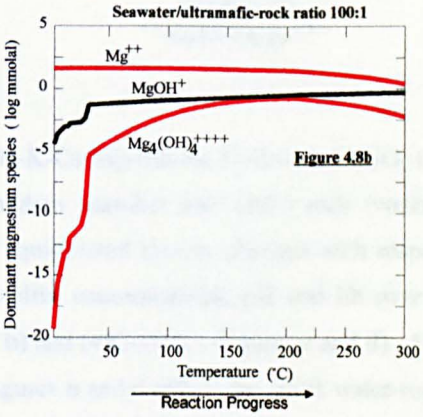
Seawater/ultramafic-rock ratio 100:1
Mg++
MgOH+
Mg4(OH)4++++
Figure 4.8b
Dominant magnesium species (log mmolal)
Temperature (°C)
Reaction Progress

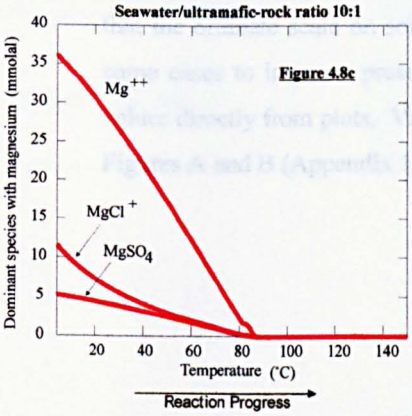
Seawater/ultramafic-rock ratio 10:1
Figure 4.8c
Mg++
MgCl+
MgSO4
Dominant species with magnesium (mmolal)
Temperature (°C)
Reaction Progress

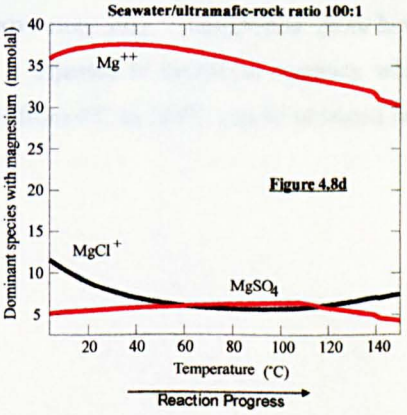
Seawater/ultramafic-rock ratio 100:1
Mg++
Figure 4.8d
MgCl+
MgSO4
Dominant species with magnesium (mmolal)
Temperature (°C)
Reaction Progress

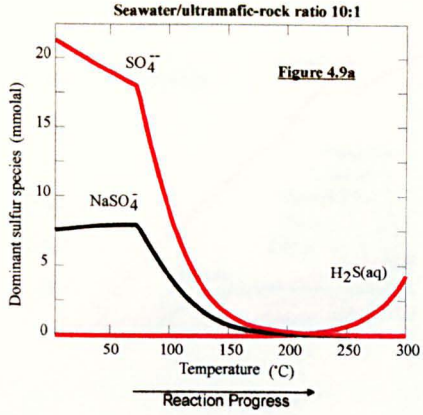
Seawater/ultramafic-rock ratio 10:1
Figure 4.9a
SO_4^{--}
$NaSO_4^-$
$H_2S(aq)$
Dominant sulfur species (mmolal)
Temperature (°C)
Reaction Progress

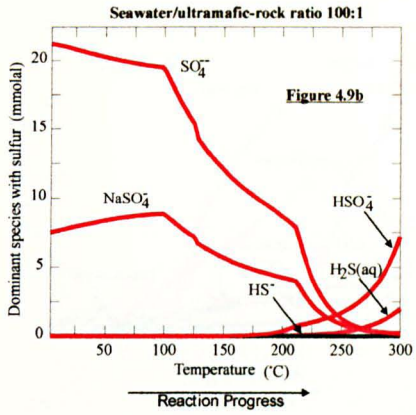
Seawater/ultramafic-rock ratio 100:1
Figure 4.9b
SO_4^{--}
$NaSO_4^-$
HSO_4^-
$H_2S(aq)$
HS^-
Dominant species with sulfur (mmolal)
Temperature (°C)
Reaction Progress

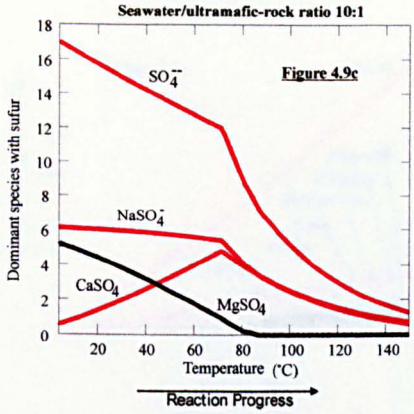
Seawater/ultramafic-rock ratio 10:1
Figure 4.9c
SO_4^{--}
$NaSO_4^-$
$CaSO_4$
$MgSO_4$
Dominant species with sufur
Temperature (°C)
Reaction Progress

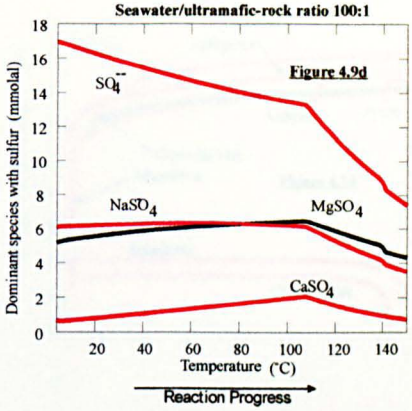
Seawater/ultramafic-rock ratio 100:1
Figure 4.9d
SO_4^{--}
$NaSO_4$
$MgSO_4$
$CaSO_4$
Dominant species with sulfur (mmolal)
Temperature (°C)
Reaction Progress

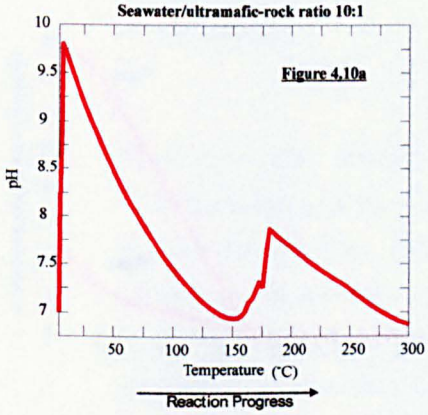
Seawater/ultramafic-rock ratio 10:1
Figure 4.10a
pH
Temperature (°C)
Reaction Progress

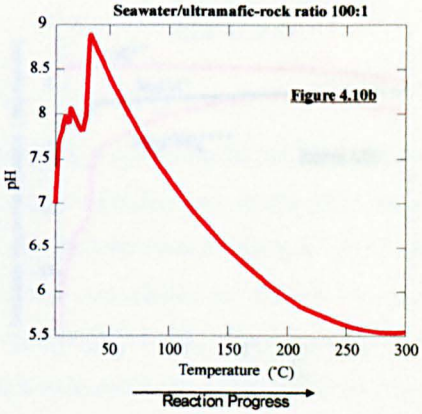
Seawater/ultramafic-rock ratio 100:1
Figure 4.10b
pH
Temperature (°C)
Reaction Progress

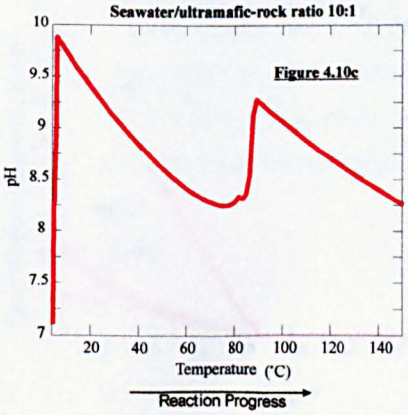
Seawater/ultramafic-rock ratio 10:1
Figure 4.10c
pH
Temperature (°C)
Reaction Progress

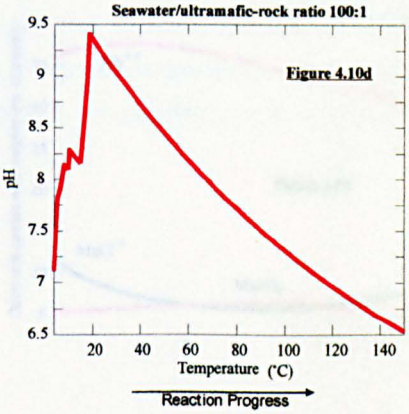
Seawater/ultramafic-rock ratio 100:1
Figure 4.10d
pH
Temperature (°C)
Reaction Progress

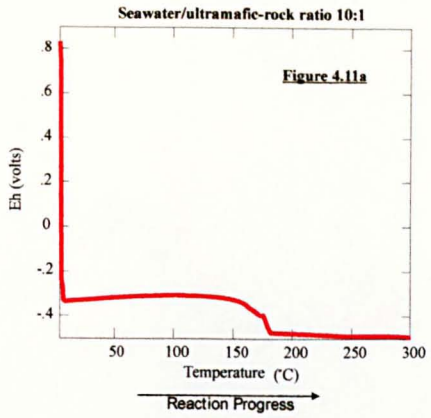

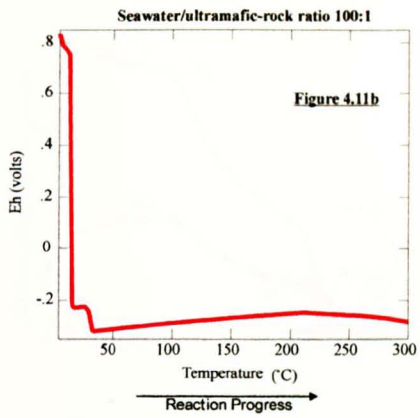

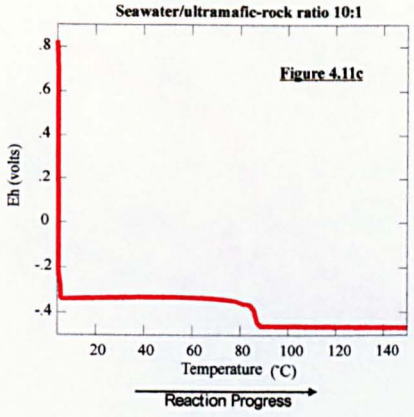

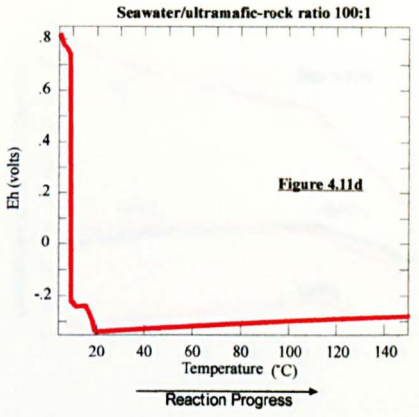

Figures 4.7a,b,c,d, to 4.11a,b,c,d. Reaction products in the Na-K-Ca-Mg-Mn-Ba-Sr-Zn-Fe-Al-SiO_2-CO_2-H_2O-Cl-S system as a result of the reaction between modern seawater and ultramafic rock (water-rock ratio = 1kg/100g and 1kg/10g). Plots show how the equilibrated system changes with respect to mineral precipitation and dissolution, magnesium and sulfur concentrations, pH and Eh over two different polythermal paths (4°C to 300°C, **a**,**b**) and (4°C-150°C, **c**,**d**). Figures suffixed with **a** and **c** reflect the 10:1 water-rock ratio model, while Figures suffixed with **b** and **d** reflect the 100:1 water-rock model. All plots generated using the GWB REACT program and GWB database *thermo.dat* (Bethke, 1996). Note that the ordinate scale on some of the plots above may vary. In some cases logarithmic plots were used to improve presentation, and in others, scales were adjusted to maximise accuracy when reading data values directly from plots. Values for neutral pH from 4°C to 300°C can be obtained from Figures A and B (Appendix 1A). MHSH is magnesium hydroxide sulfate hydrate.

Table 4.7 Rock-dominated mafic system		
Water-rock ratio 10:1	Temperature (300°C)	Temperature (150°C)
Mineral products **Figures 4.2a, 4.2c**	mainly Ca-rich smectites, with lesser amounts of feldspar, epidote, and amphibole, some sulfide	greater quantity of Ca-rich smectites and feldspar than at 300°C, and lesser amounts of anhydrite, epidote, slightly more sulfide than at 300°C, no amphibole
Magnesium loss **Figures 4.3a, 4.3c**	rapid, complete removal at ~20% of reaction progress	rapid, complete removal at ~25% of reaction progress
Sulfate loss **Figures 4.4a, 4.4c**	rapid, complete removal at ~20%, sulfide precipitates at higher temperatures (~9 mmolal)	steady loss, more pronounced at ~65% of reaction progress, incomplete (~2.5 mmolal remaining)
pH **Figures 4.5a, 4.5c**	immediate increase from 7 to 8, followed by sharp decline to 7 until Mg^{2+} is used up, sharp increase to 7.7, possibly due to loss of sulfate and calcium as anhydrite precipitates, sharp decrease to 7.7 to final pH of 5.8	initial increase from 7.1 to 8, followed by decrease to 7.6, sharp increase at ~25% reaction progress, possibly due to calcium loss as prehnite and saponite-Ca precipitate
Final Eh **Figures 4.6a, 4.6c**	relatively reduced (-0.3)	relatively reduced (-0.3)

Table 4.8 Water-dominated mafic system		
Water-rock ratio 100:1	Temperature (300°C)	Temperature (150°C)
Mineral products **Figures 4.2b, 4.2d**	mainly sulfate and magnesium-rich smectite	mainly anhydrite and magnesium-rich smectite, though overall concentrations are much less than rock-dominated system,
Magnesium loss **Figures 4.3b, 4.3d**	slow, incomplete, some magnesium remaining (~11 mmolal)	slow, incomplete, magnesium remaining (~21 mmolal)
Sulfate loss **Figures 4.4b, 4.4d**	rapid after ~30% of reaction progress to complete removal at 100%, some sulfide precipitation (~2.5 mmolal),	slow, incomplete, ~6 mmolal total sulfate remaining
pH **Figures 4.5b, 4.5d**	initial sharp increase from 7 to 7.5, followed by a gradual decrease to 4.5	initial sharp increase from 7.1 to 7.8, followed by a gradual decrease to 5.7
Final Eh **Figures 4.6b, 4.6d**	relatively reduced (-0.15)	relatively reduced (-0.15)

Table 4.9 Rock-dominated ultramafic system		
Water-rock ratio 10:1	Temperature (300°C)	Temperature (150°C)
Mineral products **Figures 4.7a, 4.7c**	mainly brucite with lesser amounts of antigorite, magnetite, magnesium-rich chlorite, and some pyrite and calcite	mainly brucite and antigorite, with lesser amounts of magnetite, anhydrite, magnesium-rich chlorite, pyrite, calcite
Magnesium loss **Figures 4.8a, 4.8c**	rapid, though less pronounced than water- dominated mafic system, complete removal at 55% of reaction progress	rapid, though less pronounced than water- dominated mafic system, complete removal at 55% of reaction progress
Sulfate loss **Figures 4.9a, 4.9c**	initially a steady loss, rapid loss after ~25% of reaction progress, possibly due to anhydrite precipitation	initially a steady loss, rapid loss after ~50% of reaction progress, possibly due to anhydrite precipitation
pH **Figures 4.10a, 4.10c**	immediate increase from 7 to 7.9, followed by a sharp decrease to 7 at ~50% of reaction progress, sharp increase to 8, followed by a gradual decrease to 7	immediate increase from 7.1 to 9.9, followed by a relatively gradual decrease to 8.3 at ~60% of reaction progress, sharp increase to 9.3, followed by a gradual decrease to 8.3
Final Eh **Figures 4.11a, 4.11c**	relatively reduced (-0.5)	relatively reduced (-0.48)

Table 4.10 Water-dominated ultramafic system		
Water-rock ratio 100:1	Temperature (300°C)	Temperature (150°C)
Mineral products **Figures 4.7b, 4.7d**	mainly brucite and anhydrite, with lesser amounts of antigorite, and some chlorite,	mainly brucite and anhydrite, with lesser amounts of antigorite and pyrite
Magnesium loss **Figures 4.8b, 4.8d**	no overall loss, perhaps slight increase	no overall change
Sulfate loss **Figures 4.9b, 4.9d**	steady loss after ~35% of reaction progress, probably due to anhydrite precipitation	steady loss after ~85% of reaction progress, probably due to anhydrite precipitation
pH **Figures 4.10b, 4.10d**	sharp increase from 7 to 8.9 to ~15% of reaction progress, gradual decrease to 5.5	sharp increase from 7.1 to 9.3 to ~15% of reaction progress, gradual decrease to 6.5
Final Eh **Figures 4.11b, 4.11d**	relatively reduced (-0.3)	relatively reduced (-0.28)

4.3.4 Discussion

Reactant minerals were dissociated and others precipitated when the model seawater, initially at 4°C, was percolated through the mafic crust and heated in the presence of mafic rock at 300°C (Figures **a** and **b**), and 150°C (Figures **c** and **d**), and at water-rock ratios of 10:1 (Figures **a** and **c**) and 100:1 (Figures **b** and **d**).

The results of the models show the varying concentration of minerals (Figures 4.2a, to 4.2d), in particular, the magnesium minerals (saponite-Ca, saponite-Mg, tremolite, amesite-14A, beidellite-Mg, see Table 4.6) and sulfur minerals (anhydrite, pyrite) in the system, as the reaction proceeds toward equilibrium (Figures 4.2a and 4.2b), at water rock ratios of 10:1 and 100:1 respectively).

The minerals present in the fluid are indicated at the end of the reaction at the final temperatures of 300°C and 150°C, the temperatures at which each system is at equilibrium (Figures 4.2a to 4.2d and 4.7a-4.7d). To resemble a typical high-temperature black-smoker hydrothermal system (relatively high in silicates, silicate-hydroxides, such as smectites, feldspar, epidote, kaolinite, and amphibole. The final fluid composition should be low in magnesium and sulfate, reduced, acidic, and have a high HS^-/SO^{2-}_4 ratio at 300°C. Minerals such as anhydrite (high in sulfate) and pyrite (high in sulfide) should also be precipitated. The results are summarised in Tables 4.7 to 4.10.

Summarising the results by referring to Table 4.6: a water-rock ratio of 10:1 favoured the production of calcium-rich smectites such as prehnite and saponite-Ca, and feldspars such as albite (Figure 4.2a). A water-rock ratio of 100:1 favours the production of the sulfate mineral, anhydrite, $CaSO_4$ and the magnesium-rich smectite (saponite-Mg, Figure 4.2b).

The mafic model shows that total Mg^{2+} and SO_4^{2-} concentrations decrease as the water-rock reaction progresses with increasing temperature. In rock-dominated reaction conditions, concentrations of total Mg^{2+} and SO_4^{2-} drop to ~0 (Figure 4.3a, 4.3b), but in water-dominated conditions (Figures 4.4c, 4.4d) some Mg^{2+} and SO_4^{2-} are still present (total Mg^{2+} ~21 mmolal, Figures 4.3b, 4.3d, and total SO_4^{2-} ~7 mmolal, Figure 4.4d) in the hydrothermal fluid but concentrations drop with increasing temperature. The calculated results for the 300°C model correspond closely to measured values given for the black-smoker fluids sampled from the NGS and OBS fields (Table 4.2).

Total sulfate concentrations (SO_4^{2-} and $NaSO_4^{2-}$) decrease from the initial levels in seawater (29 mmolal, Table 4.2) to ~0 in the hydrothermal fluid (Table 4.2), with a corresponding increase in sulfide, $H_2S_{(aq)}$ from ~0 to ~10 mmolal (Figure 4.4a), and ~1 mmolal (at a water-rock ratio of 100:1) as the seawater metamorphoses to a hydrothermal fluid. More rock (10:1, Figure 4.4a) may produce more hydrogen from the fayalite-water reaction during serpentinisation of the rock, and thus may make conditions more reducing than in 100:1 water-rock ratio model (Figure 4.4b), thus allowing more sulfide to form than in the 100:1 rock model. Thus, there is significantly less sulfide stable with mafic rock-dominated system (Figures 4.2b, 4.2d, 4.4b, 4.4d). Against expectation, pH rises, which could be explained by the fluid coming into equilibrium with the new minerals forming in the rock. So with higher water-rock ratios the final fluid is more alkaline. The rock-dominated ultramafic system produces mainly brucite ($Mg(OH)_2$) and antigorite, whereas the water-dominated ultramafic system produces mainly brucite ($Mg(OH)_2$) and anhydrite ($CaSO_4$).

4.4 The EQ3NR speciation/solubility code and the EQ6 reaction path code

4.4.1 Introduction

GWB and EQ3NR/EQ6 (Wolery and Sleep, 1976) are similar in function and logic, but not in appearance. GWB's graphical-user interface is visually more aesthetic and easier to use than EQ3NR/EQ6's UNIX command-prompt interface. EQ3NR/EQ6 requires more care and effort to prepare and successfully run input files. Though simple codes could be written to extract the required data from the large EQ6 output files (one run can produce >100 A4 size pages of data), manual extraction, unit conversions, and plotting of data from one run can take hours of valuable time and is prone to human error. With GWB, the user can choose from logarithmic or linear plots of, elemental compositions, minerals, gases, aqueous species, E*h* and pH, and variety of measurement units to choose from, are plotted almost immediately. EQ3NR/EQ6 requires considerable skills in the UNIX programming language to install and maintain, whereas GWB is available for popular operating systems such as Windows and Macintosh which install automatically and technical support is available online. There is also an e-mail discussion forum for GWB users. EQ3NR/EQ6's technical support is somewhat limited as it is maintained by the academic community at the Lawrence Livermore National Laboratory (USA). On the other hand, the cost for the EQ3NR/EQ6 codes is substantially less than the GWB code, and the high-level documentation describing the equations is useful for the modeller to understand how the results are calculated.

The objective of this exercise was to repeat the experiments that were conducted using GWB with EQ3NR/EQ6, and then to compare and substantiate results with measured and calculated values. Hydrothermal systems were modelled using the EQ3NR speciation-solubility code (Wolery, 1983) and the EQ6 reaction path code (Wolery, 1979). Modern seawater was equilibrated at 4°C with the EQ3NR program and then reacted with mafic and ultramafic rocks at temperatures of 150°C and 300°C with the EQ6 program. Experiments with GWB were conducted using units of grams (g). Since minerals in the EQ6 code were required to be input in units of moles, the mineral composition of the rock was converted from grams to moles (mol) for input to the EQ6 reaction-path program (Table 4.11).

Table 4.11. Unit conversions for mafic and ultramafic rock

Mineral	Formula	Formula Wt. (g/mol)	100g mafic rock (g)	No of moles in 100g mafic rock (mol)	100g ultramafic rock (g)	100g ultramafic rock (mol)
Forsterite	Mg_2SiO_4	140.72	6.3	0.0448	72	0.51
Fayalite	Fe_2SiO_4	203.78	2.7	0.0133	8	0.39
Diopside	$CaMgSi_2O_6$	216.55	40	0.1847	15	0.69
Anorthite	$CaAl_2Si_2O_8$	278.25	30	0.0923	3.6	0.13
Albite	$NaAlSi_3O_8$	262.27	20	0.0763	0.4	0.015
Troilite	FeS	87.9	1	0.0114	1	0.11

4.4.2 Procedure

The systems tested with GWB were remodelled using EQ3NR and EQ6. Similarities or differences between these results and those obtained from GWB were noted.

4.4.3 EQ3NR/EQ6 results for seawater and mafic rock

Table 4.12. Initial and final pH, *Eh* for systems 1-4 (W-water, R-rock)

Temp. (°C)		W/R ratio	Initial pH		Final pH		Initial *Eh*		Final *Eh*	
W	*R*		*NBS*, Rat.*** (EQ3/6)	(GWB)	*NBS, Rat.* (EQ3/6)	(GWB)	*NBS, Rat.* (EQ3/6)	(GWB)	*NBS, Rat.* (EQ3/6)	(GWB)
4	300	10:1	5.49, 5.22	7	5.86, 5.58	5.25	0.46, 0.49	0.83	-0.35, -0.32	-0.33
4	300	100:1	5.49, 5.22	7	4.34, 4.06	4.5	0.46, 0.49	0.84	-0.13, -0.09	-0.15
4	150	10:1	5.77, 5.63	7.1	7.43, 7.29	6.8	0.65, 0.66	0.83	-0.39, -0.37	-0.3
4	150	100:1	5.77, 5.63	7.1	5.21, 5.07	5.25	0.65, 0.67	0.84	-0.14, -0.13	-0.15

* NBS (National Bureau of Standards) pH and *Eh* values are extrapolated values from an arbitrarily chosen species.
** abbreviation for rational pH scale.

4.4.4 Summaries of reaction products - Systems 1-4

Blank spaces in tables indicate that either the mineral is not available in the database or it is not precipitated, but another mineral is precipitated instead (that is, the next supersaturated mineral in the system. For example, in GWB, instead of mesolite precipitation, the minerals precipitated in its place may be albite and prehnite.

Table 4.13 - 100g mafic rock and modern seawater at 300 °C (-) data not available

Major minerals	EQ3NR/6 results (mmoles)	Approximate GWB results (mmolal)
Anhydrite	23.5	24
Albite	-	47
Epidote	32.2	35
Mesolite $Na_2Ca_2[Al_2Si_3O_{10}].8H_2O$	56.9	-
Prehnite	33.6	77
Pyrite	5.82	4
Saponite-Ca	48.5	70
Tremolite	36.3	13

Table 4.14 Experiment 2 - 10g mafic rock and modern seawater at 300 °C

(-) data not available

Major minerals	EQ3NR/6 results (mmoles)	Approximate GWB results (mmolal)
Amesite-14A	2.77	8
Anhydrite	23.1	20
Beidellite-Mg	4.24	7
Hematite	1.58	-
Pyrite	0.34	~0
Saponite-Mg	15.6	17

Table 4.15 - 100g mafic rock and modern seawater at 150 °C

(-) data not available

Major minerals	EQ3/6 results (mmoles)	Approximate GWB results (mmolal)
Unknown	14.7	-
Anhydrite	21.8	20
Calcite	2.37	-
Clinochlore-14A	0.288	-
Diopside	0.460	-
Mesolite	96.2	-
Phlogopite	6.67	-
Prehnite	18.4	98
Pyrite	8.51	9
Saponite-Ca	7.72	110

Table 4.16 - 10g mafic rock and modern seawater at 150 °C (-) data not available

Major minerals	EQ3/6 results (mmoles)	Approximate GWB results (mmolal)
Amesite-14A	5.46	
Anhydrite	2.00	1.25
Hematite	1.45	15
Mesolite	2.91	-
Muscovite	6.02	-
Pyrite	8.58	0.8
Saponite-Mg	1.75	19.95

4.4.5 EQ3NR/EQ6 results for seawater and ultramafic rock

Table 4.17. Initial and final pH, *Eh* for systems 5-8

Temperature		Water/ rock ratio	Initial pH		Final pH		Initial *Eh*		Final *Eh*	
Water	Rock		NBS	Rational	NBS	Rational	NBS	Rational	NBS	Rational
4 °C	300°C	10:1	5.49	5.22	6.64	6.37	0.46	0.49	-0.47	-0.43
4°C	300°C	100:1	5.49	5.22	5.51	5.24	0.46	0.5	-0.29	-0.26
4°C	150°C	10:1	5.77	5.63	8.23	8.08	0.65	0.67	-0.46	-0.45
4°C	150°C	100:1	5.77	5.63	6.56	6.41	0.65	0.67	-0.28	-0.27

Table 4.18. Initial and final pH, *Eh* for experiments 5-8 (W-water, R-rock) (-) data not available

Temp. (°C)		W/R ratio	Initial PH		Final PH		Initial *Eh*		Final *Eh*	
W	*R*		*NBS*, Rat.*** (EQ3/6)	(GWB)	*NBS, Rat.* (EQ3/6)	(GWB)	*NBS, Rat.* (EQ3/6)	(GWB)	*NBS, Rat.* (EQ3/6)	(GWB)
4	300	10:1	5.49, 5.22	7	6.64, 6.37	6.9	0.46, 0.49	0.81	-0.47, -0.43	-0.45
4	300	100:1	5.49, 5.22	7	5.51, 5.24	5.5	0.46, 0.5	0.85	-0.29, -0.26	-0.28
4	150	10:1	5.77, 5.63	7.1	8.23, 8.08	8.25	0.65, 0.67	-	-0.46, -0.45	-
4	150	100:1	5.77, 5.63	7.1	6.56, 6.41	6.5	0.65, 0.67	0.84	-0.28, -0.27	-0.27

4.4.6 Summaries of mineral products - Systems 5-8

Table 4.19 - 100g ultramafic rock and modern seawater at 300 °C

Major Minerals	EQ3/6 results (mmoles)	Approximate GWB results (mmolal)
Anhydrite	20.2	20
Antigorite	18.8	37
Brucite	133	135
Calcite	2.15	2
Clinochlore-14A	13.8	13
Magnetite	27.0	27
Monticellite	36.7	37
Pyrite	7.96	8

Table 4.20 - 10g ultramafic rock and modern seawater at 300 °C (-) data not available

Major Minerals	EQ3/6 results (mmoles)	Approximate GWB results (mmolal)
Anhydrite	10.4	16.5
Antigorite	1.99	3.5
Brucite	16.7	18.5
Clinochlore-14A	1.38	1.5
Hematite	4.21	-
Pyrite	0.485	~0
MHSH($Mg_{1.5}$)	-	4.5

Table 4.21 - 100g ultramafic rock and modern seawater at 150 °C

(-) data not available

Major Minerals	EQ3/6 results (mmoles)	Approximate GWB results (mmolal)
Unknown	12.8	-
Anhydrite	17.4	17
Antigorite	18.8	37
Brucite	172	175
Calcite	2.39	2
Clinochlore-14A	13.7	17
Magnetite	17.7	20
Pyrite	10.4	12

Table 4.22 - 10g ultramafic rock and modern seawater at 150 °C

(-) data not available

Major Minerals	EQ3/6 results (mmoles)	Approximate GWB results (mmolal)
Anhydrite	6.93	12.6
Antigorite	1.99	3.16
Brucite	14.6	15.9
Clinochlore-14A	1.38	1
Dolomite-ord	1.16	-
Hematite	3.86	-
Pyrite	1.18	1.99

4.5 Conclusions

Mafic system

The production of the MgOH-bearing silicates (saponite-Ca, saponite-Mg, tremolite, amesite-14A, beidellite-Mg) together with the decrease in Mg^{2+} concentration, sulfate/sulfide ratio and pH and E*h* (in Figures 4.2a to 4.6d), indicated that the model behaved correctly in showing that Mg^{2+} in seawater is converted to minerals containing magnesium hydroxides, and that the fluid is relatively reduced compared with seawater (Initial Eh is approx. +0.8 V, whereas final Eh is -3.2 V for the 10:1 water-rock model, and approx. -1.4 V for the 100:1 water-rock model), and neutral to acidic (final pH is ~5.8 for 10:1 water-rock model, and ~ 4.5 for the 100:1 water-rock model).

The computed levels of total Mg^{2+} and SO_4^{2-} (Figures 4.3a, 4.3b, and Figures 4.4a, 4.4b) generally agree with the measured values given in Table 4.2: the lower the water-rock ratio the lower the Mg precipitation. The loss of sulfate from the seawater appears to be predominantly due to the formation of anhydrite during the water-rock reactions and in the case of sulfide formation is indicative of the thermal abiogenic reduction of sulfate (Figures 4.4a to 4.4d). In the model, the sulfide concentration is approximately 9 mmolal at 300°C. However, the sampled fluids have a slightly lower concentration of sulfide (6.6 mmolal) at 273°C, and 7.3 mmolal at 350°C. Seyfried and Bischoff (1979) argue that at 150°C and a water-rock ratio of 10, magnesium in seawater and calcium in the rock undergo exchange reactions. Ca passes from mafic rock to the final fluid (Mottl and Holland, 1978) to balance the ion charge. Once all the magnesium has removed all the Ca, there is an excess of magnesium at higher water rock ratios. Iron and magnesium-rich smectite were the major products. The pH is lower due to magnesium silicate precipitation. Temperature also affects

magnitude and direction of each change. Seyfried and Bischoff's (1979) final pH at 150°C were 5.5 and 5.6 after an initial decrease.

Seyfried and Bischoff also state that at temperatures above 200°C is from the precipitation of anhydrite from seawater. Anhydrite does not precipitate out of seawater at <150°C, therefore the assumption is that anhydrite precipitation at >150°C is mainly from the Ca in the basalt used in their experiments.

Overall, the ratio of sulfate to sulfide shown at equilibrium however, is reasonably correct with respect to the values given in Table 4.2. Initial and final concentrations may vary by a few mmolal, but it is the magnitude of the increase and decrease in concentrations that are particularly relevant here. However, we cannot be sure that the concentrations of species present during the course of the reaction path reflect the real system, since a real system would be maintained at disequilibrium, thus intermediate values of the real system are not calculated.

On comparison with $H_2S_{(aq)}$ values from the NGS and OBS fields (6.57 and 7.3 mmolal respectively, Table 4.2) the sulfide concentration in the model (Figure 4.4a) is slightly higher than expected. Figures 4.4a and 4.4b indicate that the oceanic crust is a major sulfur sink. The Mg and H_2S content of the black smoker model fluid agreed with the measured values of Von Damm, 1985. The pH decrease in the model is appropriate, as seawater is initially slightly alkaline, and black-smoker hydrothermal fluids typically acidic. The final pH value (pH ~5.8) agrees closely with observed values. To answer the question whether pH is dependent on the concentration of magnesium which is present in the original seawater, we can see that the curves showing the rate of depletion of magnesium in Figures 4.3a and 4.3b corresponds to a general rate of decrease in pH in Figure 1.4. Although some sulfates might be expected in an acidic solution, the reducing conditions ensure that $H_2S_{(aq)}$ is the dominant sulfur species at the end of the reactions (Figures 4.4a and 4.4b). Some HSO_4^- (bisulfate) may persist in higher water-rock ratios 100:1. Figure 4.7b suggests MHSH as an alteration product. However, temperature-induced precipitation of anhydrite and MHSH from seawater, rather than alteration of rock, were evident in peridotite-seawater experiments at 300°C, except when Ca reached high enough concentrations in solution to replace MHSH with anhydrite (Janecky and Seyfried, 1986).

The decrease in pH and Mg^{2+} is related to the precipitation of $Mg(OH)_2$ minerals as the seawater is converted to the hydrothermal fluid.

The initial rises in pH are most likely caused by reaction and dissolution of minerals possibly due to the rising temperature during the course of the reaction. However, during the course of the reaction, pH rises again sharply several times whereas the concentration of Mg species continues to decrease. This could be explained by the fluid coming into equilibrium with the new minerals forming in the rock. The pH is also dependent on the water-rock ratio. At the same temperature, pH is lowered as more rock is reacted with aqueous fluid. Lower pH is attained with low water-rock ratio at high temperature. When the seawater comes into contact with the mafic rock, the seawater rapidly transforms from being highly oxidised to a highly reduced fluid. With 100 g of mafic rock reacted up to a temperature of 150°C, the final value of the pH is the same as with half as much of the same rock reacted at the same temperature. For the ultramafic system, brucite ($Mg(OH)_2$) is the dominant precipitate with some antigorite at a seawater-rock ratio of 10:1. However, it is mainly brucite ($Mg(OH)_2$) and anhydrite (CaSO4) at the seawater-rock ratio of 100:1. The final pH of the fluid produced from ultramafic rock is higher (pH 6.5) than the final pH (pH 5.25) of the fluid produced from a similar amount of mafic rock reacted over the same temperature range (Figure 2.4). Thus the results shows that ultramafic rock influences pH differently and becomes more alkaline at an early stage and less acid at a later stage. This behaviour adds to the possibility of a relationship between magnesium concentrations in the rock and fluid pH (that is, the magnesium bearing rock cannot accept even more Mg by replacement). Seyfried *et al.* (1991) suggest that the $pH_{(25°C)}$ is a direct result of the dissociation of H^+ and OH^- bearing aqueous complexes species which are more stable at elevated temperatures and pressures than at STP (25°C / 1 atmosphere), and that at temperatures below 300°C, $pH_{(25°C)}$ is characterised by high values owing to the relative lack of $HCl^0_{(aq)}$ at these temperatures and the existence of slight but nevertheless still significant amounts of OH- bearing species.

On comparison of the EQ3NR/EQ6 results, overall they are very similar, though there are a few discrepancies. They show that the initial E*h* and pHs are low for the EQ3NR/EQ6 model compared with the GWB model. In the EQ3NR/EQ6 model, the initial redox state is required to be set by a redox couple (Wolery and Daveler, 1992), in this case, the Cu^{2+}/Cu^+ couple. The E*h* was not directly specified at the start of the reaction in the GWB model and thus the initial E*h* and pH values are different. The final Eh and pH values are however in very good agreement since the system is rock-dominated and therefore not really affecting the final Eh and pH of the system. In addition, the GWB database is lacking in some important minerals as can be seen by the number of blank entries in the tables. However, the final mineral assemblage is similar, but intermediate stages might well be disimilar. The

model may be improved upon by constraining the initial redox directly (for example, setting the initial E*h*) or indirectly with a redox couple (for example, $O_{2(aq)}/H_2O$).

In general, the results indicate that the lower the water-rock ratio the lower the Mg precipitation. This agrees with Seyfried and Bischoff's (1979) experiments that water-rock ratios greater than 50 do not allow complete removal of magnesium from seawater.

Black smokers require anhydrite precipitation (none in Hadean) and anhydrite precipitation requires alkalinisation. However, the Hadean ocean may well have been acidic due to high levels of CO_2. But it is possible that 400°C springs of similar chemistry would have existed.

The downside of the results are that for 100g and 10g of rock reacted, the pH results at same temperatures don't make much sense, they should be the same after 10% of reaction progress with 10g of rock and with 100g rock, and this is clearly not the case.

In addition, the models are equilibrium models and are thus limited in that the intermediate reaction paths are not verifiable (Bethke, 1996; p48). Many of the intermediate water-rock reactions would not proceed to completion at such low temperatures.

An alternative approach would be to heat the seawater to 150°C and 300°C on its own first then react it with the rock and see how this affects the results.

Another idea would be to obtain data for lower or higher temperature black smokers (and lower water-rock ratios) and see if their chemistry will also agree with reaction modelling results. If so, reaction modelling could be used to predict/extrapolate the fluids history/path.

The 300°C hydrothermal fluid produced in the model (seawater and mafic/or ultramafic rock) could also be reacted with iron-rich Hadean Ocean (equilibrated with 10 bars CO_2) to investigate the hydrothermal system that would result.

To determine whether pH is therefore independent of mass of rock reacted, further tests with different masses of rock may be required to be confident in making a statement about this. If so, this would strengthen the argument for the relationship between Mg^{2+} and pH.

Other weaknesses in the model could be that the values in Table 4.2 may be unreliable due to the difficulties in sampling, measuring overall E*h*, and in electrode poisoning by mineral particulates.

Chapter 5 - Mineral Buffers

5.1 Introduction

Groups of minerals in the Earth's crust that coexist in thermodynamic equilibrium with respect to each other (and any fluids or gases that may be present) are known as mineral assemblages. Some assemblages can act as buffers controlling gas fugacities. The influence of minerals in the crust range from buffering the redox states and activities of the fluids and gases that surround them (Shock, 1992a), to serving as chromatographic media (Washington, 2000). In surface sediments or hydrothermal systems, minerals may act as catalytic surfaces to remove activation energy barriers for organic synthesis (Wächtershäuser, 1988a; Huber and Wächtershäuser, 1997; Huber and Wächtershäuser, 1998). The composition of the crust varies with depth and in the degree of its metamorphic alteration from its original igneous or sedimentary composition. Thus, the group of minerals that are involved in buffering a fluid or gas depends on the path which the fluid or gas is taking through the crust (Shock, 1992a). The presence of certain mineral assemblages can remove (or introduce) kinetic barriers for local aqueous geochemical reactions that can then proceed via alternative reaction pathways and thus allow organic compounds to form in environments previously thought to be unsuitable for organic syntheses. It is for these reasons that mineral buffers feature strongly in origin of Life theories and experiments when considering the potential for organic synthesis from hydrothermal fluids. However, it should be made clear that the minerals themselves are not always used in experimental work. Experimental results may be compared to the theoretical fugacity of a gas or the activity of an aqueous species fixed by a particular mineral assemblage or even a theoretical one. Geochemists often use the calculated redox power of a theoretical mineral assemblage to provide activity or fugacity values as reference points and to predict whether a reaction can proceed under certain redox conditions.

The driving force for organic synthesis is the energy harnessed from the redox reactions occurring between an assemblage of interdependent minerals present in the early crust. The mineral assemblage of pyrrhotite, $Fe_{1-x}S$; pyrite, FeS_2; and magnetite Fe_3O_4 (denoted PPM), has been used extensively to control experimental conditions such as redox states and sulfur activities and conversely, sulfur activities can be controlled to buffer the reducing power of PPM. (Frost, 1985; Shock and Schulte, 1988; Seyfried *et al.*, 1991; Hennet *et al.*, 1992). These minerals or close analogues, for example marcasite (orthorhombic FeS_2) instead of pyrite (Krasnov *et al.*, 1995) are present in anoxic, but acidic environments (Table 2.1, §2.4.1) such as the vent chimneys, plumes and mineral deposits of

sedimented submarine hydrothermal systems (Duckworth *et al.*, 1995; Butler *et al.*, 1998; Krasnov *et al.*, 1995). Pyrite and magnetite are also abundant in deeper sections of the crust but occurrences of the iron monosulfides, pyrrhotite (slightly S-rich, $Fe_{1-x}S$) and troilite (stoichiometric FeS), are more sporadic. Marcasite and pyrite are the most abundant iron sulfide minerals found in ancient sediments, and marcasite is reported to be present in modern vent systems (Krasnov *et al.*, 1995).

Native metals such as Ni and Fe and their alloys can promote geocatalysis, but conversely some minerals can introduce energy or chemical gradients, preventing magmatic gases such as CO_2 from being reduced to CH_4 on cooling. This 'kinetic hinderance' gives the opportunity for many metastable states of organic molecules to exist in hydrothermal fluids (Shock, 1992a; Seewald, 2001). For example, dissolved CO_2, escaping during magmatic cooling or from fluid inclusions (Chivas *et al.*, 1987; Gerlach, 1989a; Sakai *et al.*, 1990; Biellmann *et al.*, 1993; Von Damm, 2000; Lowenstern, 2001), is prevented from reaching stable equilibrium with CH_4. Organic reaction intermediates can then remain stable in the reaction fluid as long as the temperature, pH and redox conditions remain constant. Evidence for this comes from isotopic studies which show that for the C-H-O system at temperatures above 500°C and conditions buffered by PPM, CO_2 is the only stable form of the carbon redox couple CH_4/CO_2 that can exist (see Shock, 1992a). As escaping CO_2 moves towards the surface and temperatures in the crust begin to fall below 500°C, some CO_2 would normally be reduced to CH_4. However, the reduction to CH_4 is hindered by the oxidising conditions (kinetic barrier) the gas meets as it approaches the surface. If CO_2 cannot be reduced to CH_4 then alternative C-O-H molecules may form. These metastable molecules may include biologically important inorganic molecules such as acetates (CH_3COO^-). Further indications of the possible existence of metastable organic compounds are in the studies of organic compounds derived from sedimentary basin brines and modelling of oil reservoirs. These showed that CH_4 did not exist in the metastable state, thus providing further support for the existence of alternative C-H-O compounds (Shock, 1992a; and references within). Of course these molecules need to remain stable for as long as it takes for chemical evolution to occur. Fluids can be trapped and buffered in some hydrothermal systems for up to 10^4 years (Cathles, 1990). This is thought to be sufficient time for polymerisation and concentration to occur, and for some kinetically slow reactions to drive to completion.

The absence of redox control imposed by buffers in many experiments indicates that many conclusions from previous investigations, and the subsequent extrapolation of

experimental results to natural systems, now bear a high degree of uncertainty. This is because important environmental variables, such as oxidation state and sulfur activities, were not buffered at geologically reasonable values (Shock, 1990a; Seewald, 2001). As indicated above, the minerals pyrite, pyrrhotite, and magnetite (PPM) are assumed to control the redox state of hydrothermal systems and their fluids at the crust and seawater interface. At greater depths within these systems, it is assumed that the fayalite (Fe_2SiO_4), magnetite, and quartz (SiO_2), or FMQ assemblage has the major influence in buffering reactions and controlling reaction rates in the crust today (Shock, 1990a). On a prebiotic Earth, if heavy bombardment of the early crust by iron-nickel meteorites is contemplated, such impacts would have increased the native iron and nickel content of the crust, thus rendering the crust more reducing than it is today (Righter and Drake, 1997). Meteoritic dust may also have contributed iron and nickel to the Hadean ocean (Kasting and Brown, 1998). Recent evidence from Archaean amphibolites suggest that primitive magmas may have been up to 30% richer in Fe than today; the ferropicrites of Francis *et al.* (1999). The crust at near-surface depths may then have been controlled by i) the relatively more reduced FMQ mineral assemblage rather than PPM (Canil, 1997; Kasting and Brown, 1998); ii) the even more reducing iron-wüstite (IW) assemblage (Saxena, 1989; Righter and Drake, 1997); or perhaps iii), the awaruite-pyrrhotite-pentlandite-(± magnetite) assemblage (Eckstrand, 1975). Awaruite (Ni_3Fe) is a truly *native* nickel-iron mineral in that it is of terrestrial origin, and it is commonly found in placers. It is associated with rocks such as serpentinised peridotites and dunites which are of oceanic origin. Its formation is thought to take place during serpentinisation (by reduction of nickel-bearing silicates or sulfides with nascent hydrogen as a possible reducing agent), and at low temperatures (Krishnarao, 1964; Frost, 1985; Eckstrand, 1975). Obtaining theoretical values of the redox power of the awaruite-pyrrhotite-pentlandite-(± magnetite) assemblage would be useful since it would allow the production of a model perhaps more representative of the early crust.

5.2 Objectives

This chapter evaluates the proposition that mineral assemblages provided a ubiquitous source of energy to drive organic synthesis (by reducing CO or CO_2 to activated metastable organic compounds) in and around early hydrothermal systems (Neal and Stanger, 1983, 1984; Shock, 1992a; Hennet *et al.*, 1992; Russell and Hall, 1997). The ability of the Geochemist's Workbench (GWB, Bethke, 1998) code to evaluate a variety of mineral assemblages that may have been present on the early Earth is tested. Assemblages which are reducing relative to PPM are evaluated for their influence on carbon redox equilibria. To validate the results obtained by thermodynamic equilibrium calculations in this study, the

work of others (Shock, 1992a; Schoonen *et al.*, 1999) were frequently referred to. The information obtained may be used to provide geochemical constraints when considering the influence of a more reducing crust in the production of key prebiotic molecules.

5.3 Methods

A series of experiments were devised to investigate the relative reducing potentials of selected mineral assemblages and their influence on the equilibria of carbon redox couples. Here, the relative reducing potential of each mineral assemblage is considered in a system by measuring its ability to buffer oxygen to various fugacities over a temperature range of 0°C to 300°C. Their position is then used to predict the most likely stable carbon redox couple that could exist in a more reduced crust in the Hadean. Oxygen fugacity ($\log f O_2$) is used as a measurement variable to calculate relative redox potentials and its use is not an indication of O_2 fugacity levels in the early crust.

Thermodynamic data, equilibrium equations and parameters for all calculations were obtained from the LLNL database *thermo.com.v8.r6.full* (Delaney and Lundeen, 1990) and the GWB database *thermo.dat* (Bethke, 1998). Oxygen fugacities were calculated from equilibrium constants (K) of the equilibria in Table 5.1 and Table 5.2 over a temperature range of 0°C to 300°C. The selected mineral and carbon equilibria shown in Tables 5.1 and 5.2 respectively were evaluated using the GWB code. Assemblages evaluated include hematite-magnetite (HM), nickel-bunsenite, (Ni/NiO), pyrrhotite-pyrite/magnetite (PPM), fayalite-magnetite/quartz (FMQ) and iron/wüstite Fe/FeO, corresponding to the equations in Table 5.1. Note that mineral assemblages and carbon redox couples are *generally* written in the convention such that the relatively reduced species appear on the left.

Thermodynamic data for NiO were obtained from the NiO analogue bunsenite. Thermodynamic data for wüstite were obtained from the FeO entry in the database. The assemblage FMQ/graphite could not be evaluated due to the inability of the modelling code to incorporate graphite into the FMQ equation (Equation 5.4). Thermodynamic data was not available for awaruite at the temperatures to be tested. Therefore it was not possible to evaluate the awaruite-pyrrhotite-pentlandite-(± magnetite) mineral assemblage (Krishnarao, 1964; Frost, 1985; Eckstrand, 1975). For the hematite-magnetite (HM) assemblage, the smaller thermodynamic database, *thermo.dat* (supplied with the GWB program) was used as it contained the necessary data. For the majority of calculations, the thermodynamic data was obtained from the LLNL database, *thermo.com.v8.r6.full.* In addition, the PPM

assemblage was tested by both the *thermo.com.v8.r6.full* and *thermo.dat* databases to compare the results.

5.4 Results

Table 5.1
Redox reactions of selected mineral assemblages†

Mineral Assemblage‡	Equilibrium Equation	
$4\ Fe_3O_4 + O_{2(g)} \rightleftharpoons 6\ Fe_2O_3$ magnetite hematite	$\log K_1 = -\log f O_{2(g)}$	*(5.1)*
$2\ Ni + O_{2(g)} \rightleftharpoons 2\ NiO$ nickel bunsenite	$\log K_2 = -\log f O_{2(g)}$	*(5.2)*
$3\ Fe_{1-x}S + O_{2(g)} \rightleftharpoons ½\ Fe_3O_4 + 1½\ FeS_2$ pyrrhotite magnetite pyrite	$\log K_3 = -\log f O_{2(g)}$	*(5.3)*
$3\ Fe_2SiO_4 + O_{2(g)} \rightleftharpoons 2\ Fe_3O_4 + 3\ SiO_2$ fayalite magnetite quartz	$\log K_4 = -\log f O_{2(g)}$	*(5.4)*
$2\ Fe + O_{2(g)} \rightleftharpoons 2\ FeO$ iron wüstite	$\log K_5 = -\log f O_{2(g)}$	*(5.5)*

Table 5.1. Reaction equilibria of various mineral assemblages with respect to O_2 fugacities.
†All reactions written so that $\log K = -\log f O_{2(g)}$.
‡Equations produced using GWB code (Bethke, 1998) and LLNL/GWB databases (Delaney and Lundeen, 1990; Bethke, 1998).

The relative stability phases of carbon redox equilibria and various mineral buffers with respect to temperature can be described by the fugacity of $O_{2(g)}$ imposed by each equilibria at various temperatures. (Figures 5.1 and 5.2 respectively).

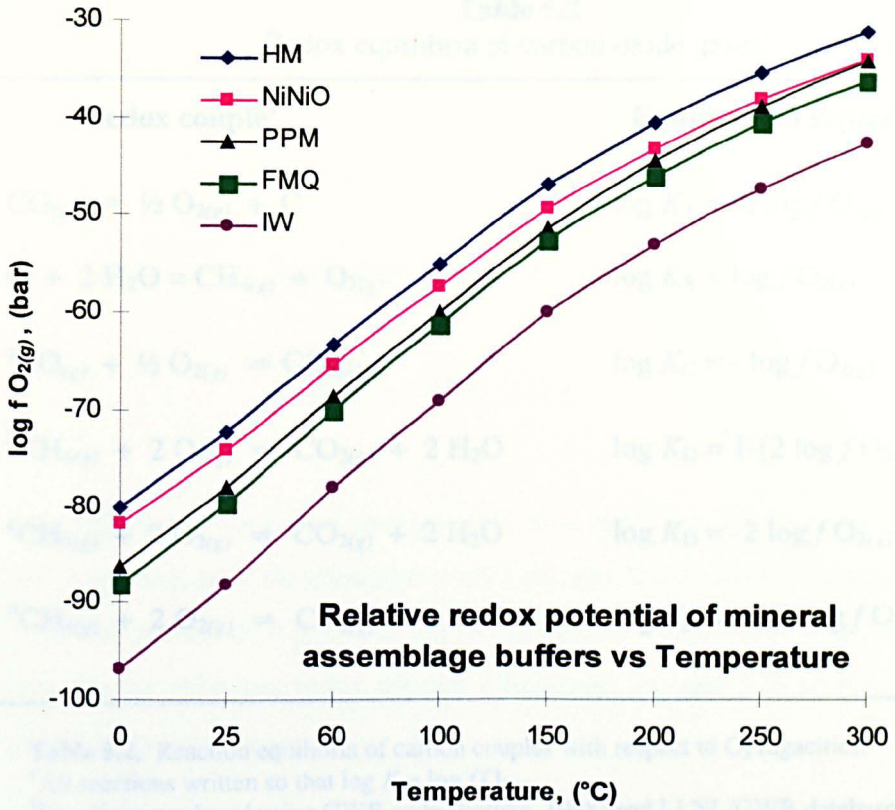

Figure 5.1. Log fugacity values of oxygen buffered by various mineral assemblages, where HM = hematite/magnetite, Ni/NiO = nickel/bunsenite, PPM = pyrrhotite/pyrite/magnetite, FMQ = fayalite/magnetite/ quartz and Fe/FeO = iron/wüstite. Fugacities calculated from equilibrium constants of equations in Table 5.1. Thermodynamic data obtained from LLNL/GWB databases (Delaney and Lundeen, 1990; Bethke, 1998). Decreasing $f\ O_2$ corresponds to increases in temperature and more reducing conditions, therefore oxidised species are stable above each line, reduced species stable below each line, see Figure 3.15b, §3.2.2

Phase boundaries were evaluated for the carbon redox couples CO/CO_2 and CH_4/CO_2 (Table 5.2) and graphed in Figure 5.2.

Table 5.2
Redox equilibria of carbon oxide gases[†]

Redox couple[‡]	Equilibrium Equation	
$CO_{(g)} \rightleftharpoons \frac{1}{2} O_{2(g)} + C$	$\log K_A = \frac{1}{2} \log fO_{2(g)}$	*(5.6)*
$C + 2 H_2O = CH_{4(g)} + O_{2(g)}$	$\log K_B = \log fO_{2(g)}$	*(5.7)*
$^{a}CO_{(g)} + \frac{1}{2} O_{2(g)} \rightleftharpoons CO_{2(g)}$	$\log K_C = - \log fO_{2(g)}$	*(5.8)*
$^{b}CH_{4(g)} + 2 O_{2(g)} \rightleftharpoons CO_{2(g)} + 2 H_2O$	$\log K_D = 1-[2 \log fO_{2(g)}]$	*(5.9)*
$^{c}CH_{4(g)} + 2 O_{2(g)} \rightleftharpoons CO_{2(g)} + 2 H_2O$	$\log K_D = -2 \log fO_{2(g)}$	*(5.10)*
$^{d}CH_{4(g)} + 2 O_{2(g)} \rightleftharpoons CO_{2(g)} + 2 H_2O$	$\log K_D = -1-[2 \log fO_{2(g)}]$	*(5.11)*

Table 5.2. Reaction equilibria of carbon couples with respect to O_2 fugacities.
[†]All reactions written so that $\log K = \log fO_{2(g)}$.
[‡]Equations produced using GWB code (Bethke, 1998) and LLNL/GWB databases (Delaney and Lundeen, 1990; Bethke, 1998).
[a]Assumptions implicit in equilibrium equation: fugacity of $CO_{2(g)}$ = 1 bar.
[b]Activity of H_2O = 1, $CO_{2(g)}/CH4_{(g)}$ = 10.
[c]Activity of H_2O = 1, $CO_{2(g)}/CH4_{(g)}$ = 1.
[d]Activity of H_2O = 1, $CO_{2(g)}/CH4_{(g)}$ = 0.1.

Oxygen fugacities can be calculated from log K values as in the example shown below for Equation *5.10*.

$$K_D = \frac{fCO_2.a[H_2O]^2}{fCH_4.f[O_2]^2}$$

The partial pressures of $CO_{2(g)}$ and $CH_{4(g)}$ are unknown. Therefore the ratio of $CO_{2(g)}$ to $CH_{4(g)}$ was tested with arbritary values of 10, 1, and 0.1 (Equations 5.9, 5.10 and 5.11 and Figure 5.2). Water activity was set to 1 (Table 5.2), since activities of H_2O rarely stray far from unity in hydrothermal fluids, except at extremes of concentration (Helgeson, 1985). For example, equation *5.10* can be simplified to evaluate $\log fO_{2(g)}$, as shown below,

$$K_D = \frac{1}{f[O_2]^2}$$

$$f[O_2]^2 = \frac{1}{K_D}$$

$$2\log f[O_2] = -\log K_D$$

$$\log K_D = -2\log f[O_2]$$

The other equations were also manipulated in a similar manner to generate the desired equation. However, only the equations with a gas-gas redox couple (Equations *5.8*, 5.9, *5.10* and *5.11*) were plotted on a graph of $\log f\,O_{2(g)}$ against temperature (Figure 5.2), as the $\log f\,O_2$ results for the solid-gas redox couples (Equations *5.6* and *5.7*) seemed to be contradict what should have been expected.

Figure 5.3 below shows the relative positions of redox potentials of mineral buffers and carbon redox couples. Positions of carbon redox couples indicate stability with respect to redox conditions imposed by mineral buffers.

Table 5.3 lists the calculated $O_{2(g)}$ fugacities for all the redox equilibria tested at 100°C and 250°C (Figure 5.3), as calculated by the Geochemist's Workbench RXN program (Bethke, 1998). Note values of $\log f\,O_{2(g)}$ for PPM obtained from both databases for comparison.

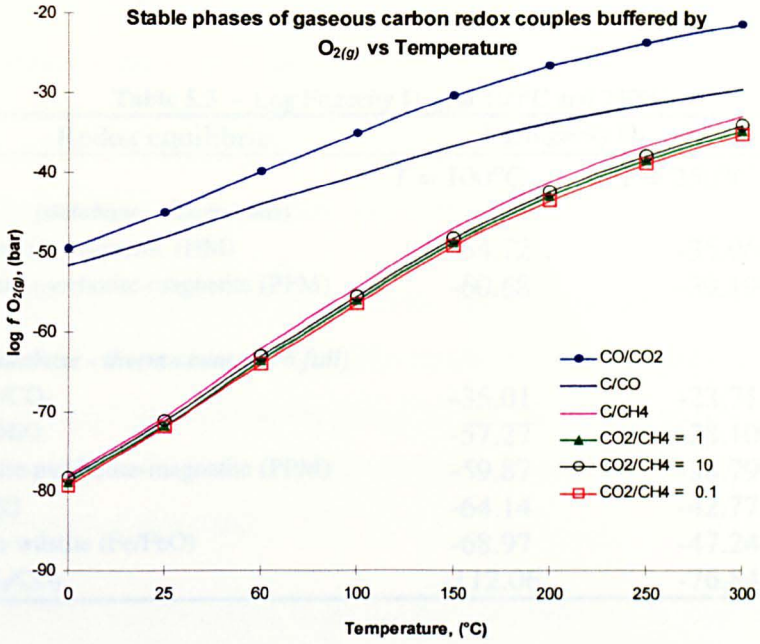

Figure 5.2. Log fugacities of $O_{2(g)}$ for the carbon redox equilibria described in Table 5.2, calculated from equilibrium constants obtained from LLNL/GWB databases (Delaney and Lundeen, 1990; Bethke, 1998). All reactions at pressures corresponding to the boiling curve of water (Appendix 1A, Figure B). Decreasing $f\,O_2$ corresponds to increases in temperature and more reducing conditions, therefore oxidised species are stable above each line, reduced species are stable below each line, see Figure 3.15b, §3.2.2

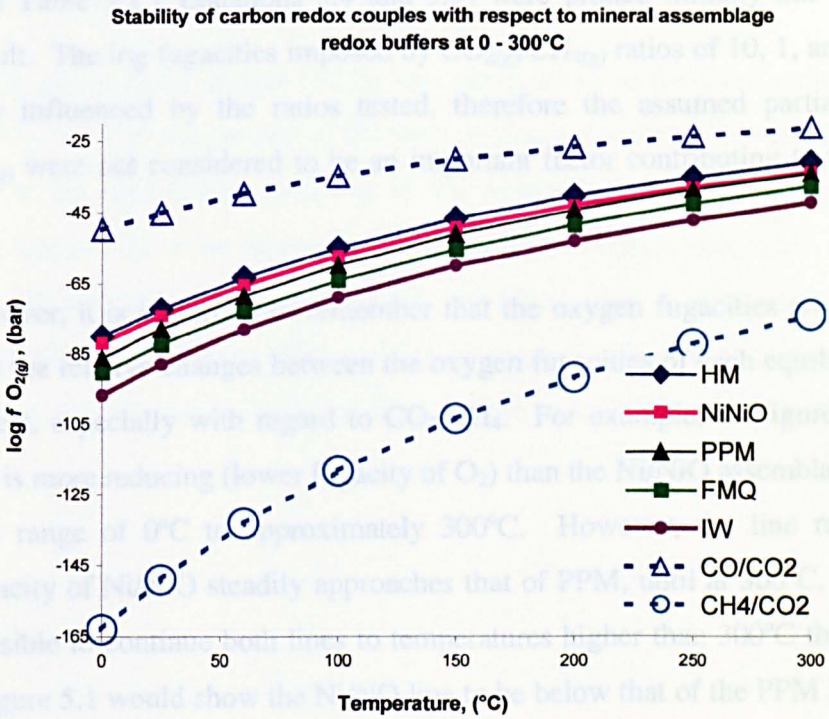

Figure 5.3 Stabilities of carbon redox couples buffered by various mineral assemblages, as function of temperature (0°C to 300°C). The lines describe the relative positions of the redox potentials of mineral buffers and carbon redox couples. CO/CO_2, $CO_{2(g)}/CH_{4(g)}$ ratio = 1:1.

Table 5.3 - Log Fugacity $O_{2(g)}$ at 100°C and 250°C

Redox equilibria	log fugacity $O_{2(g)}$ (bar)	
	T = 100°C	T = 250°C
(database - thermo.dat)		
hematite-magnetite (HM)	-54.72	-35.06
pyrite-pyrrhotite-magnetite (PPM)	-60.68	-39.19
(database - thermo.com.v8.r6.full)		
CO/CO_2	-35.01	-23.71
Ni/NiO	-57.27	-38.10
pyrite-pyrrhotite-magnetite (PPM)	-59.87	-38.79
FMQ	-64.14	-42.77
iron-wüstite (Fe/FeO)	-68.97	-47.24
CH_4/CO_2	-112.06	-76.84

5.5 Discussion

The immediate conclusions that can be drawn from these results is that the reducing power of each of the equilibria tested decreases with increasing temperature (0°C to 300°C), and that the iron-wüstite (IW) assemblage is the most reducing of the solid buffers tested. The CH_4/CO_2 couple is the most reducing of the gaseous buffers tested. The solid/gas equilibria in Table 5.2 (Equations *5.4* and *5.5*) were plotted initially but did not give a sensible result. The log fugacities imposed by $CO_{2(g)}/CH_{4(g)}$ ratios of 10, 1, and 0.1 were not significantly influenced by the ratios tested, therefore the assumed partial pressures of $CO_{2(g)}/CH_{4(g)}$ were not considered to be an important factor contributing to the unexpected results.

However, it is important to remember that the oxygen fugacities are just numerical values. It is the relative changes between the oxygen fugacities of each equilibria tested that are of interest, especially with regard to CO_2/CH_4. For example, in Figure 5.1, the PPM assemblage is more reducing (lower fugacity of O_2) than the Ni/NiO assemblage between the temperature range of 0°C to approximately 300°C. However, the line representing the oxygen fugacity of Ni/NiO steadily approaches that of PPM, until at 300°C, they converge. Were it possible to continue both lines to temperatures higher than 300°C they would cross over and Figure 5.1 would show the Ni/NO line to be below that of the PPM line. Similarly, in Figure 5.2, the CH_4/CO_2 couple is more reducing than the CO/CO_2 couple at the temperatures tested, but their respective lines converge. Again, at higher temperatures the lines would meet and then cross over. This would then show the opposite to what is

demonstrated in Figures 5.2 and 5.3 - that the CO/CO_2 couple is more stable than CH_4/CO_2 at higher temperatures (Shock, 1992a).

It would be desirable in this case to be able to model the higher temperatures that are present in the crust for further analyses to further test for the nature of the relationship.

Results agree with Kasting and Brown's (1998) estimate of a iron-wüstite buffered early crust would be 1-4 log units below FMQ. The results in this study show values ranging from 6 log units at 0°C to 4.5 log units lower than FMQ at 300°C, and so are fairly close to their estimate. The result for PPM is in agreement with Schoonen *et al.* (1999) and Figure 3.15b §3.2.2, who also confirm this trend.

In conclusion the iron-wüstite couple is among the most reducing of those tested.

However, it was not possible to model novel buffers rich in nickel-iron such as awaruite-pyrrhotite-pentlandite-(± magnetite) and compare them with iron-wüstite as the required thermodynamic data at appropriate temperatures was not available. The Ni/NiO couple evaluated instead showed that it's redox state lies between the relatively oxidised HM and PPM values, whereas it would have been preferable to model a more reducing assemblage such as awaruite-pyrrhotite-pentlandite-(± magnetite).

The solid-gas phase redox couple C/CH_4 was expected to be the most reducing (i.e., more than CH_4/CO_2) but it plotted as one of the most oxidising couples. This could have been due to an error in the calculations, possibly in the assumed number of electrons transferred. However, it was not felt to be appropriate to spend time to pursue this model further until the theoretical principles were reassessed to provide more confidence in the model. Consultation with others in the field seemed to suggest a flaw in the approach used here (Craig Bethke, *person. comm.*), or an error in the calculations (Henry Kerfoot, *person. comm.*)

Chapter 6. Modelling the Stability of Amino acids within a Hadean Submarine Hydrothermal System.

6.1 Introduction

Inorganic compounds such as H_2O, H_2, CO, CO_2, NH_3, and simple organic compounds such as alcohols, ketones, aldehydes are postulated or have already been shown to exist in many unexpected extreme environments, both terrestrial and extraterrestrial (Shock, 1996, 1997). This has led many to assume that important prebiotic organic molecules, in particular the protonated and deprotonated α-amino acids, required for protein synthesis, were available for inclusion in the first microbes. Amino acids could have been synthesised on the early Earth from relatively simple inorganic compounds such as CO_2 and NH_3 available at that time (Kasting, 1993; Simakov, 1998). However, the energetic requirements to produce amino acids from these simple compounds are often too high to proceed in moderate environments. Alternatively, ready-made complex organic molecules could have been delivered from an extraterrestrial source to be eventually broken down to smaller molecules such as alcohols, aldehydes and ketones. In fact, there are many chemical routes to the formation of amino acids and not all require as large an input of energy as would be required with CO_2 and NH_3. Other reaction pathways include reactants such as hydrogen cyanide (HCN), HCN polymers (aminonitriles) and cyanide (CN^-) radicals. The HCN reaction pathway offers a more favourable thermodynamic route to the formation of amino acids.

In 1973 an unexpected infrared emission feature was discovered from two planetary nebulae (Gillet *et al.*, 1973). The signal was initially ascribed to interplanetary dust particles (IPDs) but the emission spectra of these IPDs and of the terrestrial polycyclic aromatic hydrocarbons (PAHs) that are found in smoke soot were almost identical. This presented strong evidence for the presence of complex, organic compounds in dense interstellar clouds. PAHs are present in comets and meteorites and predominate over other organic compounds in extraterrestrial space (Allamandola *et al.*, 1997). Additionally, PAHs detected in Martian meteorites can be differentiated from terrestrial PAHs by their relatively high carbon 13 isotopic signature. With respect to amino acids, PAHs are more complex molecules and are situated *thermodynamically uphill.* Thus, the thermodynamic route to form amino acids is again easier from PAHs than from CO_2 and NH_3.

The PAH molecules can break down into esters, ketones and aldehydes from which several varieties of amino acids could be easily formed. PAHs are favoured by some to be the astrobiological precursors of Life on Earth. Indeed, we await results from numerous

experiments attempting to establish the stability of PAHs on delivery to Earth, even after seemingly destructive events such as atmospheric entry or meteoritic impact with the crust. Investigations are underway to see whether organic molecules on meteorites can survive through atmospheric entry (the European Space Agency's STONE and BIOPAN project) and impact (McKay and Borucki, 1997). Deuterium (D_2) enrichment indicates the possibility that these amino acids may have been of extraterrestrial origin (Krishnamurthy *et al.*, 1992; Lerner *et al.*, 1993; Hayatsu *et al.*, 1972). However, the extraterrestrial delivery of organic molecules is just the first among many hurdles to be met on the early Earth. Therefore, the present study takes the view that synthesis of amino acids may have formed *in-situ* in 'protected' hydrothermal systems where organic molecules can form and eventually Life could flourish.

6.2 Formation and stability of amino acids in hydrothermal systems

The current state of knowledge stipulates that surface conditions on the early Earth were neutral to mildly oxidising, with carbon, nitrogen and hydrogen present mainly in their oxidised forms - CO_2, N_2 and H_2O (Kasting, 1990, 1993; Kasting and Brown, 1998; Shock, 1990b; and references therein). This challenges the Oparin (1938), Haldane (1929) and Urey (1952) hypotheses of an early reducing atmosphere, and questions the import of Miller's (1953) synthesis of organic molecules. Miller's amino acids were readily synthesised using reduced forms of carbon, nitrogen and hydrogen (CH_4, NH_3 and H_2) and since lightning (electric-spark) was a key requirement, he proposed a surface environment with a reduced atmosphere for the origin of Life. Sagan and Khare's (1971) successful irradiation of a reducing mixture of CH_4, NH_3, H_2O and H_2S with long wave UV light, to produce amino acids, with HCN and aldehydes as possible reaction intermediates is similarly suspect. This is because amino acids and other organic molecules do not form as easily in oxidising environments and this is where the thermodynamically uphill challenge for Life lay on the early Earth.

Since Miller's (1953) electric-spark discharge experiments, several researchers have successfully synthesised many biologically important amino acids using alternative reactants, reaction pathways and under a range of environmental conditions (Oró, 1960; Lowe *et al.*, 1963; Fox and Windsor, 1970; Sagan and Khare, 1971; Hennet *et al.*, 1992; Marshall, 1994). These studies have reported the abiogenic formation of organic molecules starting with the oxidised forms of carbon and nitrogen and hydrogen. Glycine, alanine, and aspartic acid are the predominant amino acids formed in many of these experiments, though cysteine, methionine, serine, threonine, glutamic acid, leucine, tyrosine, valine, histidine and

phenylalanine are also formed in minor to trace amounts. Less biologically significant amino acids such as β-alanine, α-amino-n-butyric acid, diaminosuccinic acid, and a host of other organic molecules have also been noted in the references cited above (Shock, 1992b; and references therein). Lowe *et al.* (1963) synthesised amino acids, amino acid polymers, fatty acids and purines from ammonium cyanide (HCN) at 90°C. Oró (1960) synthesised adenine from ammonium cyanide. Fox and Windsor (1970) synthesised amino acids with ammonium hydroxide (NH_4OH), formaldehyde (HCHO), and H_2 at 185°C under hydrothermal conditions. Hennet *et al.* (1992) used a mixture of CO_2, H_2, NH_3, KCN and formaldehyde (HCOH) at 150°C and 10 atmospheres in an attempt to realistically model hydrothermal conditions, with redox conditions buffered by pyrite-pyrrhotite-magnetite. Additionally, at 150°C and with moderately alkaline starting conditions (pH ~7 to pH~8.8), the sample mixture resembled the hydrothermal fluids circulating in off-axis systems, perhaps on the flanks of spreading ridges (e.g., Kelley *et al.*, 2001). Platinum was used as an oxygen sink and titanium oxide for the autoclave liners (*it must be noted that these may have acted as additional catalysts and buffers*).

Oparin proposed a role for carbides in primordial reactions as early as 1924, and since then others have synthesised amino acids and other organic molecules in relatively low temperature aqueous solutions containing carbides (Marshall, 1994; Yanagawa and Egami, 1981), assuming them to be available in hydrothermal systems from meteoritic additions to the crust. Marshall (1994) and Berndt *et al.* (1996) demonstrated how the predominant and stable CO_2 and N_2 phases of carbon and nitrogen on the early Earth could be reduced under various conditions and reaction pathways. Marshall (1994) presented evidence of rapid synthesis of amino acids under hydrothermal conditions at 200-275°C from ethene (C_2H_2), H_2 and O_2 (in the presence of a carbide, CaC_2 and peroxide H_2O_2) by reaction with aqueous ammonium bicarbonate (NH_4HCO_4). However, concentrations of reactants used were much higher than would have been available on the early Earth. Additionally, ethene concentrations could have been much lower in sedimented systems (see Shock, 1992a).

These experiments established that it is difficult, but not impossible, to synthesise amino acids under oxidising conditions. Additionally, many of the syntheses were performed over a wide range of pressures, and temperatures ranging from 25°C to >1000°C (see Shock (1992b) for a more detailed history and review of amino acid synthesis experiments, and Ferris (1992) for a discussion on the availability of organic precursors on the early Earth). It should be of no surprise then that complex organic structures have been discovered or are speculated to exist in extreme conditions such as the Earth's subsurface or

outer space (Gillett *et al.*, 1973). Seventy-four amino acids were identified in the Murchison Meteorite, of which 19 are biologically significant (Cronin *et al.*, 1988). The amino acids synthesised in Miller's (1953) experiments were also identified in the meteorite and their relative distribution is the similar to that of the meteorite.

On the Earth, Haberstroh and Karl (1989) reported 5-445μM of dissolved amino acids in moderately heated (5-100°C) sediment-covered hydrothermal systems in the Guyamas Basin. Sediment-covered hydrothermal systems have only been found so far on divergent margins close to continents. They are distinctly different from sediment-free systems in that they have a higher pH (~6) than systems without sediments (pH ~4), and contain a rich variety of potential metallic catalysts as well as extended thermal and chemical gradients (Holm, 1992; Ferris, 1992; Simoneit, 1992). However, it is likely that the organic molecules found by Haberstroh and Karl (1989) were derived from the breakdown of organisms. HCN, amino acids, amino sugars and complex organic structures have also been detected in freshly collected volcanic ash, and in volcanic bombs from Kamchatka, Indonesia, (Muhkin, 1976; Markhinin and Podkletov, 1977), though the detection of sugars in ash samples suggests a biological origin. This gives rise to the possibility of a source of amino acids and other organic molecules from other types of vent emissions from the crust. The crustal processes from which vent fluids originate may also provide the physical and chemical gradients necessary for complex organic structures to form (Corliss, 1986b).

In the present crust, two mineral assemblages, pyrite-pyrrhotite-magnetite (PPM) and quartz-fayalite-magnetite (FMQ) are thought to be important in controlling redox conditions in seawater-basalt systems (Shock, 1992a, 1992b). However, the redox state of the crust may have been quite different on the early Earth if the crust was altered by heavy bolide impacts. For example, if it were buffered by an iron-wüstite (IW) mineral assemblage (§5.1), CH_4 and NH_3 would have at least been present in greater concentrations than today. Near-surface processes, for example hydrothermal systems on an early Earth, could have been the vehicle for the ideal reducing conditions, rather than the difficult oxidising surface conditions for producing amino acids. If this is the case, CO_2 and the predominantly stable form of nitrogen, N_2 (Kasting and Brown, 1998), would have to have been transported to the early oceanic crust, perhaps by deep marine currents or via magmatic devolatilisation. Thermodynamic studies by Shock (1992a) indicate that at depths where the environment is buffered at FMQ conditions and temperatures are above 500°C, CO_2 and N_2 are the dominant phases of carbon and nitrogen. Fluids containing CO_2 and N_2 then pass through reducing crustal zones which tend to convert the oxidised CO_2 and N_2 to their reduced counterparts

CH_4 and NH_3. These fluids circulate to parts of the crust where temperatures are relatively cooler, perhaps 50-250°C (Shock and Schulte, 1998). Allowing for some kinetic hinderance, CO_2 and N_2 are prevented from being converted completely to their reduced forms (CH_4 and NH_3) and form metastable intermediates instead (such as acetates RCOO-, hydrogen cyanide, HCN, and aldehydes, RCOH). The energy released from the mixing of hot and cold fluids may also provide a route for organic synthesis (Shock and Schulte, 1998).

Amino and carboxylic acid formation is probably via the Strecker synthesis reaction (Miller, 1957) or Fischer-Tropsch Type (FTT) reaction. Strecker synthesis reactions produce amino and carboxylic acids from NH_3, HCN, ketones, and aldehydes. Strecker synthesis reactions are thermodynamically favourable in hydrothermal environments (Schulte and Shock, 1995). The initial concentrations of aldehydes, ketones, and HCN that would have been required to form significant quantities of amino acids may not be available from a hydrothermal system (Schulte and Shock, 1995), though concentrations may have been strongly enhanced by molecular sieving in the hydrothermal mound (Russell and Hall, WWW, 2001). As indicated earlier in this chapter, there is also the possibility that the Strecker synthesis was the mechanism by which amino acids were formed in the Murchison Meteorite.

$$RCHO + HCN + NH_3 \rightleftharpoons RC(NH_2)CN + H_2O \rightarrow RCH(NH_2)CO(NH_2) + H_2O \rightarrow RCH(NH_2)COOH \quad (A)$$

$$RCHO + HCN \rightleftharpoons RC(OH)CN + H_2O \rightarrow RCH(OH)CONH_2 + H_2O \rightarrow RCH(OH)COOH \quad (B)$$

The mechanism by which this reaction proceeds according to Henrici-Olivé and Olivé, (1984) is discussed within the context of the Russell and Hall hypothesis in Russell *et al.* (1998). In general, the reaction can be described as follows: R-CHO (aldehydes, or ketones, RCOR) combine with hydrogen cyanide and ammonia in a condensation reaction to form α-aminonitriles, $RC(NH_2)CN$. α-Aminonitriles then undergo hydrolysis to give an amino amide, $RCH(NH_2)CO(NH_2)$. Further hydrolysis of the amide gives rise to the α-amino acid, $RCH(NH_2)COOH$. To form carboxylic acids (hydroxy acids) the reaction proceeds as in (A) but the amino group attached to the α-carbon is replaced by the hydroxyl group to give a hydroxy acid instead of an amino acid (B)

FTT reactions have been shown to produce HCN, acetonitriles (CH_3CN), carboxylates, heterocyclic compounds, and small amounts of amino acids from CO, H_2, NH_3, and in some cases deuterium, D_2 (Ferris, 1992). Hydrothermal systems may be able to provide the high temperatures, high pressures, and metallic or mineral catalysts required for

FFT reactions (Ferris, 1992). Berndt *et al.* (1996) suggested that CO_2 reduction to CH_4 occurs during serpentinisation of olivine. The magnetite produced from serpentinisation may catalyse the FTT reaction, not to mention the significant quantities of $H_{2(g)}$ often required for FTT reactions This is supported by detection of significant quantities of CO_2 and CH_4 (up to 50 mol% and 43 mol% respectively) in fluid inclusions in rocks sampled from the Southwest Indian Ridge (Kelley, 1996, 1999; Kelley and Früh-Green, 2001; and also see Holloway, 1984 and Horita and Berndt, 1999). However, the activation energies (25kcal/mol) involved in the Berndt *et al.* (1996) analogy of the Fischer-Trospch reaction suggest that at low temperatures, this route may take millions of years just to produce significant quantities of the intermediate reactants, such as acetates, HCN and aldehydes. Furthermore, Schulte and Shock's (1995) study of the thermodynamics of Strecker synthesis and similar reactions highlighted the need for sufficient concentrations of these intermediates to be able to form important biomolecules such as amino acids. Similarly, the mineral-catalysed reduction of N_2 (degassing from the Earth's interior), NO_2^- and NO_3^- (possibly from electrical discharge or cometary impacts), to NH_3 was noted by Brandes (1998).

If metastable equilibria *are* formed as suggested by Shock (1992a), there are assumed to be surmountable kinetic pathways leading to the synthesis of the organic compounds (Shock and Helgeson, 1990; and see Seewald, 2001). Prevented from being completely reduced by kinetic barriers, metastable species of the redox couples CH_4/CO_2 and NH_3/N_2 may have then remained buffered in a metastable state long enough to be carried to the surface to potential 'life reactors' (Shock, 1990, 1992a). This idea was disputed by Miller and Bada (1988), who argued and demonstrated that amino acids decompose at high temperatures. Bernhardt *et al.* (1984) also reported that biomolecules were 'unstable' in black-smoker conditions. To counter this argument a series of thermodynamic calculations were performed by Shock (1990). Shock emphasised that the equilibrium conditions typical of experiments such as those performed by Miller and Bada (1988), may be quite different under hydrothermal environments (Shock, 1990). His calculations demonstrated that the synthesis from organic starting materials and stability of the 20 of the protein forming amino acids were energetically favoured in hydrothermal conditions at 100°C (Amend and Shock 1998) or perhaps even up to 250°C (Shock, 1990). He rejected the idea of decomposition, and suggested that the equilibrium conditions associated with the laboratory experiment were responsible for the change in the distribution of the amino acids tested (alanine, leucine, aspartic acid, and serine). Rather than some of the amino acids being irreversibly decomposed, Shock (1990) suggests that the redistribution of amino acids at higher temperatures merely favoured the stability of alanine, leucine and glycine in solution.

This revelation suggests that there have been many other instances of inadequately controlled laboratory experiments that may have been used to incorrectly confirm or disconfirm proposals such as those made by Miller and Bada (1988) on the basis of their experiments alone. In their conclusions, Shock (1990) and others (Andersson and Holm, 2000) highlighted the practical difficulties of maintaining redox states in a laboratory to realistically simulate hydrothermal environments. For this reason, many researchers have increasingly turned to thermodynamic calculations to overcome this difficulty. With thermodynamic calculations it is possible to impose the necessary constraints for hydrothermal situations, and then to assess the stability or formation of amino acids and other organic molecules in these environments. Many thermodynamic studies have shed light on what should be occurring chemically in inaccessible places such as hydrothermal systems, and reveal that the chemistry of hydrothermal systems perhaps may be not be best elucidated from comparisons with reactions at surface conditions. Thus perhaps organic species may not be destroyed as suggested by Miller and Bada (1988), and the unusual conditions in hydrothermal systems may allow them to remain stable at higher temperatures and pressures. It is then of particular importance to use theoretical models to investigate how organic molecules might really behave under various temperatures, pressures and oxidation states or perhaps unusual conditions that cannot be easily created or sustained in laboratory experiments.

6.3 Objectives

The thermodynamic study in this chapter attempts to propose a mechanism for the formation of protein-forming α-amino acids in or around the myriad of alkaline hydrothermal seepages that are present on the flanks of ridge systems. The study tests the feasibility of primitive inorganic reactants such as CO/CO_2 as the source of the carboxyl (COO^-) and N_2/NH_3 as the source of the amino (NH_2^+) functional groups, both of which are present in amino acids. The model will also serve to examine the likely distribution and behaviour of these amino acids under hydrothermal conditions and compare the results with the published work. Finally, the suitability of the Geochemist's Workbench (GWB) software package (Bethke, 1998), and the LLNL thermodynamic database *thermo.com.v8.r6.full* (§1.4) for this experiment is discussed. The calculations performed in this chapter attempt to model the formation of organic intermediates from simple inorganic molecules such as CO/CO_2 and N_2/NH_3, which were more likely to have been available in sufficient concentrations in the vicinity of the hydrothermal system itself (as performed by Shock and Schulte (1998)). Specifically, the calculations attempt to demonstrate that the simplest amino acid, glycine (NH_2CH_2COOH), could be synthesised autotrophically from

these simple inorganic materials, and then function as a basic building block for the formation of other amino acids. Glycine (thought to be ubiquitous in the Universe), in the presence of CO_2 and H_2 could have been instrumental in the formation of higher carbon number amino acids, with longer side-chains, such as leucine$_{(aq)}$, alanine$_{(aq)}$ and valine$_{(aq)}$. The overall model is designed to investigate how the composition and redox properties of the Hadean atmosphere, ocean and crust might have encouraged or discouraged the stability of any amino acids that may have been formed. Whatever the outcome, the calculations will help towards a better understanding of their role and behaviour, perhaps help in the imposition of experimental constraints for further research, and may support theories for the emergence of life within or on the exit sites of submarine hydrothermal systems.

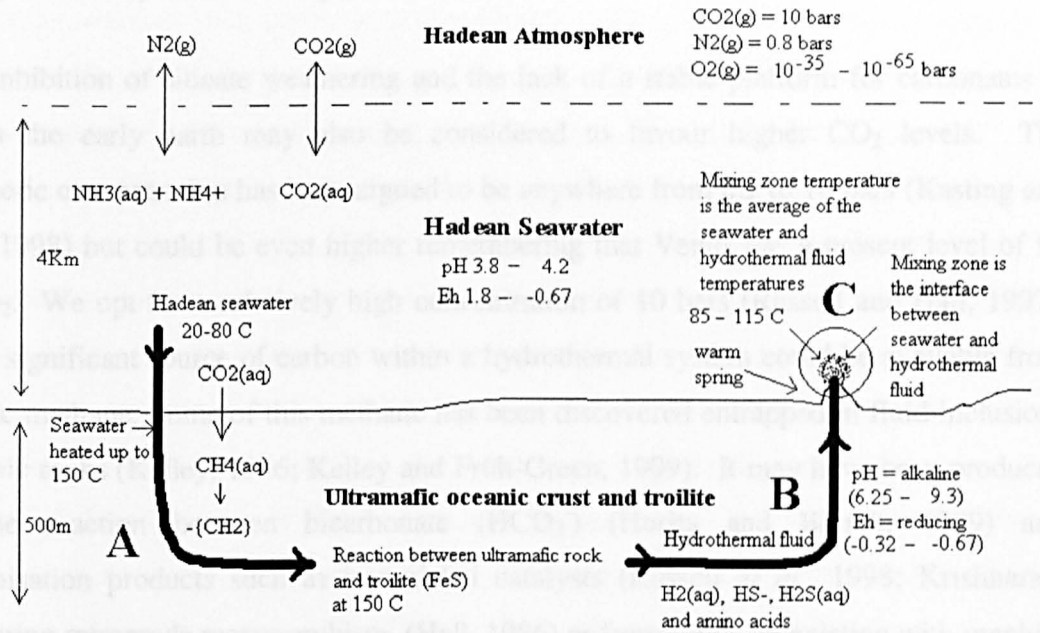

Figure 6.1. A theoretical model of an early Hadean environment showing seawater seeping down into the oceanic crust and being heated at depth (**A**), its conversion to an alkaline hydrothermal fluid after reactions with the crust (**B**), and its exit back into cold seawater at warm springs or hydrothermal seepages (**C**). The mixing ratio at **C** is assumed to be 1:1. The assumed depth of the ocean and crust, and the possible range of environmental variables such as temperature, *Eh*, pH, and fugacities are indicated. Double-sided arrows indicate equilibrium between the atmosphere and the ocean

6.3 Method

Thermodynamic models were created using GWB to demonstrate the potential for autotrophic synthesis of amino acids from the reactions between a CO_2, CO, and NH_4^+ bearing, warm (20°C–80°C), acidic (pH = 3.2-5.6) Hadean ocean, with its ultramafic crust (Figure 6.1). Experiments are conducted using Hadean seawater-ultramafic rock ratios of 10:1 and 1:1. A redox mechanism for the formation from glycine, of alanine, valine, and

leucine (the simplest protein-forming α-amino acids) was also investigated. To model the reactions in terms of a prebiotic environment (Figure 6.1) we associate both the pH of the seawater and the source of carbon for the amino acids from the reduction (during the serpentinisation of olivine) of dissolved atmospheric $CO_{2(g)}$ by hydrogen in seawater (Berndt *et al*, 1996). As explained in Chapter 2, the amount of atmospheric $CO_{2(g)}$ in the Hadean could be dependent on several factors;

(i) the rate of CO_2 exhalation

(ii) the rate of cometary delivery

(iii) carbonation of silicates (*cf.* Griffiths and Shock, 1995) in the crust and as dust generated by meteorite impact.

Inhibition of silicate weathering and the lack of a stable platform for carbonates to form on the early earth may also be considered to favour higher CO_2 levels. The atmospheric concentration has been argued to be anywhere from 0.2 to 10 bars (Kasting and Brown, 1998) but could be even higher remembering that Venus has a present level of 90 bars CO_2. We opt for a relatively high concentration of 10 bars (Russell and Hall, 1997). Another significant source of carbon within a hydrothermal system could be available from abiogenic methane. Some of this methane has been discovered entrapped in fluid inclusions in plutonic rocks (Kelley, 1996; Kelley and Früh-Green, 1999). It may have been produced from the reaction between bicarbonate (HCO_3^-) (Horita and Berndt, 1999) and serpentinisation products such as iron-nickel catalysts (Russell *et al.*, 1998; Krishnarao, 1964) during retrograde metamorphism (Hall, 1986) or from fluids co-existing with graphite (Holloway, 1984). $H_{2(g)}$ is also produced in the subsurface from the serpentinisation reactions (§2.1) and its concentrations in the models are determined by the water-rock reaction reactions (see Models 1a-8d, Appendix 3). The presence of nitrogen (~0.8 bar) on the early earth (Kasting and Brown, 1998) and its conversion to ammonia as a result of mineral-catalysed reduction at 300°C in hydrothermal environments on the early earth has been suggested (Brandes *et al*, 1998).

Overall, the models designed in this chapter are designed to reflect most of these conditions. Though concentrations of HCN, NH_3, and NH_4^+ are more likely to be required in organic synthesis, the normally unreactive atmospheric nitrogen (N_2) is used to constrain the nitrogen that is available in the models. This is acceptable since the kinetic inhibition of the N_2 to NH_3 reduction is not being investigated in this model. The redox conditions are

intrinsically controlled by the other variables in the model, and will ultimately determine the form of the nitrogen that is available. Though unintentional, using $N_{2(g)}$ as an input to the model might help the visualisation of a possible reaction pathway of nitrogen from the atmosphere to the subsurface where the formation of amino acids in the model is taking place (Figure 6.1). It is necessary to choose a reasonable arbitrary value for the calculations, therefore it is assumed that the mixing ratio between the hydrothermal fluid and the seawater is 1:1). The system in the mixing zone is assumed to be the average temperature of the two fluids

The constraints for the seawater and crust are listed in Table 6.1, which describes proposed concentrations of chemical species in Hadean seawater and the minerals in an ultramafic rock. In order to determine whether amino acids could be formed at all from the components available to a prebiotic hydrothermal system, and then remain stable in a hydrothermal fluid it was necessary to examine the generation of the hydrothermal fluid. This was engendered by equilibrating seawater with a CO_2 atmosphere (Figure 6.1, and Table 6.2A), and then using the equilibrated seawater in reactions with the ultramafic crust to produce the fluid (Figure 6.1, and Tables 6.1, 6.2B). The newly formed acids are tested for stability upon re-mixing with seawater. Mixing was effected by collecting the hydrothermal fluid and reacting it with more of the equilibrated seawater. Since the $f\,O_{2(g)}$ of the early crust is poorly constrained (Canil, 1997), it is necessary to test a range of oxidation states, though a highly reduced crust has been suggested by Kasting and Brown (1998). An added advantage of this approach is that it facilitates assessment of the influence of different oxidation states on amino acid production. Therefore, the experiments were carried out over a wide range of oxidation states ($\log f\,O_2$(g) –35 to –65), since it is not certain which redox state may have existed on the early Earth. The ranges of oxidation states may be chosen from oxygen fugacities derived from modelling various mineral assemblages (see Chapter 5).

Seawater (1kg) - Major/Trace Species		Simple ultramafic rock composition (g)	
Species	mmoles	*multiply by 10 for 1:1 water rock/ratio	
Mg++	1.E-03	Forsterite	72
SO4--	1.E-06	Fayalite	8
Na+	5.E-03	Diopside	15
Cl-	7.E-03	Anorthite	3.6
Al+++	1.E-06	Albite	0.4
SiO2(aq)	1.E-06	Troilite	1
Fe++	1.E-06	Troilite	1

Table 6.1. Chemical and mineral composition of a 10:1 ratio for 1kg of the model seawater and 100g of the simplified ultramafic crust.

Each experiment varies only in the fugacity levels of oxygen, temperature, the water-rock ratio and charge balance species, (Table 6.2A). Table 6.2B shows the concentrations of dissolved gases and other properties of the seawater after equilibration with the atmosphere. In Appendix 3, models 1a-8d show the recorded initial and final values of key products after each experimental run. These include initial and final values of oxygen fugacities, temperature, pH and Eh. Furthermore, quantities and types of dissolved amino acids, dissolved chemical species of sulfur (SO_4^{2-}, H_2S, HS^-), nitrogen (N_2, NH_3, NH_4^+), carbon (CO_2, CH_4) and hydrogen (H_2) as well as minerals precipitated during seawater-crust reactions and seawater-hydrothermal fluid reactions were also recorded.

Table 6.2A - Experimental Constraints

	Model 1	Model 2	Model 3	Model 4	Model 5	Model 6	Model 7	Model 8
				Atmosphere *f* (bar)				
CO2	10	10	10	10	10	10	10	10
O2	-35.00	-45.00	-55.00	-65.00	-35.00	-45.00	-55.00	-65.00
N2	0.8	0.8	0.8	0.8	0.8	0.8	0.8	0.8
				Seawater 1kg at T (°C)				
	20-80	20-80	20-80	20-80	20-80	20-80	20-80	20-80
				Major & trace species (*mmoles*)				
Mg++	1.E-03	1.E-03	1.E-03	1.E-03	1.E-03	1.E-03	1.E-03	1.E-03
SO4--	1.E-06	1.E-06	1.E-06	1.E-06	1.E-06	1.E-06	1.E-06	1.E-06
mmol Na+	5.E-03	5.E-03	5.E-03	5.E-03	5.E-03	5.E-03	5.E-03	5.E-03
mmol Cl-	7.E-03	7.E-03	7.E-03	7.E-03	7.E-03	7.E-03	7.E-03	7.E-03
mmol Al+++	1.E-06	1.E-06	1.E-06	1.E-06	1.E-06	1.E-06	1.E-06	1.E-06
mmol SiO2(aq)	1.E-06	1.E-06	1.E-06	1.E-06	1.E-06	1.E-06	1.E-06	1.E-06
mmol Fe++	1.E-06	1.E-06	1.E-06	1.E-06	1.E-06	1.E-06	1.E-06	1.E-06
charge balance	H+	H+	H+	H+/Cl-	H+	H+	H+	H+
Rock mass (g)	100	100	100	100	1000	1000	1000	1000
Seawater/Rock ratio	10:1	10:1	10:1	10:1	1:1	1:1	1:1	1:1

Table 6.2B - Equilibrated Seawater Products

	Temp	Dissolved species in seawater (mmoles)						log f O2(g)		pH
	(°C)	N2(aq)	NH3(aq)	CO2(aq)	CH4(aq)	H2(aq)	NH4+	*Initial (atmos)*	*Final (s/w)*	*Final (s/w)*
Models	20	0.581	~0	412	~0	~0	~0	-35	-34.75	3.39
1 and 5	40	0.446	~0	244	~0	~0	~0	-35	-34.78	3.45
	60	0.385	~0	166	~0	~0	~0	-35	-34.8	3.52
	80	0.362	~0	127	~0	~0	~0	-35	-34.82	3.6
Models	20	0.581	~0	412	~0	~0	~0	-45	-44.75	3.39
2 and 6	40	0.446	~0	244	~0	~0	~0	-45	-44.78	3.45
	60	0.385	~0	166	~0	~0	~0	-45	-44.8	3.52
	80	0.362	~0	127	~0	~0	4.25E-08	-45	-44.84	3.6
Models	20	0.581	~0	412	~0	~0	2.15E-09	-55	-54.75	3.39
3 and 7	40	0.446	~0	244	~0	~0	4.50E-06	-55	-54.78	3.45
	60	0.385	6.30E-08	166	~0	~0	3.69E-03	-55	-54.82	3.53
	80	0.362	8.03E-05	127	3.84E-09	3.38E-07	5.48E-01	-55	-54.84	3.8
Models	20	0.581	6.38E-08	412	~0	~0	0.0626	-65	-64.75	3.42
4 and 8	40	0.446	0.00061	244	5.60E-06	1.24E-07	7.72E+00	-65	-64.78	4.75
	60	2.34E-05	11.2	2.20E-06	3180	0.0075	9250	-65	-68.7	5.62
	80	Failed run								

(Except for log f O2(g), values below 1e-9 are given as approximately zero)

Table 6.2A and 6.2B. Constraints used for models 1 to 8, the results of which are tabulated in Appendix 3 Oxygen fugacity varies from log *f* -35 to log *f* -65.

The condensation reactions to form the amino acids were produced by Geochemist's Workbench (Bethke, 1998). The formation of glycine ($H_2NCH_2COOH_{(aq)}$) from carbon dioxide, hydrogen and ammonia is represented by Equation *6.1*, though there are variants of this reaction which incorporate NH_4^+ in place of $NH_{3(aq)}$ (for examples, see Shock *et al*, 1998).

$$2CO_{2(aq)} + 3H_{2(g)} + NH_{3(aq)} \rightleftharpoons H_2NCH_2COOH_{(aq)} + 2H_2O_{(l)} \qquad (6.1)$$

The equilibrium reaction between glycine and alanine ($H_2NCHCH_3COOH_{(aq)}$) is modelled in terms of redox. If the present atmosphere were to be evaluated in the model, their relationship could be expressed in terms of the oxygen fugacity, as shown in the stoichiometric equation *6.2* below,

$$2\,H_2NCHCH_3COOH_{(aq)} + 3O_{2(g)} \rightleftharpoons 2\,H_2NCH_2COOH_{(aq)} + CO_{2(g)} + H_2O_{(l)} \quad (6.2)$$

where $alanine_{(aq)}$ is oxidised to $glycine_{(aq)}$, carbon dioxide and water. However, the reaction is proposed to take place under *anoxic* conditions, and in the presence of 10 bars of $CO_{2(g)}$ in the Hadean atmosphere. Thus the reaction is written in terms of the consumption of hydrogen and carbon dioxide (Equation *6.3*).

$$Glycine_{(aq)} + 2H_{2(g)} + CO_{2(g)} \rightleftharpoons Alanine_{(aq)} + H_2O_{(l)} \quad (6.3)$$

This expression was more appropriate, as it more closely resembles the metabolic reactions in the reverse Krebs cycle, as described in Hartman (1975) and Russell and Hall (1997). In this cycle, CO_2 is reduced to the $-\{CH_2\}$ groups *(6.4)*, which are used in this model to make the progressively larger amino acids (alanine, valine and leucine) from glycine, on each addition of a $-\{CH_2\}$ group.

$$3\,H_2 + CO_2 \rightarrow 2\,H_2O + -\{CH_2\} \quad (6.4)$$

Using Le Chatelier's principle, Equations *6.1*, *6.2*, *6.3* and *6.4* indicate that were the activity of H_2O to be decreased, the reactions should be pulled to the right. Consequently, the production of more alanine would be favoured, as can be seen in Figure 6.3. As expected, Figure 6.3 indicates that a decrease in the activity of H_2O would assist the production of a higher yield of amino acids, since condensation reactions result in the loss of water. Though it should be noted that activities of H_2O rarely stray far from unity in hydrothermal fluids (Helgeson, 1985) except on mineral surfaces.

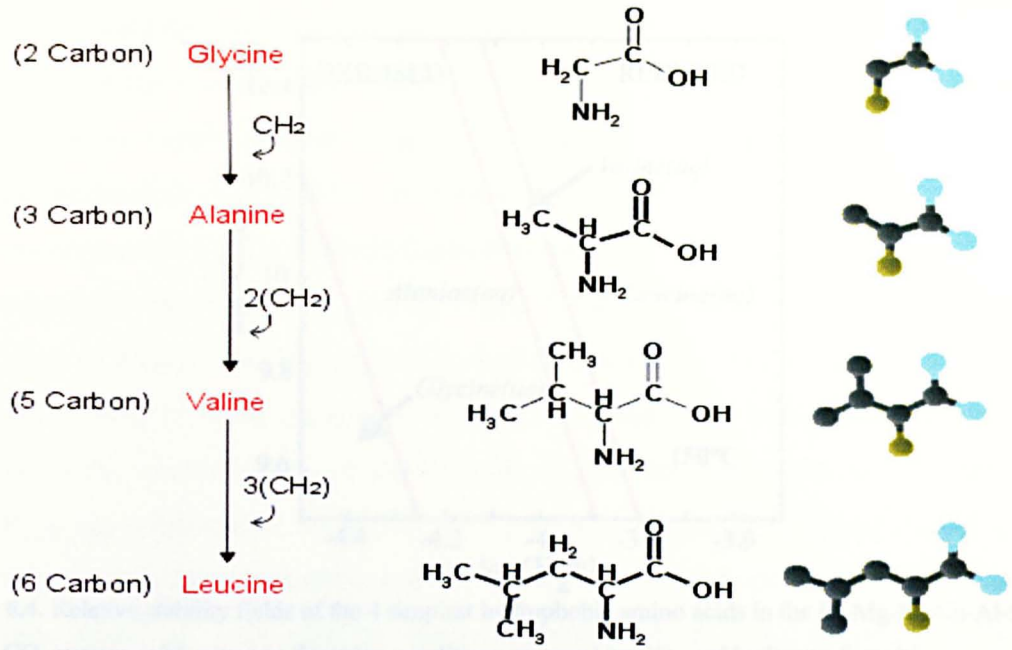

Figure 6.2. Structural formulae of the amino acids, starting with the simplest, glycine. The other amino acids differ in multiples of one carbon atom and two hydrogen atoms, represented by $-\{CH_2\}$. Carbon and hydrogen atoms are provided by reduced CO_2. The ball and stick representations on the right exclude hydrogen atoms.

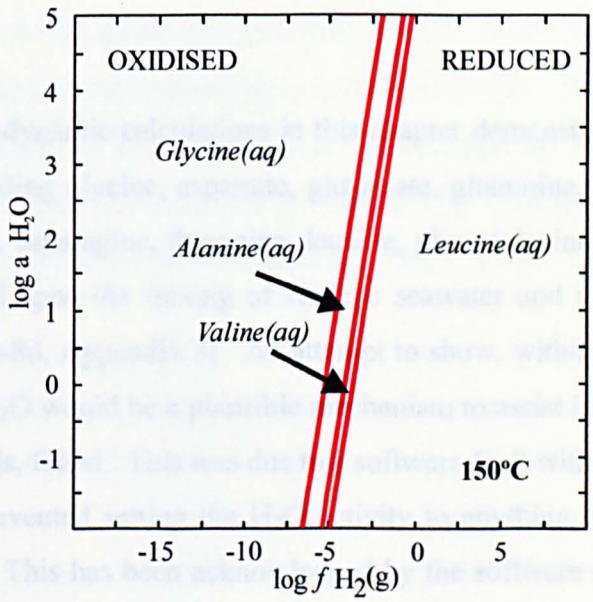

Figure 6.3. Relative stability fields of the 4 simplest hydrophobic amino acids in the Fe-Mg-Na-Ca-Al-SiO_2-Cl-S-H_2O-CO_2 system, with repect to the redox conditions imposed by water activity and hydrogen fugacity.

Figure 6.3 and equation (6.*3*) show that as the activity of H_2O (log a H_2O) decreases, alanine becomes more stable. The sequence of formation of amino acids, going from relatively oxidised to relatively reduced conditions (Glycine → Alanine → Valine → Leucine, see Figure 6.2), is from the addition of carbon and hydrogen atoms (from the reduction of CH_4 which is itself produced by the reduction of CO_2). Produced using Geochemist's Workbench (Bethke, 1998).

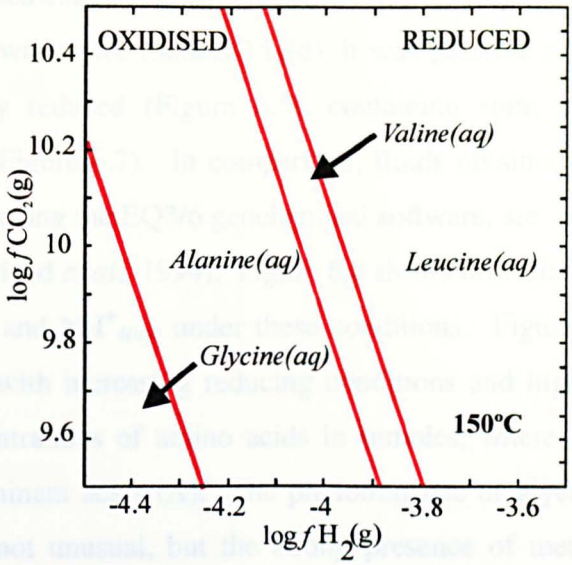

Figure 6.4. Relative stability fields of the 4 simplest hydrophobic amino acids in the Fe-Mg-Na-Ca-Al-SiO_2-Cl-S-H_2O-CO_2 system, with repect to the redox conditions imposed by CO_2 and hydrogen fugacities.

Figure 6.4 shows the stability of amino acids in terms of redox and suggests that the reduction of CO_2 by hydrogen to produce the -{CH_2} group (equation *6.4*) will, starting with glycine, favour the formation of progressively more complex amino acids.

6.4 Results

The thermodynamic calculations in this chapter demonstrate that 15 protein-forming amino acids (including glycine, aspartate, glutamate, glutamine, methionine, serine, valine, isoleucine, alanine, asparagine, threonine, leucine, phenylalanine, tyrosine, and tryptophan) could have formed upon the mixing of Hadean seawater and rock within a hydrothermal system (Models 1a-8d, Appendix 3). An attempt to show, within the model, that a decrease in the activity of H_2O would be a plausible mechanism to assist in the production of a higher yield of amino acids, failed. This was due to a software fault within this version of the GWB program which prevented setting the H_2O activity to anything other than the unit activity (unit activity =1). This has been acknowledged by the software manufacturer and the fault has been rectified in new versions of the code.

Figures 6.5 to 6.10 show the products generated from a seawater-rock interaction (see Model 1a, Appendix 3 for constraints and concentrations of products) from an initial seawater temperature of 20°C, log f O_2(g) –35 and a water rock ratio of 10:1) and the properties of the newly formed hydrothermal fluid at 150°C, as well as the production of just some of the minerals (magnetite and pyrite) from the seawater-crust reaction. From left to right, the graphs show the physical and chemical changes to the system as the temperature of the system is increased from 20°C to 150°C.

By setting the seawater-rock ratio to 10:1, and varying the fugacity of $O_{2(g)}$ and the temperature of the seawater (see models 1a-8d), it was possible to produce a hydrothermal fluid, which is highly reduced (Figure 6.5), containing some sulfur (Figure 6.6), and increasingly alkaline (Figure 6.7). In comparison, fluids obtained from similar water-rock experiments modelled using the EQ3/6 geochemical software, are also reduced, alkaline and containing sulfur (Macleod *et al.*, 1994). Figure 6.8 shows how dissolved nitrogen $N_{2(aq)}$ can be reduced to $NH_{3(aq)}$ and $NH^{+}_{4(aq)}$ under these conditions. Figure 6.9 shows pyrite being reduced to magnetite with increasing reducing conditions and higher temperature. Figure 6.10 shows the concentrations of amino acids in mmoles, where glycine, methionine and alanine are the predominant acids (**A**). The predominance of glycine and alanine over the other amino acids is not unusual, but the strong presence of methionine (an amino acid containing sulfur) is. Although an essential amino acid, in living systems methionine is present in barely detectable quantities. However, in this sulfur-rich environmental model, it is one of the more dominant amino acids and thus does not reflect the biological systems that are understood today. The second cluster of amino acids (**B**), show aspartic acid, serine, asparagine, valine, glutamic acid, threonine, glutamine, isoleucine and leucine, and phenylalanine. Note that some of these amino acids in cluster **B** undergo phase changes as the temperature increases (for example, leucine is stable to ~100°C, whereas isoleucine is stable between ~100°C to 150°C). Both are represented by only one line on the graph. Cluster **C** represents the concentrations of tyrosine (top line) and tryptophan (bottom line). See Model 1a in Appendix 3 for concentrations of the amino acids and constraints used in the models.

Lower seawater-rock ratios (1:1 rather than 10:1) give higher concentrations of sulfur and a higher pH, but the determination of the amount of seawater circulation through the early crust is necessarily speculative. However, during the growth of the hydrothermal system a period of low water-rock ratios must be met. Evidence from drill samples of ultramafic bodies (Eckstrand, 1975; Frost, 1985), indicates that some rocks may give higher concentrations of sulfur in a hydrothermal fluid. Models 5a-8d use a 1:1 seawater-rock ratio that seems to overwhelm the chemistry of the system. Regardless of the values of the initial pH, *Eh* or $\log f O_2$, of the seawater-rock reaction, the final values are unchanging, suggesting that the large volume of rock is buffering the system.

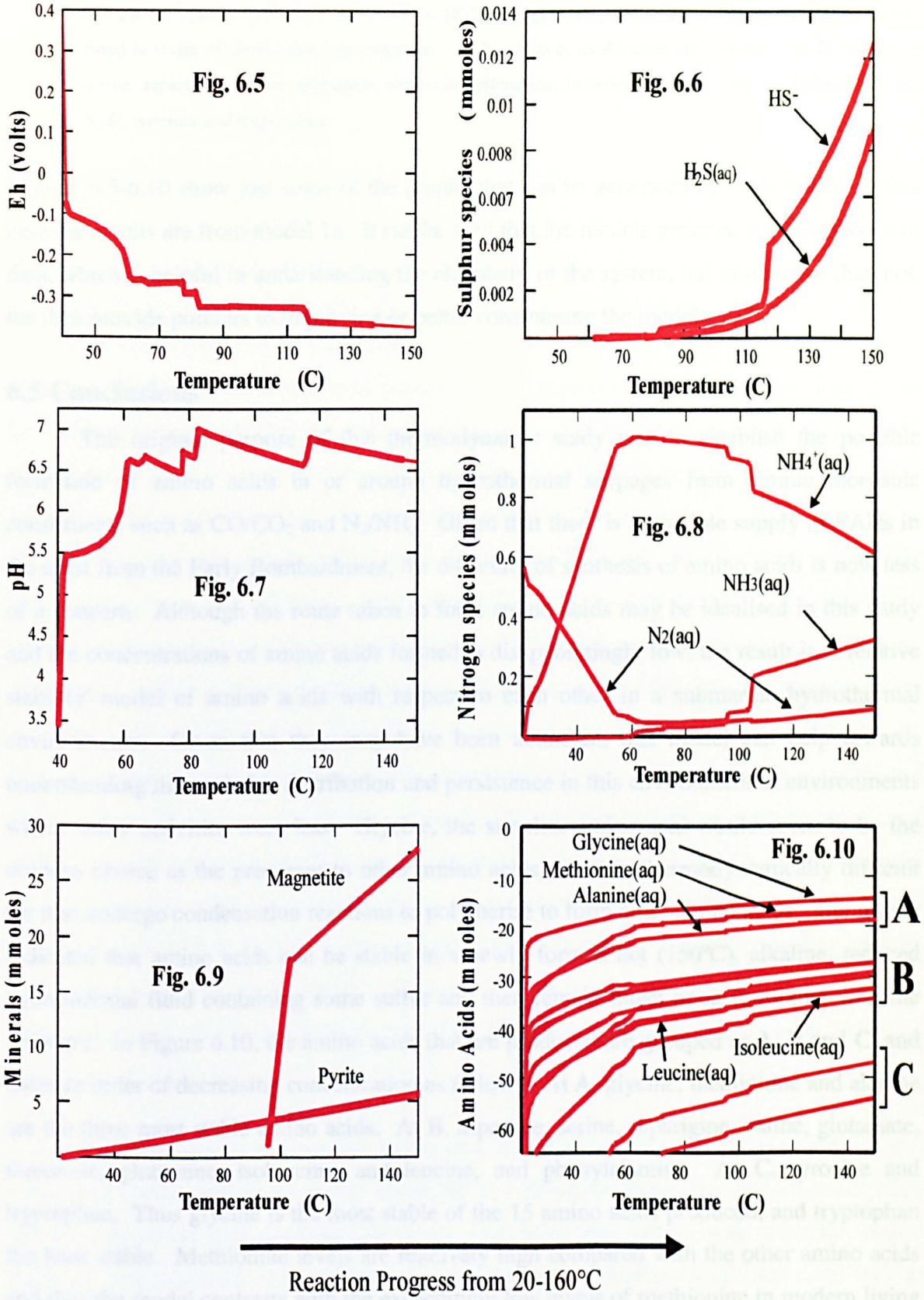

Figures 6.5-6.10. Reaction products in the Fe-Mg-Na-Ca-Al-SiO_2-Cl-S-H_2O-CO_2 system as a result of the reaction between modern seawater and ultramafic rock (water-rock ratio = 10:1). Plots show how the equilibrated system changes with respect to *Eh* (Fig.6.5), sulfide concentrations (Fig. 6.6), pH (Fig. 6.7), dominant nitrogen species (Fig.6.8), iron mineral precipitation and dissolution (Fig. 6.9), and amino acid concentrations (Fig. 6.10) over a polythermal path (20°C to 160°C). Total fugacity CO_2 = 10 bars, inital fugacity $O_2 = 10^{-3.5}$ bars, initial fugacity N_2 = 0.8 bars. Total mmol $Mg^{2+} = 1E^{-3}$,

$SO^{2-}_4 = 1E^{-6}$, $Na^+ = 5E^{-3}$, Cl- = $7E^{-3}$, $Al^{3+} = 1E^{-6}$, $SiO_{2(aq)} = 1E^{-6}$, $Fe^{2+} = 1E^{-6}$. Figure 6.10, amino acids listed in order of decreasing concentration. At **A**, glycine, methionine and alanine. At **B**, aspartate, serine, asparigine, valine, glutamate, threonine, glutamine, isoleucine, and leucine, and phenylalanine. At **C**, tyrosine and tryptophan.

Figures 6.5-6.10 show just some of the graphs that can be generated by each model, in this case the results are from model 1a. It can be seen that the models generate a large amount of data, which is helpful in understanding the chemistry of the system, but more often than not, the data provide pointers to improving or better constraining the models.

6.5 Conclusions

The original purpose of this thermodynamic study was to establish the possible formation of amino acids in or around hydrothermal seepages from simple inorganic constituents such as CO/CO_2 and N_2/NH_3. Given that there is a possible supply of PAHs in the crust from the Early Bombardment, the difficulty of synthesis of amino acids is now less of a concern. Although the route taken to form amino acids may be idealised in this study and the concentrations of amino acids formed is disappointingly low, the result is a 'relative stability' model of amino acids with respect to each other in a submarine hydrothermal environments. Given that they may have been abundant, this model can help towards understanding their relative distribution and persistence in this environment in environments where water activities were less. Glycine, the simplest amino acid would seem to be the obvious choice as the precursor to other amino acids, but it is thermodynamically difficult for it to undergo condensation reactions to polymerise to form other amino acids. The results indicated that amino acids can be stable in a newly formed hot (150°C), alkaline, reduced hydrothermal fluid containing some sulfur and then remain intact upon re-mixing with the seawater. In Figure 6.10, the amino acids that are produced are grouped as **A**, **B** and **C**, and listed in order of decreasing concentration as follows: At **A**, glycine, methionine and alanine are the three most stable amino acids. At **B**, aspartate, serine, asparigine, valine, glutamate, threonine, glutamine, isoleucine, and leucine, and phenylalanine. At **C**, tyrosine and tryptophan. Thus glycine is the most stable of the 15 amino acids produced, and tryptophan the least stable. Methionine levels are relatively high compared with the other amino acids and thus the model contrasts with the exceedingly low levels of methionine in modern living systems. Perhaps methionine had a larger role to play in early Life, or perhaps the model is not an accurate representation of the desired system and production of methionine in the model should have been suppressed. However, this anomaly aside, the formation, stability and possibility of redox reactions between the other acids in the hydrothermal fluid as well as in seawater, coupled with a continuous supply of hydrogen from seawater and ultramafic

rock reactions, lend support to the notion that submarine hydrothermal environments may have provided favourable conditions for the emergence of life.

The initial temperature of the seawater had an influence on the pH of the hydrothermal fluid produced on reaction with the oceanic crust. However, the seawater-rock ratio had a much greater effect on the pH of the fluid (see Chapter 4). The increase in concentration of reduced variants of redox couples such as $SO4^{2-}/HS^-$ and/or H_2S (Figure 6.6), N_2/NH_3 and/or NH_4^+ (Figure 6.8), and CO_2/CH_4 (see Tables in Appendix 3) after the seawater-crust interaction, is consistent with the reduced nature of the hydrothermal fluid (Figure 6.5). Retention, rather than recombination of these and other reduced species has been shown to be favourable in subsea vents by free energy calculations (Clark *et al.*, 1998). These results are in agreement with Amend and Shock's (1998) finding that the production of 11 key amino acids has been shown to be energetically favoured at 100°C. Here, the experiments produce 15 key amino acids (Figure 6.10), albeit, here only in analytically undetectable quantities. There is an increasingly held view that FMQ conditions were unlikely in the early crust (Kasting and Brown, 1998), and in any case, would have been too oxidising for NH_3 to predominate over N_2. There was some difficulty in imposing more reduced conditions between 60 °C to 80 °C in these models (see failed runs, models 4c, 4d, 8c and 8d) and as such we only approach theoretical $\log f O_2$ values for FMQ, as calculated in Chapter 6. This prevents evaluation of more reduced oxidation states imposed by mineral buffers such as iron-wüstite (IW), but further tests could assess amino acid stability under IW conditions at relatively lower or higher temperatures to those tested, or greater crustal depths or even with a different crustal composition. However, the deduction that must be made from these results, is that the ranges of $f O_2$ and temperature tested do not impact significantly on the concentrations of the three predominant amino acids, glycine, methionine and alanine.

The seawater:rock reactions in the rock-dominated system (Models 5a-8d) do not allow any amino acid to be stable above 80°C. However, when the hydrothermal fluid produced from the rock-dominated system comes back into contact with seawater, amino acids are still produced. As a consequence of altering the seawater:rock ratio from 10:1 to 1:1, the change in the relative proportion of amino acids is evident in models 5a-8d (Appendix 3). In order of decreasing concentration, glycine, methionine and alanine in the water-dominated system are now replaced by methionine, glycine and alanine in the rock-dominated system. Thus methione production in the model is clearly related to sulfur availability which is itself determined by the amount of rock reacted.

The minerals produced from the seawater-crust reaction model include pyrite and magnetite and in some cases graphite (Figure 6.9 and see models 1a-8d). Magnetite and pyrite have been used in mineral-catalysis experiments, showing that in combination with reducing conditions (Figure 6.5), the reduction of the normally stable N_2 to NH_3 and NH_4^+ (Figure 6.8) is promoted (Brandes *et al*, 1998). The conversion of Fe(II) in olivine to Fe(III) in magnetite to produce H_2 and conversion of CO_2 to reduced-C species (in this case, methane and graphite) has also been demonstrated (Berndt *et al*, 1996).

The yields of amino acids in the model are extremely low. Further experiments (in which the formation of carbon minerals such as graphite and the nitrogen species, NH_3, were suppressed), increased the yield of the amino acids by several orders of magnitude and in certain scenarios, this suppression could be justified. Experiments investigating the stability of amino acids in PPM buffered assemblages at 200°C/3 bar (Andersson and Holm, 2000), and 150°C/10 bar (Hennet *et al.*, 1992) showed that amino acids can be stable over extended periods of time as hydrothermal pathways are traversed. Hennet *et al.* (1992), reported higher concentrations, generally in the *m*M region when compared to Andersson and Holm's (2000) μM values. However, the difficulty of constraining the hydrothermal conditions, especially during the measurement stage, is clearly stated by Andersson and Holm (2000). Furthermore, decomposition of higher carbon amino acids, such as serine tend to contribute to the total analytical concentrations of lower carbon amino acids such as glycine, making the assessment of the stability of individual amino acids difficult.

It is concluded that, given the presence of nitrogen and carbon in some reduced form (NH_3 /NH_4^+(reduced) or CH_4), the formation of 15 key amino acids is possible under hydrothermal conditions. The models predict the simpler amino acids as the more stable species under the tested conditions. Glycine was found to be the predominantly stable amino acid to be followed by methionine and alanine. An increase in the quantity of rock reacted with seawater, or increase in temperature and decrease in log $f\,O_2$ did not produce any significant increase in concentration of the simple amino acids.

Chapter 7. Conclusions

"The model orders, integrates and unifies a vast amount of experimental data and theoretical considerations coming from many disciplines. It meets the requirement of physical laws, simplicity, self-organisation, selection, continuity and testability". This statement (Muller, 1995; in reference to his own hypothesis) was in response to Oparin's (1938) 'materialistic' criteria for an origin of life model. The Russell and Hall theory (1997) meets all of these criteria. In the present study, the final criteria, testability, is applicable to the early stages (at least thermodynamically) of the Russell and Hall (1997) model, and its probability can be ascertained (Bernal 1960). However, as in most theses, the time allocated for study is limited. It was not possible to attempt to test all of the stages in the Russell and Hall hypothesis (1997), nor to verify each claim or counterclaim of the results of others. This was due in part to the sometimes limited thermodynamic data available at the temperatures and pressures of interest. However, given the required data, this should be surmountable.

The result of this study is essentially a feasibility study of the Russell and Hall model, and an acquisition of the basics skills necessary to model such hypotheses. As far as the chemistry is concerned, much of it has been shown to be thermodynamically feasible. Furthermore, the chemistry of the Russell and Hall hypothesis has increasingly been demonstrated over the last ten years (Cody, Huber and Wächtershäuser, Heinen and Lauwers, Rickard *et al.*, 2001) perhaps an indication that it is built on sensible proposals.

The conclusions of this thesis are summarised below

Hydrogen and pH

It was demonstrated that in the environment envisaged in the Russell-Hall (1997) model, vent systems occurring on off-axis slow-spreading ridges, where seawater circulates deeper into the ultramafic oceanic crust through fractures and fissures, than at on-axis spreading centres, can produce hydrogen-rich (up to ~40 mmol), alkaline (up to pH ~9.5) fluids at relatively low temperatures (<150°C). pH was thought to be controlled by the loss of magnesium from seawater and loss of calcium from the oceanic rock.

Sulfur

The availability of reduced sulfur in hydrothermal fluids is determined by the composition of the crust and thus the mineral assemblage by which the crust is buffered.

The results in this thesis indicate that ~10 mmolar of sulfur would have been available. In addition they suggest that increased reducing conditions such as those resulting from hydrogen generation in serpentinisation reactions could increase sulfur availability.

Wächtershäuser's 'pyrite-pulled' theory was confirmed to be theoretically unsound, and the approach used to demonstrate this point and many others, indicated the power and flexibility of geochemical modelling codes, in particular the Geochemist's Workbench.

The high-temperature hydrothermal systems modelled seemed to be a good representation of the types of systems found so far by others (Corliss, *et al.*, 1979; Kelley *et al.*, 2001). In addition the models also gave similar results to the many water-rock experiments conducted by Seyfried , Mottl and others (see Bibliography and Chapter 4).

The mineral buffer experiments indicated that a more reduced crust may have promoted organic synthesis by preventing (hindering) the complete reduction of CO_2 to CH_4

Amino acids were shown to be stable under a variety of conditions and perhaps able to condense into larger molecules due to changes in water activtiy. With the ability to represent chemical, physical and even biological processes, this hints at how useful a prediction tool geochemical modelling can be.

Bibliography

Adams, D. (1979). The Hitchhikers Guide to the Galaxy. Ballantine Books, ISBN: 0-345-39180-2.

Adams, M.W.W. 1992. Novel iron-sulfur centers in metalloenzymes and redox proteins from extremely thermophilic bacteria. *Advances in Organic Chemistry,* **38**, 341-396.

Allamandola, L. J., Bernstein, M. P., & Sandford, S. A. 1997. Photochemical evolution of interstellar/precometary organic material. In: *Astronomical and Biochemical Origins and the Search for Life in the Universe*, C.B. Cosmovici, S. Bowyer, & D. Werthimer (eds.), Proc. 5th International Conf. on Bioastronomy, IAU Coll. #161, Capri, 1-5 July 1996, (Editrice Compositori: Bologna), 23-47.

Alt, J.C., Honnorez, J., Laverne, C. & Emmerman, R. 1986. Hydrothermal alteration of a 1 km section through the upper oceanic crust, Deep Sea Drilling Project Hole 504b: Mineralogy, chemistry, and the evolution of seawater-basalt reactions. *Journal of Geophysical Research*, **91**, 10309-10335.

Amend, J.P. & Shock, E.L. 1998. Energetics of amino acid synthesis in hydrothermal ecosystems. *Science*, **281**, 1,659-1,662.

Amend, J.P. & Shock, E.L. 2001. Energetics of overall metabolic reactions of thermophilic and hyperthermophilic Archaea and Bacteria. *FEMS Microbiological Reviews*, **25**, 175-243.

Andersson, E. & Holm, N.G. 2000. The stability of some selected amino acids under attempted redox constrained hydrothermal conditions. *Origins of Life and Evolution of the Biosphere*, **30**, 9-23.

Appel, P.W.U., Rollinson, H.R. & Touret, J.L.R. 2001. Remnants of an early Archean (>3.75 Ga) sea-floor nydrothermal system in the Isua Greenstone Belt. *Precambriam Research*, **112**, 27-49.

Appelo, C.A.J. & Postma, D. 1993. Geochemistry, groundwater and pollution. A.A. Balkema Publishers, USA.

Arnórsson, S. & Gunnlaugsson, E. 1985. New gas geothermal exploration-calibration and application. *Geochimica et Cosmochimica Acta*, **49**, 1,307-1,325.

Arrhenius, G. 1986. Dysoxic environments as models for primordial mineralisation. In Cairns-Smith *et al.*, A.G. & Hartman, H.(eds) *Clay and Clay Minerals and the Origin of Life*. Cambridge University Press, 97-104.

Baker, E.T. 1994. A six-year time series of hydrothermal plumes over the Cleft segment of the Juan de Fuca Ridge. *Journal of Geophysical Research*, 99, 4889-4904.

Ballhaus, C. & Ellis, D.J. 1996. Mobility of core melts during Earth's accretion. *Earth and Planetary Science Letters,* **143**, 137-145.

Banks, D 1985. A fossil hydrothermal worm assemblage from the Tynagh lead-zinc deposit in Ireland. *Nature* , **313**, 128-131.

Barker, W.W., Santelli, C. M., Welch, S.A. & Banfield, J.F. 2001. Biomineralization of extracellular polymers by iron oxyhydroxides. *Abstract*: *Astrobiology Science Conference Abstracts,* http://www.astrobiology.com.

Barnes, S.J. & Hill, R.E.T. 2000. Metamorphism of komatiite-hosted nickel sulfide deposits. In: Spry, P.G., Marshall, B. & Vokes, F.M. (eds). *Reviews in Economic Geology*, **11**, 203-215.

Barnes, H.L. & Kullerud, G. 1961. Equilibration in sulfur-containing aqueous solutions in the system Fe-S-O, and their correlation during ore deposition. *Economic Geology*, **56**, 648-688.

Barns, S.M., Fundyga, R.E., Jeffries, M.W. & Pace, N.R. 1994. Remarkable archaeal diversity in a Yellowstone hot spring environment. *Proc. Natl. Acad. Sci. USA.*, **91**, 1609-1613.

Barns, S.M., Delwich, C.F., Palmer, J.D. Dawson, S.C. Herschberger, K.L. & Pace, N.R. 1996. Phylogenetic perspective on microbial life in hydrothermal ecosystems, past and present. In: Evolution of Hydrothermal Ecosystems on Earth (and Mars?)," G.R. Bock, and J.A. Goode (eds.), Wiley Press, Chichester, 24-32.

Baross, J.A. & Hoffman, S.E. 1985. Submarine hydrothermal vents and associated gradient environments as sites for the origin and evolution of life. *Origins of Life and Evolution of the Biosphere,* **15,** 327-345.

Battista, J.R., Earl, A.M. & Park, M-J. 1999. Why is *Deinococcus radiodurans* so resistant to ionizing radiation? *Trends in Microbiology*, **7**, 362-365.

Bernal, J.D. 1949. The physical basis of Life. *Proceedings of the Physical Society, London*, **62**, 537-558.

Bernal, J.D. 1951. *The Physical Basis of Life.* Routledge and Kegan Paul, London.

Bernal, J.D. 1960. The problem of stages in biopoesis. *In*: Florkin, M. (ed.) *Aspects of the Origin of Life*, .New York, Pergamon Press, 30-45.

Berndt, M.E., Allen, D.E. & Seyfried, W.E. 1996. Reduction of CO_2 during serpentinization of olivine at 300°C and 500 bar. *Geology*, **24**, 351-354.

Berner R. A. 1981. A new geochemical classification of sedimentary environments. *Journal of edimentary Petrology*, **51**, 2,359-2,365

Bernhardt, G., Ludemann, H.-D., Jaenicke, R., König, H. ans Stetter, KO. 1984. Biomolecules are unstable under "black smoker" conditions. *Naturwissenschaften*, **71**, 583-586.

Bethke, C.M. 1996. *Geochemical Reaction Modelling.* Oxford University Press. ISBN 0-19-509475-1.

Bethke, C. M. 1998. *The Geochemist's Workbench, Release 3.0*, Hydrogeology Program, University of Illinois.

Biellmann, C., Gillet, P., Guyot, F., Peyronneau, J. & Reynard, B. 1993. Experimental evidence for carbonate stability in the Earth's lower mantle. *Earth and Planetary Science Letters* **118**, 31-41.

Bischoff, J.L. & Dickson, F.W. 1975. Seawater-basalt interaction at 200°C and 500 bars: implications for origin of seafloor heavy metal deposits and regulation of seafloor chemistry. *Earth and Planetary Science Letters*, **25**, 385-397.

Bischoff, J.L. & Rosenbauer, R.J. 1984. The critical point and two-phase boundary of seawater, 200-500°C. *Earth and Planetary Science Letters*, **68**, 172-180.

Bischoff, J.L. & Pitzer K. S. 1989. Liquid-vapour relations for the system NaCl-H_2O: summary of the P-T-x surface from 300° to 500°C. *American Journal of Science*, **289**, 217-248.

Boyce, A.J., Coleman, M.L. & Russell, M.J. 1983. Formation of fossil hydrothermal chimneys and mounds from Silvermines, Ireland. *Nature*, **306**, 545-550.

Bonomi, F., Werth, M.T. & Kurtz, D.M. 1985. Assembly of $Fe_nS_n(SR)^{2-}$ (n=2,4) in aqueous media from iron salts, thiols and sulfur, sulfide, thiosulfide plus rhodonase. *Inorganic Chemistry*, **24**, 4331-4335.

Brandes, J.A., Boctor, N. Z., Cody, G.D., Cooper, B.A., Hazen, R.M. & Yoder, H.S. 1998. Abiotic nitrogen reduction on the early Earth. *Nature*, **395**, 365-367.

Brock, T.D., Madigan, M.T., Martinko, J.M. & Parker, J. 1997. *Biology of Microorganisms.* 8th Edition. Prentice Hall International Inc. (UK) Limited, London.

Brown, G.C., Hawkesworth, C.J. & Wilson, R.C.L. (eds.). 1992. *Understanding the Earth: a new synthesis,* Cambridge University Press. ISBN 0-521-37020-5.

Brown, G.M., Emeleus C. H., Holland J. G., & Phillips R. 1970. Petrographic, minerologic, and x-ray fluorescence analysis of lunar igneous-type rocks and spherules. *Science*, **167**, 599-601.

Buchanan, B.B. & Arnon, D.I. 1990. A reverse Krebs cycle in photosynthesis: Consensus at last. *Photosynthesis Research,* **24**, 47-53.

Butler, I.B., Fallick, A.E. & Nesbitt, R.W. 1998. Mineralogy, sulphur isotope geochemistry and the development of sulphide structures at the Broken Spur hydrothermal vent site, 29°10'N, Mid-Atlantic Ridge. *Journal of the Geological Society*, **155**, 773-785.

Butterfield, D.A., Massoth, G.J., McDuff, R.E., Lupton, J.E. & Lilley, M.D. 1990. Geochemistry of hydrothermal fluids from Axial Seamount Hydrothermal Emmisions Study Vent Field, Juan de Fuca Ridge: subseafloor boiling and subsequent fluid-rock interaction. *Journal of Geophysical Research*, **95**, 12,895-12,921.

Canil, D. 1997. Vanadium partitioning and the oxidation state of Archaean komatiite magmas. *Nature:Letters*, **389**, 842-845.

Cathles, L.M. 1990. Scales and Effects of fluid flow in the upper crust. *Science*, **248**, 323-329.

Chivas, A.R., Barnes, I., Evans, W.C., Lupton, J.E. & Stone, J.O. 1987. Liquid carbon dioxide of magmatic origin and its role in volcanic eruptions. *Nature*, **326**, 587-589.

Chyba, C. 1998. Buried beginnings. *Nature*, **395**, 329-330.

Clark, P. D., Dowling, N. I. & Huang, M. 1998. Comments on the role of H_2S in the chemistry of Earth's early atmosphere and in prebiotic synthesis. *Journal of Molecular Evolution*, **47**, 127-132.

Cody, G. D., Boctor, N. Z., Filley, T. R., Hazen, R. M., Scott, J. H., Sharma, A. & Yoder Jr, H. S. 2000. Primordial carbonylated iron-sulfur compounds and the synthesis of pyruvate. *Science*, **289**, 1337-1340.

Cody, G.D., Boctor, N.Z., Hazen, R.M., Brandes, J.A., Morowitz, H.J. & Yoder, H.S. 2001. Geochemical roots of carbon fixation: Hydrothermal experiments in the system citric acid, H2O-(FeS)-(NiS). *Geochimica et Cosmochimica Acta*, **65**, 3557-3576.

Collin, J. 1988. Double carbonylation reaction : a review.

Corliss, J.B., Dymond, J., Gordon, L.I., Edmond, J.M., von Herzen, R.P., Ballard, R.P., Green, K.K., Williams, D., Bainbridge, A., Crane, K. & van Andel, T.H. 1979. Submarine thermal springs on the Galapagos rift. *Science*, **203**, 1073-1083.

Corliss, J.B., Baross, J.A. & Hoffman, S.E. 1981. An hypothesis concerning the relationship between submarine hot springs and the origin of life on Earth. *Oceanololica Acta*, No. Sp, 59-69.

Corliss, J.B. 1986a. On the role of submarine hot springs on the Archaean Earth: The chemistry of sea water, degassing, and the oxidation/reduction balance. *Origins of Life and Evolution of the Biosphere*, **19**, 192-193.

Corliss, J.B. 1986b. On the creation of living cells in submarine hot spring flow reactors: Attractors and bifurcations in the natural hierarchy dissipative systems. *Origins of Life and Evolution of the Biosphere*, **19**, 381-382.

Coveney (Jr), R.M., Goebel, E.D., Zeller, E.J., Dreschhoff, G.A.M. & Angino, E.E. 1987. Serpentinization and the origin of hydrogen gas in Kansas. *The American Association of Petroleum Geologists Bulletin*, **71**, No. 1. 39-48.

Cronin, J.R., Pizzarello, S. & Cruikshank, D.P. 1988. Organic matter in carbonaceous chondrites, planetary satellites, asteroids and comets. *In*: Kerridge, J.F. & Matthews, M.D., *Meteorites and the Early Solar System.* Tucson, University of Arizona Press, 819-857.

Daniel, R.M. 1992. Modern life at high temperatures. Marine hydrothermal systems and the origin of Life, *Origins of Life and Evolution of the Biosphere*, **22**, 33-42.

Daniel, R.M. & Danson, M.J. 1995. Did primitive microorganisms use nonheme iron proteins in place of NAD/P? *Journal of Molecular Evolution*, **40**, 559-563.

Daniels, L., Belay N., Basvapatna R.S. & Weimer P.J. 1987. Bacterial methanogenesis and growth from CO_2 with elemental iron as the sole source of electrons. *Science,* **237**, 509-511.

Darwin, C.C.R. 1859. *On the origin of species by means of natural selection.* London : Murray.

Dayhoff, M. O., LippinCott, E. R., Eck, R. V. & Nagarajan, G. 1967. Therodynamic equilibrium in prebiological atmospheres of C, H, O, N, P, S, and Cl. *Scientific and Technical Information Division, NASA.*

de Duve, C. 1991. *Blueprint for a Cell: The Nature and Origin of Life.* Burlington, North Carolina, Neil Patterson Publishers.

de Duve, C., & Miller, S.L. 1991. Two-dimensional life? *Proceedings of the National Academy of Science USA*, **88**, 10014-10017.

de Duve, C. 1995. Vital dust: life as a cosmic imperative. Basic Books, Harper-Collins, New York.

Delaney, J.M. & Lundeen, S.R. 1990. The LLNL thermochemical database. Lawrence Livermore National Laboratory Report. UCRL-21658, p150.

de Ronde, C.E.J., de Wit, M.J. & Spooner, E.T.C. 1994. Early Archean (>3.2 Ga) Fe-oxide-rich, hydrothermal discharge vents in the Barberton greenstone belt, South Africa. *Geological Society of America Bulletin*, **106**, 86-104.

de Wit, M., Hart, R., Martin, A. & Abbot, P. (1982). Archaean abiogenic and probable biogenic structures associated with mineralized hydrothermal vent systems and regional metasomatism, with implications for greenstone belt studies. *Economic Geology*, **77**, 1783-1801.

de Vusse, V. & Powell, R. 1983. The interpretation of pyrrhotine – pentlandite – tochilinite – magnetite – magnesite textures in serpentinities from Mount Keith, Western Australia. *Mineralogical Magazine*, **47**, 501-505.

Deamer, W.D. 1986. Role of amphiphilic compounds in the evolution of membrane structure on the early Earth. *Origins of Life and Evolution of the Biosphere*, **17**, 3-25.

Deming, D. (1992). Catastrophic release of heat and fluid flow in the continental crust. *Geology*, **20**, 83-86.

Dobbek, H., Svetlitchnyi, V., Gremer, L., Huber, R. & Meyer, O. (2001). Crystal structure of a carbon monoxide dehydrogenase reveals a [Ni-4Fe-5S] cluster. *Science*, **293**, 1281-1285.

Doolittle, W. F. 1998. A paradigm gets shifty. *Nature*, **392**, 15-16.

Drever, J.I. 1988. The Geochemistry of Natural Waters. Second Edition. Prentice-Hall, Englewood Cliffs, New Jersey, p437.

Drobner, E., Huber, H. & Wächtershäuser, G., Rose, D. & Stetter, O. 1990. Pyrite formation linked with hydrogen evoluton under anaerobic conditions. *Nature*, **346**, 724-744.

Duckworth, R.C., Knott, R., Fallick. A.E., Rickard, D., Murton, B.J., & Van Dover, C. 1995. Mineralogy and sulphur isotope geochemistry of the Broken Spur sulphides, 29°N, Mid-Atlantic Ridge. *In*: Parson, L.M., Walker, C.L. & Dixon, D.R (eds). *Hydrothermmal Vents and Processes*. Geological Society Special Publication No. 87, 175-189.

Dymek, R.F. & Klein, C 1988. Chemistry, petrology and origin of banded iron-formation lithologies from the 3800 Ma Isua Supracrustal Belt, West Greenland. *Precambrian Research*, **39**, 247-302.

Eck, R.V. & Dayhoff, M.O. 1966. Evolution of the structure of ferredoxin based on living relics of primitive amino acid sequences. *Science*, **152**, 363-366.

Eckstrand, O. R. 1975. The Dumont Serpentinite: A model for control of nickeliferous opaque mineral assemblages by alteration reactions in ultramafic rocks. *Economic Geology*, **70**, 183-201.

Edmond, J. M., Measures. C., McDuff R. E., Chan L. H., Collier, R. & Grant, B., Gordon L.I. & Corliss, J.B. 1979. Ridge Crest Hydrothermal activity and the balances of the major and minor elements in the ocean: The Galapolas data. *Earth and Planetary Science Letters*, **46**, 1-18.

Edmond, J.M., Campell, A.C., Palmer, M.R., Klinkhammer, G.P., German, C.R., Edmonds, H.N., Elderfield, H., Thompson, G. & Rona.P. 1995. Time series studies of vent fluids from the TAG and MARK sites (1986, 1990) Mid-Atlantic Ridge: a new solution chemistry model and a mechanism for Cu/Zn zonation in massive sulphide orebodies. *In*: Parson, L.M., Walker, C.L. & Dixon, D.R (eds). *Hydrothermmal Vents and Processes*. Geological Society Special Publication No. 87, 77-86.

Elderfield, H. & Schultz, A. 1996. Mid-ocean ridge hydrothermal fluxes and the chemical composition of the ocean. *Annual Review Earth Planeteray Sciences*, **24**, 191-224.

Eschenmoser, A. 1994. Chemistry of potentially prebiological natural products. *Origins of Life and Evolution of the Biosphere*, **24**, 389-423.

Evans, W.C., White, L.D. & Rapp, J.B. 1988. Geochemistry of some gases in hydrothermal fluids from the southern Juan de Fuca Ridge. *Journal of Geophysical Research*, **93**, 15,305-15,313.

Farley, J. 1977. The spontaneous generation controversy from Descartes to Oparin. *The John Hopkins University Press Ltd., London*. ISBN 0-8018-1902-4.

Farquhar, J., Bao, H. & Thiemens, M. 2000. Atmospheric influence of Earth's earliest sulfur cycle. *Science*, **289**, 756-758.

Ferris, J. P. 1992. Chemical markers of prebiotic chemistry in hydrothermal systems. In: Marine hydrothermal systems and the origin of Life (ed. Holm, N.G.). *Origins of Life and Evolution of the Biosphere*, **22**, 109-134.

Ferris, J.P., Hill, A.R. Liu, R. & Orgel, L.E. 1996. Synthesis of long prebiotic oligomers on mineral surfaces. *Nature*, **381**, 59-61.

Fletcher, P. 1993. *Chemical Thermodynamics for Earth Scientists*. Longman Scientific and Technical.

Francis, D., Ludden, J., Johnstone, R. & Davis, W. 1999. Picrite evidence for more Fe in Archean mantle reservoirs. *Earth and Planetary Science Letters*, **167**, 197-213.

Frederickson, K. F. & Onstott T. C. 1996 Microbes deep inside the Earth, *Scientific American*, 43-47.

French, B.M. 1964. Stability of siderite, $FeCO_3$, and progressive metamorphism of iron formation. The Johns Hopkins University PhD Thesis, 57-68.

Freund, F., Gupta. A.D. & Kumar, D. 1999. Carboxylic and dicarboxylic acids extracted from crushed magnesium oxide single crystals. *Origins of Life and Evolution of the Atmosphere*, **29**, 489-509.

Freund, F., Staple, A. & Scoville, J. 2001. Organic protomolecule assembly in igneous minerals. *Proceedings of the National Academy of Science, USA*, **98**, No. 5. 2142-2147.

Frost, B. R. 1985. On the stability of sulphides, oxides, and native metals in serpentinite. *Journal of Petrology*, **26**, 31-63.

Fox, S.W. & Windsor, C.R. 1970. Synthesis of amino acids by the heating of formaldehyde and ammonia. *Science*, **170**, 984-986.

Fyfe, W.S. 1974. Heats of chemical reactions and submarine heat production. *Geophysical Journal of the Royal Astronomical Society*, **37**, 213-215.

Fyfe, W.S. & Price, N.J. 1973. Fluids in the Earth's crust. Amsterdam. Elsevier.

Garcia, M.O., Hulsebosch, T.P., Rhodes, J.M., Rhodes, J.M. & Lockwood, J.P. 1995, Olivine-rich submarine basalts from the southwest rift zone of Mauna Loa Volcano; implications for magmatic processes and geochemical evolution. Mauna Loa revealed; structure, composition, history, and hazards. *Geophysical Monograph*, **92**, 219-239.

Garrels, R.M. & Christ, C.L. 1965. *Minerals, Solutions and Equilibria.* New York, Harper Row.

Garrels, R.M. & MacKenzie, F.T. 1967. Origin of the chemical compositions of some springs and Lakes. *In*: R.F. Gould (Ed), Equilibrium Concepts in Natural Water Systems. (Advances in Chemistry Series 67). *American Chemical Society*, Washington, D.C., p. 222-242.

Gerlach, T.M. 1989a. CO_2 from magma-chamber degassing. *Nature*, **337**, 124.

Gerlach, T.M. 1989b. Degassing of carbon dioxide from basaltic magma at spreading centers: I. Afar transitional basalts. *Journal of Volcanic and Geothermal Research*, **39**, 211-219.

German, C.R., Baker, E.T. & Klinkhammer, G. 1995. Regional setting of hydrothermal activity. *In*: Parson, L.M., Walker, C.L. & Dixon, D.R (eds). *Hydrothermal Vents and Processes.* Geological Society Special Publication No. 87, 3-15.

Gillett, F.C., Forrest, W.J. & Merrill, K.M. 1973. 8-13 micron Observations of Titan. *Astrophys. J.*, **184**, 93-95

Gislason, S. R. & Eugster, H. P. 1987. Meteoric water-basalt interactions. I: A laboratory study. *Geochimica et Cosmochimica Acta*, **51**, 2,827-2,840.

Greenwood, H.J. 1977. Short course in application of thermodynamics to petrology and ore deposits. *Mineralogical Association of Canada.* Evergreen Press Limited.

Griffith, L.L. & Shock, E.L. 1995. A geochemical model for the formation of hydrothermal carbonates on Mars. *Nature*, **377**, 406-408.

Haberstroh, P.R. & Karl, D.M. 1989. Dissolved free amino acids in hydrothermal vent habitats of the Guyamas Basin. *Geochimica et Cosmochimica Acta*, **53**, 2,937-2945.

Hahn, J. & Haug, P. 1986. Traces of Archaebacteria in ancient sediments. Archaebacteria 1985 Proceedings, *System. Appl. Microbiol*, **7**, 178-183.

Haldane, J.B.S. 1929. The origin of Life. *The Rationalist Annual*, **3**.

Hall, D.O., Cammack, R. & Rao, K.K. 1971. Role for ferredoxins in the origin of life and biological evolution. *Nature*, **233**, 136-138.

Hall, A.J. 1986, Pyrite-pyrrhotite redox reactions in nature, *Mineralogical Magazine*, **50**, 223-229.

Hall, A.J., Boyce, A.J. & Fallick, A.E. 1987. Iron-sulphides in metasediments:isotopic support for a retrogressive pyrrhotite to pyrite reaction. *Chem. Geol.*, Isotope Geoscience section, **65**, 305-310.

Hartman, H. 1975. Speculations on the origin and evolution of metabolism. *Journal of Molecular Evolution*, **4**, 359-370.

Hayatsu, R., Studier, M.H., Moore, L.P. & Anders, E. 1972. Origin of organic matter in the solar system VI. Catalytic synthesis of nitriles, nitrogen bases and porphyrin-like-pigments. *Geochimica et Cosmochimica Acta*, 36, 555-571.

Heezen, M.C., Tharp, M. & Ewing, M. 1959. The floors of the oceans. I - The North Atlantic. *The Geological Society of America.* Special Paper 65, p122 .

Heinen, W. & Lauwers, A.M. 1996. Organic sulfur compounds resulting from the interaction of iron sulfide, hydrogen sulfide and carbon dioxide in an anaerobic aqueous environment. *Origins of Life and Evolution of the Biosphere*, **26**, 131-150.

Heinen, W. & Lauwers, A.M. 1997. The iron-sulfur world and the origins of life: Abiotic synthesis from metallic iron, H_2S and CO_2: a comparison of the thiol generating FeS/HCl(H_2S)/CO2-system and its $Fe^0/H_2S/CO_2$-counterpart. Proceedings Koninklijke Nederlandse Akademie van Wetenschappen, Amsterdam, **100**, 11-25.

Helgeson, H.C. 1968. Evaluation of irreversible reactions in geochemical processes involving minerals and aqueous solutions: I. Thermodynamic relations. *Geochimica et Cosmochimica Acta*, **32**, 853-877.

Helgeson, H.C. 1969. Thermodynamics of hydrothermal systems at elevated temperatures and pressures. *American Journal of Science*, **267**, 729-804.

Helgeson, H.C. 1970. A chemical and thermodynamic model of ore deposition in hydrothermal systems. *In*: Mineralogical Society of America Special Paper 3, Mineralogical Society of America, Washington, D.C. p155-186

Helgeson, H.C. & Kirkham, D. H. 1974a. Theoretical prediction of the thermodynamic behaviour of aqueous electrolytes at high pressures and temperatures. **I.** Summary of the thermodynamic/electrostatic properties of the solvent. *American Journal of Science*, **274**, 1089-1198.

Helgeson, H.C. & Kirkham, D. H. 1974b. Theoretical prediction of the thermodynamic behaviour of aqueous electrolytes at high pressures and temperatures. **II.** Debye-Huckel parameters for activity co-efficients and relative partial molal properties. *American Journal of Science*, **274**, 1089-1198.

Helgeson, H.C., Kirkham, D.H., & Flowers, G.C. 1981. Theoretical prediction of the thermodynamic behavious of aqueous electrolytes at high pressures and temperatures: III. Equation of state for aqueous species at infinite dilution. *American Journal of Science*, **276**, 97-240.

Helgeson, H.C. 1985. Some thermodynamic aspects of geochemistry. *Pure and Applied Chemistry*, **57**, 31-44.

Hennet, R.J.C., Holm, N.G. & Engel, M.H. 1992. Abiotic synthesis of amino acids under hydrothermal conditions and the Origin of Life: a perpetual phenomenon? *Naaturwissenschaaften*, **79**, 361-365.

Henrici-Olivé, G. & Olivé, S. 1984. Mechanism of the Fischer-Tropsch synthesis- origin of oxygenates. *Journal of Molecular Catalysis*, **24**, 7-13.

Hochella, Jr. M. F. & White, A. F. *(eds.)* 1990. Mineral-water interface geochemistry. *Reviews in Mineralogy*. Mineralogical Society of America, pp603.

Holland, H. D. 1984. The chemical evolution of the atmosphere and oceans. Princeton University Press, ISBN 0-691-08348-7.

Holloway, J. R. 1984. Graphite-CH_4-H_2O-CO_2 equilibria at low-grade metamorphic conditions. *Geology*, **12**, 455-458.

Holm, N. G., (ed.). 1992. Marine hydrothermal systems and the origin of Life. *Report of SCOR Working Group 91*. Kluwer Academic Publishers.

Holm, N.G. 1992. Why are hydrothermal systems proposed as plausible environments for the origin of Life? *In*: Holm, N. G., (ed.), *Marine Hydrothermal Systems and the Origin of Life. Origins of Life and Evolution of the Atmosphere*, **22**, 5-14. Kluwer Academic Publishers.

Holm, N.G. & Hennet, R.J. 1992. Hydrothermal systems: their varieties, dynamics, and suitability for prebiotic chemistry. *In*: Marine hydrothermal systems and the origin of Life. *Origins of Life and Evolution of the Atmosphere*, **22**, 5-14.

Horita, J. & Berndt, M. E. 1999. Abiogenic methane formation and isotopic fractionation under hydrothermal conditions. *Science*, **285**, 1,055-1,057.

Huber, R., Kurr, M., Jannasch, H.W. & Stetter, K.O. 1989. A novel group of abyssal methanogenic archaebacteria (*Methanopyrus*) growing at 110°C. *Nature*, **342**, 833-834.

Huber, C. & Wächtershäuser, G. 1997. Activated acetic acid by carbon fixation on (Fe,Ni)S under primordial conditions. *Science*, **276**, 245-247.

Huber, C. & Wächtershäuser, G. 1998. Peptides by activation of amino acids with CO on (Ni, Fe) surfaces: implications for the origin of life. *Science*, **281**, 670-672.

Imai, E., Honda, H., Hatori, K., Brack, A. & Matsuno, K. 1999. Elongation of oligopeptides in a simulated submarine hydrothermal system. *Science*, **283**, 831-833.

Irifune, T. & Isshiki, M. 1998. Iron partitioning in a pyrolite mantle and the nature of the 410-km seismic discontinuity. *Nature*, **392**, 702-704.

Jakosky, B. M. & Shock, E. L. 1998. The biological potential of Mars, the early Earth, and Europa. *Journal of Geophysical Research*, **103**, 19,359-19,364.

Janecky, D. R. & Seyfried, J. R. 1986. Hydothermal serpentinization of peridotite within the oceanic crust: experimental investigations of mineralogy and major element chemistry. *Geochimica et Cosmochimica Acta*, **50**, 1357-1378.

Jenkins W. T. 1994. Balancing enzymological equations by thermodynamic bookkeeping. *Modern Enzymology: Problems and Trends*, Nova Science Publishers, Inc. ISBN 1-56072-167-7

Jenkins, W. T. & Patrick J. S. 1986. Catalysis of the dephosphorylation of an ATP-molybdate complex by calcium and magnesium ions. *Journal of Inorganic Biochemistry*, **27**, 163-172.

Jenkins, W. T. 1988. Reactions of dysprosium with adenine nucleotides. *Journal of Inorganic Biochemistry*, **32**, 269-275.

Jenkins, W. T. 1998. Three solutions of the protein solubility problem. *Protein Science*, **7**, 376-382.

Jochum, K. P., Arndt, N. T. & Hofmann, A. W. 1991. Nb-Th-La in komatiites and basalts: Constraints on komatiite petrogenesis and mantle evolution. *Earth and Planetary Science Letters.*

Johnson, J.W., Oelkers, E.H. & Helgeson, H.C. 1992. SUPCRT92: A software package for calculating the standard molal thermodynamic properties of minerals, gases, aqueous species and reactions from 1 to 5000 bars and 0° to 1000°C. *Computers in Geosciences*, **18**, 899-947.

Jupp, T. & Schultz, A. 2000. A thermodynamic explanation for black smoker temperatures. *Nature*, **403**, 880-883.

Kanavarioti, A. 1997. Dimerisation in highly concentrated solutions of phosphoimidazolide activated mononucleotides. *Origins of Life and Evolution of the Atmosphere*, **27**, 357-376.

Kaschke, M., Russell, M.J. & Cole, J.W. 1994. [FeS/FeS_2]. A redox system for the origin of life. *Origins of Life and Evolution of the Biosphere,* **24**, 43-56.

Kassim, J., Baird, T. & Fryer, J.R. 1982. Electron microscope studies of iron corrosion products in water at room temperature. *Corrosion Science*, **22**, 147-158.

Kasting, J.F. 1990. Bolide impacts and the oxidation state of carbon in the Earth's early atmosphere. *Origins of Life and Evolution of the Biosphere*, **20**, 199-231.

Kasting, J.F. 1993. Earth's earliest atmosphere. *Science*, **259**, 920-926.

Kasting, J.F., Eggler, D.H. & Raeburn, S.P. 1993. Mantle redox evolution and the oxidation state of the Archaean atmosphere. *The Journal of Geology*, **101**, 245-257.

Kasting, J.F. & Brown, L.L. 1998. The early atmosphere as a source of biogenic compounds. In *The Molecular Origins of Life*, Brack, A., editor, Cambridge University Press, 35-56.

Keefe, A.D., Miller, S.L., McDonald, G. and Bada, J. 1995. Investigation of the prebiotic synthesis of amino acids and RNA bases from CO_2 using FeS/H_2S as a reducing agent. *Proceedings of the National Academy of Science USA*, **92**, 11,904-11,906.

Kelley, D.S. 1996. Methane-rich fluids in the oceanic crust. *Journal of Geophysical Research*, **101**, 2,943-2,962.

Kelley, D.S. & Früh-Green, G.L. 1999. Abiogenic methane in deep-seated mid-ocean ridge environments: Insights from stable isotopes analyses. *Journal of Geophysical Research*, **104**, 10,439-10,460.

Kelley, D. S. & Früh-Green, G. L. 2001. Magmatic and hydrothermal abiogenic methane ($\pm H_2 \pm$hydrocarbon) production in the oceanic crust. *Eleventh Annual V. M. Goldschmidt Conference.*

Kelley, D. S., Karson, J. A., Blackman, D. K., Früh-Green, G. L., Butterfield, D. A., Lilley, M. D., Olson, E. J., Schrenk, M. O., Roe, K. K., Lebon, G. T., Rivizzigno, P. & the AT3-60 Shipboard Party. 2001. An off-axis hydrothermal vent field near the Mid-Atlantic Ridge at 30 °N. *Nature*, **412**, 145-149

Kempe, S. & Degens, E. T. 1985. An early soda ocean? *Chemical Geology*, **53**, 95-108.

Kempe, S. & Kaźmierczak, J. 1994. The role of alkalinity in the evolution of ocean chemistry, organization of living systems, and biocalcification processes. *Bulletin de l'Institut océanographique*, **13**, 61-117.

Kling, G.W., Tuttle, M.L. & Evans, W.C. 1989. The evolution of thermal structure and water chemistry in Lake Nyos. *Journal of Volcanology and Geothermal Research,* **39**, 151-165.

Klinkhammer, G., Rona, P., Greaves,M.J. & Elderfield, H. 1985. Hydrothermal manganese plumes over the Mid-Atlantic Ridge rift valley. *Nature*, **314**, 727-731.

Knobel, R., Breuer, H. & Freund, F. 1984. Abiotic synthesis of organic molecules from minerals containig traces of dissolved H_2O, CO_2, N_2. Part II: Experimental Data. *Origins of Life*, **14**, 197-204.

Kohara, M. G., Yanagawa, T. & Kobayashi, H. 1997. Stability of amino acids in simulated hydrothermal vent environments. *Chemistry Letters*, **10**, 1053-1054.

Kral T. A., Brink, K. M., Miller, S. L. & McKay, C. P. 1998. Hydrogen consumption by methanogens on the early Earth. *Origins of Life and Evolution of the Biosphere,* **28**, 311-319.

Krasnov, S.G., Cherkashev, G.A., Stepanova, T.V., Batuyev, B.N., Krotov, A.G., Malin, B.V., Maslov, M.N., Markov, V.F., Poroshina, I.M., Samovarov, M.S., Ashadze, A.M., Lazareva, L.I. & Ermolayev, I.K. 1995. Detailed geological studies of hydrothermal fields in the North Atlantic. *In*: Parson, L.M., Walker, C.L. & Dixon, D.R (eds). *Hydrothermmal Vents and Processes.* Geological Society Special Publication No. 87, 43-64.

Krauskopf, K.B. 1967. *Introduction to Geochemistry.* McGraw-Hill LCCCN 67-13903

Krishnamurthy, R.V., Yuen, G.U., Epstein, S, Cronin, J.R. 1992. Isotopic and molecular analyses of hydrocarbons and monocarboxylic acids of the Murchison Meteorite. *Geochimica et Cosmochimica Acta*, **56**, 4045-4058.

Krishnamurthy, R. Arrhenius, G & Echenmoser, A. 1999. Formation of glycolaldehyde phosphate from glyceraldehyde in aqueous solution. *Origins of Life and Evolution of the Biosphere*, **29**, 333-354.

Krishnarao, J.S.R. 1964. Native nickel-iron alloy, its mode of occurrence, distribution and origin. *Economic Geology*, **59**, 443-448.

Krumholz, L.R. 1998. Microbial ecosystems in the Earth's subsurface. *American Society for Microbiology (ASM News)*, **64**, No. 4.

Krupp, R.E. 1994. Phase relations and phase transformations between the low-temperature iron sulfides mackinawite, greigite, and smythite. *European Journal of Mineralogy*, **6**, 265-278.

Lafon, G.M. & Mackenzie, F.T. 1974. Early evolution of the oceans: a weathering model, In: Hay, W.W. (ed) Studies in Paleo-oceanography, Special Publication, Society of Economic Paleontolgists and Mineralogists 20, Tulsa, 205-218.

Larter, R.C.L., Boyce, A.J. & Russell, M.J. 1981. Hydrothermal pyrite chimneys from the Ballynoe baryte deposit, Silvermines, County Tipperary, Ireland. *Mineralium Deposita*, **16**, 309-318.

Lavrentiev, G.A., Strigunkova, T.F. & Egorov, I.A. 1984. Abiological synthesis of amino acids, purines and pyrimidines under conditions simulating the volcanic ash-gas cloud. *Origins of Life*, **14**, 205-212.

Le Pichon, X. 1968. Sea-floor spreading and continental drift. *Journal of Geophysical Research*, **73**, 3661-3679.

Lennie, A.R., Redfern, S.A.T., Schofield, P.F. & Vaughan, D.J. 1995. Synthesis and Rietveld crystal structure refinement of mackinawite, tetragonal FeS. *Mineralogical Magazine*, **59**, 677-683.

Lerner, N.R., Peterson, E. & Chang, S. 1993. The strecker synthesis as a source of amino acids in carbonaceous chondrites: deuterium retention during synthesis. *Geochimica et Cosmochimica Acta*, **57**, 4713-4723.

Liu, S.V., Zhou, J., Zhang, C., Cole, D.R., Josifovska, M.G. & Phelps, T.J. 1997. Thermophilic Fe(III)-reducing bacteria from the deep subsurface: the evolutionary implications. *Science*, **277**, 1106-1109.

Lovelock, E.J. 1989. Geophysiology. *Transactions of the Royal Society of Edinburgh: Earth Sciences*, **80**, 169-175.

Lovely, D.R. & Goodwin, S. 1988. Hydrogen concentrations as an indicator of the predominant terminal electron-accepting reactions in aquatic sediments. *Geochimica et Cosmochimica Acta*, **52**, 2993-3003.

Lowe, C.U., Rees, M.W. & Markham, R. 1963. Synthesis of complex organic compounds from simple precursors: Formation of amino acids, amino acid polymers, fatty acids and purines from ammonium cyanide. *Nature*, **199**, 219-222.

Lowenstern, J.B. 2001. Carbon dioxide in magmas and implications for hydrothermal systems. *Mineralium Deposita*, **36**, 490-502.

MacLeod, G., Mckeown, C., Hall, A.J. & Russell, M.J. 1994. Hydrothermal and oceanic pH conditions of possible relevance to the Origin of Life. *Origin of Life and Evolution of the Biosphere*, **24**, 19-41.

Madigan, M.T., Martinko, J.M. & Parker, J. 1997. Brock: Biology of Microorganisms, 8th *Edn.* Prentice Hall, ISBN (0-13-571225-4).

Markhinin, E.K. & Podkletnov, N.E. 1977. The phenomenon of formation of prebiological compounds in volcanic processes. *Origins of Life*, **8**, 225-235.

Marshall, W.L. 1994. Hydrothermal synthesis of amino acids. *Geochimica et Cosmochimica Acta*, **58**, 2099-2106.

Martin, W., Müller, M. 1998. The hydrogen hypothesis for the first eukaryote. *Nature*, **392**, 37-41.

McCollom, T.M. & Shock, E.L. 1997. Geochemical constraints on chemolithoautotrophic metabolism by micro-organisms in seafloor hydrothermal systems. *Geochimica et Cosmochimica Acta*, **61**, 4375-4391.

McDonald, I. 1993, PhD Thesis. The analysis of the platinum-group elements by neutron activation analysis and their behaviour in fire-assay and natural igneous melts in the presence of a carbonaceous volatile phase. *A thesis presented for the degree of Doctor of Philosophy.* Department of Geological Sciences, University of Cape Town.

McDowall, M.A. 1977. Theory of surface metabolism. Commentary by Max A. McDowell. *Personal Communication*, maxamcd@melbpc.org.au

McKay, C.P., Pollack, J.B. & Courtin, R. 1991. The greenhouse and antigreenhouse effects on Titan. *Science*, **253**, 1,118-1,121.

McKay, C.P. & Borucki, W. J. 1997. Organic synthesis in experimental impact shocks. *Science*, **276**, 390.

McKenzie, D.P. & Parker, R.L. 1967. The North Pacific: An example of tectonics on a sphere. *Nature*, **216**, 1276-1280.

Melchior, D.C. & Bassett, R.L. (eds). 1990. Chemical modelling of aqueous systems II. *American Chemical Society*, Washington DC. ACS SYMPOSIUM SERIES 416.

Mellersh, A. R. 1993. A model for the prebiotic synthesis of peptides which throws light on the origin of the genetic code and the observed chirality of life, *Origin of Life and Evolution of the Biosphere* **23**, 261-274.

Mellersh, A.R. & Wilkinson, A-S. 2000. RNA bound to a solid phase can select an amino acid and facilitate subsequent amide bond formation. *Origins of Life and Evolution of the Biosphere*, **30**, 3-7.

Mellersh, A.R. 1993. A model for the prebiotic synthesis of peptides which throws light on the origin of the genetic code and the observed chirality of life. *Origins of Life and Evolution of the Biosphere*, **23**, 261-274.

Mellersh, A.R. 1994. The origin of Life: Which came first, proteins or RNA? *Natural History*, **6/94**, 10-13.

Melosh, H.J. 1989. Impact cratering: A Geologic Process. Oxford University Press.

Merlivat, L., Pineau, F. & Javoy, M. 1987. Hydrothermal vent waters at 13°N on the East Pacific Rise: isotopic composition and gas concentration. *Earth and Planetary Science Letters*, 84, 100-108.

Meyer, C. 1988. Ore deposits as guides to geologic history of the Earth. *Annual Reviews in Earth and Planetary Sciences*, **16**, 147-171.

Michaelis, W. & Albrecht, P. 1979. Molecular fossils of Archaebacteria in kerogen. *Naturwissenschaften*, **66** (8) , 420-422.

Miller, S.L. 1953. A production of amino acids under possible primitive Earth conditions. *Science*, **117**, 529-529.

Miller, S.L. 1957. The mechanism of synthesis of amino acids by electric discharges. *Biochimica et Biophysica Acta*, **23**, 480-489.

Miller, S.L. & Bada, J.L. 1998. Submarine springs and the origin of Life, *Nature*, **334**, 609-611.

Minard, R.D., Hatcher, P.G., Gourley, R.C. & Matthews, C.N. 1998. Structural investigations of hydrogen cyanide polymers: New insights using TMAH Thermochemolysis/GC-MS. *Origins of Life and Evolution of the Atmosphere*, **28**, 461-473.

Moody, J.B. 1976. Serpentinisation: a review. *Lithos*, **1**, 125-138.

Moorbath, S., O'Nions, R.K. & Pankhurst. R.J. 1973. Early Archean age for the Isua iron formation, West Greenland. *Nature*, **245**, p138.

Morgan, W.J. 1968. Rises, Trenches, Great Faults, and Crustal Blocks. *Journal of Geophysical Research*, **73**, 1959-1982.

Morowitz, H.J., Kostelnik, J.D., Yang, J. & Cody, G.D. 2000. The origin of intermediary metabolism. *Proceedings of the National Academy of Science USA*, **97**, 7704-7708.

Mottl, M.J. & Holland, H.D. 1978. Chemical exchange during hydrothermal alteration of basalt by seawater – I. Experimental results for major and minor components of seawater. *Geochimica et Cosmochimica Acta*, **42**, 1103-1115.

Mottl, M.J. 1983. Metabasalts, axial hot springs, and the structure of hydrothermal systems at mid-ocean ridges. *Geological Society of America Bulletin*, **94**, 161-180.

Mottl, M.J. 1983. Metabasalts, axial hot springs and the structure of of hydrothermal systems at mid-ocean ridges. *Geological Society of America Bulletin*, **94**, 161-180.

Mottl, M.J. & Wheat, C.G. 1994. Hydrothermal circulation through mid-ocean ridge flanks: Fluxes of heat and magnesium. *Geochimica et Cosmochimica Acta*, 58, 2225-2237.

Mottl, M.J., Wheat, G. *et al.*, 1998. Warm springs discovered on 3.5 Ma oceanic crust, eastern flank of the Juan de Fuca Ridge. *Geology*, **26**, 51-54.

Mukhin, L.M. 1976. Volcanic processes and the synthesis of simple organic compounds on primitive Earth. *Origins of Life and Evolution of the Biosphere*, **7**, 355-368

Muller, A.W.J. 1995. Were the first organisms heat engines? A new model for biogenesis and the early evolution of biological energy conversion. *Progress in Biophysics and Molecular Biology*, **63**, 193-231.

Murton, B.J., Klinkhammer, G., Becker, K., Briais, A., Edge, D., Hayward, N., Millard, N., Mitchell, I., Rouse, I., Rudnicki, M., Sayanagi, K., Sloan, H. & Parson, L.M. 1994. Direct evidence for the distribution and occurrence of hydrothermal activity between 27-30°N on the Mid-Atlantic Ridge. *Earth and Planetary Science Letters*, **125**, 119-128.

Neal, C. & Stanger, G. 1983. Hydrogen generation from mantle source rocks in Oman. *Earth and Planetary Science Letters*, **66**, 315-320.

Neal, C. & Stanger, G. 1984. Calcium and magnesium hydroxide precipitation from alkaline groundwater in Oman, and their significance to the process of serpentinization. *Mineralogical Magazine*, **48**, 237-241.

Nehlig, P. & Juteau, T. 1988. Flow porosities, permeabilities and preliminary data on fluid inclusions and fossil thermal gradients in the crustal sequences of the Sumail ophilite (Oman). *Tectonophysics*, **151**, 199-221.

Nisbet, E.G. 1987. Uniquely fresh 2.7 Ga komatiites from the Belingwe Greenstone Belt, Zimbabwe. *Journal of Geology*, **15**, 1147-1150.

Oberholzer, T., Albizio, M. & Luisi, P.L. 1995. Polymerase chain reaction in liposomes. *Chemistry and Biology*, **2**, 677-682.

Oparin, A.I. 1938. *The Origin of Life*. New York, Dover.

Oró, J. 1960. Synthesis of adenine from ammonium cyanide. *Biochem. Biophys. Res. Commun.*, **2**, 407-412

Oró, J., Miller, S.L. & Lazcano, A. 1990. The origin and early evolution of Life on Earth. *Annual Review of Earth and Planetary Sciences*, **18**, 317-356.

Pedersen, K. 1997. Microbial Life in deep granitic rock. *Microbiology Reviews*, **20**, 399-414.

Pinto, J.P., Gladstone, G.R. & Yung, Y.K. 1980. Photochemical production of formaldehyde in Earth's primitive atmosphere. *Science* , **210**, 183-185.

Plummer, L.N. 1992. Geochemical modeling of water rock interaction : past, present,future, In: *Water Rock Interaction*, Vol. I, Geological Survey, Kharaka and Maest (eds), 1992, Balkema, Rotterdam.

Pourbaix, M.J.N. 1949. *Thermodynamics of Dilute Aqueous Solutions*. London, Arnold.

Pourbaix, M.J.N., Van Muylder, J. & de Zhoubov, N. 1963. *Atlas d'Eqhilbres Electrochimiques à 25°C.* Paris, Gauthier-Villars.

Pringle, J.W.S. 1953. The origin of Life. *Symposia of the Society for Experimental Biology, Number VII, Evolution.* Cambridge University Press, 1-21.

Raff A.D. & Mason, R.G. 1961. Magnetic survey off the west coast of North America, 40°N latitude to 52°N latitude. *Geological Society of America Bulletin*, **72**, 1,267-1,270.

Rasmussen, B. 2000. Filamentous microfossils in a 3,235 million-year-old volcanogenic massive sulphide deposit. *Nature*, **405**, 676-679.

Reysenbach, A.-L., Wickham, G.S. & Pace, N.R. 1994. Phylogenetic analysis of the hyperthermophilic "pink filament" community in Octopus Spring, Yellowstone National Park. *Appl. Environ. Microbiol.*, **60**, 2113-2119.

Rickard, D. 1995. Kinetics of FeS precipitation: Part 1. Competing reaction mechanisms. *Geochimica Cosmochimica Acta*, **59**, 4367-4379.

Rickard, D., Butler, I.B. & Oldroyd, A. 2001. A novel iron sulphide mineral switch and its implications for Earth and planetary science. *Earth and Planetary Science Letters*, **189**, 85-91.

Righter, K. & Drake, M.J. 1997. Metal-silicate equilibrium in a homogeneously accreting earth: new results for Re. *Earth and Planetary Science Letters*, **146**, 541-553.

Righter, K. Drake, M.J. & Yaxley, G. 1997. Prediction of siderophile element metal-silicate partition coefficients to 20 GPa and 2,800°C: the effects of pressure, temperature, oxygen fugacity, and silicate and metallic melt compositions. *Physics of the Earth and Planetary Interiors* **100**, 115-134.

Robie, R. A., Hemingway, B. S. & Fischer, J.R. 1978. Thermodynamic properties of minerals and related substances at 298.15 K and 1 bar pressure and at higher presssures: *U.S.G.S. Bulletin*, **1452**, 456.

Röckmann, T., Brenninkmeijer, C. A.M., Saueressig, G., Bergamaschi, P., Crowley, J.N., Fischer, H. & Crutzen, P.J. 1998. Mass- independent oxygen isotope fractionation in atmospheric CO as a result of the reaction CO + OH. *Atmospheric Chemistry Division*, **281**, 544-545.

Rona, P.A., Widenfalk, L and Boström. 1987. Serpentinized ultramafics and hydrothermal activity at the Mid-Atlantic Ridge crest near 15°N. *Journal of Geophysical Research* **92B**, 1417-1427.

Russell, M.J., Hall, A.J. & Turner, D. 1989. In vitro growth of iron sulphide chimneys: Possible culture chambers for origin-of-life experiments. *Terra Nova*, **1**, 238-241.

Russell, M.J., Daniel, R.M., Hall, A.J. & Sherringham, J. 1994. A hydrothermally precipitated catalytic iron sulphide membrane as a first step toward life. *Journal of Molecular Evolution*, **39**, 231-243.

Russell, M.J. & Hall, A.J. 1997. The emergence of Life from iron monosulphide bubbles at a submarine hydrothermal redox and pH front. *Journal of the Geological Society*, **154**, 377-402.

Russell, M.J. Daia D.E. & Hall, A.J. 1998. The emergence of life from FeS bubbles at alkaline hot springs in an acid ocean. in *Thermophiles: The keys to molecular evolution and the origin of life*, eds Wiegel J. & Adams, M.W.W. Taylor and Francis, Washington, 77-125.

Russell, M., Ingham, J.K., Zedef, V., Maktav, D., Sunar, F., Hall, A.J. & Fallick, A.E. 1999. Search for signs of ancient Life on Mars: expectations from hydromagnesite microbialities, Salda Lake, Turkey. *Journal of the Geological Society*, **156**, 869-888.

Russell, M.J., Hall, A.J., Rahman, L. & Turner, D. 2001. Abiotic organic syntheses in deep submarine, alkaline hydrothermal systems catalysed by Fe^0, mackinawite, violarite and green rust. In *Eleventh Annual V.M. Goldschmidt Conference,* Abstract #3090. LPI Contribution No. 1088, Lunar and Planetary Institute, Houston (CD_ROM).

Russell, M.J., Hall, A.J., & Rahman, L. 2003. Hydrothermal and ocean chemistries: Initial conditions for the onset of life. *Natural and Laboratory Simulated Thermal Geochemical Processes* ed. R. Ikan, Kluwer Academic Publishers, Dordrecht.

Sagan, C and Khare, B.N. 1971. Long-wavelength ultraviolet photoproduction of amino acids on the primitive Earth. *Science*, **173**, 417-420.

Sakai, H., Gamo, T., Kim, E-S., Tsutsumi, M., Tanaka, T., Ishibashi, J., Wakita, H., Yamano, T. & Oomori, T. 1990. Venting of carbon dioxide-rich fluid and hydrate formation in Mid-Okinawa Trough Backarc Basin. *Science*, **248**, 1,093-1,096.

Saxena, S.K. 1989. Oxidation state of the mantle. *Geochimica et Cosmochimica Acta*, **53**, 89-95.

Schoonen, M.A.A., Xu, Y. & Bebie, J. 1999. Energetics and kinetics of the prebiotic synthesis of simple organic and amino acids with the $FeS\text{-}H_2/FeS_2$ redox couple as reductant. *Origins of Life and Evolution of the Biosphere*, **29**, 5-32.

Schopf, J.W. 1983. *Earth's Earliest Biosphere: Its Origin and Evolution.* Princeton University Press, New Jersey.

Schulte, M.D. & Shock, E.L. 1995. Thermodynamics of Strecker synthesis in hydrothermal systems. *Origins of Life and Evolution of the Biosphere*, **25**, 161-173.

Schwartzman, D.W., Shore, S.N., Volk, T. & McMenamin, M. 1994. Self-organization of the Earth's biosphere - geochemical or geophysiological? *Origins of Life & Evolution of the Biosphere*, **24**, 435-450.

Seewald, J.S. 2001. Aqueous geochemistry of low molecular weight hydrocarbons at elevated temperatures and pressures: Constraints from mineral buffered laboratory experiments. *Geochimica et Cosmochimica Acta,* **65**, No. 10, 1641-1664.

Seyfried W.E., Bischoff, J.L. 1979. Low temperature basalt alteration by seawater: An experimental study at 70°C and 150°C. *Geochimica et Cosmochimica Acta*, **43**, 1937-1947.

Seyfried, W.E. & Dibble, W.E. 1980. Seawater- peridotite interaction at 300°C and 500°C bars: Implications for the origin of oceanic serpentinites. *Geochimica et Cosmochimica Acta*, **44**, 309-321.

Seyfried, W.E. & Bischoff, J.L. 1981. Experimental seawater-basalt interaction at 300°C, 500 bars. Chemical exchange, secondary mineral formation and implications for the transport of heavy metals. *Geochimica et Cosmochimica Acta*, **45**, 135-147.

Seyfried, W.E. & Janecky, D.R. 1985. Heavy metal and sulfur transport during subcritical hydrothermal alteration of basalt composition and crystallinity. *Geochimica et Cosmochimica Acta*, **49**, 2,545-2,560.

Seyfried, W.E., Ding, K. & Berndt, M.E. 1991. Phase equilibria constraints on the chemistry of hot spring fluids at mid-ocean ridges. *Geochimica et Cosmochimica Acta*, **55**, 3,559-3,580.

Seyfried, W.E. & Ding, K. 1992. Determination of Fe-Cl complex in the low pressure supercritical region (NaCl Fluid): Iron solubility constraints on pH of subseafloor hydrothermal fluids. *Geochimica et Cosmochimica Acta*, **56**, 3681-3692.

Shanks, W.C., Böhlke, J.K. & Seall, R.R. 1995. Stable isotopes in mid-ocean ridge hydrothermal systems: Interactions between fluids, minerals and organisms. In: *Seafloor Hydrothermal Systems: Physical, Chemical Biological and Geological Interactions.* Humphris *et al.*, (eds), Geophys. Monograph,Series., Vol. 91 pp. 194-221, AGU, Washington, D.C.

Shapiro, R. 1995. The prebiotic role of adenine: A critical analysis. *Origins of Life and Evolution of the Biosphere*, **25**, 83-98.

Shock, E.L. 1990. Do amino acids equilibrate in hydrothermal fluids? *Geochimica et Cosmochimica Acta*, **54**, 1,185-1,189.

Shock, E.L. & Helgeson, H.C. 1990. Calculation of the thermodynamic and transport properties of aqueous species at high pressures and temperatures: Standard partial

molal properties of organic species. *Geochimica et Cosmochimica Acta*, **52**, 2009-2036.

Shock, E.L. 1992a. Chemical environments of submarine hydrothermal systems. In: Marine hydrothermal systems and the origin of Life (ed. Holm, N.G.). *Origins of Life and Evolution of the Biosphere*, **22**, 67-107.

Shock, E.L. 1992b. Hydrothermal organic synthesis experiments. In: Marine hydrothermal systems and the origin of Life (ed. Holm, N.G.). *Origins of Life and Evolution of the Biosphere*, **22**, 135-146.

Shock, E.L., McCollom, T. & Schulte, M. D. 1993. Geochemical constraints on chemolithoautotrophic reactions in hydrothermal systems. *Origins of Life and Evolution of the Biosphere*, **25**, 141-159.

Shock, E.L. 1995. Organic acids in hydrothermal solutions: Standard molal thermodynamic properties of carboxylic acids and estimates of dissociation constants at high temperatures and pressures. *American Journal of Science*, **295**, 496-580.

Shock, E.L. 1996. Hydrothermal systems as environments for the emergence of life. *Evolution of Hydrothermal Ecosystems on Earth (and Mars?)*, CIBA Foundation Symposium No. 202, 40-52.

Shock, E.L. 1997. High-temperature life without photosynthesis as a model for Mars. *Journal of Geophysical Research*, **102**, 23,687-23,694.

Shock, E.L. & Schulte, M. D. 1998. Organic synthesis during fluid mixing in hydrothermal systems. *Journal of Geophysical Research*, **103**, 28,513-28,527.

Shock, E.L., McCollom, T. & Schulte, M.D. 1998. The emergence of metabolism from within hydrothermal systems. *Thermophiles: the keys to molecular evolution and the origin of life?* (eds) Wiegel J. & Adams, M.W.W. Taylor and Francis, Washington 59-76.

Sigurdsson, H., Devine, J.D., Tchoua, F.M., Presser, T.S., Pringle, M.K.W. & Evans, W.C. 1987. Origin of the lethal gas burst from Lake Monoun, Cameroun. *Journal of Volcanology and Geothermal Research*, **31**, 1-16.

Silver, J. 1993. Chemistry of Iron. Chapman & Hall. ISBN 0-7514-0062-9.

Simakov, S.K. 1998. Redox state of Earth's upper mantle peridotites under the ancient cratons and its connection with diamond genesis. *Geochimica et Cosmochimica Acta*, **62**, 1811-1820.

Simoneit. B.R. 1992. Aqueous organic geochemistry at high temeprature/high pressure. In: Marine hydrothermal systems and the origin of Life (ed. Holm, N.G.). *Origins of Life and Evolution of the Biosphere*, **22**, 43-65.

Sleep, N.H. & Zahnle, K. 2001. Carbon dioxide cycling and implications for climate on ancient Earth. *Journal of Geophysical Research*, **106**, 1,373-1,399.

Sleep, N.H., Zahnle, K.J., Kasting, J.F. & Morowitz, H.J. 1989. Annihilation of ecosystems by large asteroid impacts. *Nature*, **342**, 139-142.

Solomon, M. & Walshe, J.L. 1979. The formation of massive sulfide deposits on the sea floor. *Economic Geology*, **74**, 797-813.

Solomons, T.W.G. 1980. *Organic Chemistry, 2nd Edition.* John Wiley & Sons, Inc. p785.

Sörenson, S.P.L. 1909. Enzyme Studies II. The measurement and meaning of hydrogen ion concentration in enzymatic processes. *Biochemische Zeitschrift*, **21**, 131-200.

Stahl, D.A., D.J. Lane, G.J. Olsen, and N.R. Pace. 1985. Characterization of a Yellowstone hot spring microbial community by 5S ribosomal RNA sequences. *Applied Environmental Microbiology*. **49**, 1,379-1,384.

Steele, A., Toporski, J.K.W., Stapleton, D. & McKay, D.S. 2001. The imaging of terrestrial microbial contamination of meteorites. *Microscopy and Analysis*, May, 5-7.

Stetter, K.O., Lauerer, G., Thomm, M. & Neuner, A. 1987. Isolation of extremely thermophilic sulfate reducers - evidence for a novel branch of archaebacteria. *Science*, **236**, 822-824.

Stetter, K.O. 1996. Hyperthermophilic procaryotes. *FEMS Microbiology Reviews*, **18**, 149-158.

Stevens, T.O., McKinley, J. P. 1995. Lithoautotrophic microbial ecosystems in deep basalt aquifers. *Science*, **270**, 450-454.

Stevenson, D. J. 1999. Life-sustaining planets in interstellar space? *Nature*, **400**, 32.

Swart, P.K., Wortmann, U.G., Mitterer, R.M., Malone, M.J., Smart, P.L., Feary, D.A., & Hine, A.C. 2000. Hydrogen sulfide-rich hydrates and saline fluids in the continental margin of South Australia. *Geology*, **28**, 1,039-1,042.

Taylor, P., Rummery, T.E. & Owen, D.G. 1979. Reactions of iron monosulfide solids with aqueous hydrogen sulfide up to 160 °C. *Journal of inorganic nuclear Chemistry*, **41**, 1683-1687.

Thauer, R.K., Jungermann, K. & Decker, K. 1977. Energy conservation in chemotrophic anaerobic bacteria. *Bacteriologic Reviews*, **41**, 100-180.

Tingle, T.N., Mathez, E.A. & Hochella (Jnr), M.F. 1991. Carbonaceous matter in peridotites and basalts studied by XPS, SALI, and LEED. *Geochimica et Cosmochimica Acta*, **55**, 1,345-1,352.

Treiman, A. & Wallendahl, A. 1998. Hydrogen chemistry of basalt aquifers. *Science: Letters*, **282**, 2196.

Turcotte D.L. 1980. On the thermal evolution of the Earth. *Earth and Planetary Science Letters*, **48**, 53-58.

Urey, H.C. 1952. The planets: Their origin and development, Yale University Press, Newhaven, Conn.

Urey, H.C. 1952. On the Early Chemical History of the Earth and the Origin of Life. *Proceedings of the National Academy of Science*, **38**, 351-363.

van der Sluijs, J. P., Jan de Bruyn, G. & Westbroek, P. 1996. Biogenic feedbacks in the carbonate-silicate geochemical cycle and the global climate. *American Journal of Science*, **296**, 932-953.

Vargas, M., Kashefi, K., Blunt-Harris, E.L. & Lovley, D.R. 1998. Microbiological evidence for Fe(III) reduction on early Earth. *Nature*, **395**, 65-67.

Vaughan, D.J. & Lennie, A.R. 1991. The iron sulphide minerals: their chemistry and role in nature. *Sci. Progress*, **75**, 371-388.

Vine, F. & Matthews, D.H. 1963. Magnetic Anomalies over Oceanic Ridges. *Nature*, **199**, 947-949.

Von Damm, K.L. 1990. Sea floor hydrothermal activity: Black smoker chemistry and chimneys. *Annual Review of Earth and Planetary Sciences*, **18**, 173-204.

Von Damm, K.L. 1995. Controls on the chemistry and temporal variability of seafloor hydrothermal fluids. In: *Seafloor Hydrothermal Systems: Physical, Chemical Biological and Geological Interactions.* Humphris *et al.*, (eds), *Geophys. Monograph,Series.*, **Vol. 91**, pp. 222-247, AGU, Washington, D.C.

Von Damm, K.L. 2000. Chemistry of hydrothermal vent fluids from 9°-10°N, East Pacific Rise: "Time zero", the immediate posteruptive period. *Journal of Geophysical Research*, **105B**, 11,203-11,222.

Wächtershäuser, G. 1988a. Pyrite formation, the first energy source for life: A hypothesis. *Systematic Applied Microbiology*, **10**, 207-210.

Wächtershäuser, G. 1988b. Before enzymes and templates: theory of surface metabolism. *Microbiological Reviews*, **52**, 452-484.

Wächtershäuser, G. 1990. Evolution of the first metabolic cycles. *Proceedings of the National Academy of Sciences USA*, **87**, 200-204.

Wächtershäuser, G. 1992. Groundworks for an evolutionary biochemistry: The iron-suphur world. *Progress in Biophysics and Molececular Biology*, **58**, 85-201.

Wächtershäuser, G. 1997. The origin of life and its methodological challenge. *Journal of Theoretical Biology*, **187**, 483-94

Wächtershäuser, G. 1998. Towards a reconstruction of ancestral genomes by gene cluster alignment. *Systematic Applied Microbiology*, **21**, 473-477.

Wächtershäuser, G. 2000. Life as we don't know it. *Science* **289**, 1307-1308.

Walker, J.C.G. 1985. Carbon dioxide on the early Earth. *Origins of Life and Evolution of the Biosphere*, **16**, 117-127.

Walker, J.C.G. & Brimblecombe, P. 1985. Iron and sulfur in the pre-biological ocean. *Precambrian Research*, **28**, 205-222.

Walter, M.R. 1983. Archaean stromatolites: Evidence for the Earth's earliest benthos. In: Schopf, J.W. (ed) Earth's earliest biosphere: its origin and evolution. Princeton University Press, NJ, 187-213.

Washington, J. 2000. The possible role of volcanic aquifers in prebiologic genesis of organic compounds and RNA. *Origins of Life and Evolution of the Biosphere*, **30**, 53-79.

Weber, A.L. 1987. The triose model: glyceraldehyde as a source of energy and monomers for prebiotic condensation reactions. *Origins of Life*, **17**, 107-119.

Weber, A.L. 1997. Energy from redox disproportionation of sugar carbon drives biotic and abiotic synthesis. *Journal of Molecular Evolution*, **44**, 354-360.

Weber, A.L. 2000. Sugars as the optimal biosynthetic carbon substrate of aqueous Life throughout the Universe. *Origins of Life and Evolution of the Biosphere*, **30**, 33-43.

Westheimer, F.H. 1987. Why nature chose phosphates. *Science*, **235**, 1173.

Woese, C.R., Kandler, O. & Wheelis, M.L. 1990. Towards a natural system of organisms: Proposals for the domains Archaea, Bacteria, and Eucarya. *Proceedings of the National Academy of Science USA*, **87**, 4576-4579.

Wöhler, F. 1828. La formation artificielle de l'urée. *Annal. Chim. Phys.*, **37**, 330-334.

Wolery, T.J. 1979. Calculation of chemical equilibrium between aqueous solutions and minerals: The EQ3/6 software package. UCRL-52658, Lawrence Livermore National Laboratory, Livermore, CA.

Wolery, T.J. 1983. EQ3NR, a computer program for geochemical aqueous speciation-solubility calculations: User's Guide and Documentation, Lawrence Livermore National Laboratory Report UCRL–53414, Livermore, CA.

Wolery, T.J. & Sleep, N.H. 1976. Hydrothermal circulation and geochemical flux at mid-ocean ridges. *Journal of Geology*, **84**, 249-275.

Wolery, T.J. 1992. EQ3NR A computer program for geochemical aqueous speciation-solubility calculations: Theoretical Manual, User's Guide, and Related Documentation (Version 7.0), UCRL–MA-110662, PT III. Lawrence Livermore National Laboratory, Livermore, CA.

Wolery, T.J. & Daveler, S.A. 1992. EQ6 A computer program for reaction path modeling of aqueous geochemical systems: Theoretical Manual, User's Guide, and Related Documentation, UCRL–MA-110662, PT IV. Lawrence Livermore National Laboratory, Livermore, CA.

Wood, H.G. 1991. Life with CO or CO_2 and H_2 as a source of carbon and energy. *The FASEB Journal*, **5**, 156-163.

Wrigglesworth, J. 1997. Energy and Life. Taylor and Francis Ltd. ISBN (0-7484-0433-3).

Yamagata, Y., Wanatabe, H., Saitoh, M. & Namba, T. 1991. Volcanic production of polyphosphates and its relevance to prebiotic evolution. *Nature*, **352**, 516-519.

Yanagawa, H. & Egami, F. 1981. Is carbon suboxide a new candidate as starting material for the synthesis of biomolecules on the primitive Earth? *Precamb. Res.*, **14**, 75-80.

Zachara, J. M., Fredrickson, J. K., Smith, S.C. & Gassman, P.L. 2001. Solubilization of Fe(III) oxide-bound trace metals by a dissimilatory Fe(III) reducing bacterium. *Geochimica et Cosmochimica Acta*, **65**, 75-93.

Zolotov, M.Y., Seewald, J.S. & McCollom, T.M. 2001. Experimental investigation of aqueous cabon monoxide reactivity under hydrothermal conditions. *Eleventh Annual V.M. Goldschmidt Conference.*

Web Directory (WWW)

Barker, *et al.*, 2001. *in prep.* Biomineralization of extracellular polymers by iron oxyhydroxides. *Astrobiologyweb*, First International Conference 2001, Abstracts, http://www.astrobiology.com/

Little, C. & Herrington, R. 1995. Silurian-age (430 million years ago) fossil assemblage from the Yaman Kasy VMS deposit in the Urals of Russia, http://www.nhm.ac.uk/mineralogy/intro/project5/

Moore, J.N. 2001 Geology 431 - Environmental Geochemistry, Past Lectures. http://www.cs.umt.edu/GEOLOGY/classes/Geol431/G431page.htm

Nelson, J. Stromatolites, Our mysterious ancient feefs, http://www.lakesuperior.com/online/192/192strom.html

Russell, M.J. Hall, A.J. Rahman, L & Turner, D.. The Geochemical Origins of Life, 2001 site. http://www.gla.ac.uk/projects/originoflife.

McDowall, M.A. 1998. *In*: Russell, M.J. Hall, A.J. Rahman, L & Turner, D. The Geochemical Origins of Life, 1998 site accessible from Russell *et al.*, WWW, 2001. http://www.gla.ac.uk/projects/originoflife.

Sumner, D. Y. Archaean stromatolites. http://www.gps.caltech.edu/~sumner/Dmicrob.html

Sumner, D. Y. Morphological Evidence for Archean Microbe Segregation into Distinct Communities. Accepted by the 30th IGC Meeting, Beijing. http://www.gps.caltech.edu/~sumner/DIGC.html

The Calvin Cycle, http://tidepool.st.usm.edu/crswr/darkmov.html

Appendices

Appendix 1A

Figures A and B. Change of neutral pH with temperature. Neutral pHs (Figure A) calculated from ionization constant data (-log K_w) in Krauskopf (*Figure 2.1*, 1967, p34) and plotted in Figure B.

Figure A

Neutral pH values at 0-300°C

Temperature (°C)	Neutral pH
0	7.5
25	7
50	6.6
100	6.1
125	5.9
150	5.8
225	5.7
300	5.9

Figure B
Temperature vs Neutral pH of H_2O

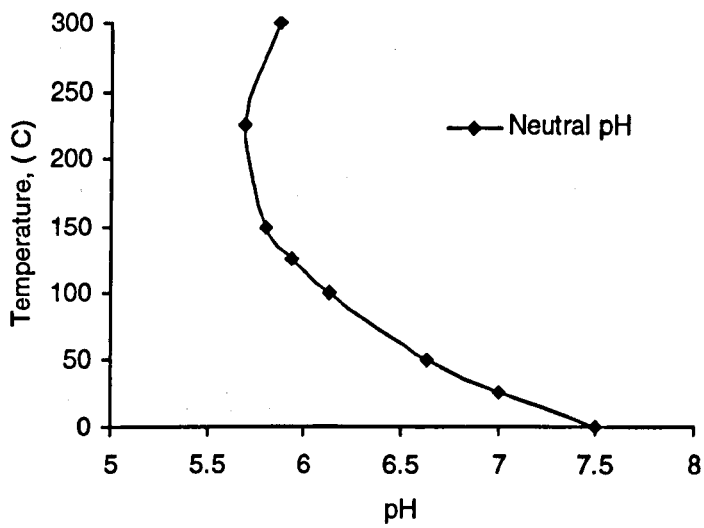

Table A . Pressures corresponding to Boiling Curve of H_2O

Temperatures (°C)	0.01	25	60	100	150	200	250	300
Pressures (bar)	1.0132	1.0132	1.0132	1.0132	4.7572	15.5365	39.7365	85.8378

Table showing pressures corresponding to the boiling curve of water at each temperature, as used in all models in this thesis. Data obtained from the *thermo.com.v8.r6.full* thermodynamic database (Johnson *et al.*, 1992).

Appendix 1B Figures

Table A1. Products resulting from 1 mmol Fayalite reacted with 1kg of seawater at various temperatures.

Table A1 Fayalite and Water

Temp	(°C)	10	50	90	150	200	250
Amount Reacted							
Fayalite	*(mmol)*	1	1	1	1	1	1
Water	*(kg)*	1	1	1	1	1	1
Reaction Products							
Minerals	Greenalite	0.5	0.5	0.48	0.35		
(mmol)	Magnetite	0.17	0.17	0.175	0.32	0.67	0.67
	Hematite	~0	~0				
log fH2(g)	Init (s/w)	-18	-15	-12.5	-7	-3	0
(bar)	Fin (fluid)	-1.0	0.0	-1.0	-0.5	0.0	0.0
log fO2(g)	Init (s/w)	-53	-46	-40	-40	-40	-40
(bar)	Fin (fluid)	-86	-74	-64	-52.5	-46	-40.5
Eh	Init (s/w)	0.1	0.07	0.05	-0.11	-0.25	-0.401
(volts)	Fin (fluid)	-0.5	-0.48	-0.45	-0.42	-0.41	-0.416
pH	Init (s/w)	7.25	6.62	6.2	5.8	5.61	5.54
	Fin (fluid)	9.25	8.4	7.16	6.3	5.81	5.59

Table A2. Products resulting from 1 mmol Forsterite reacted with 1kg of seawater at various temperatures.

Table A2 Forsterite and Water

Temp	(°C)	10	50	90	150	200	250
Amount Reacted							
Forsterite	*(mmol)*	1	1	1	1	1	1
Water	*(kg)*	1	1	1	1	1	1
Reaction Products							
Minerals	Brucite	0.5	0.5	0.51	0.53	0.55	0.57
(mmol)	Antigorite	0.06	0.06	0.06	0.06	0.06	0.06
log *f* H2(g)	Init (s/w)	-24	-17.5	-12.5	-7	-3	0
(bar)	Fin (fluid)	-24	-17.5	-12.5	-7	-3	0
log *f* O2(g)	Init (s/w)	-40	-40	-40	-40	-40	-40
(bar)	Fin (fluid)	-40	-40	-40	-40	-40	-40
Eh	Init (s/w)	0.265	0.16	0.05	-0.11	-0.25	-0.4
	Fin (fluid)	0.065	-0.025	-0.12	-0.26	-0.39	-0.52
pH	Init (s/w)	7.25	6.6	6.25	5.8	5.6	5.55
	Fin (fluid)	10.75	9.5	8.6	7.6	7.07	6.7

Table A3. Products resulting from 0.1 mmol Fayalite, 0.9 mmol Forsterite reacted with 1kg of seawater at various temperatures.

Table A3 Fayalite, Forsterite and Water

Temp	(°C)	10	50	90	150	200	250
Amount Reacted							
Total Rock	*(mmol)*	1	1	1	1	1	1
Forsterite	*(mmol)*	0.9	0.9	0.9	0.9	0.9	0.9
Fayalite	*(mmol)*	0.1	0.1	0.1	0.1	0.1	0.1
Water	*(kg)*	1	1	1	1	1	1
Reaction Products							
Minerals	Brucite	0.3	0.295	0.31	0.33	0.35	0.37
(mmol)	Magnetite	0.067	0.085	0.067	0.067	0.067	0.067
	Antigorite	0.059	0.059	0.059	0.059	0.059	0.058
log *f* H2(g)	Init (s/w)	-18	-15	-13	-7	-3	-0.22
(bar)	Fin (fluid)	-1.1	-1.0	-1.0	-1.1	-1.2	-0.2
log *f* O2(g)	Init (s/w)	-52	-46	-40	-40	-39	-40
(bar)	Fin (fluid)	-86	-73	-63	-51	-44	-40
Eh	Init (s/w)	0.1	0.07	0.05	-0.11	-0.25	-0.4
	Fin (fluid)	-0.58	-0.56	-0.53	-0.51	-0.48	-0.52
pH	Init (s/w)	7.25	6.65	6.25	5.8	5.6	5.55
	Fin (fluid)	10.8	9.5	8.6	7.6	7.1	6.7

Table A4. Products resulting from 1 mmol Fayalite reacted with 1kg of seawater at 0.0003 bar $CO_{2(g)}$ and various temperatures.

Table A4 Fayalite, CO2 (0.0003 bar) and Water

Temp	(°C)	10	50	90	150	200	250
Amount Reacted							
Fayalite	*(mmol)*	1	1	1	1	1	1
Water	*(kg)*	1	1	1	1	1	1
log *f* CO2(g)	*(bar)*	-3.5	-3.5	-3.5	-3.5	-3.5	-3.5
Reaction Products							
Minerals	Greenalite	0.5	0.5	0.485	0.34		
(mmol)	Magnetite	0.17	0.17	0.175	0.325	0.66	0.67
log *f* H2(g)	Init (s/w)	-23.5	-18	-12.6	-7	-3.2	-0.23
(bar)	Fin (fluid)	-1.00	-0.75	-0.67	-0.45	-0.25	-0.03
log *f* O2(g)	Init (s/w)	-41	-40	-40	-40	-40	-40
(bar)	Fin (fluid)	-86	-74	-64	-53	-46	-40.4
log *f* CO2(g)	Init (s/w)	-3.5	-3.5	-3.5	-3.5	-3.5	-3.5
(bar)	Fin (fluid)	-23	-18.8	-14.6	-10.7	-8.6	-4.32
log *f* CH4(g)	Init (s/w)	-73	-55	-39	-21	-9.6	-0.35
(bar)	Fin (fluid)	-2.5	-2.5	-2.5	-2.5	-2.8	-0.35
Eh	Init (s/w)	0.34	0.21	0.08	-0.19	-0.25	-0.401
	Fin (fluid)	-0.5	-0.43	-0.45	-0.42	-0.41	-0.416
pH	Init (s/w)	5.6	5.75	5.85	5.76	5.6	5.55
	Fin (fluid)	9.2	8.05	7.15	6.26	5.8	5.59

Table A5. Products resulting from 1 mmol Fayalite reacted with 1kg of seawater at 1 bar $O_{2(g)}$ and various temperatures. Fugacities are in units of bars.

Table A5 Fayalite, CO2 (1 bar) and Water

Temp	(°C)	10	50	90	150	200	250
Amount Reacted							
Fayalite	*(mmol)*	1	1	1	1	1	1
Water	*(kg)*	1	1	1	1	1	1
log *f* CO2(g)	*(bar)*	0	0	0	0	0	0
Reaction Products							
Minerals	Quartz	1	0.75	0.34			
(mmol)	Siderite		1.12	1.6			
	Magnetite				0.64	0.66	0.67
log *f* H2(g)	Init (s/w)	-24.2	-17.8	-12.6	-6.9	-3.2	-0.23
(bar)	Fin (fluid)	-10.00	-8.00	-5.40	-2.70	-1.90	-0.23
log *f* O2(g)	Init (s/w)	-40	-40	-40	-40	-40	-40
(bar)	Fin (fluid)	-69	-59	-54.5	-48.4	-42.5	-40
log *f* CO2(g)	Init (s/w)	0	0	0	0	0	0
(bar)	Fin (fluid)	0.032	-0.06	-0.09	-0.017	-0.011	-0.01
log *f* CH4(g)	Init (s/w)	-62	-51	-35	-17.5	-6.1	3.15
(bar)	Fin (fluid)	-14	-12.5	-6.5	-1	-1.1	3.15
Eh	Init (s/w)	0.45	0.325	0.2	0.01	-0.162	-0.337
	Fin (fluid)	-0.025	-0.06	-0.15	-0.225	-0.25	-0.352
pH	Init (s/w)	3.88	4	4.15	4.41	4.7	4.93
	Fin (fluid)	5.3	5.25	5.25	5.11	4.98	5.07

Table A6. Products resulting from 1 mmol Fayalite reacted with 1kg of seawater at 10 bar $CO_{2(g)}$ and various temperatures.

Table A6 Fayalite, CO2 (10 bar) and Water

Temp	(°C)	10	50	90	150	200	250
Amount Reacted							
Fayalite	*(mmol)*	1	1	1	1	1	1
Water	*(kg)*	1	1	1	1	1	1
log *f* CO2(g)	*(bar)*	1	1	1	1	1	1
Reaction Products							
Minerals	Quartz	0.95	0.77	0.35			
(mmol)	Siderite			1.07	1.72		
	Magnetite					0.64	0.67
	Graphite						148
log *f* H2(g)	Init (s/w)	-24.2	-17.7	-12.6	-6.8	-3.18	0.17
(bar)	Fin (fluid)	-10.8	-8.3	-7.1	-4.1	-2.19	0.17
log *f* O2(g)	Init (s/w)	-40	-40	-40	-40	-40	-40.8
(bar)	Fin (fluid)	-67	-58	-51	-45.5	-42	-40.8
log *f* CO2(g)	Init (s/w)	1	1	1	1	1	-0.604
(bar)	Fin (fluid)	0.997	0.993	0.99	0.998	0.998	-0.604
log *f* CH4(g)	Init (s/w)	-71	-51	-35	-16.5	-5.1	4.15
(bar)	Fin (fluid)	-17.5	-12.5	-12.5	-5.5	-1.1	4.15
Eh	Init (s/w)	0.48	0.36	0.23	0.05	-0.115	-0.386
	Fin (fluid)	0.05	0	-0.025	-0.125	-0.205	-0.397
pH	Init (s/w)	3.37	3.5	3.65	3.9	4.15	5.2
	Fin (fluid)	4.3	4.55	4.55	4.6	4.6	5.3

Table A7. Products resulting from 1 mmol Forsterite reacted with 1kg of seawater at 0.0003 bar $CO_{2(g)}$ and various temperatures.

Table A7 Forsterite, CO2 (0.0003 bar) and Water

Temp	(°C)	10	50	90	150	200	250
Amount Reacted							
Forsterite	*(mmol)*	1	1	1	1	1	1
Water	*(kg)*	1	1	1	1	1	1
log *f* CO2(g)	*(bar)*	-3.5	-3.5	-3.5	-3.5	-3.5	-3.5
Reaction Products							
Minerals	Brucite	0.48	0.49	0.51	0.53	0.55	0.57
(mmol)	Antigorite	0.06	0.06	0.06	0.06	0.06	0.06
log *f* H2(g)	Init (s/w)	-24	-17.7	-12.6	-6.85	-3.2	-0.2306
(bar)	Fin (fluid)	-24	-17.7	-12.6	-6.85	-3.2	-0.2303
log *f* O2(g)	Init (s/w)	-40	-40	-40	-40	-40	-40
(bar)	Fin (fluid)	-40	-40	-40	-40	-40	-40
log *f* CO2(g)	Init (s/w)	-3.5	-3.5	-3.5	-3.5	-3.5	-3.5
(bar)	Fin (fluid)	-8.25	-6.7	-5.6	-4.4	-3.73	-3.5
log *f* CH4(g)	Init (s/w)	-75	-54.8	-38.9	-21	-9.55	-0.35
(bar)	Fin (fluid)	-79.8	-57.9	-41	-21.9	-9.79	-0.35
Eh	Init (s/w)	0.35	0.22	0.075	-0.11	-0.25	-0.4
	Fin (fluid)	0.07	-0.025	-0.12	-0.26	-0.39	-0.52
pH	Init (s/w)	5.6	5.75	5.8	5.75	5.6	5.75
	Fin (fluid)	10.8	9.5	8.6	7.65	7.07	6.7

Table A8. Products resulting from 1 mmol Forsterite reacted with 1kg of seawater at 1 bar $CO_{2(g)}$ and various temperatures.

Table A8 Forsterite, CO2 (1 bar) and Water

Temp	(°C)	10	50	90	150	200	250
Amount Reacted							
Forsterite		1	1	1	1	1	1
Water	*(kg)*	1	1	1	1	1	1
log *f* CO2(g)	*(bar)*	0	0	0	0	0	0
Reaction Products							
Minerals	Quartz	0.95	0.77	0.34			
(mmol)	Magnesite				0.92	0.48	0.54
	Talc				0.15		
	Antigorite					0.05	0.06
log *f* H2(g)	Init (s/w)	-24.2	-17.7	-12.6	-6.85	-3.18	-0.23
(bar)	Fin (fluid)	-24.2	-17.7	-12.6	-6.85	-3.18	-0.22
log *f* O2(g)	Init (s/w)	-40	-40	-40	-40	-40	-40
(bar)	Fin (fluid)	-40	-40	-40	-40	-40	-40
log *f* CO2(g)	Init (s/w)	0	0	0	0	0	0
(bar)	Fin (fluid)	-0.032	-0.085	-0.17	-0.13	-0.06	-0.04
log *f* CH4(g)	Init (s/w)	-71.62	-51.28	-35.42	-17.5	-0.606	3.15
(bar)	Fin (fluid)	-71.64	-51.36	-35.59	-17.6	-6.11	3.15
Eh	Init (s/w)	0.45	0.33	0.2	0	-0.16	-0.34
	Fin (fluid)	0.37	0.22	0.065	-0.13	-0.29	-0.46
pH	Init (s/w)	3.86	4	4.2	4.4	4.65	4.9
	Fin (fluid)	5.33	5.62	6	6	6	6.1

Table A9. Products resulting from 1 mmol Forsterite reacted with 1kg of seawater at 10 bar $CO_{2(g)}$ and various temperatures.

Table A9 Forsterite, CO2 (10 bar) and Water

Temp	*(°C)*	10	50	90	150	200	250
Amount Reacted							
Forsterite	*(mmol)*	1	1	1	1	1	1
Water	*(kg)*	1	1	1	1	1	1
log *f* CO2(g)	*(bar)*	1	1	1	1	1	1
Reaction Products							
Minerals	Magnesite					1.45	
(mmol)	Graphite						149
	Antigorite						0.06
	Brucite						0.52
	Quartz	0.95	0.77	0.34	0.375		
log *f* H2(g)	Init (s/w)	-24.22	-17.7	-12.6	-6.85	-3.18	0.17
(bar)	Fin (fluid)	-24.22	-17.7	-12.6	-6.85	-3.18	0.17
log *f* O2(g)	Init (s/w)	-40	-40	-40	-40	-40	-40.8
(bar)	Fin (fluid)	-40	-40	-40	-40	-40	-40.8
log *f* CO2(g)	Init (s/w)	0	0	0	0	0	0
(bar)	Fin (fluid)	-0.032	-0.085	-0.17	-0.13	-0.06	-0.04
log *f* CH4(g)	Init (s/w)	-71.62	-51.28	-35.42	-17.5	-6.06	3.15
(bar)	Fin (fluid)	-71.64	-51.36	-35.59	-17.6	-6.11	3.15
Eh	Init (s/w)	0.45	0.33	0.2	0	-0.16	-0.34
	Fin (fluid)	0.37	0.22	0.065	-0.13	-0.29	-0.46
pH	Init (s/w)	3.86	4	4.2	4.4	4.65	4.9
	Fin (fluid)	5.33	5.62	6	6	6	6.1

Table A10. Products resulting from 0.1 mmol Fayalite, 0.9 mmol Forsterite reacted with 1kg of seawater at 0.0003 bar $CO_{2(g)}$ and various temperatures.

Table A10 Fayalite, Forsterite, CO2 (0.0003 bar) and Water

Temp	*(°C)*	10	50	90	150	200	250
Amount Reacted							
Total Rock	*(mmol)*	1	1	1	1	1	1
Forsterite	*(mmol)*	0.9	0.9	0.9	0.9	0.9	0.9
Fayalite	*(mmol)*	0.1	0.1	0.1	0.1	0.1	0.1
Water	*(kg)*	1	1	1	1	1	1
log *f* CO2(g)	*(bar)*	-3.5	-3.5	-3.5	-3.5	-3.5	-3.5
Reaction Products							
Minerals	Brucite	0.29	0.29	0.31	0.326	0.35	0.36
(mmol)	Magnetite	0.067	0.067	0.067	0.067	0.067	0.067
	Antigorite	0.058	0.059	0.058	0.058	0.058	0.058
log *f* H2(g)	Init (s/w)	-23	-17.7	-12.6	-6.8	-3.2	-0.23
(bar)	Fin (fluid)	-5	-1.3	-1.2	-1.2	-1.25	-0.205
log *f* O2(g)	Init (s/w)	-41	-40	-40	-40	-40	-40
(bar)	Fin (fluid)	-79	-72.5	-60.3	-51.2	-43.8	-40.05
log *f* CO2(g)	Init (s/w)	-3.5	-3.5	-3.5	-3.5	-3.5	-3.5
(bar)	Fin (fluid)	-9	-16.2	-12.5	-7.7	-4.5	-3.6
log *f* CH4(g)	Init (s/w)	-73	-55	-38	-21	-9.5	-0.35
(bar)	Fin (fluid)	-2	-2	-2.5	-2.5	-3	-0.35
Eh	Init (s/w)	0.34	0.2	0.08	-0.11	-0.25	-0.4
	Fin (fluid)	-0.49	-0.55	-0.52	-0.5	-0.475	-0.52
pH	Init (s/w)	5.6	5.75	5.8	5.75	5.6	5.55
	Fin (fluid)	10.8	9.5	8.6	7.6	7.08	6.7

Table A11. Products resulting from 0.1 mmol Fayalite, 0.9 mmol Forsterite reacted with 1kg of seawater at 1 bar $CO_{2(g)}$ and various temperatures.

Table A11 Fayalite, Forsterite, CO2 (1 bar) and Water

Temp	(°C)	10	50	90	150	200	250
Amount Reacted							
Total Rock	*(mmol)*	1	1	1	1	1	1
Forsterite	*(mmol)*	0.9	0.9	0.9	0.9	0.9	0.9
Fayalite	*(mmol)*	0.1	0.1	0.1	0.1	0.1	0.1
Water	*(kg)*	1	1	1	1	1	1
log *f* CO2(g)	*(bar)*	0	0	0	0	0	0
Reaction Products							
Minerals	Quartz	0.95	0.77	0.34			
(mmol)	Siderite			0.175			
	Magnesite				0.72	0.28	0.33
	Talc				0.15	0.065	0.057
	Magnetite				0.06	0.065	0.067
	Antigorite					0.05	
log *f* H2(g)	Init (s/w)	-24.2	-17.7	-12.6	-6.8	-3.18	-0.23
(bar)	Fin (fluid)	-11.2	-8.2	-5.2	-2.8	-2.19	-0.22
log *f* O2(g)	Init (s/w)	-40	-40	-40	-40	-40	-40
(bar)	Fin (fluid)	-66	-58	-54.8	-47.8	-42	-40.01
log *f* CO2(g)	Init (s/w)	0	0	0	0	0	0
(bar)	Fin (fluid)	-0.032	-0.085	-0.16	-0.12	-0.046	-0.028
log *f* CH4(g)	Init (s/w)	-71	-51	-35	-17.5	-6	3.15
(bar)	Fin (fluid)	-20	-31	-7	-2	-2.1	3.15
Eh	Init (s/w)	0.45	0.325	0.2	0	-0.16	-0.34
	Fin (fluid)	0.02	-0.075	0.2	-0.29	-0.34	-0.455
pH	Init (s/w)	3.88	4	4.2	4.4	4.66	4.9
	Fin (fluid)	5.32	5.6	6	6	6	6.05

Table A12. Products resulting from 0.1 mmol Fayalite, 0.9 mmol Forsterite reacted with 1kg of seawater at 10 bar $CO_{2(g)}$ and various temperatures.

Table A12 Fayalite, Forsterite, CO2 (10 bar) and Water

Temp	(°C)	10	50	90	150	200	250
Amount Reacted							
Total Rock	*(mmol)*	1	1	1	1	1	1
Forsterite	*(mmol)*	0.9	0.9	0.9	0.9	0.9	0.9
Fayalite	*(mmol)*	0.1	0.1	0.1	0.1	0.1	0.1
Water	*(kg)*	1	1	1	1	1	1
log *f* CO2(g)	*(bar)*	1	1	1	1	1	1
Reaction Products							
Minerals	Quartz	0.95	0.77	0.33			
(mmol)	Siderite				0.18		
	Magnesite				0.18	1.25	
	Magnetite					0.07	0.067
	Graphite						149
	Brucite						0.32
	Antigorite						0.058
log *f* H2(g)	Init (s/w)	-24.2	-17.7	-12.6	-6.8	-3.18	0.17
(bar)	Fin (fluid)	-12.8	-9	-7.3	-4.1	-2.42	0.17
log *f* O2(g)	Init (s/w)	-40	-40	-40	-40	-40	-40.8
(bar)	Fin (fluid)	-63	-57.2	-50.5	-45.6	-41.5	-40.8
log *f* CO2(g)	Init (s/w)	1	1	1	1	1	-0.604
(bar)	Fin (fluid)	0.997	0.992	0.986	0.982	0.986	-0.604
log *f* CH4(g)	Init (s/w)	-70	-50	-34.5	-16.5	-5.1	4.15
(bar)	Fin (fluid)	-25	-15	-13	-5.4	-2.1	4.15
Eh	Init (s/w)	0.48	0.35	0.235	0.05	-0.12	-0.385
	Fin (fluid)	0.11	0.02	-0.04	-0.18	-0.26	-0.515
pH	Init (s/w)	3.37	3.5	3.65	3.9	4.15	5.2
	Fin (fluid)	4.3	4.75	4.87	5.3	5.3	6.45

Arrows on plots indicate direction of reaction between initial and final states of the system.

Figures A1 – A5. Products resulting from 1 mmol Fayalite reacted with 1kg seawater at various temperatures

Figure A1
Minerals

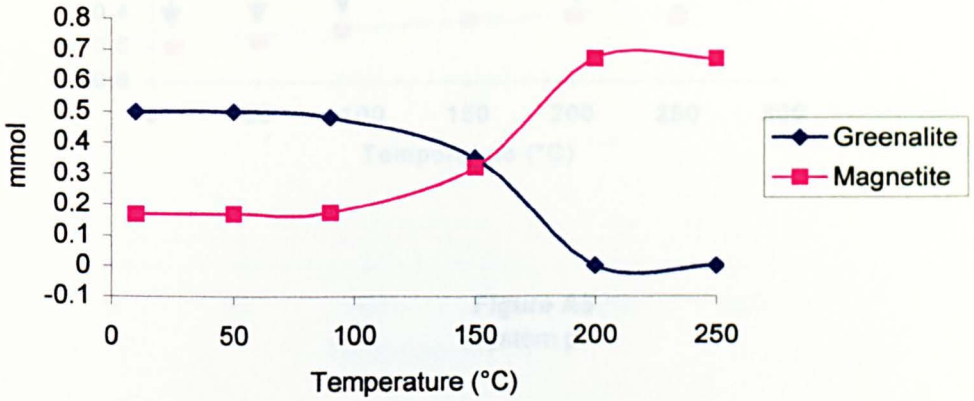

Figure A2
Hydrogen Fugacity

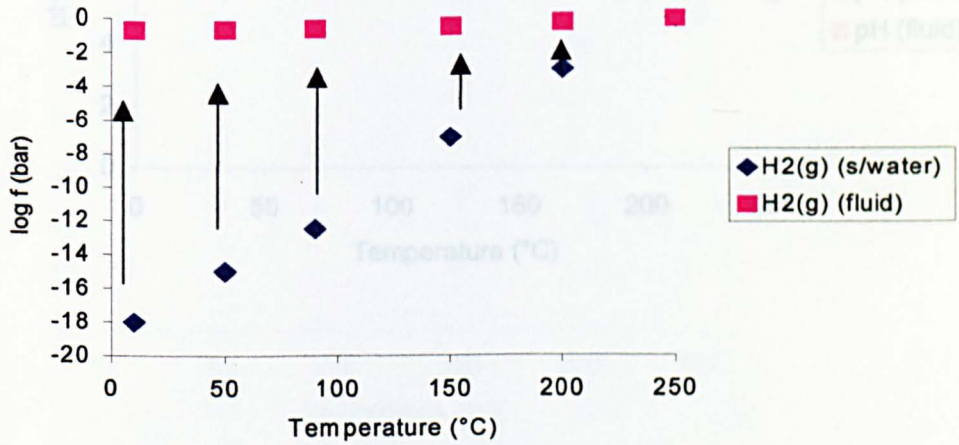

Figure A3
Oxygen Fugacity

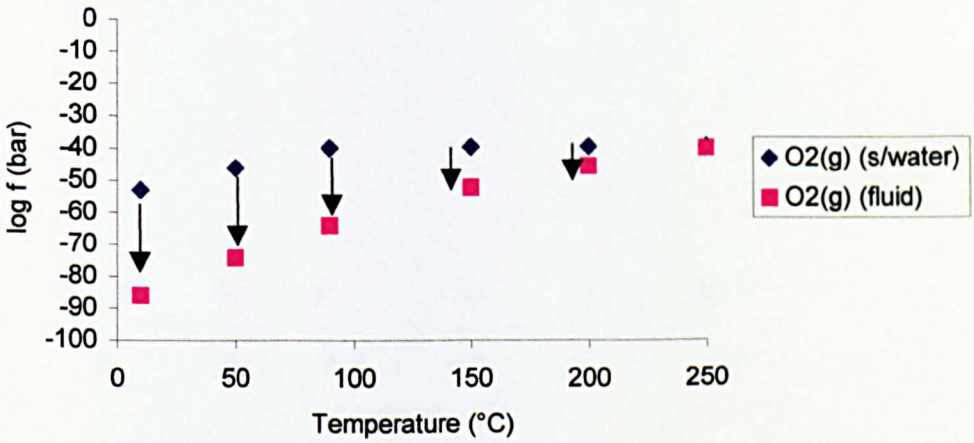

Figure A4
Oxidation State

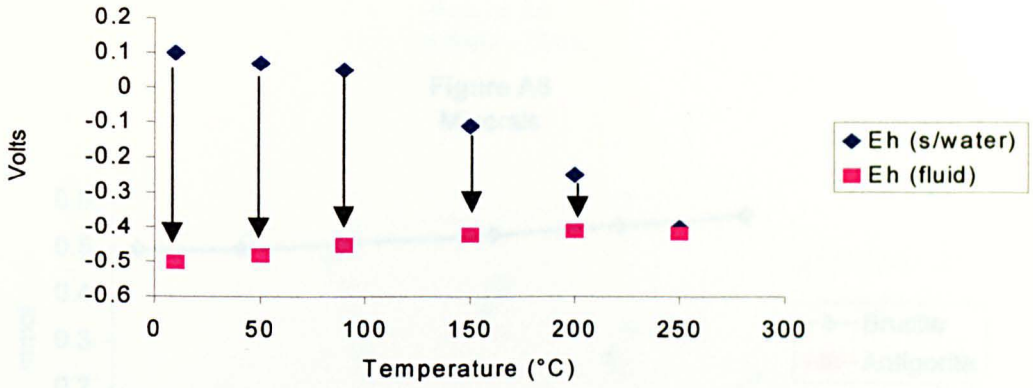

Figure A5
System pH

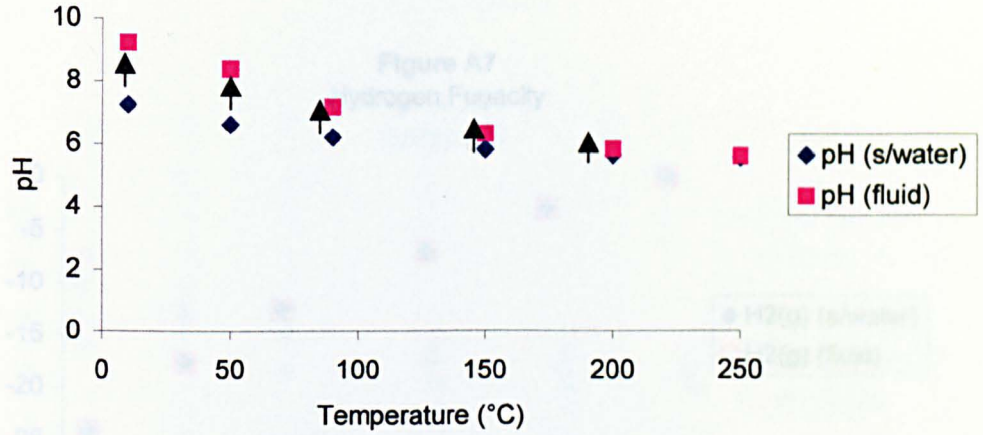

Figures A6 – A10. Products resulting from 1 mmol Forsterite reacted with 1kg seawater at various temperatures

Figure A6
Minerals

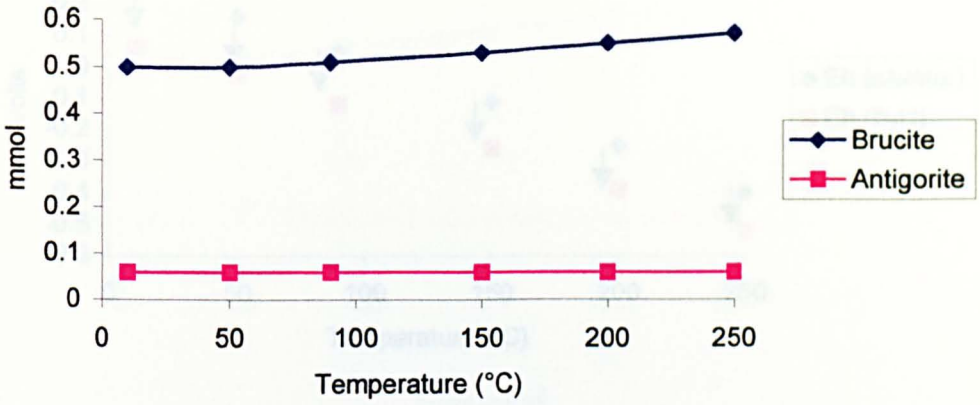

Figure A7
Hydrogen Fugacity

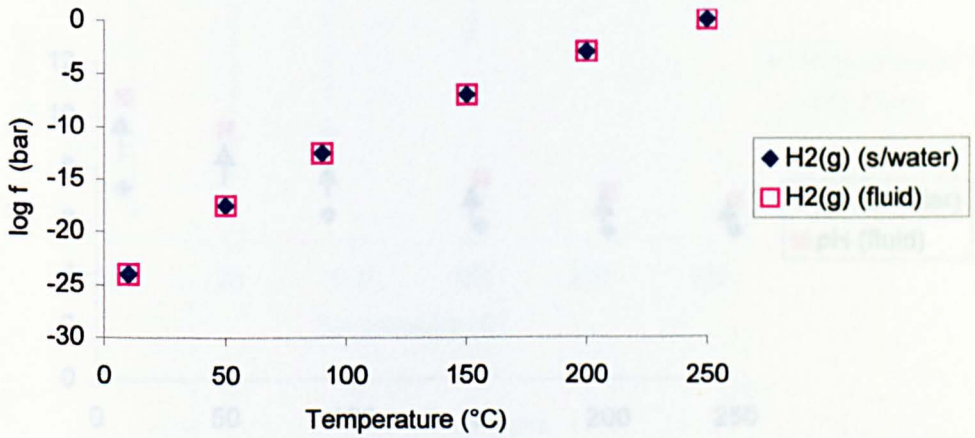

Figure A8
Oxygen Fugacity

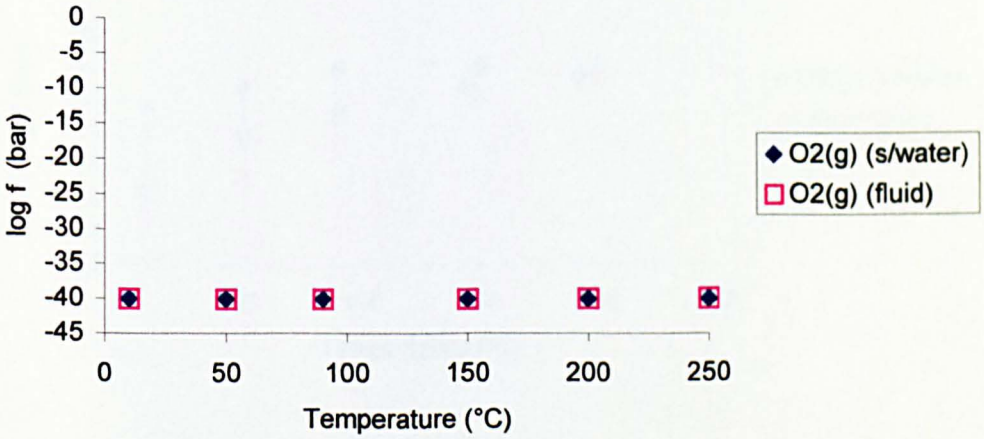

Figure A9
Oxidation State

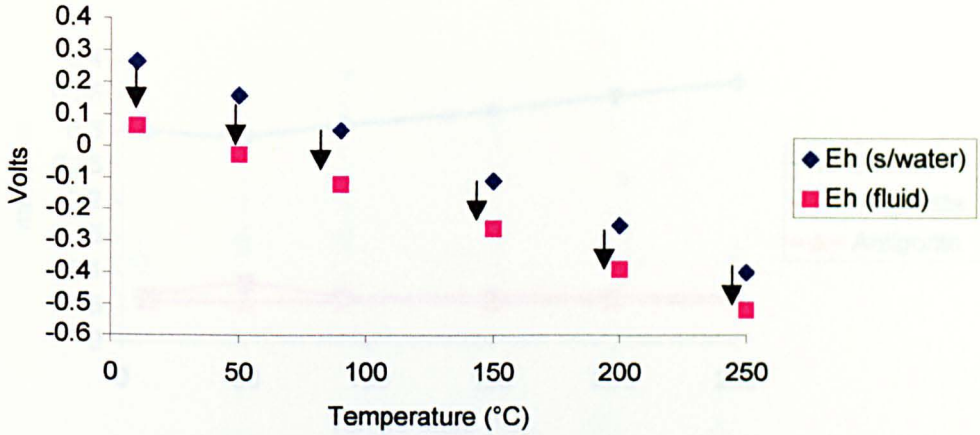

Figure A10
System pH

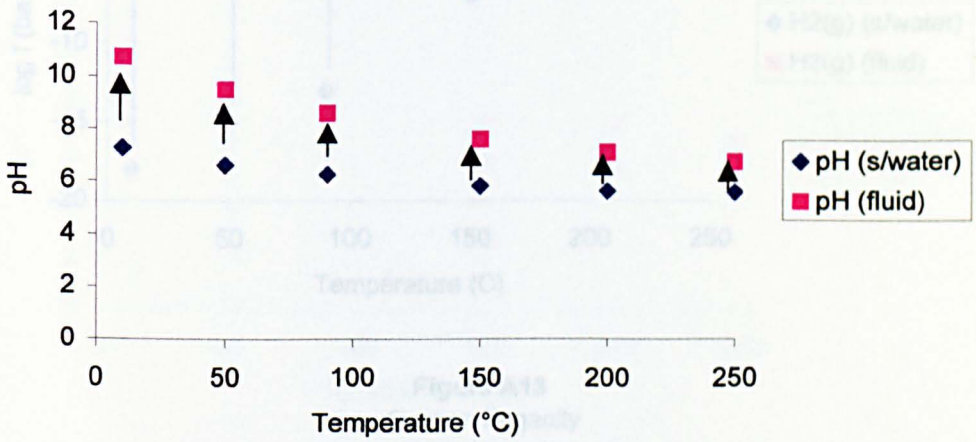

Figures A11-A15. Products resulting from 0.9 mmol Forsterite and 0.1 mmol Fayalite reacted with 1kg seawater at various temperatures

Figure A11
Minerals

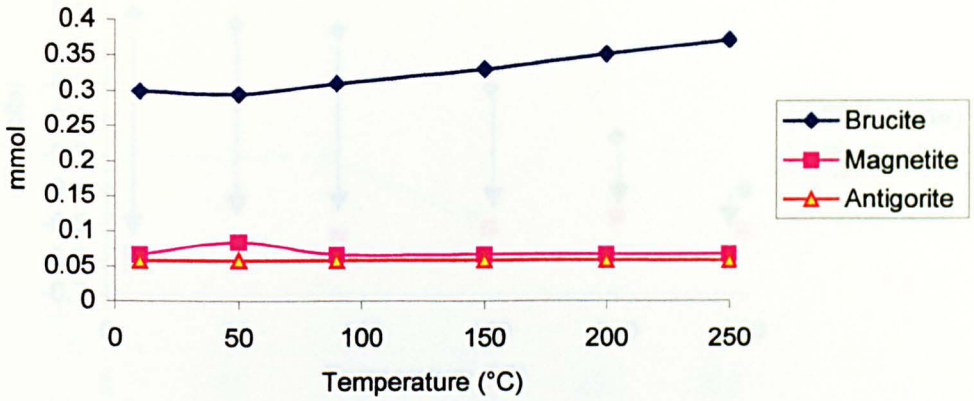

Figure A12
Hydrogen Fugacity

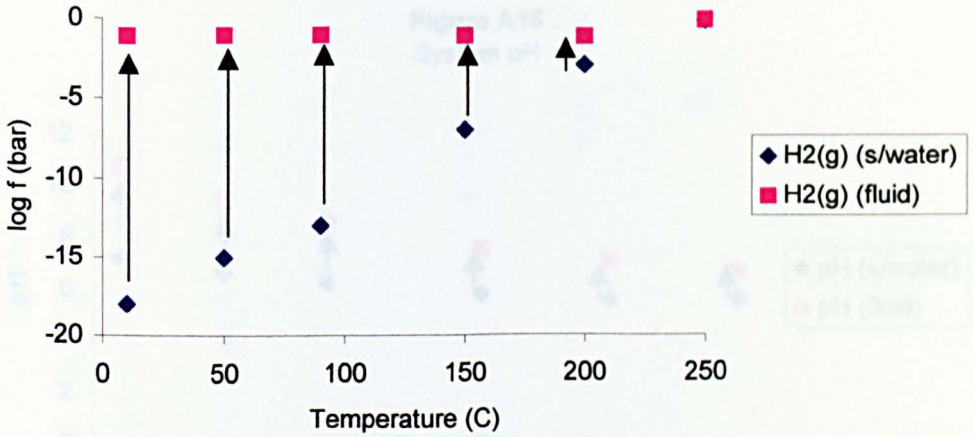

Figure A13
Oxygen Fugacity

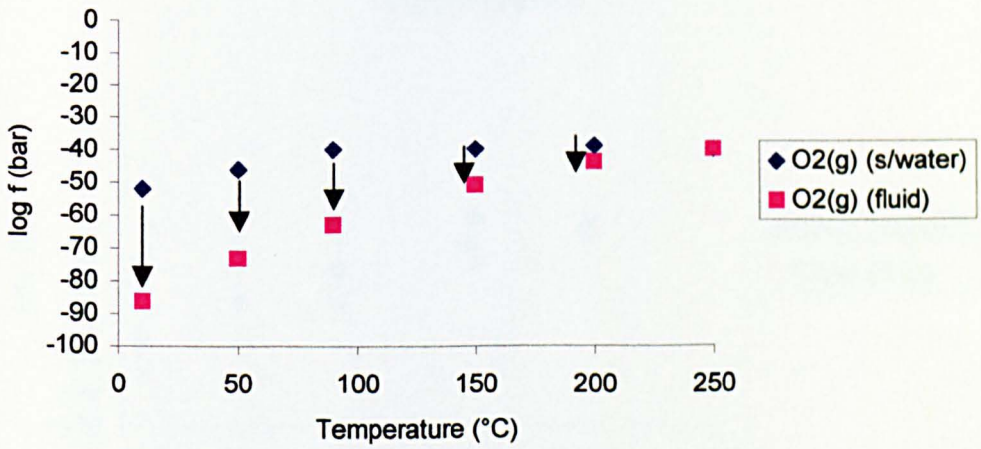

Figure A14
Oxidation State

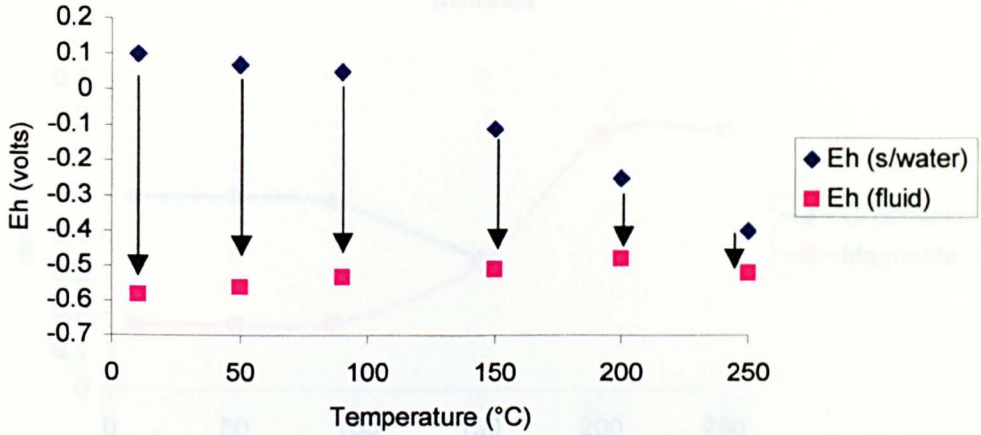

Figure A15
System pH

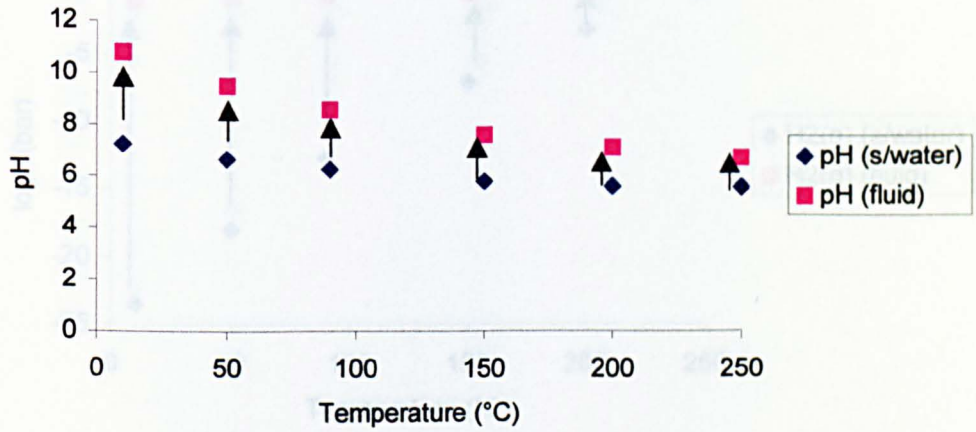

Figures A16-A22. Products resulting from 1 mmol Fayalite and 0.0003 bar CO2 reacted with 1kg seawater at various temperatures

Figure A16
Minerals

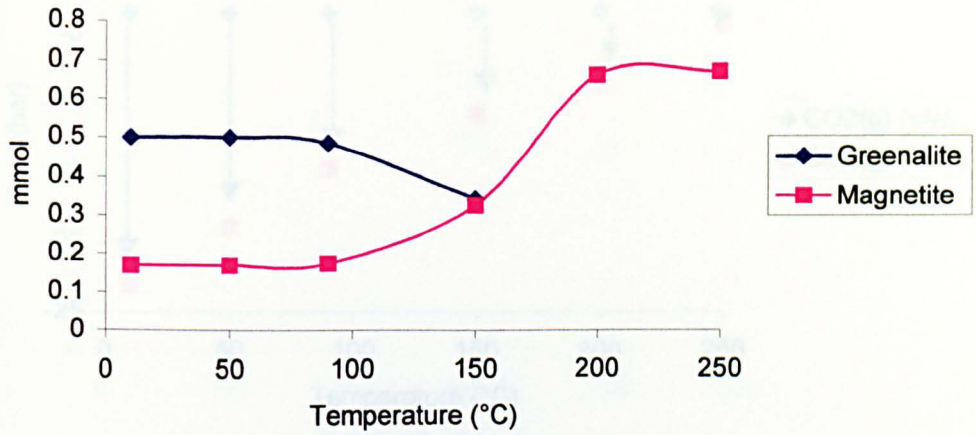

Figure A17
Hydrogen Fugacity

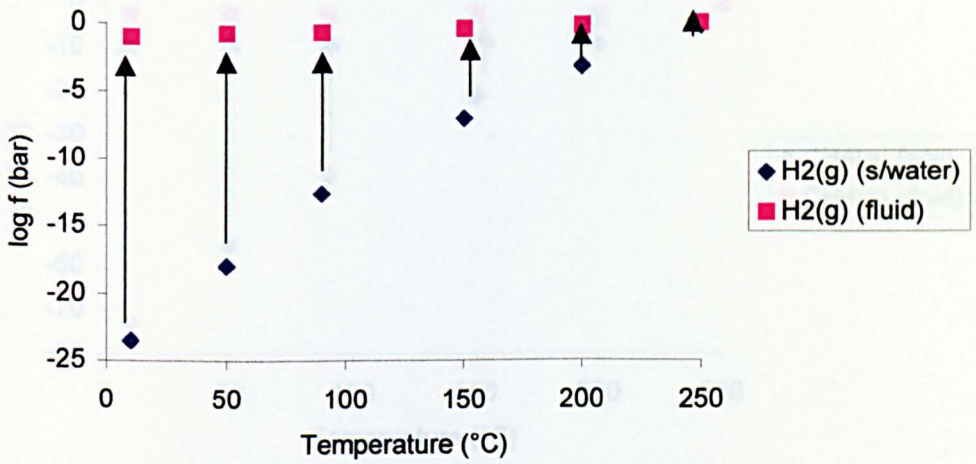

Figure A18
Oxygen Fugacity

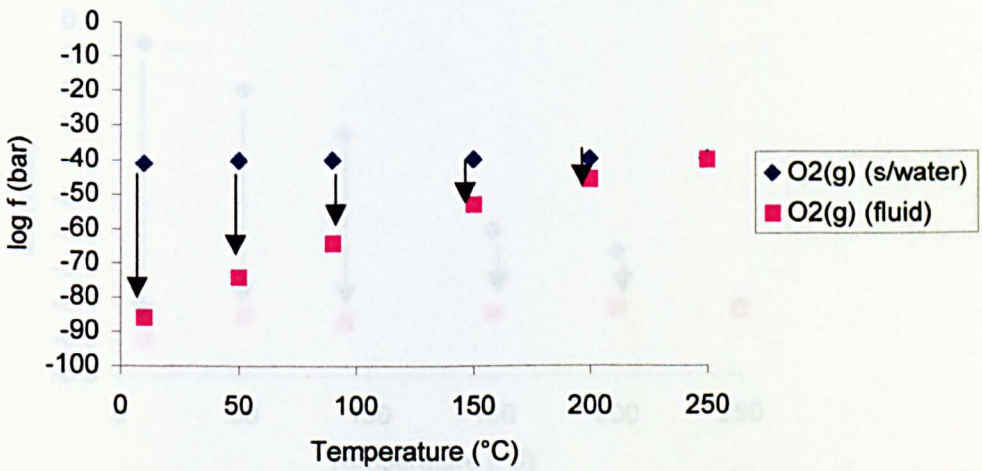

Figure A19
CO2 Fugacity

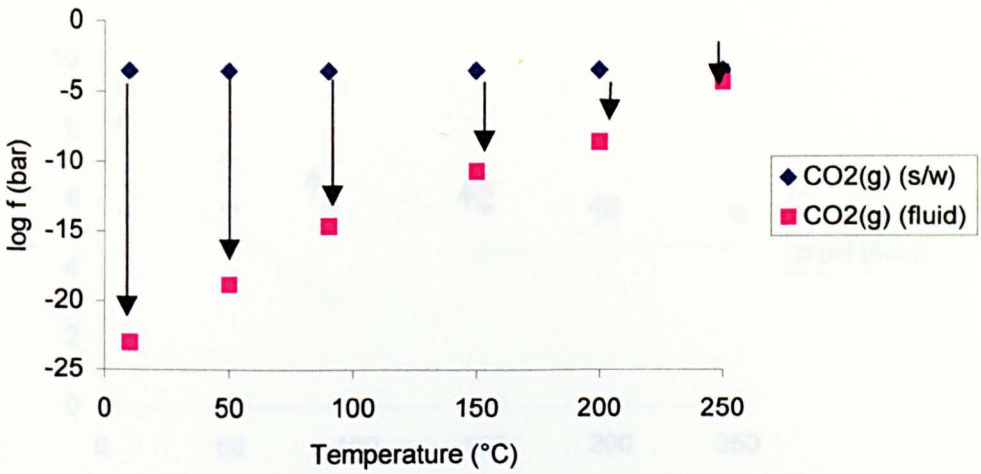

Figure A20
Methane Fugacity

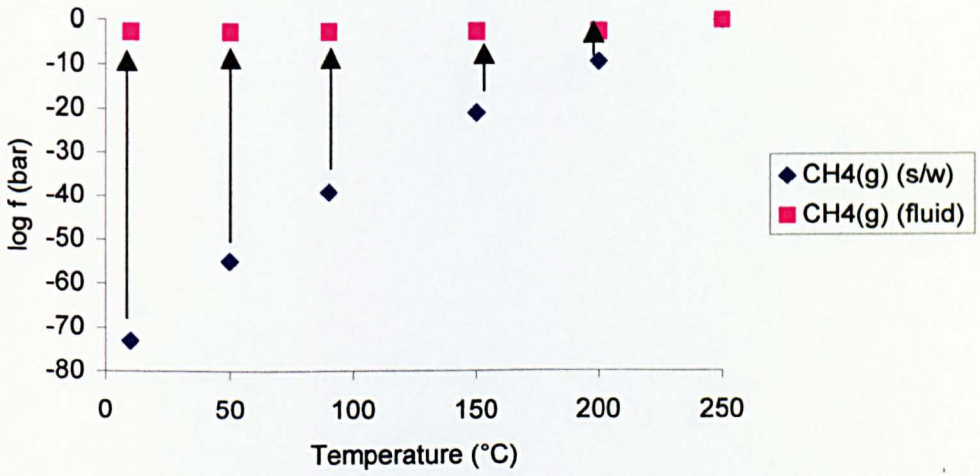

Figure A21
Oxidation State

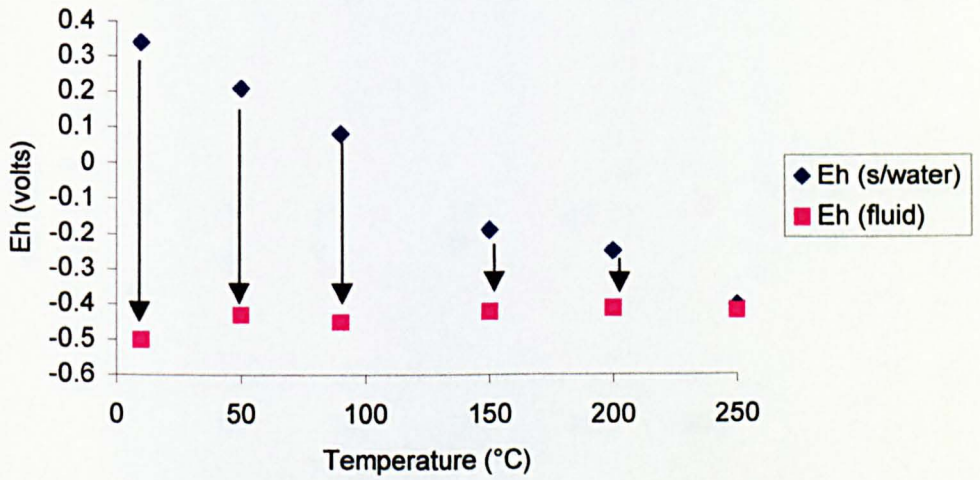

Figure A22
System pH

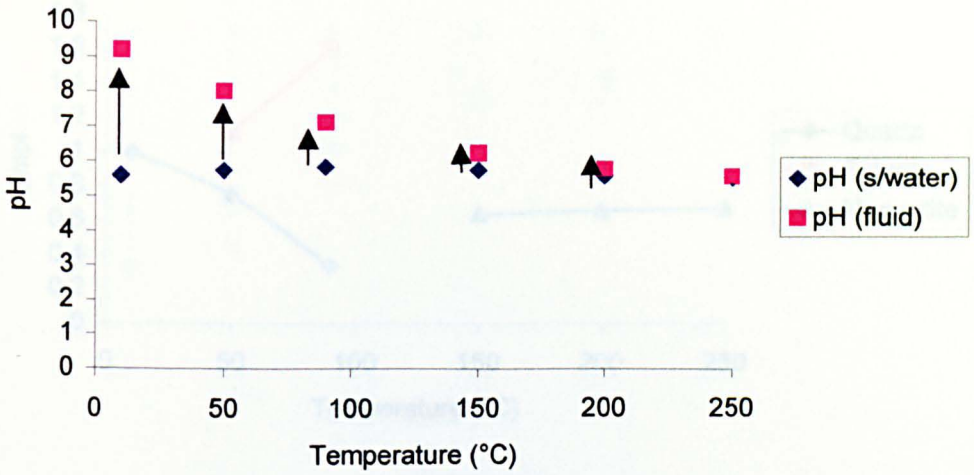

Figures A23-A29. Products resulting from 1 mmol Fayalite and 1 bar CO2 reacted with 1kg seawater at various temperatures

Figure A23
Minerals

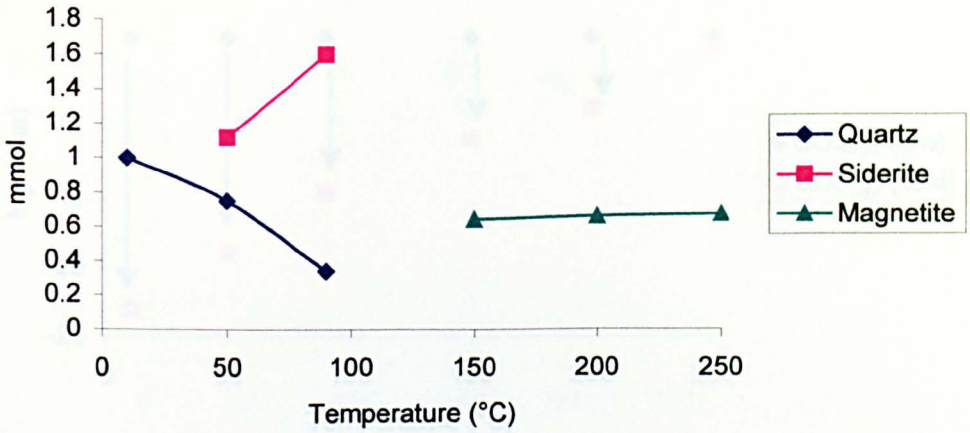

Figure A24
Hydrogen Fugacity

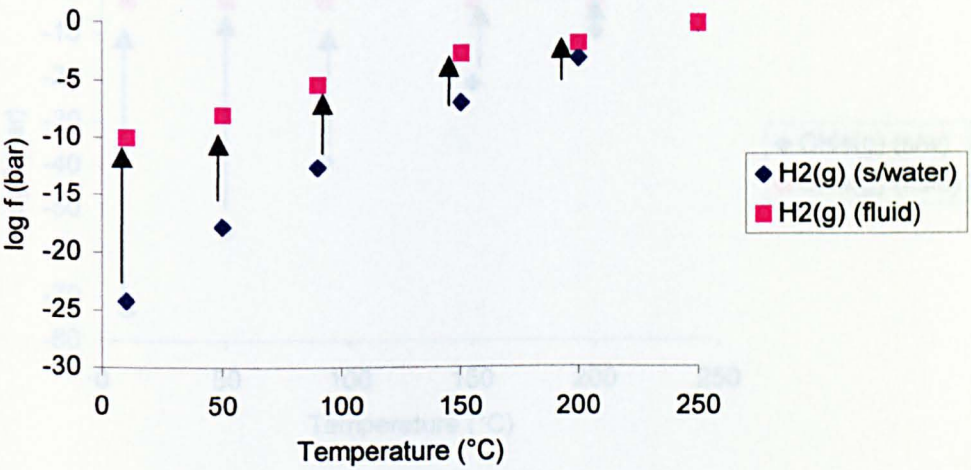

Figure A25
Oxygen Fugacity

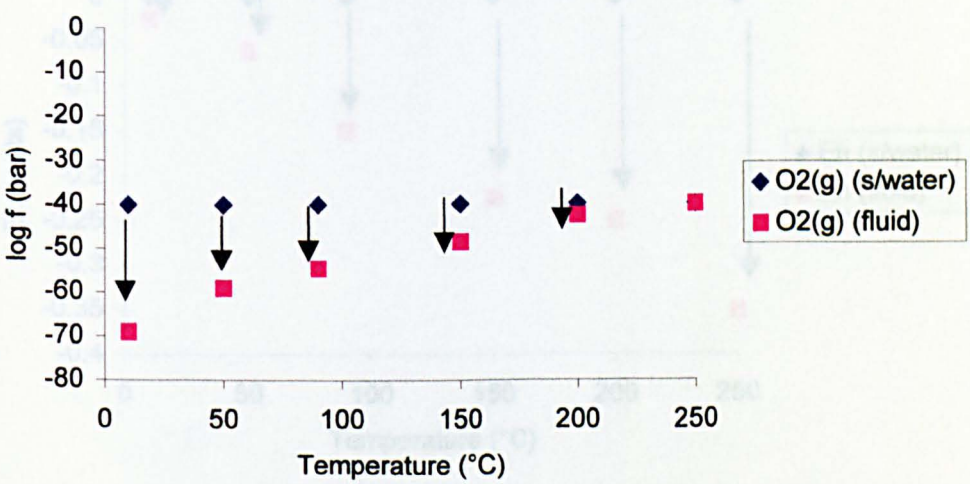

Figure A26
CO2 Fugacity

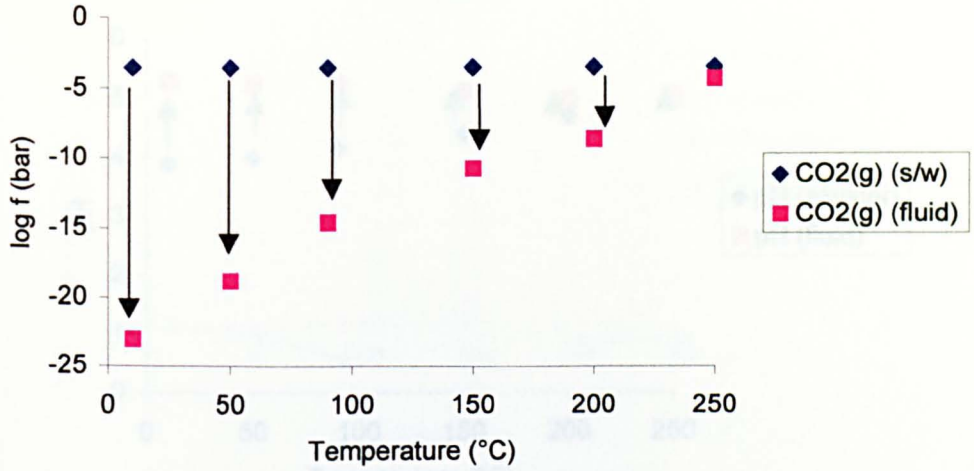

Figure A27
Methane Fugacity

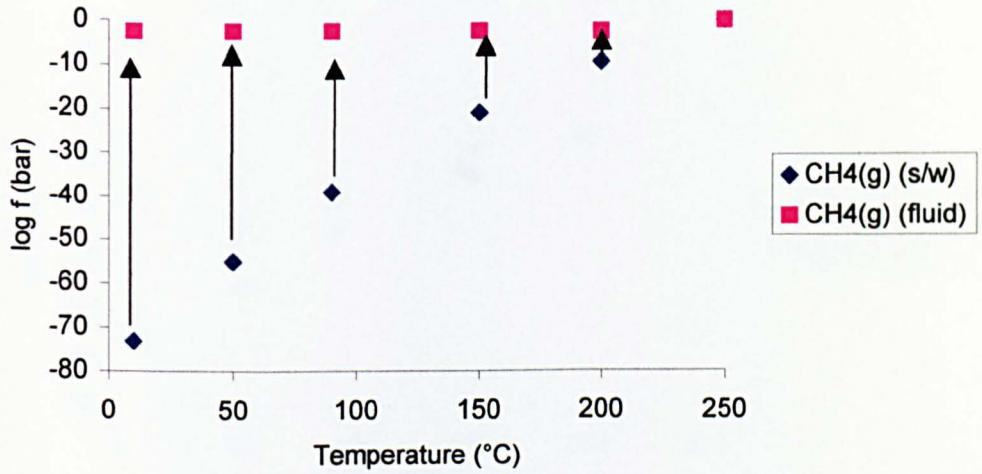

Figure A28
Oxidation State

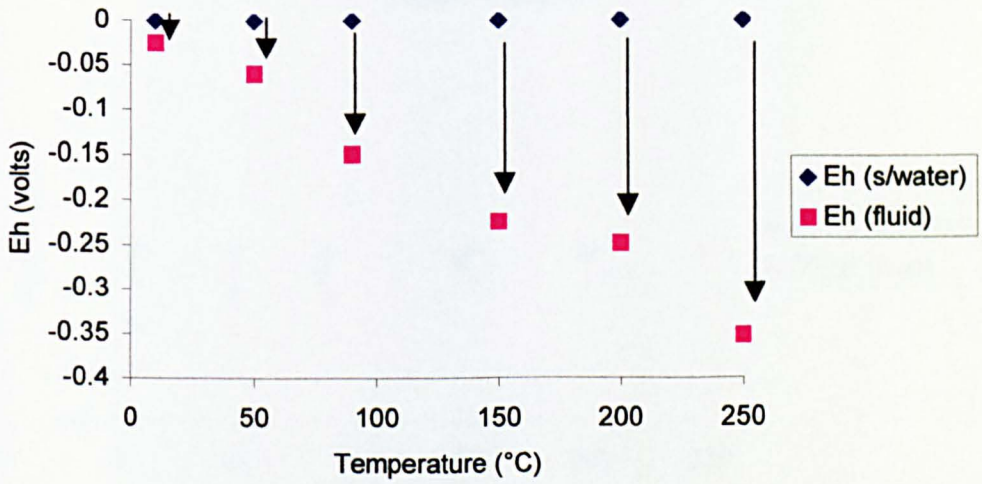

Figure A29
System pH

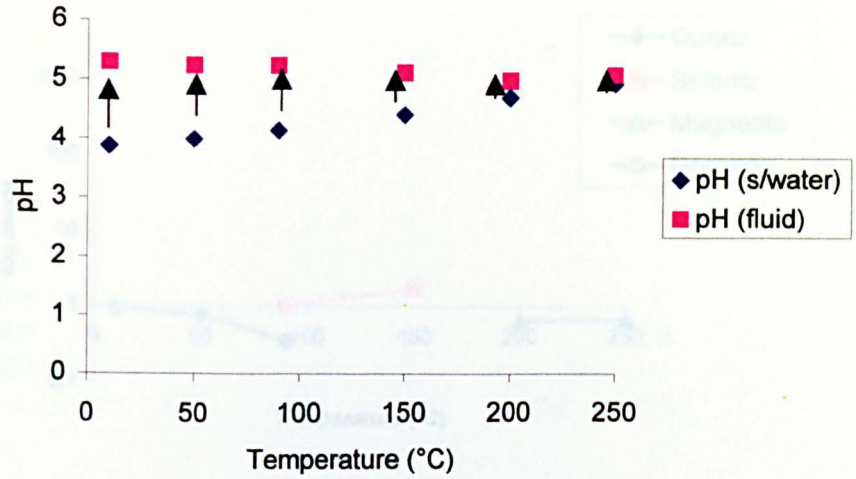

Figures A30-A36. Products resulting from 1 mmol Fayalite and 10 bar CO2 reacted with 1kg seawater at various temperatures

Figure A30
Minerals

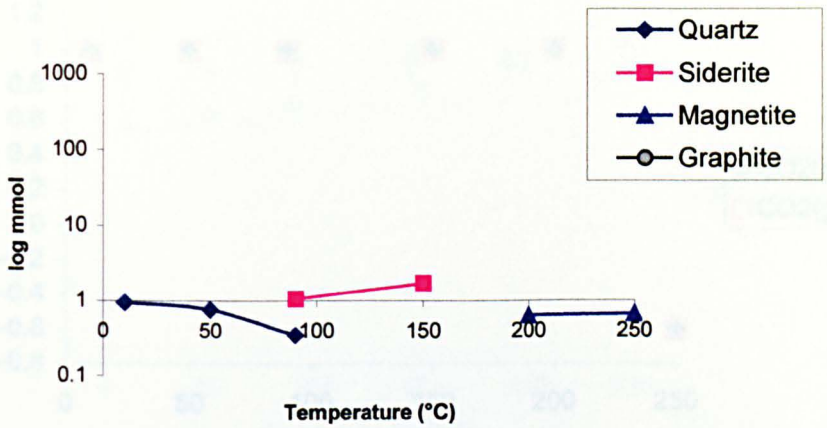

Figure A31
Hydrogen Fugacity

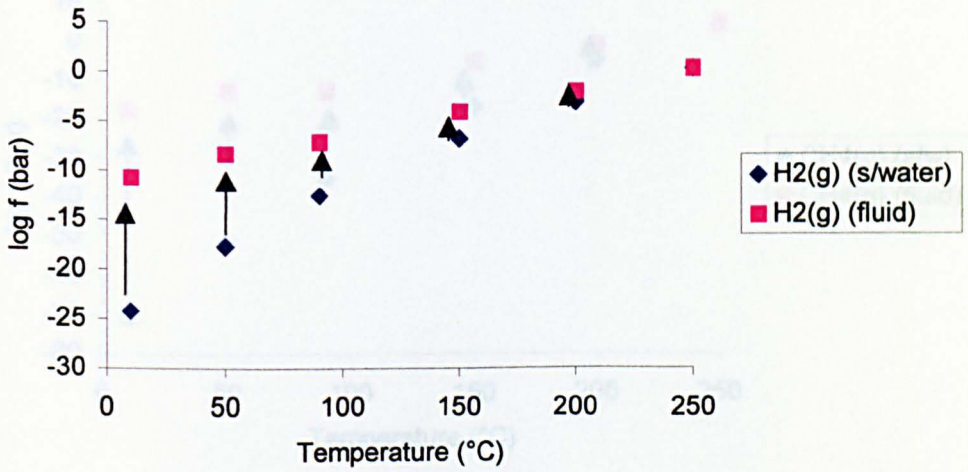

Figure A32
Oxygen Fugacity

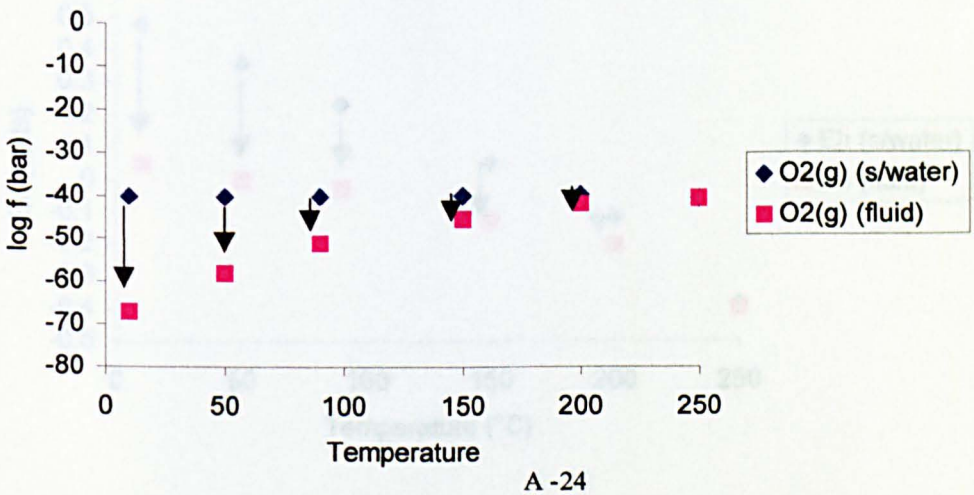

Figure A33
CO2 Fugacity

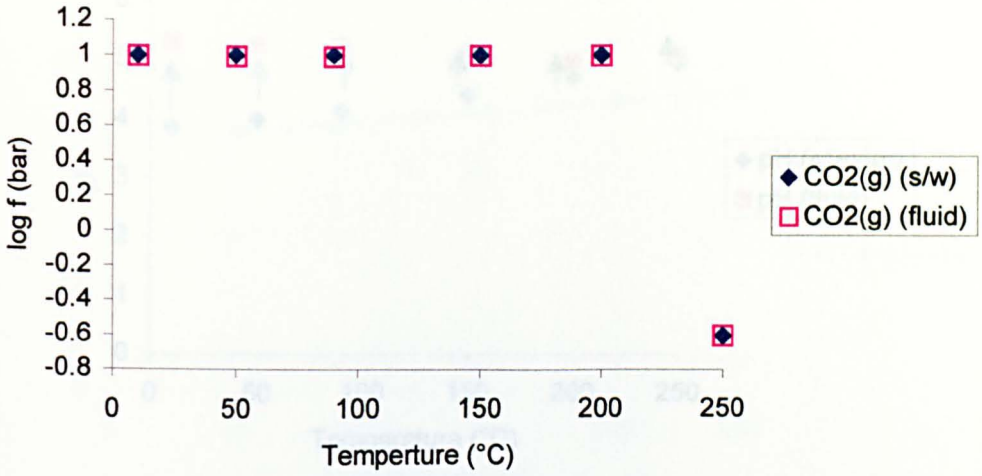

Figure A34
Methane Fugacity

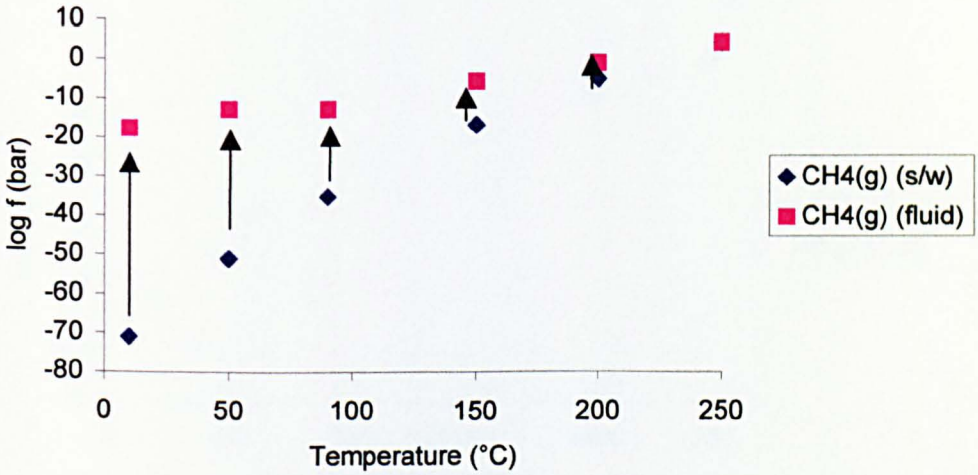

Figure A35
Oxidation State

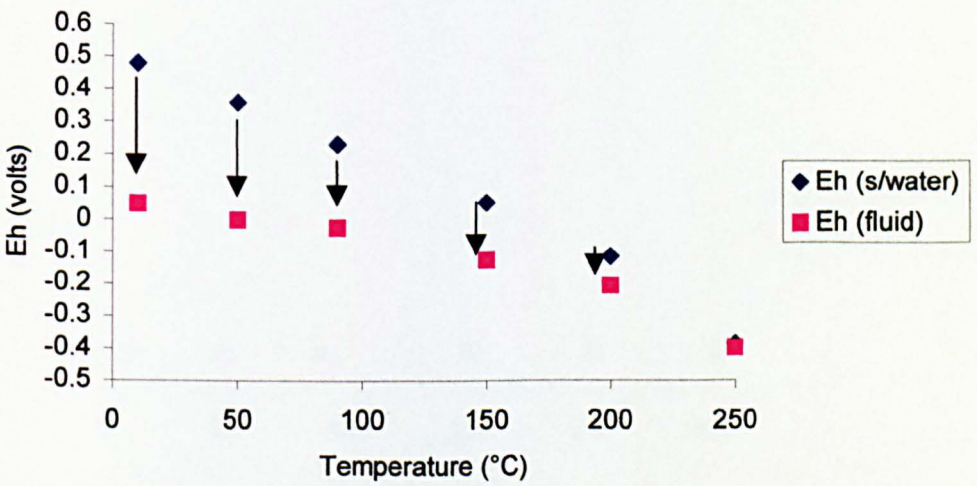

Figure A36
System pH

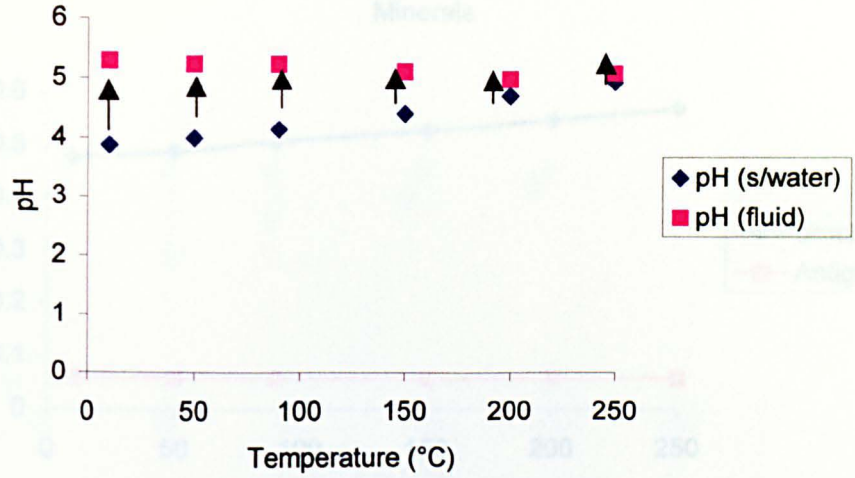

Figures A37-A43. Products resulting from 1 mmol Forsterite and 0.0003 bar CO2 reacted with 1kg seawater at various temperatures

Figures A37
Minerals

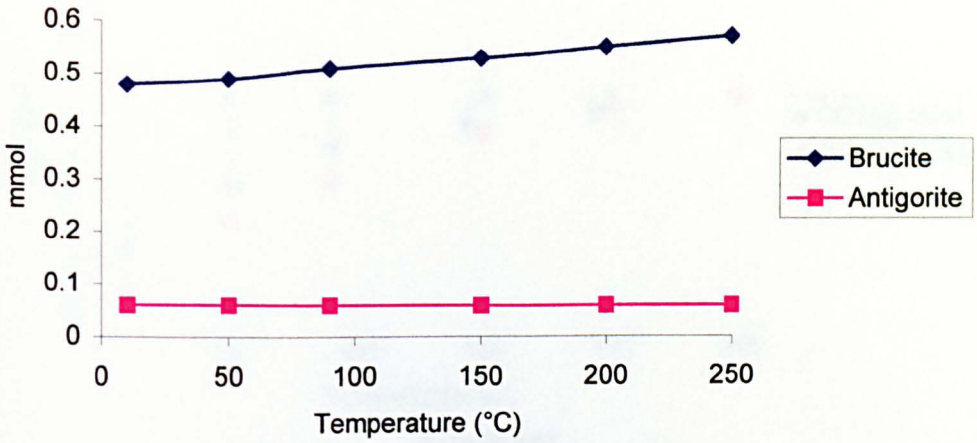

Figure A38
Hydrogen Fugacity

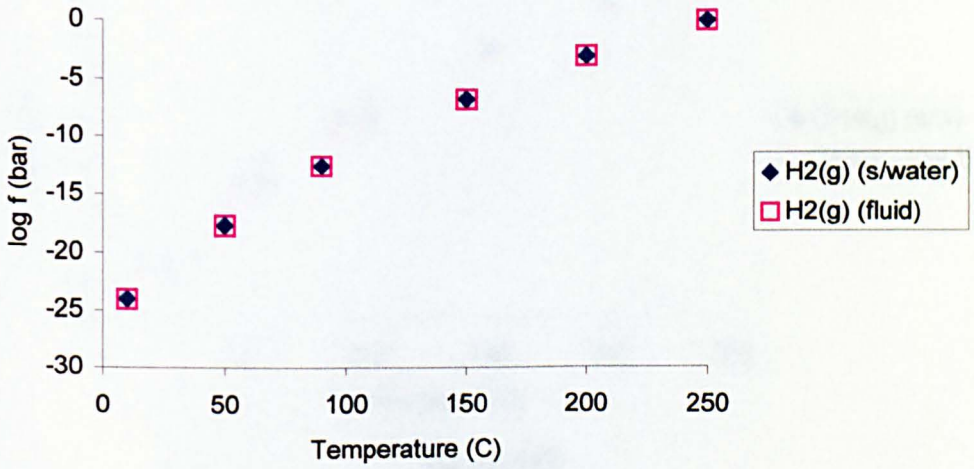

Figures A39
Oxygen Fugacity

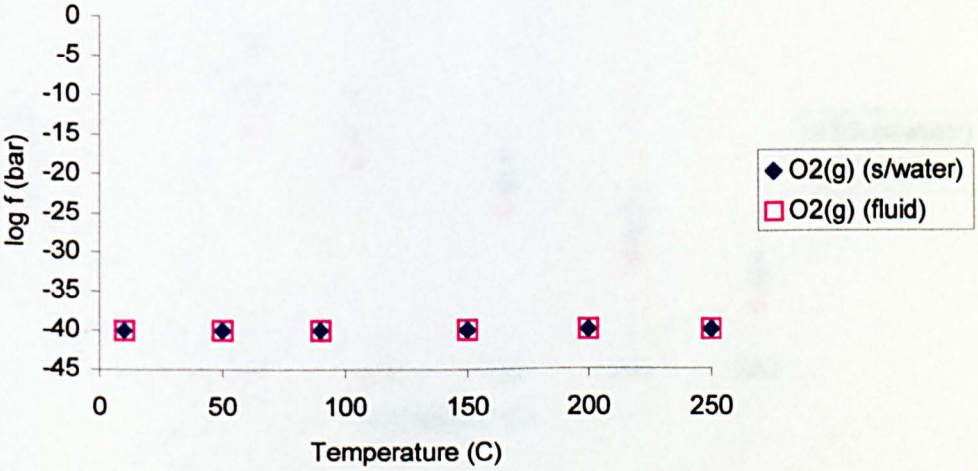

Figure A40
CO2 Fugacity

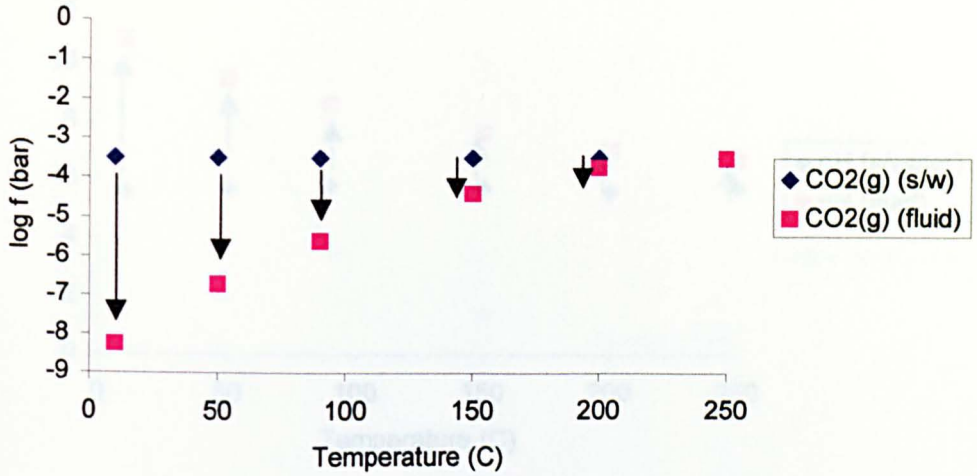

Figure A41
Methane Fugacity

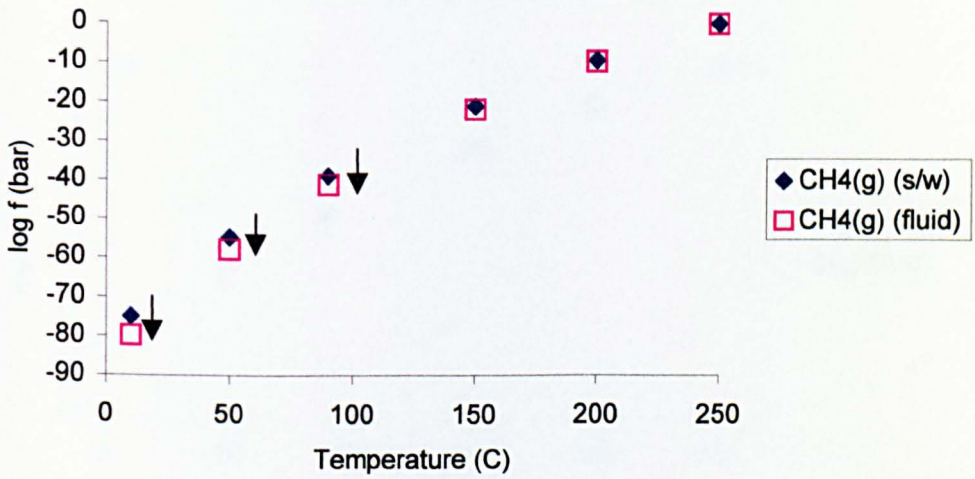

Figure A42
Oxidation State

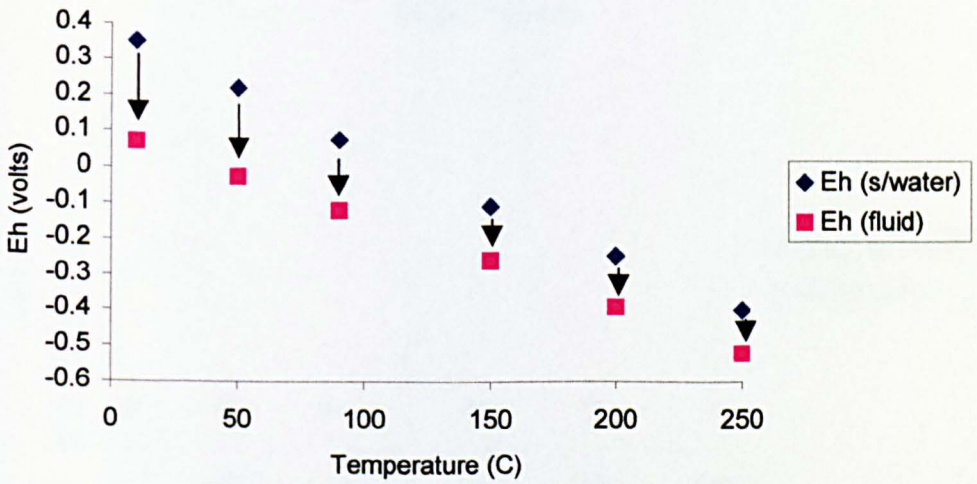

Figure A43
System pH

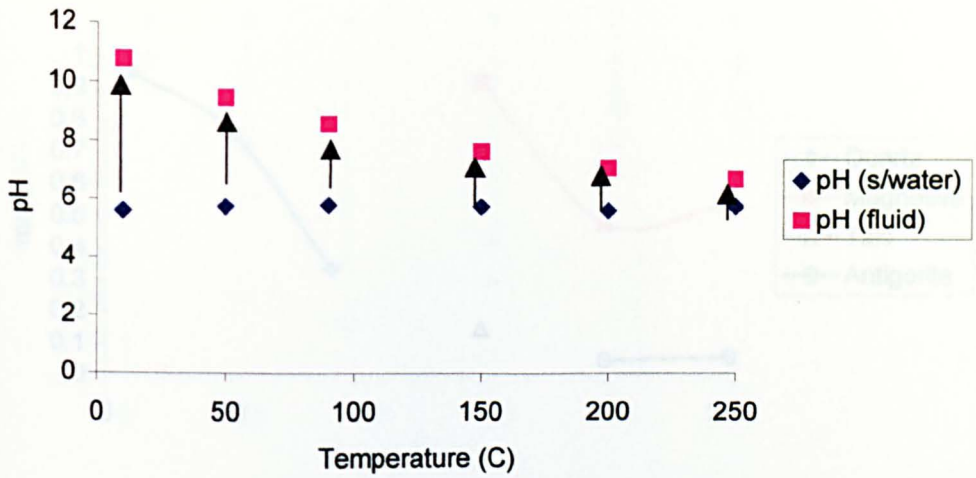

Figures A44-A50. Products resulting from 1 mmol Forsterite and 1 bar CO2 reacted with 1kg seawater at various temperatures

Figure A44
Minerals

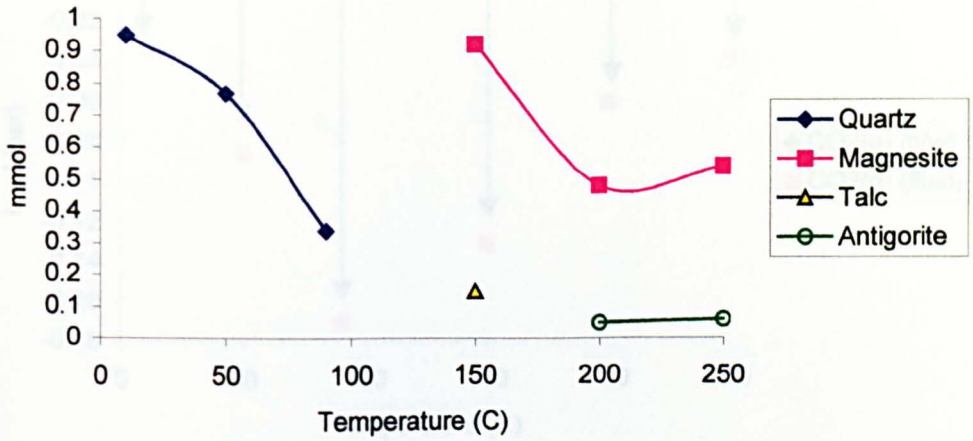

Figure A45
Hydrogen Fugacity

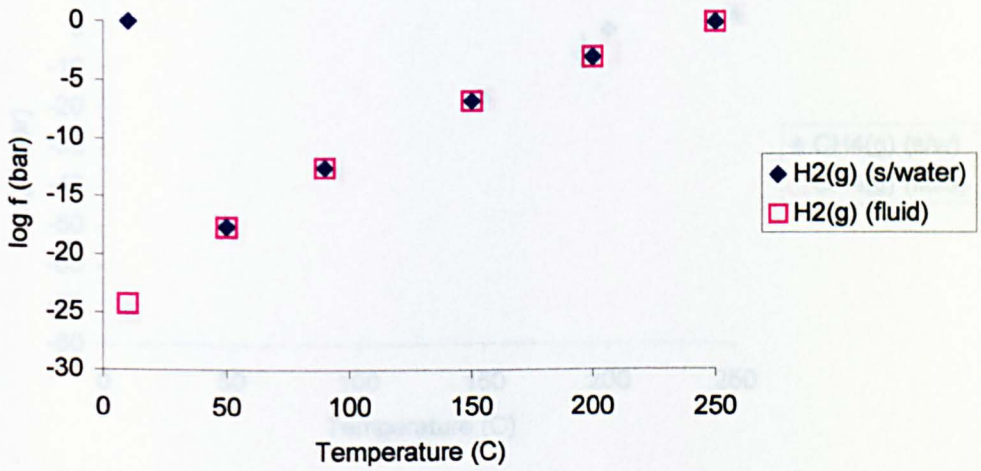

Figure A46
Oxygen Fugacity

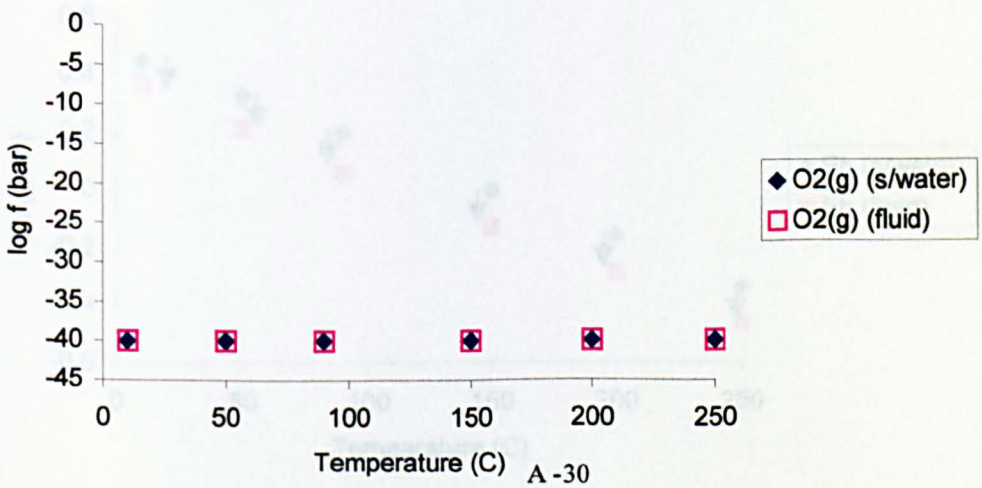

Figure A47
CO2 Fugacity

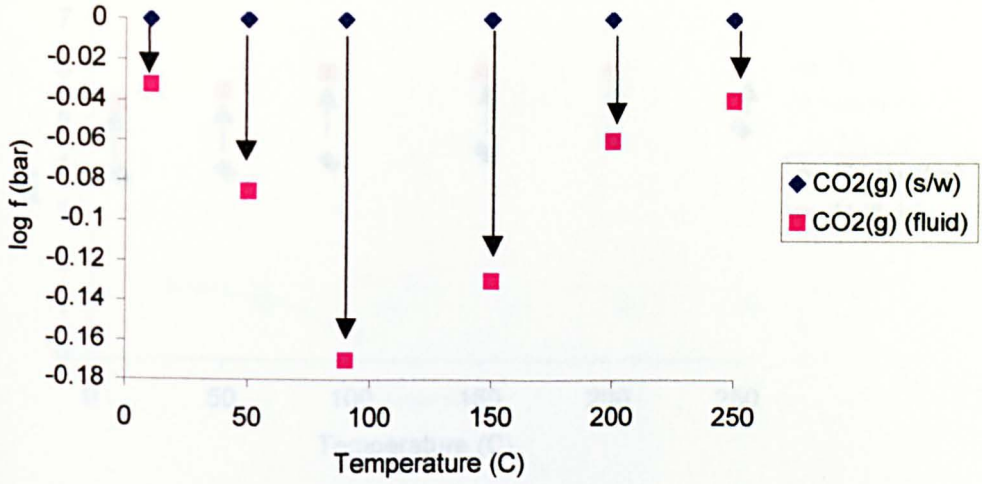

Figure A48
Methane Fugacity

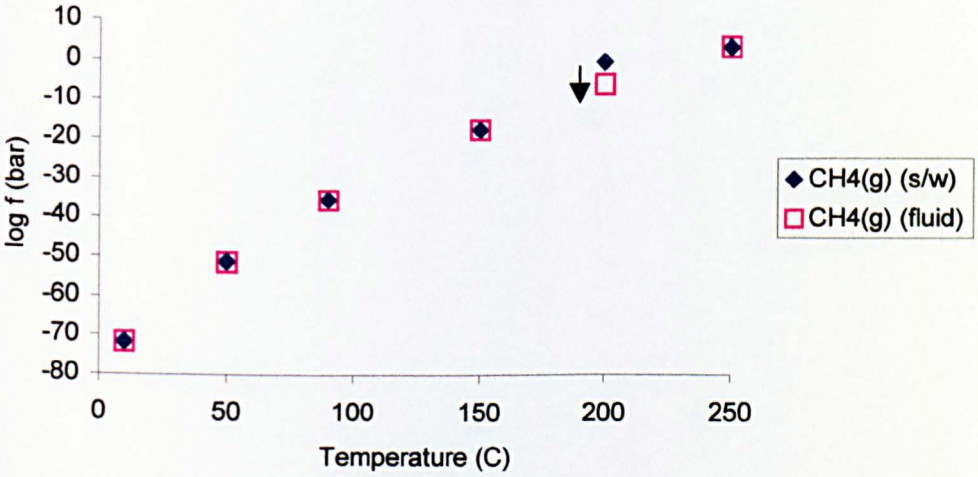

Figure A49
Oxidation State

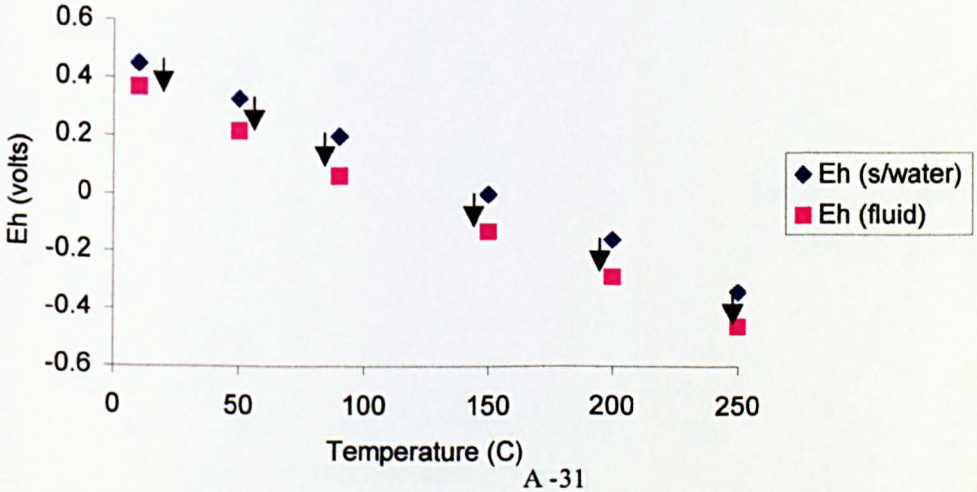

Figure A50
System pH

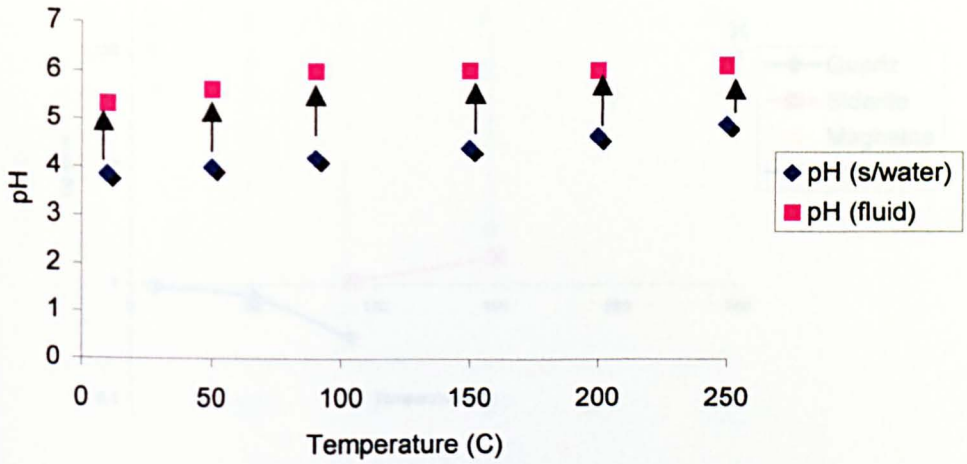

Figure A51 - A57. Products resulting from 1 mmol Forsterite and 10 bar CO2 reacted with 1kg seawater at various temperatures

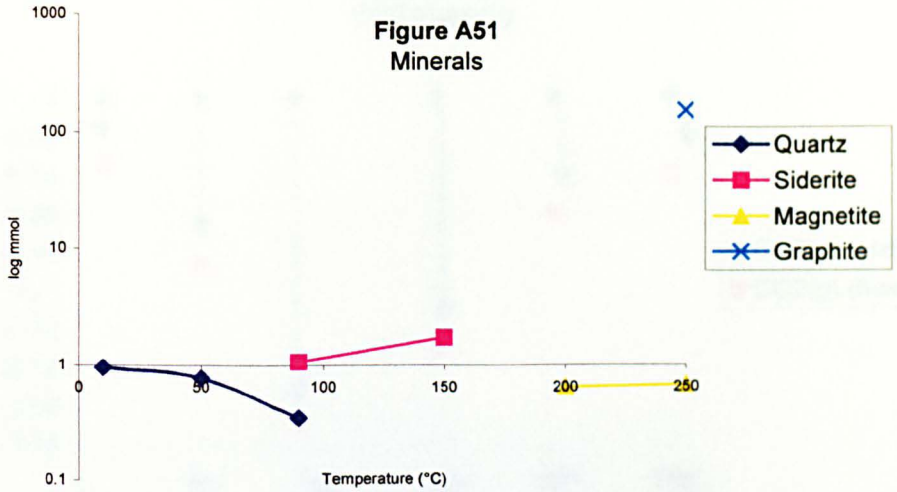

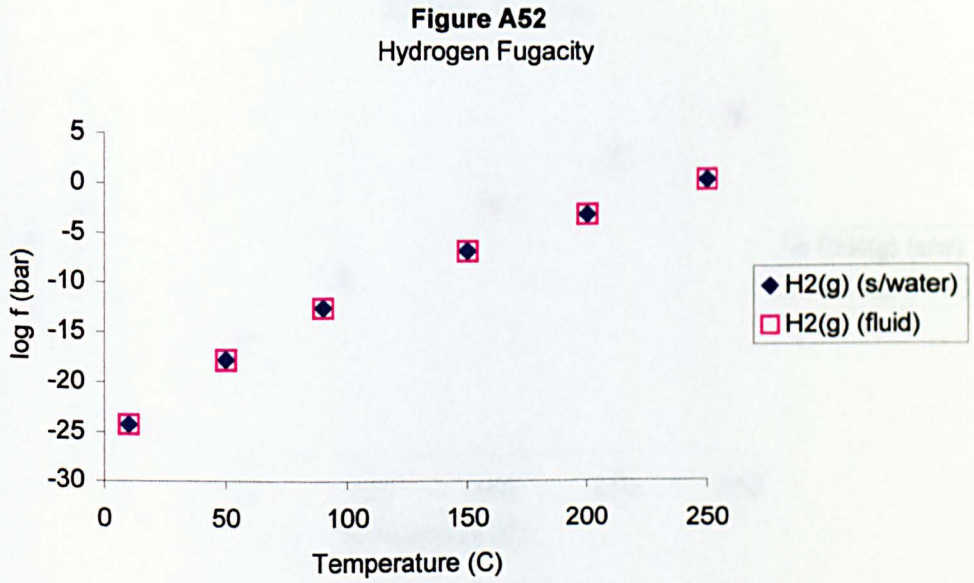

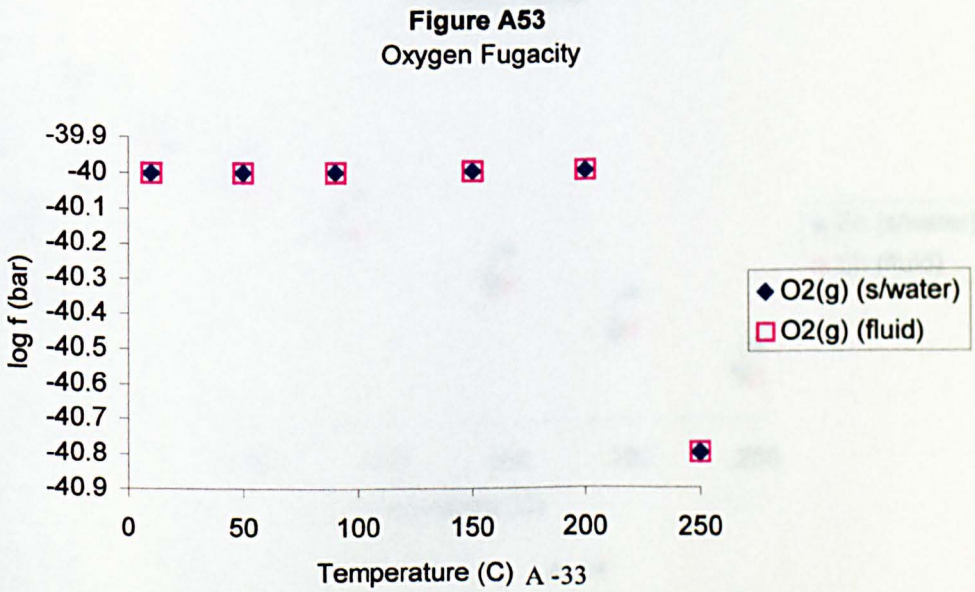

Figure A54
CO2 Fugacity

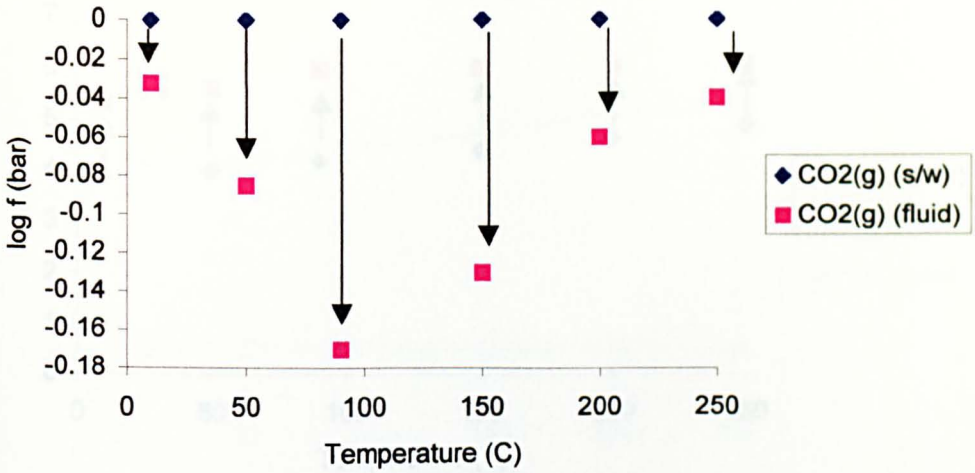

Figure A55
Methane Fugacity

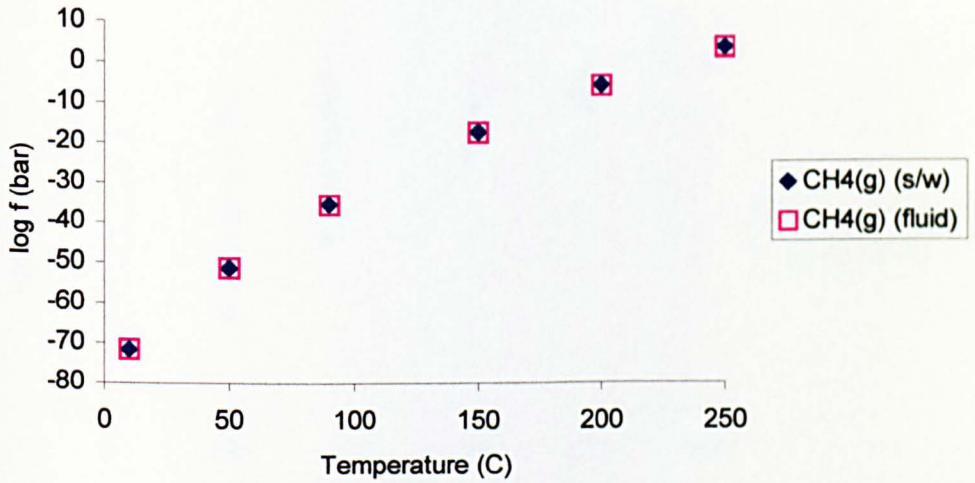

Figure A56
Oxidation State

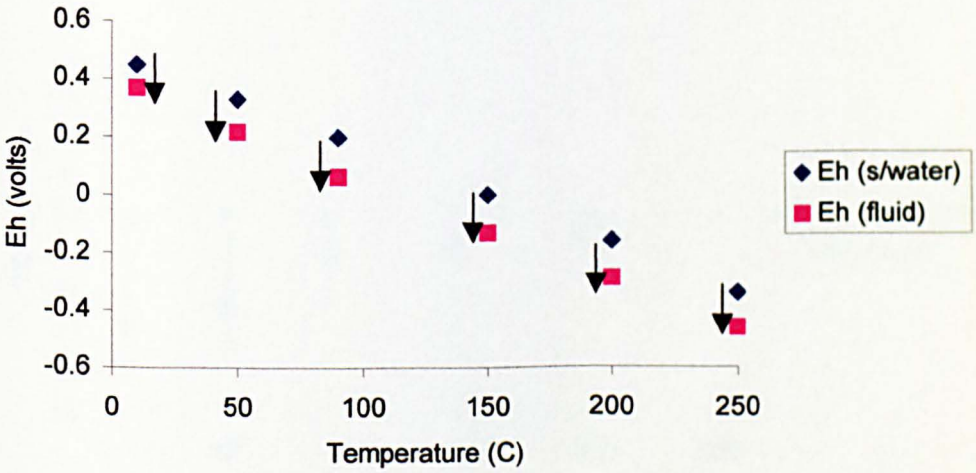

Figure A57
System pH

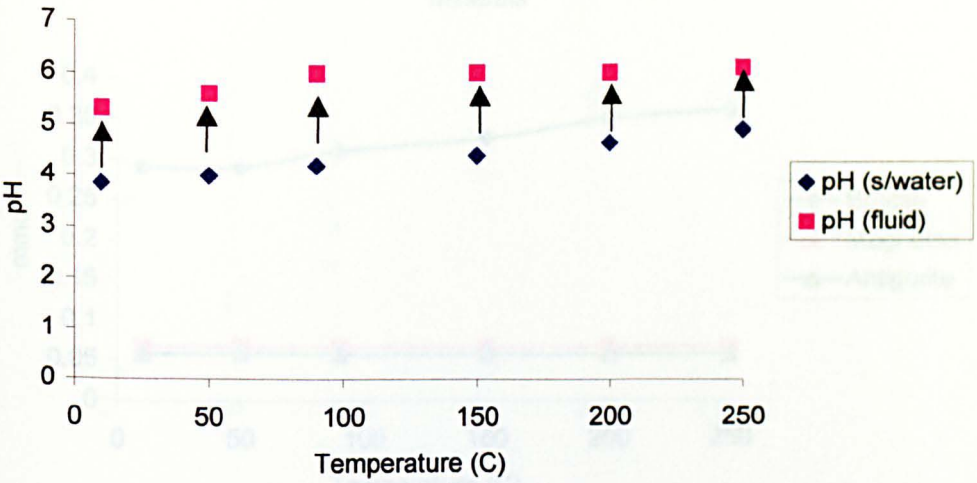

Figures A58-64 Products resulting from 1 mmol Forsterite, Fayalite and 0.0003 bar CO2 reacted with 1kg seawater at various temperatures

Figure A58
Minerals

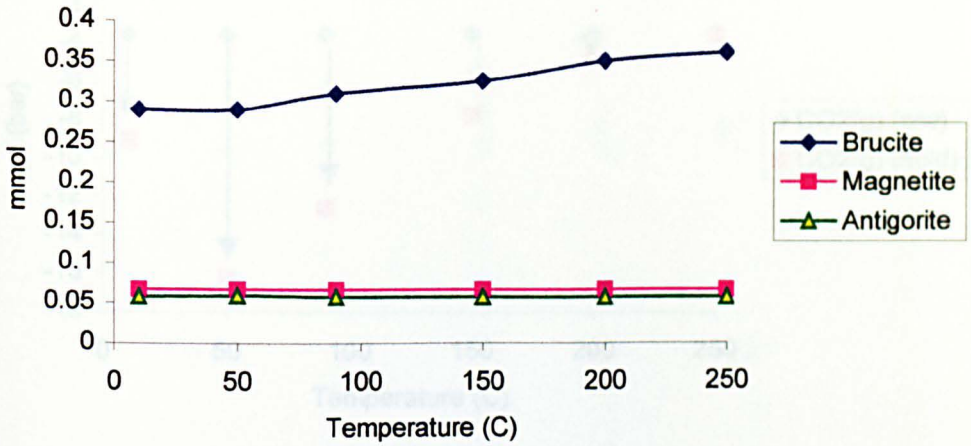

Figure A59
Hydrogen Fugacity

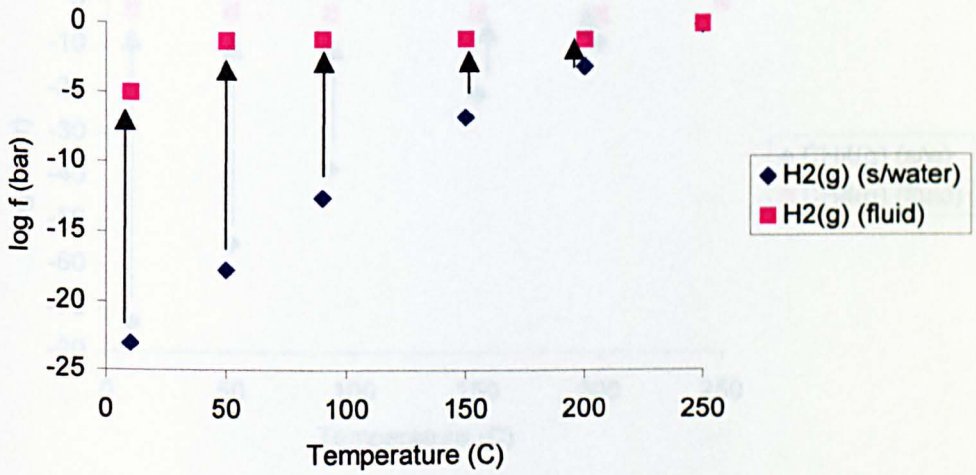

Figure A60
Oxygen Fugacity

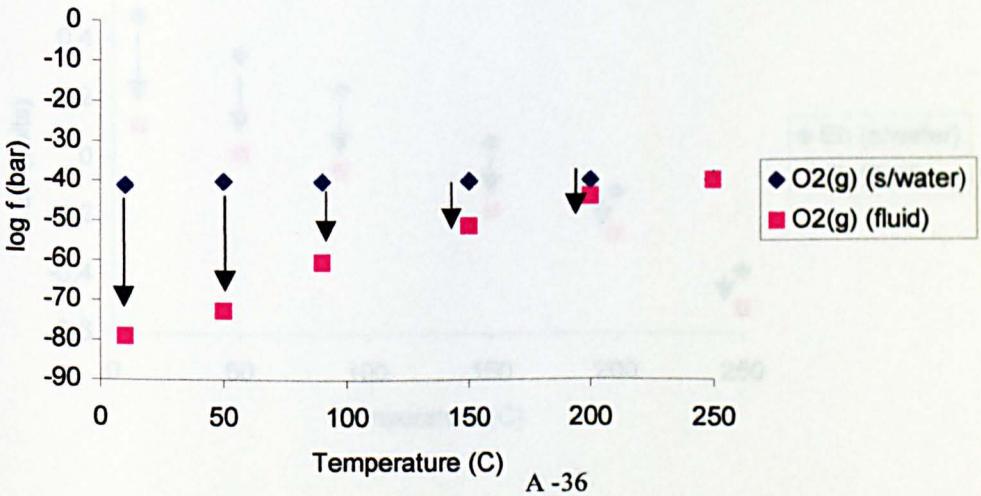

Figure A61
CO2 Fugacity

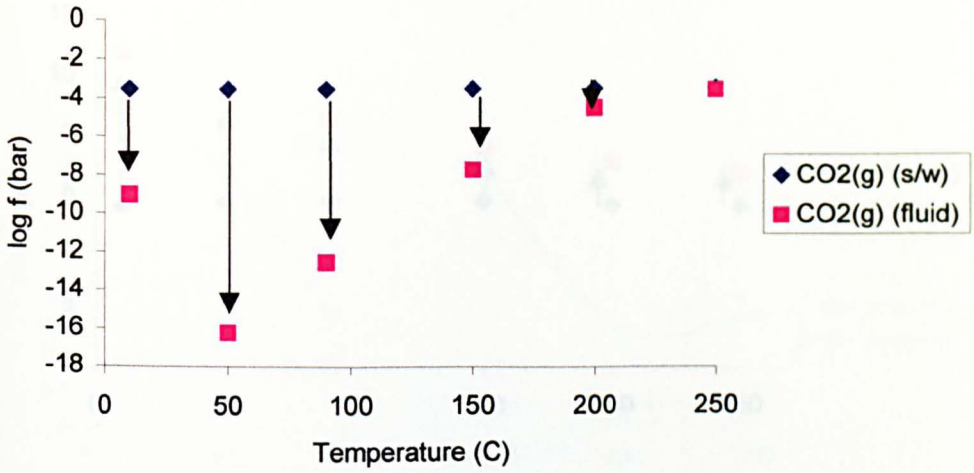

Figure A62
Methane Fugacity

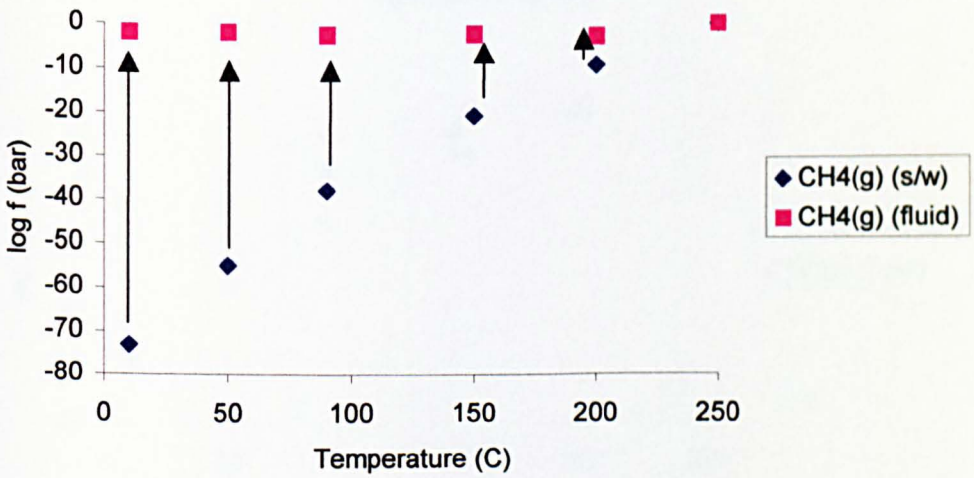

Figure A63
Oxidation State

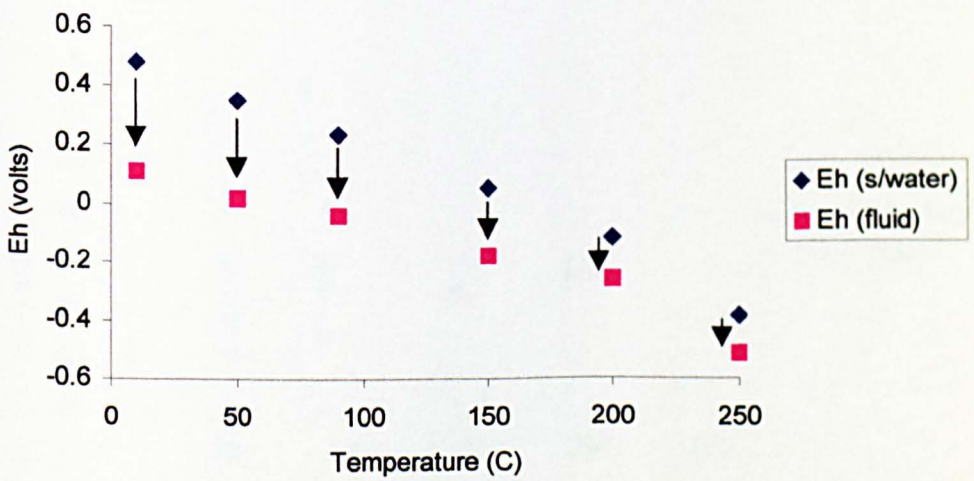

Figure A64
System pH

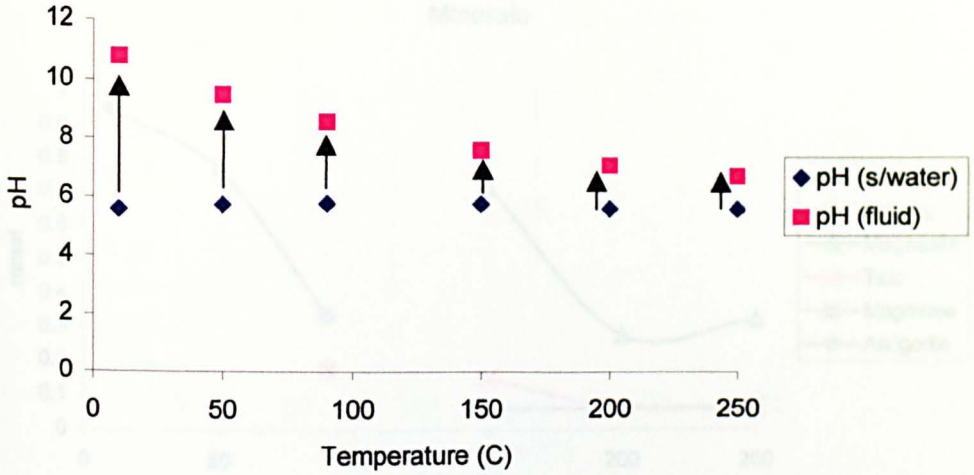

Figures A65 - A71. Products resulting from 1 mmol Forsterite, Fayalite and 1 bar CO2 reacted with 1kg seawater at various temperatures

Figure A65
Minerals

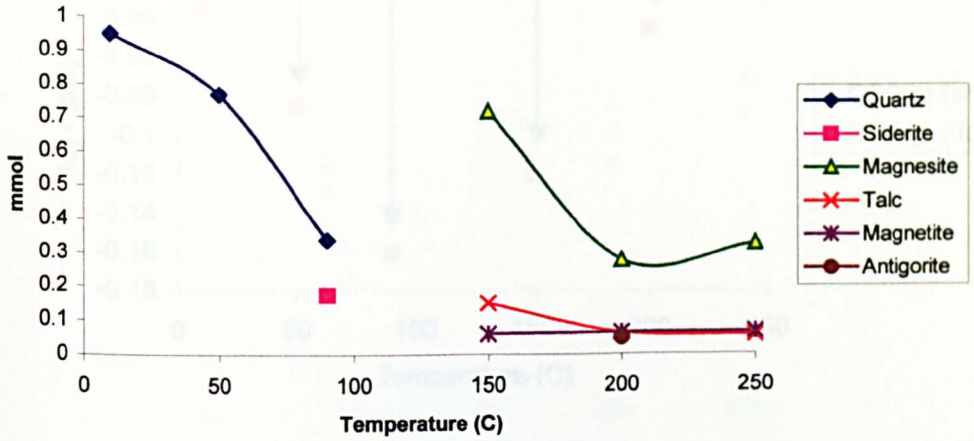

Figure A66
Hydrogen Fugacity

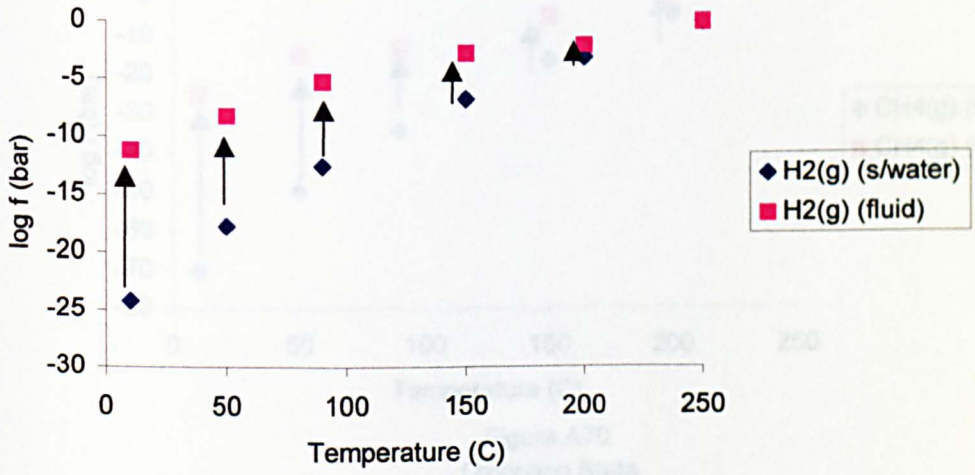

Figure A67
Oxygen Fugacity

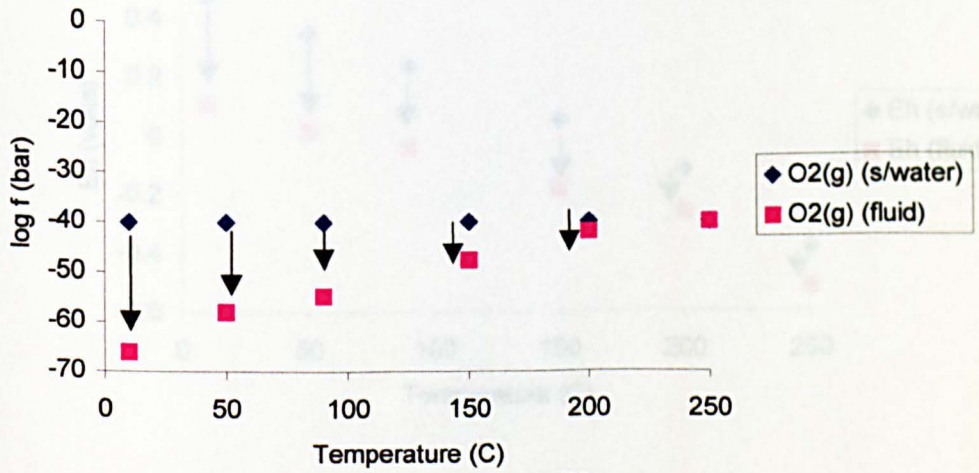

Figure A68
CO2 Fugacity

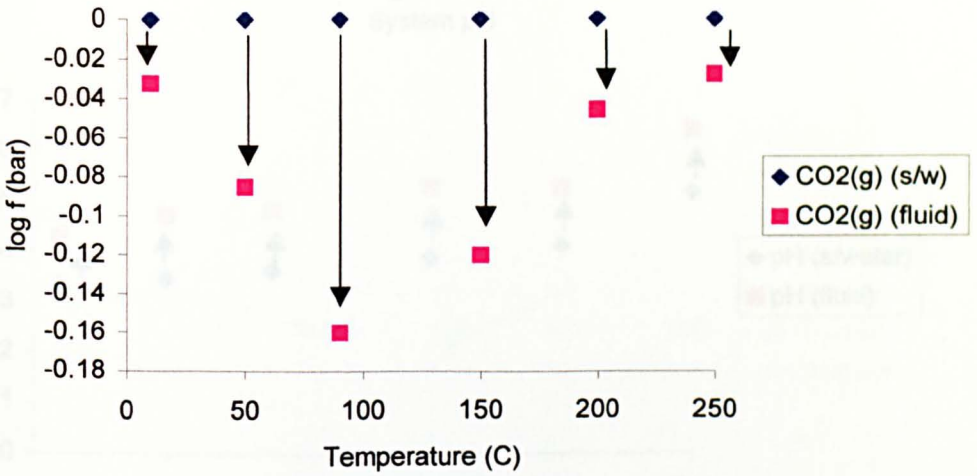

Figure A69
Methane Fugacity

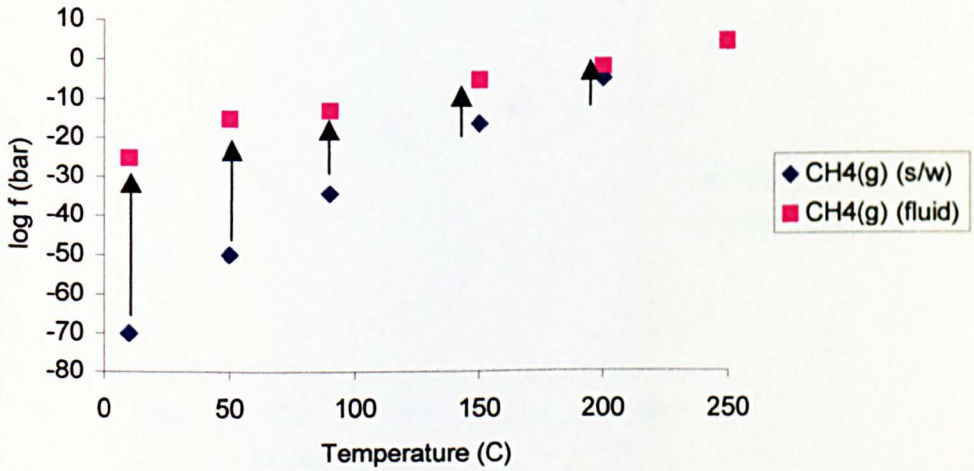

Figure A70
Oxidation State

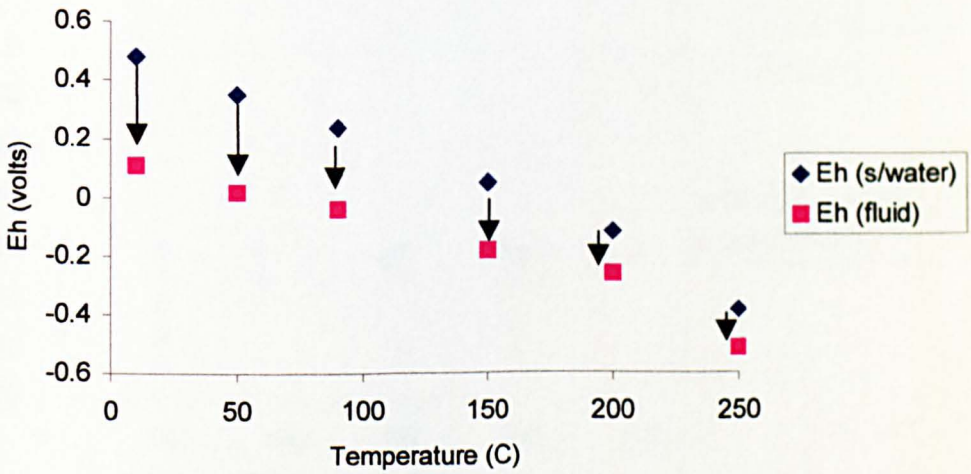

Figure A71
System pH

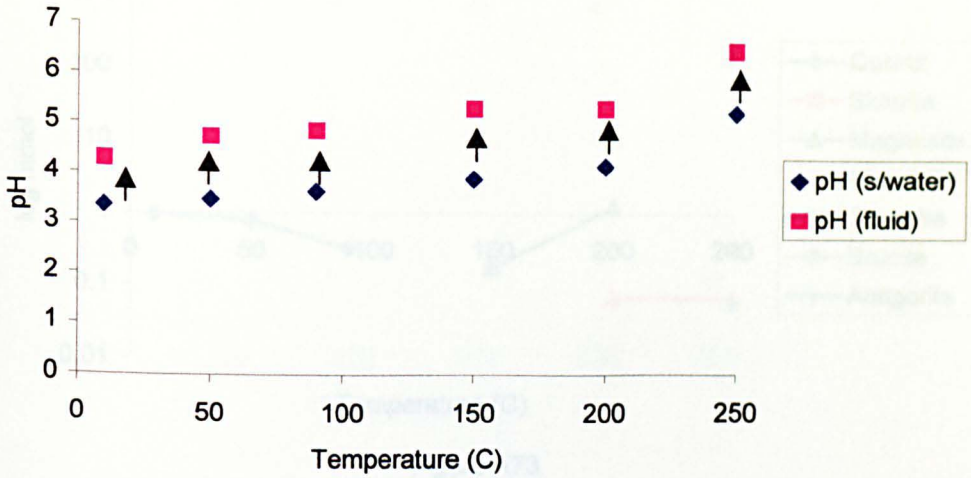

Figures A72-A78. Products resulting from 1 mmol Forsterite, Fayalite and 10 bar CO2 reacted with 1kg seawater at various temperatures

Figure A72
Minerals

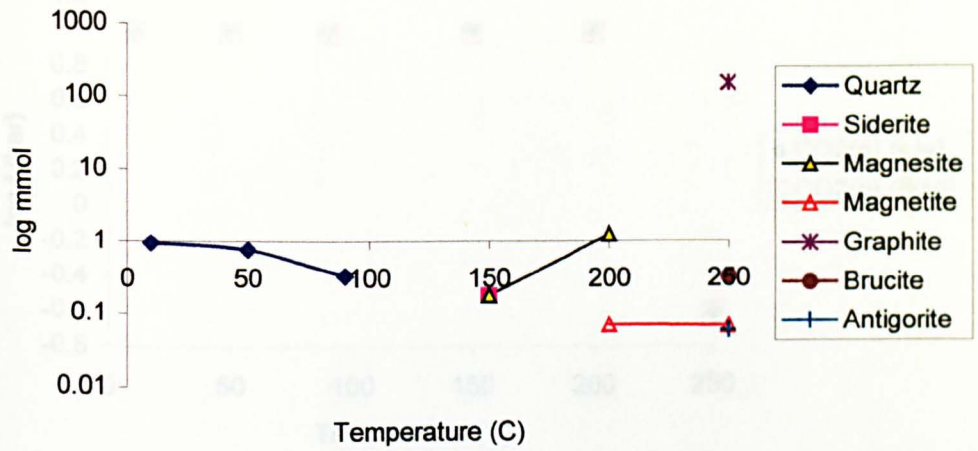

Figure A73
Hydrogen Fugacity

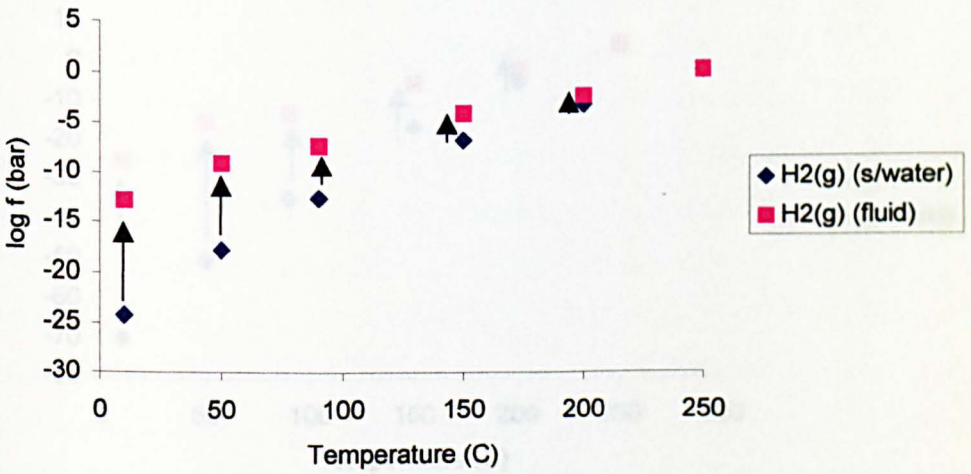

Figure A74
Oxygen Fugacity

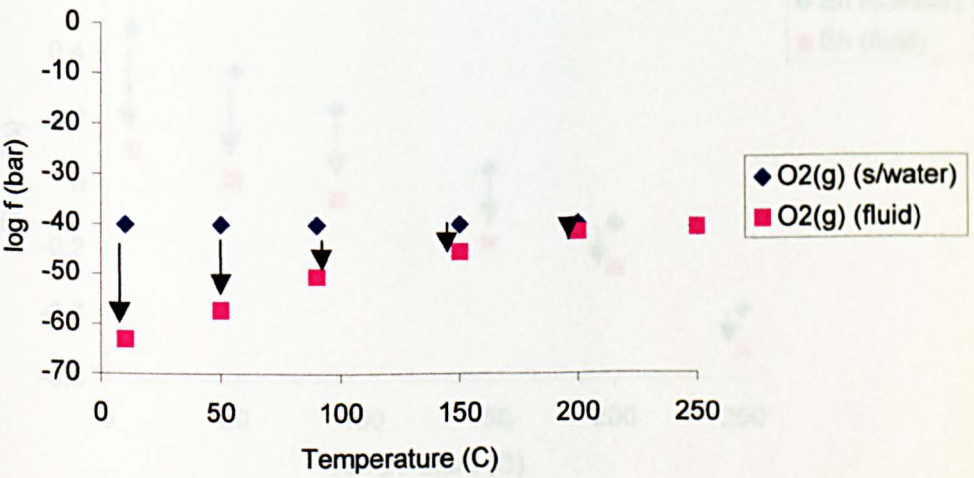

Figure A75
CO2 Fugacity

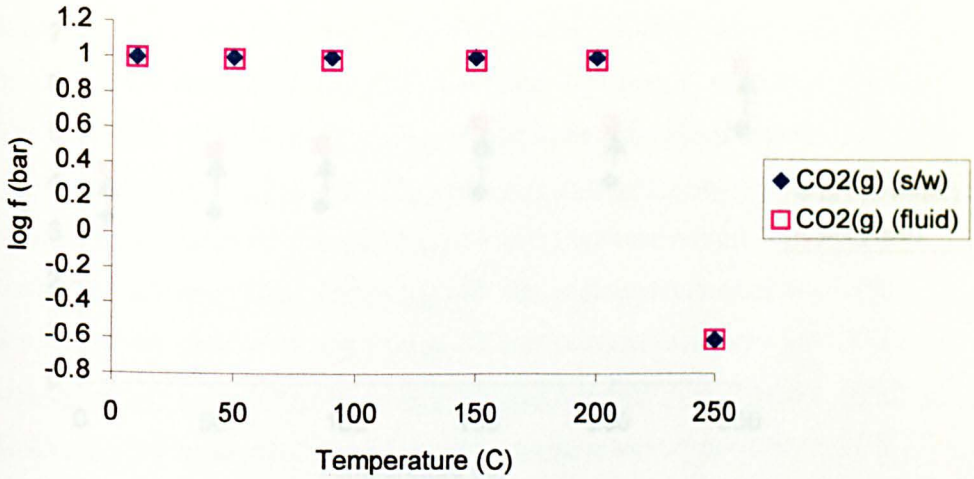

Figure A76
Methane Fugacity

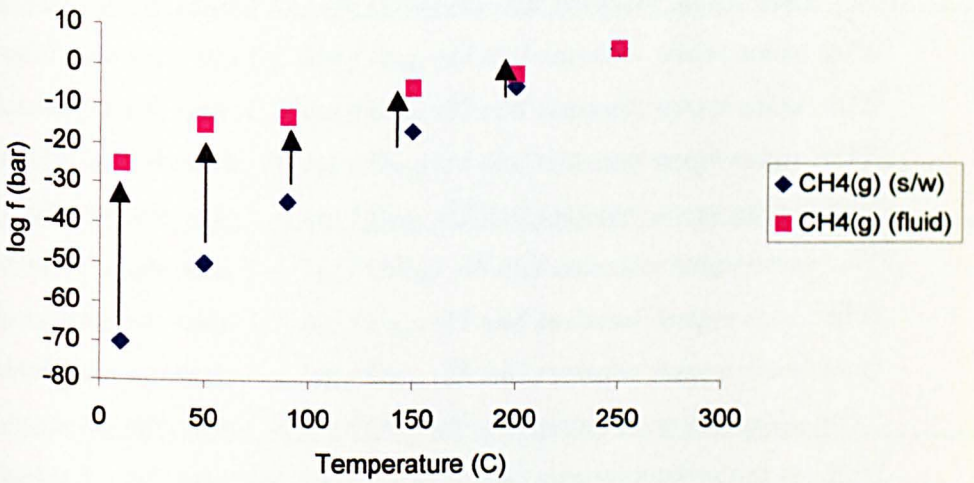

Figure A77
Oxidation State

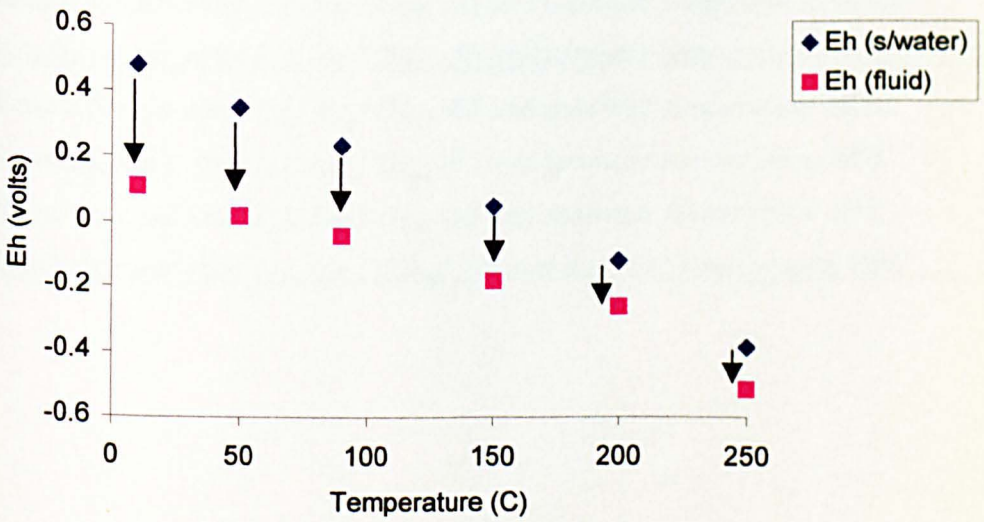

Figure A78
System pH

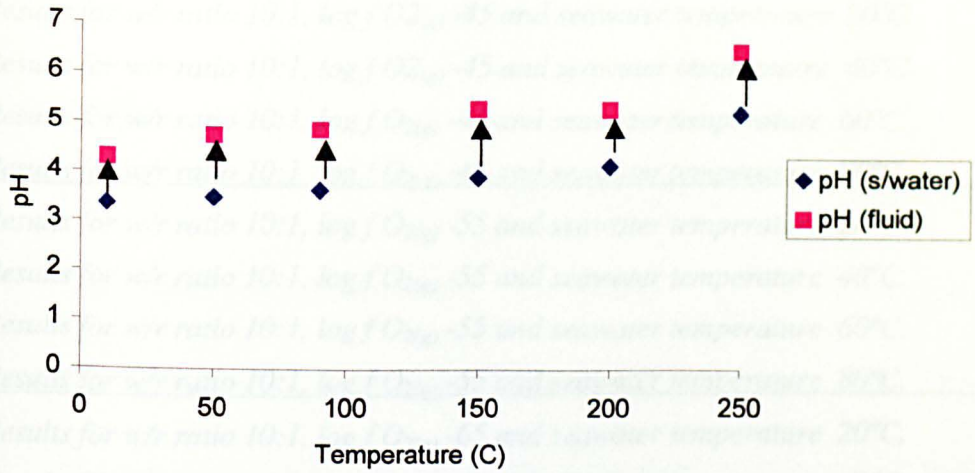

Appendix 3

	Model
Results for w/r ratio 10:1, log f $O_{2(g)}$ -35 and seawater temperature 20°C	*Model 1a*
Results for w/r ratio 10:1, log f $O_{2(g)}$ -35 and seawater temperature 40°C.	*Model 1b*
Results for w/r ratio 10:1, log f $O_{2(g)}$ -35 and seawater temperature 60°C.	*Model 1c*
Results for w/r ratio 10:1, log f $O_{2(g)}$ -35 and seawater temperature 80°C.	*Model 1d*
Results for w/r ratio 10:1, log f $O2_{(g)}$ -45 and seawater temperature 20°C.	*Model 2a*
Results for w/r ratio 10:1, log f $O2_{(g)}$ -45 and seawater temperature 40°C.	*Model 2b*
Results for w/r ratio 10:1, log f $O_{2(g)}$ -45 and seawater temperature 60°C.	*Model 2c*
Results for w/r ratio 10:1, log f $O_{2(g)}$ -45 and seawater temperature 80°C.	*Model 2d*
Results for w/r ratio 10:1, log f $O_{2(g)}$ -55 and seawater temperature 20°C.	*Model 3a*
Results for w/r ratio 10:1, log f $O_{2(g)}$ -55 and seawater temperature 40°C.	*Model 3b*
Results for w/r ratio 10:1, log f $O_{2(g)}$ -55 and seawater temperature 60°C.	*Model 3c*
Results for w/r ratio 10:1, log f $O_{2(g)}$ -55 and seawater temperature 80°C.	*Model 3d*
Results for w/r ratio 10:1, log f $O_{2(g)}$ -65 and seawater temperature 20°C.	*Model 4a*
Results for w/r ratio 10:1, log f $O_{2(g)}$ -65 and seawater temperature 40°C.	*Model 4b*
Results for w/r ratio 10:1, log f $O_{2(g)}$ -65 and seawater temperature 60°C.	*Model 4c*
Results for w/r ratio 10:1, log f $O_{2(g)}$ -65 and seawater temperature 80°C.	*Model 4d*
Results for w/r ratio 1:1, log f $O_{2(g)}$ -35 and seawater temperature 20°C.	*Model 5a*
Results for w/r ratio 1:1, log f $O_{2(g)}$ -35 and seawater temperature 40°C.	*Model 5b*
Results for w/r ratio 1:1, log f $O_{2(g)}$ -35 and seawater temperature 60°C.	*Model 5c*
Results for w/r ratio 1:1, log f $O_{2(g)}$ -35 and seawater temperature 80°C.	*Model 5d*
Results for w/r ratio 1:1, log f O2(g) -45 and seawater temperature 20°C.	*Model 6a*
Results for w/r ratio 1:1, log f $O_{2(g)}$ -45 and seawater temperature 40°C.	*Model 6b*
Results for w/r ratio 1:1, log f $O_{2(g)}$ -45 and seawater temperature 60°C.	*Model 6c*
Results for w/r ratio 1:1, log f $O_{2(g)}$ -45 and seawater temperature 80°C.	*Model 6d*
Results for w/r ratio 1:1, log f $O_{2(g)}$ -55 and seawater temperature 20°C.	*Model 7a*
Results for w/r ratio 1:1, log f $O_{2(g)}$ -55 and seawater temperature 40°C.	*Model 7b*
Results for w/r ratio 1:1, log f $O_{2(g)}$ -55 and seawater temperature 60°C.	*Model 7c*
Results for w/r ratio 1:1, log f $O_{2(g)}$ -55 and seawater temperature 80°C.	*Model 7d*
Results for w/r ratio 1:1, log f $O_{2(g)}$ -65 and seawater temperature 20°C.	*Model 8a*
Results for w/r ratio 1:1, log f $O_{2(g)}$ -65 and seawater temperature 40°C.	*Model 8b*
Results for w/r ratio 1:1, log f $O_{2(g)}$ -65 and seawater temperature 60°C.	*Model 8c*
Results for w/r ratio 1:1, log f O2(g) -65 and seawater temperature 80°C.	*Model 8d*

Key for Appendix 3

w/r water/rock ratio

f fugacity

s/w, seawater Hadean seawater

fluid hydrothermal fluid

rock ultramafic rock

Amino acids

Gly Glycine	**Met** Methionine	**Ala** Alanine
Asp Aspartate (or Aspartic acid)	**Ser** Serine	**Asn** Asparagine
Glu Glutamate (or Glutamic acid)	**Val** Valine	**Thr** Threonine
Gln Glutamine	**Ile** Isoleucine	**Leu** Leucine
Phe Phenylalanine	**Tyr** Tyrosine	**Trp** Tryptophan

Model 1a

Experimental Results for w/r ratio 10:1, log f O2(g) -35 and s/w temperature 20°C

	Seawater/Rock Products				Fluid/Seawater Products			
	Initial	**Final**			**Swater**	**Fluid**	**Final**	
log f O2(g)	-34.75	-48			-34.75	150	-56.3	
Temp (°C)	20	150			20	150	85	
pH	3.39	6.26			3.39	6.26	4.3	
Eh(Volts)	-0.52	-0.33			0.52	-0.33	-0.8	
Minerals(mmol)	Magnesite	213	Talc	19	Graphite	1.75		
	Saponite-Mg	83	Graphite	13.4				
	Dolomite-ord	82	Antigorite	10				
	Magnetite	28	Pyrite	5.7				
Amino Acids	Gly	6.80E-15	Val	Phe	Gly	1.25E-17	Glu	Phe
(mmol)	Met	1.90E-16	Glu	Tyr	Met	3.10E-20	Val	Tyr
	Ala	5.00E-19	Thr	Trp	Ala	1.25E-23	Thr	Trp
	Asp		Gln		Asp		Gln	
	Ser		Ile		Ser		Ile	
	Asn		Leu		Asn		Leu	
Dissolved species	**SO4--**	**H2S**	**HS-**		**SO4--**	**H2S**	**HS-**	
(mmol)	~0	0.0078	0.005		~0	0.013	8.50E-05	
	N2	**NH3**	**NH4+**		**N2**	**NH3**	**NH4+**	
	0.1	0.325	0.6		~0	8.50E-04	2.25	
	CO2	**CH4**			**CO2**	**CH4**		
	~5	1.4			4.05E+02	6.80E-04		
	H2				**H2**			
	0.004				1.40E-05			

Model 1b

Experimental Results for w/r ratio 10:1, log f O2(g) -35 and s/w temperature 40°C

	Seawater/Rock Products				Fluid/Seawater Products			
	Initial	**Final**			**Seawater**	**Fluid**	**Final**	
log f O2(g)	-34.78	-49.2			-34.78	-49.2	-55	
Temp (°C)	40	150			40	150	95	
pH	3.45	6.6			3.45	6.6	4.5	
Eh(Volts)	0.46	-0.38			0.46	-0.38	-0.11	
Minerals(mmol)	Dolomite-Ord	82	Antigorite	17	Graphite	6.3		
	Magnesite	57	Graphite	9.2	Diaspore	6.50E-04		
	Saponite-Mg	35	Clinochlore-1	8				
	Magnetite	28	Pyrite	5.7				
Amino Acids	Gly	5.50E-15	Val	Phe	Gly	2.75E-17	Glu	Phe
(mmol)	Met	5.00E-16	Glu	Tyr	Met	1.70E-19	Val	Tyr
	Ala	6.50E-19	Thr	Trp	Ala	6.00E-23	Thr	Trp
	Asp		Gln		Asp		Gln	
	Ser		Ile		Ser		Ile	
	Asn		Leu		Asn		Leu	
Dissolved species	**SO4--**	**H2S**	**HS-**		**SO4--**	**H2S**	**HS-**	
(mmol)	~0	0.009	0.0125		~0	0.022	3E-04	
	N2	**NH3**	**NH4+**		**N2**	**NH3**	**NH4+**	
	0.048	0.43	0.36		~0	0.0017	1.75	
	CO2	**CH4**			**CO2**	**CH4**		
	~1	3.5			237	0.0025		
	H2				**H2**			
	0.0065				4.00E-05			

Model 1c

Experimental Results for w/r ratio 10:1, log f O2(g) -35 and s/w temperature 60°C

	Seawater/Rock Products				Fluid/Seawater Products			
	Initial	**Final**			**Seawater**	**Fluid**	**Final**	
log f O2(g)	-34.8	-50			-34.8	-50	-54	
Temp (°C)	60	150			60	150	105	
pH	3.52	7.25			3.52	7.25	4.7	
Eh(Volts)	~0	-0.47			~0	-0.47	-0.14	
Minerals(mmol)	Dolomite-ord	73	Calcite	9	Graphite	15.8		
	Magnetite	28	Pyrite	5.6				
	Antigorite	20	Saponite-Ca	2.8				
	Clinochlore-1⁴	13.2						
Amino Acids	Gly	3.10E-15	Glu	Gln	Gly	6.50E-17	Glu	Phe
(mmol)	Met	8.20E-16	Thr	Tyr	Met	4.00E-18	Val	Tyr
	Ala	5.50E-19	Ile	Trp	Ala	2.60E-22	Thr	Trp
	Asp		Leu		Asp		Gln	
	Ser		Asn		Ser		Ile	
	Val		Phe		Asn		Leu	
Dissolved species	**SO4--**	**H2S**	**HS-**		**SO4--**	**H2S**	**HS-**	
(mmol)	~0	0.012	0.16		~0	0.17	0.003	
	N2	**NH3**	**NH4+**		**N2**	**NH3**	**NH4+**	
	~0.001	0.68	0.06		0.01	0.0035	1.5	
	CO2	**CH4**			**CO2**	**CH4**		
	~0	8			155.5	0.0086		
	H2				**H2**			
	0.0155				1.00E-04			

Model 1d

Experimental Results for w/r ratio 10:1, log f O2(g) -35 and s/w temperature 80°C

	Seawater/Rock Products				Fluid/Seawater Products			
	Initial	Final			**Seawater**	**Fluid**	**Final**	
log f O2(g)	-34.82	**-51**			-34.82	-51	-52.5	
Temp (°C)	80	150			80	150	115	
pH	3.6	8.25			3.6	8.25	4.87	
Eh(Volts)	-0.35	-0.54			-0.35	-0.54	-0.15	
Minerals(mmol)	Calcite	47	Clinochlore-14A	13.7	Graphite	15.5		
	Dolomite-ord	35	Pyrite	5.2	Diaspore	0.0065		
	Magnetite	28			Pyrite	0.001		
	Antigorite	20						
Amino Acids	**None stable above 137°C**				Gly	1.80E-16	Glu	Phe
(mmol)					Met	7.00E-16	Val	Tyr
					Ala	1.25E-21	Thr	Trp
					Asp		Gln	
					Ser		Ile	
					Asn		Leu	
Dissolved species	**SO4--**	**H2S**	**HS-**		**SO4--**	**H2S**	**HS-**	
(mmol)	~0	0.0078	0.0042		~0	1.05	0.028	
	N2	**NH3**	**NH4+**		**N2**	**NH3**	**NH4+**	
	~0	~0	~0		~0	0.0077	1.4	
	CO2	**CH4**			**CO2**	**CH4**		
	~5	1.37			115.5	0.025		
	H2				**H2**			
	0.0041				0.00025			

Model 2a

Experimental Results for w/r ratio 10:1, log f O2(g) -45 and s/w temperature 20°C

	Seawater/Rock Products				Fluid/Seawater Products			
	Initial	**Final**			**Seawater**	**Fluid**	**Final**	
log f O2(g)	-44.75	-49			-44.75	-49	-56.5	
Temp (°C)	20	150			20	150	85	
pH	3.25	6.25			3.25	6.25	4.3	
Eh(Volts)	0.37	-0.34			0.37	-0.34	-0.08	
Minerals(mmol)	Magnesite	213	Talc	19	Graphite	1.74		
	Saponite-Mg	83	Graphite	13.5				
	Dolomite-ord	82	Antigorite	10				
	Magnetite	28	Pyrite	5.7				
Amino Acids	Gly	6.70E-15	Val	Phe	Gly	1.25E-17	Glu	Phe
(mmol)	Met	2.00E-16	Glu	Tyr	Met	3.30E-20	Val	Tyr
	Ala	5.00E-19	Thr	Trp	Ala	1.25E-23	Thr	Trp
	Asp		Gln		Asp		Gln	
	Ser		Ile		Ser		Ile	
	Asn		Leu		Asn		Leu	
Dissolved species	**SO4--**	**H2S**	**HS-**		**SO4--**	**H2S**	**HS-**	
(mmol)	~0	0.0078	0.005		~0	0.013	8.50E-05	
	N2	**NH3**	**NH4+**		**N2**	**NH3**	**NH4+**	
	0.1	0.326	0.6		~0	8.50E-04	2.25	
	CO2	**CH4**			**CO2**	**CH4**		
	~5	1.4			4.05E+02	7.00E-04		
	H2				**H2**			
	0.004				1.40E-05			

Model 2b

Experimental Results for w/r ratio 10:1, log f O2(g) -45 and s/w temperature 40°C

	Seawater/Rock Products				Fluid/Seawater Products			
	Initial	**Final**			**Seawater**	**Fluid**	**Final**	
log f O2(g)	-44.78	-49.3			-44.78	-49.3	-55	
Temp (°C)	40	150			40	150	95	
pH	3.5	6.6			3.5	6.6	4.5	
Eh(Volts)	0.31	-0.375			0.31	-0.375	-0.12	
Minerals(mmol)	Dolomite-ord	83	Antigorite	16.8	Graphite	6.4		
	Magnesite	56	Graphite	9.25	Diaspore	~0		
	Saponite-Mg	34	Clinochlore-14A	8				
	Magnetite	28	Pyrite	5.7				
Amino Acids	Gly	5.50E-15	Val	Phe	Gly	2.80E-17	Glu	Phe
(mmol)	Met	5.00E-16	Glu	Tyr	Met	1.70E-19	Val	Tyr
	Ala	6.50E-19	Thr	Trp	Ala	6.00E-23	Thr	Trp
	Asp		Gln		Asp		Gln	
	Ser		Ile		Ser		Ile	
	Asn		Leu		Asn		Leu	
Dissolved species	**SO4--**	**H2S**	**HS-**		**SO4--**	**H2S**	**HS-**	
(mmol)	~0	0.009	0.013		~0	0.023	0.00025	
	N2	**NH3**	**NH4+**		**N2**	**NH3**	**NH4+**	
	0.04	0.435	0.337		~0.01	0.0017	1.75	
	CO2	**CH4**			**CO2**	**CH4**		
	~1	3.55			237	0.0025		
	H2				**H2**			
	0.0065				4.00E-05			

Model 2c

Experimental Results for w/r ratio 10:1, log f O2(g) -45 and s/w temperature 60°C

	Seawater/Rock Products				Fluid/Seawater Products			
	Initial	**Final**			**Seawater**	**Fluid**	**Final**	
log f O2(g)	-44.8	-50			-44.8	-50	-53.6	
Temp (°C)	60	150			60	150	105	
pH	3.5	7.6			3.5	7.6	4.7	
Eh(Volts)	0.25	-0.47			0.25	-0.47	-0.14	
Minerals(mmol)	Dolomite-ord	73	Calcite	8.5	Graphite	15.6		
	Magnetite	27	Pyrite	5.7	Diaspore	0.006		
	Antigorite	20	Saponite-Ca	3.2	Pyrite	9.00E-04		
	Clinochlore-14A	13						
Amino Acids	Gly	2.80E-17	Val	Phe	Gly	7.00E-17	Glu	Phe
(mmol)	Met	1.70E-19	Glu	Tyr	Met	3.80E-18	Val	Tyr
	Ala	6.00E-23	Thr	Trp	Ala	2.70E-22	Thr	Trp
	Asp		Gln		Asp		Gln	
	Ser		Ile		Ser		Ile	
	Asn		Leu		Asn		Leu	
Dissolved species	**SO4--**	**H2S**	**HS-**		**SO4--**	**H2S**	**HS-**	
(mmol)	~0	0.012	0.16		~0	0.17	0.003	
	N2	**NH3**	**NH4+**		**N2**	**NH3**	**NH4+**	
	0.01	0.68	0.06		0.01	0.0035	1.5	
	CO2	**CH4**			**CO2**	**CH4**		
	~0	8			155.5	0.0085		
	H2				**H2**			
	0.015				1.00E-04			

Model 2d

Experimental Results for w/r ratio 10:1, log f O2(g) -45 and s/w temperature 80°C

	Seawater/Rock Products				Fluid/Seawater Products			
	Initial	**Final**			**Seawater**	**Fluid**	**Final**	
log f O2(g)	-44.84	-50.5			-44.84	-50.5	-52.3	
Temp (°C)	80	150			80	150	115	
pH	3.6	8.25			3.6	8.25	4.88	
Eh(Volts)	0.18	-0.55			0.18	-0.55	-0.17	
Minerals(mmol)	Calcite	46	Antigorite	20	Graphite	15.5		
	Dolomite-ord	35	Clinochlore-14A	13.8	Diaspore	0.0065		
	Brucite	30	Pyrite	4.15	Pyrite	0.001		
	Magnetite	27						
Amino Acids	**None stable above ~137°C**				Gly	1.80E-16	Glu	Phe
(mmol)					Met	7.00E-17	Val	Tyr
					Ala	1.25E-21	Thr	Trp
					Asp		Gln	
					Ser		Ile	
					Asn		Leu	
Dissolved species	**SO4--**	**H2S**	**HS-**		**SO4--**	**H2S**	**HS-**	
(mmol)	~0	0.0168	1.05		~0	1.05	0.028	
	N2	**NH3**	**NH4+**		**N2**	**NH3**	**NH4+**	
	~0	0.71	0.02		0.01	0.0077	1.4	
	CO2	**CH4**			**CO2**	**CH4**		
	~0	8			115.5	0.025		
	H2				**H2**			
	0.04				0.00025			

Model 3a

Experimental Results for w/r ratio 10:1, log f O2(g) -55 and s/w temperature 20°C

	Seawater/Rock Products				Fluid/Seawater Products			
	Initial	**Final**			**Seawater**	**Fluid**	**Final**	
log f O2(g)	-54.75	**-49**			-54.75	-49	-56.3	
Temp (°C)	20	150			20	150	85	
pH	3.4	6.3			3.4	6.3	4.3	
Eh(Volts)	0.225	-0.32			0.225	-0.32	0.08	
Minerals(mmol)	Magnesite	213	Talc	20	Graphite	1.74		
	Saponite-Mg	83	Graphite	13.4				
	Dolomite-ord	82	Antigorite	10				
	Magnetite	28	Pyrite	6				
Amino Acids	Gly	6.70E-15	Val	Phe	Gly	1.25E-17	Glu	Phe
(mmol)	Met	2.00E-16	Glu	Tyr	Met	3.25E-20	Val	Tyr
	Ala	5.00E-19	Thr	Trp	Ala	1.25E-23	Thr	Trp
	Asp		Gln		Asp		Gln	
	Ser		Ile		Ser		Ile	
	Asn		Leu		Asn		Leu	
Dissolved species	**SO4--**	**H2S**	**HS-**		**SO4--**	**H2S**	**HS-**	
(mmol)	~0	0.008	0.005		~0	0.013	8.50E-05	
	N2	**NH3**	**NH4+**		**N2**	**NH3**	**NH4+**	
	0.1	0.33	0.6		~0	8.50E-04	2.25	
	CO2	**CH4**			**CO2**	**CH4**		
	~5	1.4			4.05E+02	7.00E-04		
	H2				**H2**			
	0.004				1.40E-05			

Model 3b

Experimental Results for w/r ratio 10:1, log f O2(g) -55 and s/w temperature 40°C

	Seawater/Rock Products				Fluid/Seawater Products			
	Initial	**Final**			**Seawater**	**Fluid**	**Final**	
log f O2(g)	-54.78	**-49.3**			-54.78	-49.3	-55	
Temp (°C)	40	150			40	150	95	
pH	3.5	6.55			3.5	6.55	4.5	
Eh(Volts)	0.15	-0.375			0.15	-0.375	-0.12	
Minerals(mmol)	Dolomite-ord	82	Antigorite	17	Graphite	6.4		
	Magnesite	60	Graphite	9.2	Diaspore	6.50E-04		
	Saponite-Mg	35	Clinochlore-14A	8				
	Magetite	28	Pyrite	5.7				
Amino Acids	Gly	5.50E-15	Val	Phe	Gly	2.80E-17	Glu	Phe
(mmol)	Met	5.00E-16	Glu	Tyr	Met	1.70E-19	Val	Tyr
	Ala	6.50E-19	Thr	Trp	Ala	6.00E-23	Thr	Trp
	Asp		Gln		Asp		Gln	
	Ser		Ile		Ser		Ile	
	Asn		Leu		Asn		Leu	
Dissolved species	**SO4--**	**H2S**	**HS-**		**SO4--**	**H2S**	**HS-**	
(mmol)	~0	0.009	0.013		~0	0.022	0.00025	
	N2	**NH3**	**NH4+**		**N2**	**NH3**	**NH4+**	
	0.04	0.44	0.37		~0	0.0017	1.75	
	CO2	**CH4**			**CO2**	**CH4**		
	~1	3.5			237	0.0025		
	H2				**H2**			
	0.0065				4.00E-05			

Model 3c

Experimental Results for w/r ratio 10:1, log f O2(g) -55 and s/w temperature 60°C

	Seawater/Rock Products				Fluid/Seawater Products			
	Initial	**Final**			**Seawater**	**Fluid**	**Final**	
log f O2(g)	-54.82	-50			-54.82	-50	-53.5	
Temp (°C)	60	150			60	150	105	
pH	3.5	7.6			3.5	7.6	4.7	
Eh(Volts)	0.08	-0.47			0.08	-0.47	-0.14	
Minerals(mmol)	Dolomite-ord	73	Calcite	8.4	Graphite	15.6		
	Magnetite	28	Pyrite	5.6	Diaspore	0.006		
	Antigorite	20	Saponite-Ca	3.2	Pyrite	9.00E-04		
	Clinochlore-14A	13						
Amino Acids	**None stable above ~145°C**				Gly	7.00E-17	Glu	Phe
(mmol)					Met	4.00E-18	Val	Tyr
					Ala	2.60E-29	Thr	Trp
					Asp		Gln	
					Ser		Ile	
					Asn		Leu	
Dissolved species	**SO4--**	**H2S**	**HS-**		**SO4--**	**H2S**	**HS-**	
(mmol)	~0	0.012	0.16		~0	0.17	0.003	
	N2	**NH3**	**NH4+**		**N2**	**NH3**	**NH4+**	
	0.01	0.7	0.6		0.01	0.0035	1.52	
	CO2	**CH4**			**CO2**	**CH4**		
	~0	8			155.5	0.0085		
	H2				**H2**			
	0.015				1.00E-04			

Model 3d

Experimental Results for w/r ratio 10:1, log f O2(g) -55 and s/w temperature 80°C

	Seawater/Rock Products				Fluid/Seawater Products			
	Initial	**Final**			**Seawater**	**Fluid**	**Final**	
log f O2(g)	-54.84	**-50.9**			-54.84	-50.9	-52.3	
Temp (°C)	80	150			80	150	115	
pH	4	8.25			4	8.25	5	
Eh(Volts)	-0.048	-0.55			-0.048	-0.55	-0.175	
Minerals(mmol)	Calcite	46	Antigorite	20	Graphite	15.6		
	Dolomite-ord	36	Clinochlore-14A	13.8	Diaspore	0.0065		
	Brucite	30	Pyrite	5.1	Pyrite	0.001		
	Magnetite	28						
Amino Acids	**None stable above ~137°C**				Gly	4.50E-16	Glu	Phe
(mmol)					Met	1.80E-16	Val	Tyr
					Ala	3.10E-21	Thr	Trp
					Asp		Gln	
					Ser		Ile	
					Asn		Leu	
Dissolved species	**SO4--**	**H2S**	**HS-**		**SO4--**	**H2S**	**HS-**	
(mmol)	~0	0.017	1.05		~0	1.05	0.04	
	N2	**NH3**	**NH4+**		**N2**	**NH3**	**NH4+**	
	0.35	1.34	0.03		0.05	0.02	2.6	
	CO2	**CH4**			**CO2**	**CH4**		
	~0	8			115	0.025		
	H2				**H2**			
	0.04				0.00025			

Model 4a

Experimental Results for w/r ratio 10:1, log f O2(g) -65 and s/w temperature 20°C

	Seawater/Rock Products				Fluid/Seawater Products			
	Initial	**Final**			**Seawater**	**Fluid**	**Final**	
log f O2(g)	-64.75	-49			-64.75	-49	-56.4	
Temp (°C)	20	150			20	150	85	
pH	3.4	6.3			3.4	6.3	4.35	
Eh(Volts)	0.08	-0.34			0.08	-0.34	-0.088	
Minerals(mmol)	Magnesite	213	Talc	20	Graphite	1.7		
	Saponite-Mg	83	Graphite	13.5				
	Dolomite-ord	82	Antigorite	10				
	Magnetite	28	Pyrite	5.7				
Amino Acids	Gly	7.00E-15	Val	Phe	Gly	1.35E-17	Glu	Phe
(mmol)	Met	2.10E-16	Glu	Tyr	Met	3.60E-20	Val	Tyr
	Ala	5.40E-19	Thr	Trp	Ala	1.45E-23	Thr	Trp
	Asp		Gln		Asp		Gln	
	Ser		Ile		Ser		Ile	
	Asn		Leu		Asn		Leu	
Dissolved species	**SO4--**	**H2S**	**HS-**		**SO4--**	**H2S**	**HS-**	
(mmol)	~0	0.008	0.005		~0	0.013	9.00E-05	
	N2	**NH3**	**NH4+**		**N2**	**NH3**	**NH4+**	
	0.115	0.35	0.65		0.01	9.50E-04	0.1	
	CO2	**CH4**			**CO2**	**CH4**		
	~5	1.38			404.5	7.00E-04		
	H2				**H2**			
	0.004				1.40E-05			

Model 4b

Experimental Results for w/r ratio 10:1, log f O2(g) -65 and s/w temperature 40°C

	Seawater/Rock Products				Fluid/Seawater Products			
	Initial	**Final**			**Seawater**	**Fluid**	**Final**	
log f O2(g)	-64.78	-56.3			-64.78	-56.3	-55	
Temp (°C)	40	150			40	150	95	
pH	4.8	6.8			4.8	6.8	5.12	
Eh(Volts)	-0.1	-0.38			-0.1	-0.38	-0.16	
Minerals(mmol)	Dolomite-ord	82	Antigorite	16.5	Graphite	7.5		
	Magnesite	62	Graphite	12.5	Diaspore	0.0011		
	Saponite-Mg	36	Clinochlore-14A	7.8	Pyrite	8.00E-04		
	Magnetite	28	Pyrite	5.7				
Amino Acids	Gly	1.35E-17	Val	Phe	Gly	8.10E-16	Glu	Phe
(mmol)	Met	3.60E-20	Glu	Tyr	Met	6.20E-18	Val	Tyr
	Ala	1.40E-23	Gln	Trp	Ala	1.70E-21	Gln	Trp
	Asn		Thr		Asp		Thr	
	Asp		Ile		Asn		Ile	
	Ser		Leu		Ser		Leu	
Dissolved species	**SO4--**	**H2S**	**HS-**		**SO4--**	**H2S**	**HS-**	
(mmol)	~0	0.009	0.021		1.00E-05	0.0275	0.0013	
	N2	**NH3**	**NH4+**		**N2**	**NH3**	**NH4+**	
	2.5	3.4	1.8		3.5	0.05	13.4	
	CO2	**CH4**			**CO2**	**CH4**		
	~5	3.55			234.5	0.00252		
	H2				**H2**			
	0.0065				4.00E-05			

Failed Run:Using balance on Cl- and pH set to 4.8 instead **Model 4c**

Experimental Results for w/r ratio 10:1, log f O2(g) -35 and s/w temperature 60°C

	Seawater/Rock Products				Fluid/Seawater Products			
	Initial	**Final**			**Seawater**	**Fluid**	**Final**	
log f O2(g)	-68.7	**-53.5**			-68.7	-53.5	-60	
Temp (°C)	60	150			60	150	105	
pH	5.62	5.68			5.6	5.68	6.12	
Eh(Volts)	-0.29	-0.38			-0.29	-0.38	-0.374	
Minerals(mmol)	Saponite-Mg	82	Pyrite	0.125	Troilite	0.23		
	Antigorite	12.2			Pyrite	0.01		
	Troilite	10.8						
	Clinochlore-14A	0.21						
Amino Acids	Met	2.25E-16	Ile	Phe	Met	5.60E-13	Leu	Phe
(mmol)	Gly	4.25E-18	Leu	Tyr	Gly	4.70E-16	Ser	Tyr
	Ala	1.10E-20	Asp	Trp	Ala	1.80E-18	Asp	Trp
	Val		Gln		Val		Gln	
	Asn		Thr		Asn		Thr	
	Ser		Glu		Ile		Glu	
Dissolved species	**SO4--**	**H2S**	**HS-**		**SO4--**	**H2S**	**HS-**	
(mmol)	~0	0.24	0.063		~0	0.0275	2.00E-02	
	N2	**NH3**	**NH4+**		**N2**	**NH3**	**NH4+**	
	0.14	820	11900		0.015	8.40E+02	24600	
	CO2	**CH4**			**CO2**	**CH4**		
	4.50E-05	8484			6.00E-06	1.70E+04		
	H2				**H2**			
	0.67				2.75E-01			

Failed Run:Using balance on Cl- and pH set to 4.8 instead **Model 4d**

Experimental Results for w/r ratio 10:1, log f O2(g) -35 and s/w temperature 80°C

	Seawater/Rock Products				Fluid/Seawater Products			
	Initial	**Final**			**Seawater**	**Fluid**	**Final**	
log f O2(g)	**Didn't run!**							
Temp (°C)	80	150			80	150	115	
pH								
Eh(Volts)								
Minerals(mmol)								
Amino Acids								
(mmol)								
Dissolved species	**SO4--**	**H2S**	**HS-**		**SO4--**	**H2S**	**HS-**	
(mmol)								
	N2	**NH3**	**NH4+**		**N2**	**NH3**	**NH4+**	
	CO2	**CH4**			**CO2**	**CH4**		
	H2				**H2**			

Model 5a

Experimental Results for w/r ratio 1:1, log f O2(g) -35 and s/w temperature 20°C

	Seawater/Rock Products				Fluid/Seawater Products			
	Initial	**Final**			**Seawater**	**Fluid**	**Final**	
log f O2(g)	-34.8	-52.5			-34.8	-52.5	-56.3	
Temp (°C)	20	150			20	150	85	
pH	3.39	9.3			3.39	9.3	5.01	
Eh(Volts)	0.52	-0.66			0.52	-0.66	-0.13	
Minerals(mmol)	Brucite	1360	Magnetite	150	Graphite	158		
	Calcite	325	Clinochlore-14-A	137	Pyrite	0.001		
	Antigorite	185	Troilite	105	Diaspore	0.07		
	Andradite	165						
Amino Acids	Some acids are stable over different temperature				Met	1.15E-16	Asn	Ile
(mmol)	ranges, but none are stable above 80°C except for				Gly		Glu	Leu
	Threonine.				Ala		Val	Phe
					Asp		Thr	Tyr
					Ser		Gln	Trp
Dissolved species	**SO4--**	**H2S**	**HS-**		**SO4--**	**H2S**	**HS-**	
(mmol)	~0	0.009	7		0.01	8.5	3.00E-01	
	N2	**NH3**	**NH4+**		**N2**	**NH3**	**NH4+**	
	0.51	1.15	~0		0.08	0.004	2.1	
	CO2	**CH4**			**CO2**	**CH4**		
	~0	80			3.05E+02	8.00E-04		
	H2				**H2**			
	0.225				1.48E-05			

Model 5b

Experimental Results for w/r ratio 1:1, log f O2(g) -35 and s/w temperature 40°C

	Seawater/Rock Products				Fluid/Seawater Products			
	Initial	**Final**			**Seawater**	**Fluid**	**Final**	
log f O2(g)	-34.78	-52.5			-34.78	-52.5	-55	
Temp (°C)	40	150			40	150	95	
pH	3.45	9.3			3.45	9.3	5.4	
Eh(Volts)	0.47	-0.67			0.47	-0.67	-0.18	
Minerals(mmol)	Brucite	1600	Clinochlore-14A	137	Graphite	170		
	Andradite	220	Magnetite	115	Diaspore	0.072		
	Antigorite	180	Troilite	105	Pyrite	0.001		
	Calcite	155						
Amino Acids	Some acids are stable over different temperature				Met	5.20E-16	Glu	Phe
(mmol)	ranges, but none are stable above 80°C except for				Gly		Val	Tyr
	Threonine.				Ala		Thr	Trp
					Asp		Gln	
					Ser		Ile	
					Asn		Leu	
Dissolved species	**SO4--**	**H2S**	**HS-**		**SO4--**	**H2S**	**HS-**	
(mmol)	~0	0.009	7		0.0042	8	7.00E-01	
	N2	**NH3**	**NH4+**		**N2**	**NH3**	**NH4+**	
	~0	0.88	~0		0.07	1.06E-02	1.6	
	CO2	**CH4**			**CO2**	**CH4**		
	~0	85			1.38E+02	4.00E-03		
	H2				**H2**			
	0.23				4.50E-05			

Model 5c

Experimental Results for w/r ratio 1:1, log f O2(g) -35 and s/w temperature 60°C

	Seawater/Rock Products				Fluid/Seawater Products			
	Initial	**Final**			**Seawater**	**Fluid**	**Final**	
log f O2(g)	-34.8	-52.5			-34.8	-52.5	-54	
Temp (°C)	60	150			60	150	105	
pH	3.52	9.3			3.52	9.3	5.75	
Eh(Volts)	0.42	-0.67			0.42	-0.67	-0.22	
Minerals(mmol)	Brucite	1700	Magnetite	99	Graphite	174		
	Andradite	245	Calcite	78	Diaspore	0.072		
	Antigorite	180			Pyrite	0.001		
	Clinochlore-14A	137						
	Troilite	105						
Amino Acids	None stable above 70°C				Met	2.40E-15	Asn	Ile
(mmol)	All acids are stable between 60-70°C				Gly		Glu	Leu
					Ala		Val	Phe
					Asp		Thr	Tyr
					Ser		Gln	Trp
Dissolved species	**SO4--**	**H2S**	**HS-**		**SO4--**	**H2S**	**HS-**	
(mmol)	~0	0.009	6.9		0.00154	7.2	1.50E+00	
	N2	**NH3**	**NH4+**		**N2**	**NH3**	**NH4+**	
	~0	0.76	~0		0.11	3.10E-02	1.28	
	CO2	**CH4**			**CO2**	**CH4**		
	~0	83			6.30E+01	1.85E-02		
	H2				**H2**			
	0.23				1.50E-04			

Model 5d

Experimental Results for w/r ratio 1:1, log f O2(g) -35 and s/w temperature 80°C

	Seawater/Rock Products				Fluid/Seawater Products			
	Initial	**Final**			**Seawater**	**Fluid**	**Final**	
log f O2(g)	-34.82	-52.5			-34.82	-52.5	-53	
Temp (°C)	80	150			80	150	115	
pH	3.6	9.3			3.6	9.3	6.15	
Eh(Volts)	0.36	-0.67			0.36	-0.67	-0.275	
Minerals(mmol)	Brucite	1800	Troilite	105	Graphite	175		
	Andradite	265	Magnetite	90	Diaspore	0.072		
	Antigorite	180	Calcite	40	Pyrite	0.001		
	Clinochlore-14A	138						
Amino Acids	None stable above 86°C				Met	1.20E-14	Glu	Phe
(mmol)					Gly		Val	Tyr
					Ala		Thr	Trp
					Asp		Gln	
					Ser		Ile	
					Asn		Leu	
Dissolved species	**SO4--**	**H2S**	**HS-**		**SO4--**	**H2S**	**HS-**	
(mmol)	~0	0.0088	6.8		5.75E-04	5.7	3.00E+00	
	N2	**NH3**	**NH4+**		**N2**	**NH3**	**NH4+**	
	~0	0.75	~0		0.14	1.00E-01	1.06	
	CO2	**CH4**			**CO2**	**CH4**		
	~0	88			2.50E+01	1.00E-01		
	H2				**H2**			
	0.23				4.90E-04			

Model 6a

Experimental Results for w/r ratio 1:1, log f O2(g) -45 and s/w temperature 20°C

	Seawater/Rock Products				Fluid/Seawater Products			
	Initial	**Final**			**Seawater**	**Fluid**	**Final**	
log f O2(g)	-44.75	-52.5			-44.75	-52.5	-56.5	
Temp (°C)	20	150			20	150	85	
pH	3.39	9.3			3.39	9.3	5	
Eh(Volts)	0.38	-0.67			0.38	-0.67	-0.15	
Minerals(mmol)	Brucite	1360	Magnetite	154	Graphite	159		
	Calcite	325	Clinochlore-14A	136	Diaspore	0.0072		
	Antigorite	185	Troilite	105	Pyrite	0.001		
	Andradite	168						
Amino Acids	None stable above 55°C except Valine, Serine, Isoleucine,				Met	1.15E-16	Glu	Phe
(mmol)	Leucine, Threonine				Gly	5.00E-17	Val	Tyr
					Ala	6.00E-23	Thr	Trp
					Asp		Gln	
					Ser		Ile	
					Asn		Leu	
Dissolved species	**SO4--**	**H2S**	**HS-**		**SO4--**	**H2S**	**HS-**	
(mmol)	~0	0.009	7		0.009	8.5	3.00E-01	
	N2	**NH3**	**NH4+**		**N2**	**NH3**	**NH4+**	
	~0	1.14	~0		0.8	3.80E-03	2.1	
	CO2	**CH4**			**CO2**	**CH4**		
	~0	80			3.04E+02	8.00E-04		
	H2				**H2**			
	0.225				1.47E-05			

Model 6b

Experimental Results for w/r ratio 1:1, log f O2(g) -45 and s/w temperature 40°C

	Seawater/Rock Products				Fluid/Seawater Products			
	Initial	**Final**			**Seawater**	**Fluid**	**Final**	
log f O2(g)	-44.78	52.5			-44.78	52.5	-55	
Temp (°C)	40	150			40	150	95	
pH	3.45	9.3			3.45	9.3	5.35	
Eh(Volts)	0.32	-0.67			0.32	-0.67	-0.175	
Minerals(mmol)	Brucite	1600	Magnetite	120	Graphite	168		
	Andradite	220	Troilite	105	Diaspore	0.0072		
	Calcite	155			Pyrite	0.001		
	Clinochlore-14A	137						
Amino Acids	None stable above 36°C except for Threonine				Met	5.40E-16	Glu	Phe
(mmol)					Gly	1.40E-16	Val	Tyr
					Ala	3.70E-22	Thr	Trp
					Asp		Gln	
					Ser		Ile	
					Asn		Leu	
Dissolved species	**SO4--**	**H2S**	**HS-**		**SO4--**	**H2S**	**HS-**	
(mmol)	~0	0.009	7		0.0042	8	7.00E-01	
	N2	**NH3**	**NH4+**		**N2**	**NH3**	**NH4+**	
	~0	0.88	~0		0.08	1.10E-02	1.6	
	CO2	**CH4**			**CO2**	**CH4**		
	~0	85			1.40E+02	3.80E-03		
	H2				**H2**			
	0.225				4.75E-05			

Model 6c

Experimental Results for w/r ratio 1:1, log f O2(g) -45 and s/w temperature 60°C

	Seawater/Rock Products				Fluid/Seawater Products			
	Initial	**Final**			**Seawater**	**Fluid**	**Final**	
log f O2(g)	-44.8	-52.5			-44.8	-52.5	-54	
Temp (°C)	60	150			60	150	105	
pH	3.52	9.3			3.52	9.3	5.75	
Eh(Volts)	0.25	-0.67			0.25	-0.67	-0.225	
Minerals(mmol)	Brucite	1720	Troilite	105	Graphite	172		
	Andradite	250	Magnetite	99	Diaspore	0.0072		
	Antigorite	180	Calcite	78	Pyrite	0.001		
	Clinochlore-14A	137						
Amino Acids	None stable above 70°C				Met	2.40E-15	Glu	Phe
(mmol)					Gly	4.00E-16	Val	Tyr
					Ala	2.40E-21	Thr	Trp
					Asp		Gln	
					Ser		Ile	
					Asn		Leu	
Dissolved species	**SO4--**	**H2S**	**HS-**		**SO4--**	**H2S**	**HS-**	
(mmol)	~0	0.009	7		0.0017	7.2	1.50E+00	
	N2	**NH3**	**NH4+**		**N2**	**NH3**	**NH4+**	
	~0	0.75	~0		0.1	3.10E-02	1.28	
	CO2	**CH4**			**CO2**	**CH4**		
	~0	87			6.30E+01	1.80E-02		
	H2				**H2**			
	0.23				1.50E-04			

Model 6d

Experimental Results for w/r ratio 1:1, log f O2(g) -45 and s/w temperature 80°C

	Seawater/Rock Products				Fluid/Seawater Products			
	Initial	**Final**			**Seawater**	**Fluid**	**Final**	
log f O2(g)	-44.84	-52.5			-44.84	-52.5	-53	
Temp (°C)	80	150			80	150	115	
pH	3.6	9.3			3.6	9.3	6.15	
Eh(Volts)	1.8	-0.67			1.8	-0.67	-0.275	
Minerals(mmol)	Brucite	1800	Troilite	105	Graphite	175		
	Andradite	263	Magnetite	90	Diaspore	0.0072		
	Antigorite	175	Calcite	40	Pyrite	0.001		
	Clinochlore-14A	138						
Amino Acids	None stable above 85°C				Met	1.10E-14	Glu	Phe
(mmol)					Gly	1.20E-15	Val	Tyr
					Ala	1.60E-20	Thr	Trp
					Asp		Glu	
					Ser		Ile	
					Asn		Leu	
Dissolved species	**SO4--**	**H2S**	**HS-**		**SO4--**	**H2S**	**HS-**	
(mmol)	~0	0.009	7		5.70E-04	5.7	3.05E+00	
	N2	**NH3**	**NH4+**		**N2**	**NH3**	**NH4+**	
	~0	0.7	~0		0.14	1.00E-01	1.06	
	CO2	**CH4**			**CO2**	**CH4**		
	~0	88			2.50E+01	1.00E-01		
	H2				**H2**			
	0.23				5.00E-04			

Model 7a

Experimental Results for w/r ratio 1:1, log f O2(g) -55 and s/w temperature 20°C

	Seawater/Rock Products				Fluid/Seawater Products			
	Initial	**Final**			**Seawater**	**Fluid**	**Final**	
log f O2(g)	-54.75	-52.5			-54.75	-52.5	-56.4	
Temp (°C)	20	150			20	150	85	
pH	3.39	9.3			3.39	9.3	5	
Eh(Volts)	0.24	-0.67			0.24	-0.67	-0.14	
Minerals(mmol)	Brucite	1360	Magnetite	150	Graphite	159		
	Calcite	325	Clinochlore-14A	137	Diaspore	0.0072		
	Antigorite	187	Troilite	110	Pyrite	0.001		
	Andradite	170						
Amino Acids	None stable above 55°C except Isoleucine, Leucine				Met	1.15E-16	Glu	Phe
(mmol)	and Threonine				Gly	5.00E-17	Val	Tyr
					Ala	5.70E-23	Thr	Trp
					Asp		Gln	
					Ser		Ile	
					Asn		Leu	
Dissolved species	**SO4--**	**H2S**	**HS-**		**SO4--**	**H2S**	**HS-**	
(mmol)	~0	0.009	7		0.009	8.5	3.00E-01	
	N2	**NH3**	**NH4+**		**N2**	**NH3**	**NH4+**	
	0.575	1.14	~0		0.08	3.80E-03	2.15	
	CO2	**CH4**			**CO2**	**CH4**		
	~0	80			3.05E+02	8.00E-04		
	H2				**H2**			
	0.225				1.42E-05			

Model 7b

Experimental Results for w/r ratio 1:1, log f O2(g) -55 and s/w temperature 40°C

	Seawater/Rock Products				Fluid/Seawater Products			
	Initial	**Final**			**Seawater**	**Fluid**	**Final**	
log f O2(g)	-54.78	-52.5			-54.78	-52.5	-55.1	
Temp (°C)	40	150			40	150	95	
pH	3.45	9.3			3.45	9.3	5.35	
Eh(Volts)	0.16	-0.67			0.16	-0.67	-0.18	
Minerals(mmol)	Brucite	1600	Clinochlore-14A	137	Graphite	168		
	Andradite	223	Magnetite	115	Diaspore	0.0072		
	Antigorite	180	Troilite	105	Pyrite	0.001		
	Calcite	155						
Amino Acids	None stableabove 59°C except Threonine				Met	5.20E-16	Glu	Phe
(mmol)					Gly	1.40E-16	Val	Tyr
					Ala	3.70E-22	Thr	Trp
					Asp		Gln	
					Ser		Ile	
					Asn		Leu	
Dissolved species	**SO4--**	**H2S**	**HS-**		**SO4--**	**H2S**	**HS-**	
(mmol)	~0	0.009	7		0.0042	8	7.00E-01	
	N2	**NH3**	**NH4+**		**N2**	**NH3**	**NH4+**	
	~0	0.88	~0		0.08	1.07E-02	1.6	
	CO2	**CH4**			**CO2**	**CH4**		
	~0	85			1.38E+02	4.00E-03		
	H2				**H2**			
	0.23				4.75E-05			

Model 7c

Experimental Results for w/r ratio 1:1, log f O2(g) -55 and s/w temperature 60°C

	Seawater/Rock Products				Fluid/Seawater Products			
	Initial	**Final**			**Seawater**	**Fluid**	**Final**	
log f O2(g)	-54.82	-52.5			-54.82	-52.5	-54	
Temp (°C)	60	150			60	150	105	
pH	3.53	9.3			3.53	9.3	5.75	
Eh(Volts)	0.08	-0.67			0.08	-0.67	-0.225	
Minerals(mmol)	Brucite	1720	Troilite	105	Graphite	173		
	Andradite	250	Magnetite	99	Diaspore	0.0072		
	Antigorite	180	Calcite	78	Pyrite	0.001		
	Clinochlore-14A	137						
Amino Acids	None stable above 70°C				Met	2.50E-15	Glu	Phe
(mmol)					Gly	4.00E-16	Val	Tyr
					Ala	2.40E-21	Thr	Trp
					Asp		Gln	
					Ser		Ile	
					Asn		Leu	
Dissolved species	**SO4--**	**H2S**	**HS-**		**SO4--**	**H2S**	**HS-**	
(mmol)	~0	0.009	7		0.0017	7.25	1.50E+00	
	N2	**NH3**	**NH4+**		**N2**	**NH3**	**NH4+**	
	~0	0.88	~0		0.11	3.10E-02	1.3	
	CO2	**CH4**			**CO2**	**CH4**		
	~0	85			6.30E+01	1.80E-02		
	H2				**H2**			
	0.23				1.50E-04			

Model 7d

Experimental Results for w/r ratio 1:1, log f O2(g) -55 and s/w temperature 80°C

	Seawater/Rock Products				Fluid/Seawater Products			
	Initial	**Final**			**Seawater**	**Fluid**	**Final**	
log f O2(g)	-54.84	-52.5			-54.84	-52.5	-53	
Temp (°C)	80	150			80	150	115	
pH	3.8	9.3			3.8	9.3	6.2	
Eh(Volts)	-0.27	-0.67			-0.27	-0.67	-0.275	
Minerals(mmol)	Brucite	1750	Troilite	105	Graphite	175		
	Andradite	262	Magnetite	90	Diaspore	0.0072		
	Antigorite	175	Calcite	40	Pyrite	0.001		
	Clinochlore-14A	138						
Amino Acids	None stable above 86°C				Met	1.80E-14	Glu	Phe
(mmol)					Gly	2.00E-15	Val	Tyr
					Ala	2.75E-20	Gln	Trp
					Asp		Thr	
					Asn		Ile	
					Ser		Leu	
Dissolved species	**SO4--**	**H2S**	**HS-**		**SO4--**	**H2S**	**HS-**	
(mmol)	~0	0.009	7		6.00E-04	5.5	3.20E+00	
	N2	**NH3**	**NH4+**		**N2**	**NH3**	**NH4+**	
	~0	1.36	~0		0.4	1.75E-01	1.75	
	CO2	**CH4**			**CO2**	**CH4**		
	~0	88			2.40E+01	1.00E-01		
	H2				**H2**			
	0.23				5.00E-04			

Model 8a

Experimental Results for w/r ratio 1:1, log f O2(g) -35 and s/w temperature 20°C

	Seawater/Rock Products				Fluid/Seawater Products			
	Initial	**Final**			**Seawater**	**Fluid**	**Final**	
log f O2(g)	-64.75	-52.5			-64.75	-52.5	-56.5	
Temp (°C)	20	150			20	150	85	
pH	3.42	9.3			3.42	9.3	5.1	
Eh(Volts)	0.08	-0.67			0.08	-0.67	-0.135	
Minerals(mmol)	Brucite	1360	Magnetite	153	Graphite	158		
	Calcite	325	Clinochlore-14A	137	Diaspore	0.0072		
	Antigorite	187	Troilite	105	Pyrite	0.001		
	Andradite	170						
Amino Acids	None stable above 55°C except for Serine and				Met	1.25E-16	Glu	Phe
(mmol)	Threonine				Gly	5.50E-17	Val	Tyr
					Ala	6.00E-23	Thr	Trp
					Asp		Gln	
					Ser		Ile	
					Asn		Leu	
Dissolved species	**SO4--**	**H2S**	**HS-**		**SO4--**	**H2S**	**HS-**	
(mmol)	~0	0.009	7		0.009	8.5	3.00E-01	
	N2	**NH3**	**NH4+**		**N2**	**NH3**	**NH4+**	
	0.57	1.23	~0		0.1	4.20E-03	2.25	
	CO2	**CH4**			**CO2**	**CH4**		
	~0	80			3.05E+02	8.00E-04		
	H2				**H2**			
	0.21				1.43E-05			

Model 8b

Experimental Results for w/r ratio 1:1, log f O2(g) -65 and s/w temperature 40°C

	Seawater/Rock Products				Fluid/Seawater Products			
	Initial	**Final**			**Seawater**	**Fluid**	**Final**	
log f O2(g)	-64.78	-52.5			-64.78	-52.5	-55.2	
Temp (°C)	40	150			40	150	95	
pH	4.75	9.3			4.75	9.3	5.55	
Eh(Volts)	-0.7	-0.67			-0.7	-0.67	-0.193	
Minerals(mmol)	Brucite	1590	Clinochlore-14A	137	Graphite	168		
	Andradite	240	Magnetite	117	Diaspore	0.0072		
	Antigorite	180	Troilite	105	Pyrite	0.007		
	Calcite	163						
Amino Acids	None stable above 59°C except Threonine				Met	4.25E-15	Glu	Phe
(mmol)					Gly	1.20E-15	Gln	Tyr
					Ala	3.00E-21	Val	Trp
					Asp		Thr	
					Ser		Ile	
					Asn		Leu	
Dissolved species	**SO4--**	**H2S**	**HS-**		**SO4--**	**H2S**	**HS-**	
(mmol)	~0	0.009	7		0.0085	7.7	1.00E+00	
	N2	**NH3**	**NH4+**		**N2**	**NH3**	**NH4+**	
	~0	10.2	~0		5.5	9.00E-02	9.12	
	CO2	**CH4**			**CO2**	**CH4**		
	~0	90			1.33E+02	4.10E-03		
	H2				**H2**			
	0.23				4.80E-05			

Experimental Results for w/r ratio 1:1, log f O2(g) -65 and s/w temperature 60°C

	Seawater/Rock Products				Fluid/Seawater Products		
	Initial	**Final**			**Seawater**	**Fluid**	**Final**
log f O2(g)	-68.7	-58			-68.7	-58	-66
Temp (°C)	60	150			60	150	105
pH	5.62	6.38			5.62	6.38	6.75
Eh(Volts)	-0.28	-0.535			-0.28	-0.535	-0.525
Minerals(mmol)	Brucite	255	Troilite	114	Troilite	0.00135	
	Antigorite	200					
	Clinochlore-14A	137					
	Magnetite	137					
Amino Acids (mmol)	None stable above 66°C				None stable above 60C		
Dissolved species (mmol)	**SO4--**	**H2S**	**HS-**		**SO4--**	**H2S**	**HS-**
	~0	0.001	0.00125		~0	0.00023	7.00E-04
	N2	**NH3**	**NH4+**		**N2**	**NH3**	**NH4+**
	0.0065	3250	9500		~0	3.25E+03	22200
	CO2	**CH4**			**CO2**	**CH4**	
	~0	8484			~0	1.70E+04	
	H2				**H2**		
	135				1.35E+02		

Experimental Results for w/r ratio 1:1, log f O2(g) -65 and s/w temperature 80°C

	Seawater/Rock Products			Fluid/Seawater Products		
	Initial	**Final**		**Seawater**	**Fluid**	**Final**
log f O2(g)	**Didn't Run**					
Temp (°C)	80	150		80	150	115
pH						
Eh(Volts)						
Minerals(mmol)						
Amino Acids (mmol)						
Dissolved species (mmol)	**SO4--**	**H2S**	**HS-**	**SO4--**	**H2S**	**HS-**
	N2	**NH3**	**NH4+**	**N2**	**NH3**	**NH4+**
	CO2	**CH4**		**CO2**	**CH4**	
	H2			**H2**		